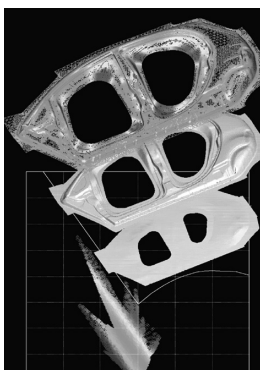


TECHNICAL REVIEW

2006 NO. 18



MITSUBISHI MOTORS



- **Cover Photograph**

The cover photograph shows a stamping simulation of the side outer panel for the Mitsubishi "i". Stamping simulations enable Mitsubishi Motors Corporation to predict splits, wrinkles, and other defects that may occur in the parts from sheet metal. They also enable us to predict thinning distribution, stress distribution, draw-in during stamping, and skid marks. By simulating stamping processes, we are able to identify and eliminate defects early in development programs, thereby promoting front-loading of work.

Published by Editorial Committee for the Technical Review
c/o Environment & Recycling Affairs Dept.
MITSUBISHI MOTORS CORPORATION,
16-4, Kohnan 2-chome, Minato-ku, Tokyo 108-8410, Japan
Phone: +81-3-6719-4207
Fax: +81-3-6719-0034
E-mail: technicalreview.et@mitsubishi-motors.com



MITSUBISHI MOTORS TECHNICAL REVIEW

2006 NO.18

Contents

Foreword

Promotion of Technical Development with Emphasis on the Environment	4
---------------------------------------------------------------------------	---

Technical Perspective

Technology Status and Future of Clean-Energy Vehicles	6
Left-Right Torque Vectoring Technology as the Core of Super All Wheel Control (S-AWC)	16

Technical Papers

Dynamic Scheduling Control for Engine and Gearshifts: Consolidation of Fuel-Economy Optimization and Reserve Power	24
Enhancement of Combustion by Means of Squish Pistons	32
Development of Optimizing System for Engine Performance Simulator	42
Development of Technique for Predicting Parts Temperatures Using Radiation Analysis	49
Basic Study for Reducing Noise in a Vehicle Cavity (Experimental and Theoretical Analyses of Structural – Acoustic Coupling Problems in a Rectangular Parallelepiped Space)	55

New Technologies

Special Feature 1 New Technology for OUTLANDER

Newly Developed Four-Cylinder MIVEC Engine	59
Overview of the Newly Developed Front Engine Front Drive Platform	62
Development of Application Technology of Aluminum Roof	68
Development of a Next Generation Electronics Platform	75
ECU Variant Coding System	80
ETACS Functionality Development for the OUTLANDER	84
Development of High Quality Premium Sound System	89

Photo in the previous page

These images are the final design sketches of the Mitsubishi "i" (a new minicar that was launched January 2006) and Mitsubishi OUTLANDER (a new sport utility vehicle that was launched in October 2005). Many of the new technologies used in the "i" and OUTLANDER are featured in this edition of the Mitsubishi Motors Technical Review.

Special Feature 2 New Technology for “i”

Newly Developed Three-Cylinder MIVEC Engine	95
Overview of the Newly Developed Mid Engine Rear Drive Platform	98
Door Keyless Operation System Using Piezoelectric Cable Sensor	102

Improvement of Vehicle Dynamic Performance by Means of In-Wheel Electric Motors	106
Development of Technique for Predicting Roof Buckling Under Snow Load	113
Development of Filter with New Function for Car Air-Conditioner	117
Parking-Guidance System Using Nose-View Cameras	121
Latest Stamping Simulation Technique	126

Technical Topics

The Road to “Concept-X”

A Glimpse into Creating a Design Icon – Understanding the Process and Method	132
Mitsubishi Concept-X Exterior Design Story	134
Creating an Interior Icon for Concept-X	136

New Products

OUTLANDER	138
i	140
LANCER EVOLUTION WAGON	142
TRITON	144
ZINGER	148



Promotion of Technical Development with Emphasis on the Environment

Tetsuro AIKAWA

Managing Director

Concern over the environment is growing as abnormal global weather and the depletion of natural resources threaten the world. The Kyoto Protocol came into effect last year and discussions on the environment have continued ceaselessly. The United States, which refused to sign the Kyoto Protocol, has started efforts to reduce domestic emissions of CO₂. Hence, the auto industry is actively working to develop environment-friendly technologies since the industry inevitably has a major impact on the environment. The auto industry showcased its environmental conservation efforts at the Tokyo Motor Show last autumn and at various other events around the world.

In January 2005 Mitsubishi Motors Corporation (MMC) announced its new revitalization plan, and in September announced a new slogan, the "*Kuruma zukuri no genten e*" (meaning "Pursuing the Origins of Car Engineering" in English. The English phrase is not used in the company's marketing efforts), which will be reflected in our products. MMC has resolved to make more attractive automobiles that offer both drivability and durability, and has promised customers to sincerely consider the environment in carrying out the plan.

As part of its environmental conservation work, MMC defined its environmental principle as a basic policy in 1999, drew up a 5-year medium-term environmental action plan in 2002 to execute that policy, and has taken various steps accordingly. For instance, the Design for Environment (DfE) promotes designing based on not only the reduction of CO₂ emitted while operating the vehicle and realizing cleaner exhaust emissions, but also on the reduction of CO₂ emitted during the production of automobiles, together with the maximizing of the recycling potential upon scrapping. In 2002, MMC set up a special division for automobile recycling to prepare for the Recycling Law which came into force in January 2005. MMC has already achieved a shredder dust recycling rate of 59.3 % in 2004, significantly exceeding the legal requirement of over 30 % in 2005 and later. Our environment-related actions and achievements are announced in the Environment Sustainability Plan in four categories: environment management, recycling, prevention of global warming and prevention of contamination of the environment.

The OUTLANDER model released last October includes specific environmental features. For instance, its exhaust emissions are 75 % lower than those mandated by Japan's 2005 LEV regulations and its fuel efficiency is 5 % higher than Japan's 2010 fuel efficiency standard, thanks to improved combustion and exhaust systems and minimized weight increase by adopting a newly developed platform. As for safety – another key factor of automobiles – even though the weight increase has been suppressed, the OUTLANDER series achieves safety equivalent to the highest 6☆ rating in the JNCAP safety performance com-

parison test by a public organization (result of in-company test), and the vehicle is designed to minimize the damage of a smaller car in the event of a crash and to improve protection for pedestrians. Meanwhile, the minicar model “i” released in January satisfied the voluntary regulation of the auto industry on Volatile Organic Compounds (VOCs) that cause the “sick-house syndrome” in order to improve the ambience inside the car. And for safety, since the “i” series adopts a rear midship layout, it creates a sufficient crush zone by using the front area without engine. Although the “i” series is a minicar, it meets the 5☆ safety rating of JNCAP (result of in-company test). These new technologies adopted on OUTLANDER and “i” are featured on this **MITSUBISHI MOTORS TECHNICAL REVIEW**.

The target low pollution model in the future environmental technologies is the next-generation electric vehicle “MIEV” which emits no gas at all. First of all, it makes exceptional use of space since the motor is contained inside a wheel and thus no large drive system is necessary. With this concept, it is easier to develop not only basic electric cars but also hybrid cars and fuel cell electric cars. The vehicle performance will also be significantly enhanced as the in-wheel motors can be controlled independently for each wheel without a transmission, differential gears or other complex drive systems. MMC will use lithium ion batteries with higher energy density to replace the conventional batteries. MMC will work hard to study the technologies required to achieve this target to make customers experience our minicar-based environment-friendly electric cars by 2010.

Today, company managers must be both environmentally and socially aware. As we promised in the revitalization plan last year, MMC will add “contribution to environmental preservation” to the “driving pleasure and safety” while putting the customer first. We will focus on achieving our targets and developing the required new technologies, which we will continue to announce in **MITSUBISHI MOTORS TECHNICAL REVIEW**. We hope you enjoy reading these articles.

Technology Status and Future of Clean-Energy Vehicles

Eizo TABO* Takashi YOSHINA*
Yasufumi SEKINE* Reiko SAITO*

Abstract

Since the Kyoto Protocol to the United Nations Framework Convention on Climate Change (commonly known as the Kyoto Protocol) came into force in February 2005, the Japanese government has been working to satisfy the targets for reduction of carbon-dioxide (CO₂) emissions. Meanwhile, however, rapid motorization in China, India, and Southeast Asia can be expected to drive continued demand for automobiles and concomitant growth in energy consumption.

Against this backdrop, automakers have a responsibility to develop and promote Low Emission Vehicles (LEVs) as a means of helping to preserve the natural environment. Like other automakers, Mitsubishi Motors Corporation (MMC) needs to take a clearly defined approach to LEV development and promotion from a long-term standpoint.

This paper gives an overview of MMC's LEV-related efforts together with information on the Japanese government's LEV strategies, the current situation regarding Clean Energy Vehicles (CEVs), and the outlook for future LEV developments.

Key words: *Technical Trend, Low-Emission Vehicle, Clean Energy Vehicle*

1. Introduction

In recent years, the effects of global warming have become increasingly evident in the form of rising air temperatures, rising sea levels, and melting permafrost. The Intergovernmental Panel on Climate Change has attributed most of the global warming in the last 50 years to human activity⁽¹⁾, and it has been reported that the greenhouse gas that most seriously exacerbates global warming is CO₂⁽²⁾.

When the Kyoto Protocol came into force in February 2005, the Japanese government established a Kyoto Target Achievement Plan. This plan calls for adoption of LEVs to be promoted as a way to achieve a reduction of about three million tons in CO₂ emissions by FY 2010⁽³⁾. Consequently, there is a need for a rapid increase in LEV adoption.

Further, in November 2005 Japan's Ministry of Economy, Trade, and Industry (METI) compiled a super-long-term energy strategy that calls for CO₂ emissions in the household and transportation sectors to be reduced to zero by 2100. This document reflects an assumption that worldwide oil production will peak in 2050 and a belief that societies must end their dependence on oil by the same year. With regard to automobiles, the strategy calls for Fuel Cell Vehicles (FCVs) and Electric Vehicles (EVs) as a proportion of total automobiles to be increased to 40 % by 2050 to enable CO₂ emissions to be reduced to zero by 2100.

Given the aforementioned circumstances, the positioning of LEVs in the socioeconomic structure is going to become increasingly important.

2. Overview of LEVs

There is no universal, clear-cut definition of a LEV. Generally speaking, though, LEVs are taken to include vehicles that emit only small quantities of atmospheric pollutants such as Hydro-carbon (HC), nitrogen oxides (NO_x), and particulate matter (PM) and vehicles that additionally emit only small quantities of CO₂. LEVs are categorized either as LEVs (gasoline and diesel vehicles that are designed for reduced exhaust emissions) or as CEVs [EVs, Compressed Natural-Gas (CNG) vehicles, Hybrid Electric Vehicles (HEVs), and other vehicles that use clean alternatives to conventional fuels].

The Japanese central government and a number of Japanese local authorities have introduced certification and purchase-subsidy programs to promote the spread of LEV adoption.

2.1 Major Japanese government incentive programs for promotion of LEVs

In a March 2002 outline of strategies for combating global warming⁽¹⁾, the Japanese government targeted adoption of 3.48 million LEV units by 2010. In the Kyoto Target Achievement Plan⁽³⁾, which it established in April 2005, the government set a revised target of 2.33 million units. To achieve this target, the government is implementing incentives that encourage the purchase of LEVs. Some of the schemes are described hereafter.

2.1.1 Green automobile taxation system⁽⁴⁾

This incentive is administered by the Ministry of Land, Infrastructure, and Transport (MLIT) and came into effect in 2001, when Japan introduced a certification system for LEVs. Under the present taxation system, anyone purchasing a low-emission and low-fuel-

* Corporate Planning Office, Environment & Recycling Affairs Dept.

Table 1 Overview of Japan's green automobile taxation system (FY 2006 – 2007)

Tax type	Applicable vehicle types	Tax reduction* ¹	Period
Annual automobile tax	EVs, FCVs, CNG vehicles, methanol vehicles and gasoline vehicles (including HEVs and LPG vehicles) qualifying for a 4☆ LEV rating ² and having fuel efficiency at least 20 % better than standard ³	– 50 %	April 2006 to March 2008 ⁵
	Gasoline vehicles (including HEVs and LPG vehicles) qualifying for a 4☆ LEV rating and having fuel efficiency at least 10 % better than standard ⁴	– 25 %	
Automobile acquisition tax	Gasoline vehicles (including LPG vehicles) qualifying for a 4☆ LEV rating and having fuel efficiency at least 20 % better than standard	Personally owned vehicles (excluding minicars): – ¥15,000 Commercially owned vehicles; minicars: – ¥9,000	April 2006 to March 2008
	Gasoline vehicles (including LPG vehicles) qualifying for a 4☆ LEV rating and having fuel efficiency at least 10 % better than standard	Personally owned vehicles (excluding minicars): – ¥7,500 Commercially owned vehicles; minicars: – ¥4,500	
	EVs, methanol vehicles, CNG vehicles, HEVs, FCVs	HEVs (passenger cars): – 2.2 % Others: – 2.7 %	April 2005 to March 2007

<Reference> The standard automobile acquisition tax rate is 5 % for personally owned vehicles (excluding minicars) and 3 % for commercially owned vehicles and for minicars.

*1: Reductions in annual automobile tax are shown as percentage reductions in payable tax amounts. Reductions in automobile acquisition tax are shown as yen reductions in payable tax amounts or as percentage reductions from the standard tax rates (e.g., 3 % for commercially owned vehicles).

*2: Vehicles with exhaust emissions at least 75 % lower than those permitted by Japan's 2005 regulations

*3: Vehicles with fuel efficiency at least 20 % better than that required by Japan's 2010 standard

*4: Vehicles with fuel efficiency at least 10 % better than that required by Japan's 2010 standard

*5: The tax reduction is applied the year after a vehicle is newly registered.

*6: It is possible to receive the above preferential treatments for both the annual automobile tax and automobile acquisition tax, but it is impossible to receive multiple preferential treatments for the automobile acquisition tax.

consumption vehicle benefits from a reduction of annual tax and acquisition tax. When a certain number of years has passed following the vehicle's registration, the annual tax is levied at an increased rate. Thus, the system not only encourages initial LEV purchases but also promotes the replacement of old vehicles with new ones.

In December 2005, the government unveiled a FY 2006 tax-system outline involving continuation of the automobile green taxation system in FY 2006. The taxation system will have revised terms: A 25 % reduction in annual automobile tax applies to any vehicle that has exhaust emissions 75 % lower than Japan's 2005 regulations (4☆ LEV rating) and has fuel efficiency at least 10 % better than Japan's 2010 fuel-efficiency standard. And a 50 % reduction in annual automobile tax applies to any vehicle that has exhaust emissions 75 % lower than Japan's 2005 regulations (4☆ LEV rating) and has fuel efficiency at least 20 % better than Japan's 2010 fuel-efficiency standard. An overview of the green taxation system to be implemented from FY 2006 to 2007 is given by **Table 1**.

2.1.2 Subsidy system for adoption of CEVs⁽⁵⁾

This system was released in FY 1998 by METI and is substantially revised every three years (The next review is scheduled for FY 2007.). It receives annual government funding of ¥8 – 10 billion. (The budget for FY 2006 is ¥9 billion.)

Under the system, anyone purchasing a CEV receives a subsidy roughly equal to half of the price difference between the CEV and the conventional model on which it is based. Also, subsidies are provided for construction of natural-gas supply stations, battery-charging facilities, and other types of infrastructure for

CEVs. The system has subsidized the purchase of numerous HEVs and CNG vehicles. An overview of the CEV subsidy system is given by **Table 2**.

2.2 The current state of CEV development and adoption

Fig. 1 shows the numbers of CEVs (EVs, HEVs, and CNG vehicles) in use in Japan from FY 2000 to 2004. The number of CEVs increased from about 60,000 in FY 2000 to 230,000 in FY 2004. Also as shown, HEVs account for the majority of the CEVs on Japan's roads. FCVs and methanol vehicles numbered only a few dozen in FY 2004.

An overview of development, sales, and launches of CEVs by Japan's major automakers from 1990 to 2005 is given in **Table 3**. The table was compiled using information released by the Japan Automobile Research Institute (JARI) and information released by the automakers. Although it is not shown in the table, the following schedules are announced: Toyota and Honda will actively launch HEVs in 2006 or later; Mazda will launch hydrogen-engine vehicles in 2006 or later; MMC and Subaru will launch EVs in the minicar category in 2010.

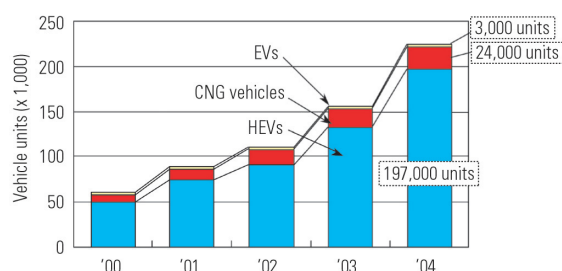
2.2.1 HEVs

A HEV has multiple power sources, whose respective advantages are combined in a way that is intended to limit both exhaust emissions and fuel consumption. The most common HEV power-source combination is an internal-combustion engine and an electric motor. The configuration of the power sources can be series, parallel, or series-parallel (**Fig. 2**).

Since a HEV has multiple power sources or energy sources, the chassis structure is complex and therefore

Table 2 Overview of Japan's CEV subsidy systems

Applicable purchased items	Administering body	Amounts of subsidies and tax reductions	Conditions
EVs, HEVs	Japan Automobile Research Institute	<ul style="list-style-type: none"> New vehicle Up to half of price difference between vehicle and base conventional-fuel model In-use vehicle converted for CNG use Up to one third of cost of conversion from gasoline/diesel use to CNG use 	<ul style="list-style-type: none"> Only private use Leased vehicles are eligible. Regional public bodies may not apply. Minimum requirement for distance driven: 6,000 km/year (This requirement applies only to HEVs. It was abolished for EVs in FY 2005.)
CNG vehicles	Japan Gas Association		
Electricity stand	Japan Eco-Service Stations Association	Commercial use: up to ¥3.5 million Non-commercial use: up to half of cost of purchase and installation	As of November 2005, rapid chargers are ineligible for subsidies.
CNG stand		Commercial use: up to ¥90 million Non-commercial use: up to half of cost of purchase and installation	Running costs are subsidized.

**Fig. 1 Numbers of CEVs on Japan's roads**

HEVs are rather expensive as compared with the conventional vehicles. However, their ability to be fuelled at existing gasoline stations means that they have become far more prevalent than other CEVs. (There were about 197,000 HEVs on Japan's roads in FY 2004.).

2.2.2 EVs

An EV has a secondary battery that powers an electric motor for propulsion. It creates a smaller environmental burden than any other type of vehicle since it runs with zero exhaust emissions.

Fig. 3 shows comparison of gasoline vehicles, HEVs, and EVs as "well-to-wheel" CO₂ emissions (total CO₂ emissions from energy production to vehicle propulsion). As shown, for performance levels corresponding to an engine displacement of 1,500 cc an EV's "well-to-wheel" CO₂ emissions are about 1/3 of those of a gasoline vehicle and about 2/3 of those of a HEV. The CO₂ emissions corresponding to electricity generation were calculated in accordance with the proportions of generation techniques used by Japan's 10 electric power companies (In FY 2002, the proportions were as follows: thermal; 60 %, nuclear; 31 %, hydroelectric; 9 %). As the generation efficiency improves and the proportion of generation systems with emitting lower CO₂ increase, CO₂ emissions corresponding to EVs will become even smaller.

Fig. 4 shows comparison of gasoline vehicles, HEVs, and EVs as running costs. The calculations assume (a) performance levels corresponding to a compact passenger car with an engine displacement of 1,500 cc; (b) a gasoline cost of ¥120 per liter; (c) a daytime electricity

cost of ¥22/kWh; and (d) a nighttime electricity cost of ¥6/kWh. They show that the running cost for an EV is 1/3 (with daytime charging) or 1/10 (with nighttime charging) of that for a gasoline vehicle and that it is 2/3 (with daytime charging) or 1/5 (with nighttime charging) of that for an HEV.

EVs are clearly superior in terms of environmental compatibility and running costs. As shown in **Fig. 1**, however, the number of EVs registered in Japan (even including micro EVs) is only slightly more than 3,000 Units. The scarcity of EVs can be attributed to strongly negative perceptions (that EVs have extremely short range, must be charged for long periods, are extremely costly, and so on) that have caused by the lead-acid batteries which most EVs on the market use.

A switch from lead-acid batteries to nickel-metal-hydride and lithium-ion batteries has resulted in higher performance from smaller batteries, in longer range, in shorter charging durations, and in lower vehicle weights. **Fig. 5** shows the progress made in development of batteries for EVs and HEVs. Whereas EV batteries must offer high energy density, HEV batteries must offer high power density. Lithium-ion batteries for EVs currently have about four times the energy density of lead-acid batteries. By about 2010, they are likely to have about six times the energy density of lead-acid batteries. Their high energy density enables lower vehicle weights. Their increased performance has made it possible to produce electric minicars and compact cars that have 200 km range.

2.2.3 FCVs

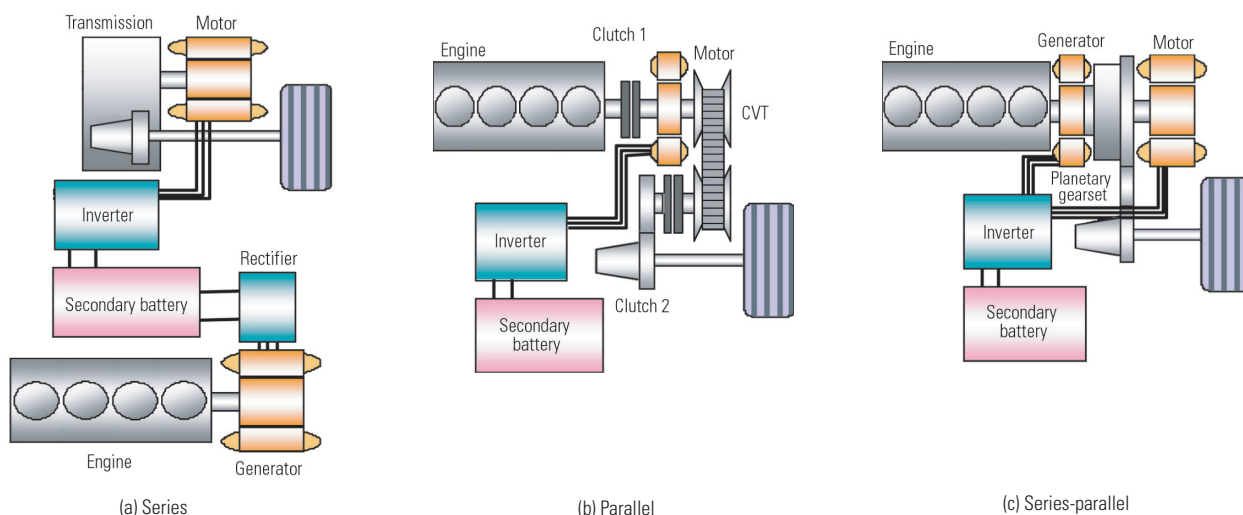
In a FCV, an electric propulsion motor is powered by electricity that is generated inside the fuel cell by a chemical reaction between hydrogen and oxygen in the atmospheric air (**Fig. 6**). The theoretical efficiency of the fuel cell is as high as 80 %, and the substance emitted by a FCV is only water vapor. However, there are several outstanding downside issues, namely a scarcity of hydrogen supply infrastructure, high vehicle production costs, and the difficulty of storing hydrogen safely and efficiently. The general public is not likely to widely adopt FCVs before about 2020 or 2030. (As of FY 2004, there were only 47 FCVs, which consisted of experimental units and units produced for limited sale, in Japan.)

Table 3 Development, sales, and planned launches of CEVs by Japan's major automakers

Company	Vehicle type	'90 – '99	'00	'01	'02	'03	'04	'05
MMC	FCV					★GRANDIS		
	EV	LIBERO						
	CNG	MINICA, MINICAB					MINICAB VAN	
Toyota	FCV				FCHV●		FCHV (motor vehicle type designation)●	
	HEV	PRIUS		CROWN, ESTIMA		New PRIUS, ALPHARD		HARRIER, KLUGER
	EV	RAV4						
	CNG					Century, Probox		
Nissan	FCV						●X-TRAIL FCV	
	HEV		TINO					
	EV	R'nessa	Hypermini					
	CNG		AD VAN			CARAVAN		
Honda	FCV				FCX●		FCX (motor vehicle type designation)●	
	HEV	insight		CIVIC			ACCORD	New CIVIC
	EV	EV PLUS						
	CNG			CIVIC				
Mazda	EV	BONGO						
	CNG		DEMIO					
Subaru	HEV							
	EV	SAMBER					LEGACY	
	CNG							
Suzuki	FCV					★WAGON R, MR WAGON		
	HEV					TWIN		
	EV	ALTO, EVERY						
	CNG		WAGON R, EVERY				WAGON R	
Daihatsu	FCV					★MOVE-FCV-K-2		
	HEV				●HIJET CARGO			HIJET CARGO
	EV	HIJET						
	CNG		HIJET, Mira		HIJET CARGO			

★: Experimental FCV Vehicle (approved by Minister of Land, Infrastructure, and Transport) ●: Available to limited customers (including lease customers) : Marketed to general public

Source: Information released by Japan Automobile Research Institute and information released by the automakers

**Fig. 2 HEV basic configurations**

Although major type of current FCVs have gas tanks filled up by high pressure hydrogen gas (35 – 70 MPa), researches for handling the hydrogen as easy as the gasoline (for example, chemical storage technique) are progressing.

2.2.4 Hydrogen-engine vehicles

A hydrogen-engine vehicle has an internal-combustion engine that uses hydrogen as fuel. Hydrogen-engine vehicles have the advantage that will allow existing engine production facilities to be used after any transition to a hydrogen-based economy. BMW and

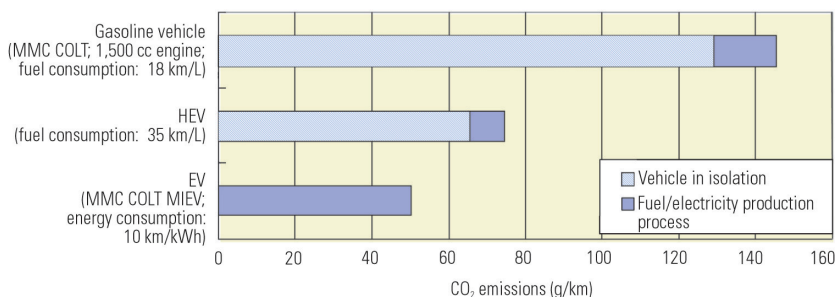
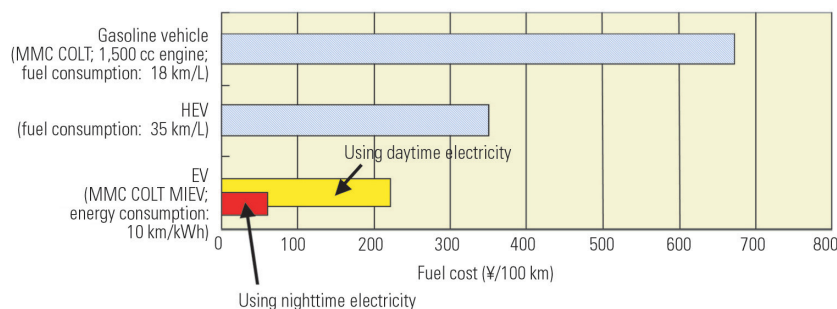
Fig. 3 Comparison of CO₂ emissions

Fig. 4 Comparison of running cost

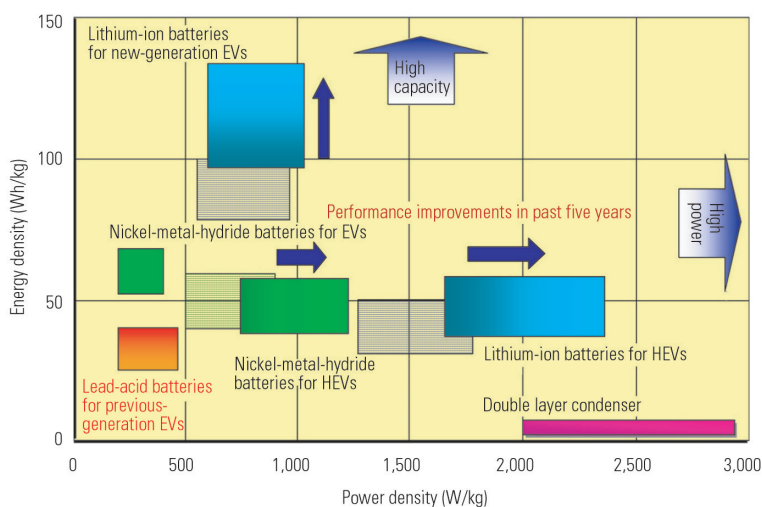


Fig. 5 Development of batteries for EVs and HEVs

Mazda are developing hydrogen-engine vehicles and plan to launch them in 2006. It is necessary to mount the special NO_x catalyst because hydrogen engine emits NO_x.

2.2.5 CNG vehicles

A CNG vehicle has an internal-combustion engine that uses CNG, the main component of which is methane, as its fuel. The merits of a CNG vehicle are that it emits no black smoke, emits only small amounts of NO_x, and has only about 80 % of the CO₂ emissions of a gasoline-engine vehicle. Since the fuel is carried in a gaseous state, however, driving range is relatively short. In FY 2004, there were about 24,000 CNG vehicles in Japan. At the end of September 2005, there were

260 CNG filling stations across Japan.

About 4.1 million CNG vehicles are in use around the world. CNG vehicles are particularly numerous in Argentina and Brazil. These countries produce a large amount of CNG (Fig. 7).

2.2.6 Methanol vehicles

A methanol vehicle has an internal-combustion engine that uses methanol (CH₃OH). When methanol vehicles were first made available, they were promoted since they emit hardly any NO_x and black smoke. Currently, however, there is hardly any methanol supply infrastructure and hardly any methanol vehicles exist.

3. The future perspective of CEV

3.1 Tightening of automobile exhaust gas regulations and fuel efficiency standard

Japan imposed the first regulations on the exhaust emissions of gasoline passenger cars in 1973. It has since made the regulations increasingly stringent; the emission levels permitted by the 2005 regulations are only about 1/100 of those permitted in 1973 (Fig. 8). It is likely that most vehicles in Japan will by about 2010 be replaced with vehicles that comply with new exhaust-emission regulations, meaning that efforts to further reduce exhaust emissions are likely to be eased for a while after 2010.

With regard to efforts to reduce fuel consumption, Japan has established 2010 fuel efficiency standard with separate requirements for individual vehicle-weight categories. Automakers have announced plans to achieve early compliance with the

requirements for all vehicle-weight categories in the 2005 – 2007 period. Efforts to reduce fuel consumption can be expected to accelerate in the years ahead. Tighter fuel efficiency standard will be adopted in 2015. It is important to note that the focus of efforts to comply with regulations from 2010 is likely to shift from exhaust emissions to fuel consumption. Clean-diesel passenger cars and HEVs are likely to be popularized.

3.2 Future outlook of oil supply

Fig. 9 shows United States Department of Energy predictions for worldwide oil production in 2000. According to these predictions, oil production will peak in about 2030 if a global economic growth rate of 3 %

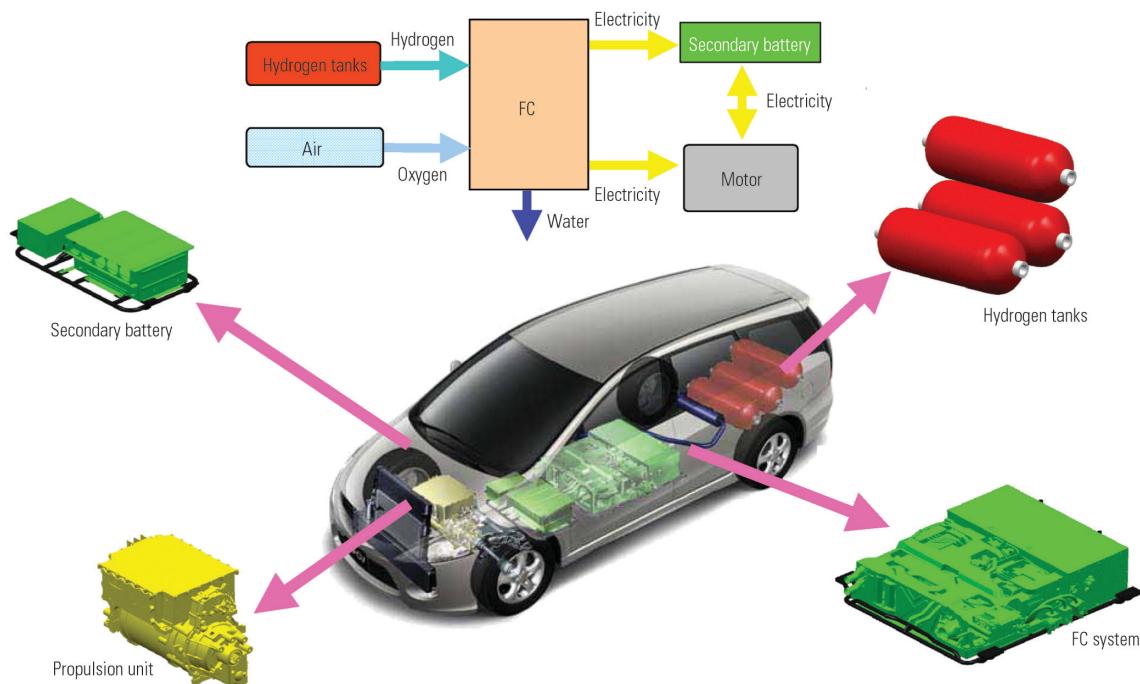


Fig. 6 Basic configuration of FCV

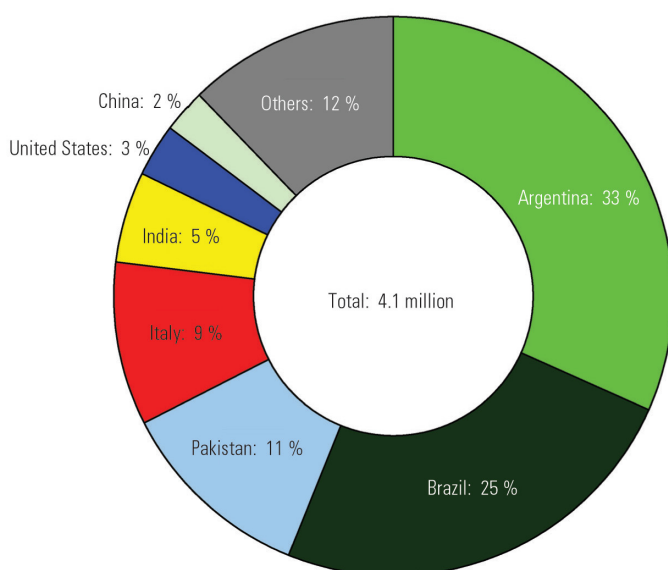


Fig. 7 Proportions of total CNG vehicles by country (As of April 2005)

(roughly equivalent to the 2005 rate of 3.2 %⁽⁶⁾) is sustained and will peak in about 2050 even if the global economic growth rate is only 1 %. As oil production approaches its peak, there is likely to be a sharp increase in oil prices and many restrictions are likely to be applied to the use of oil in the transportation sector. Public pressure for a transition from vehicles that use fossil fuels to those that use renewable energy sources can be expected to grow, so HEVs and other oil-using vehicles will have to be replaced with FCVs and EVs.

3.3 Future development of CEV

Fig. 10 shows broad forecasts for CEV adoption based on the aforementioned circumstances.

Through about 2010, there will likely be a continued effort to reduce the exhaust emissions of gasoline and diesel vehicles and a simultaneous increase in adoption of CNG vehicles; clean-running vehicles (including trucks and buses) will become increasingly prevalent. From about 2010, efforts to further reduce exhaust emissions are likely to be eased and adoption of low-fuel-consumption vehicles can be expected to accelerate, meaning that HEVs and clean-diesel passenger cars will likely be adopted on a scale not seen thus far. From about 2020, the internal-combustion engine will remain the primary propulsion technology. Owing to the approaching peak in oil production, however, high oil prices and increased demand for energy security will accelerate the transition from oil to alternative energy sources; EVs and FCVs, which do not use fossil fuels, will likely be adopted in increasing numbers.

As CEVs penetrate the market in increasing numbers, different types of CEV technology will likely be favored in different vehicle-size categories (Table 4). Among electrically powered vehicles (EVs, FCVs, and HEVs), for example, it is likely that EV technology will, in light of its distinct characteristics (a relatively small number of onboard components owing to the absence of an engine, fuel tank, and transmission; high efficiency at low vehicle speeds; and relatively short range) be adopted for a proportion of minicars and compact cars. Meanwhile, the adoption of HEV or FCV technology involves the addition to a gasoline vehicle of an electric motor, a secondary battery, and an inverter and the incorporation of space-hogging components such as a high-pressure hydrogen tank and, in the case of FCV

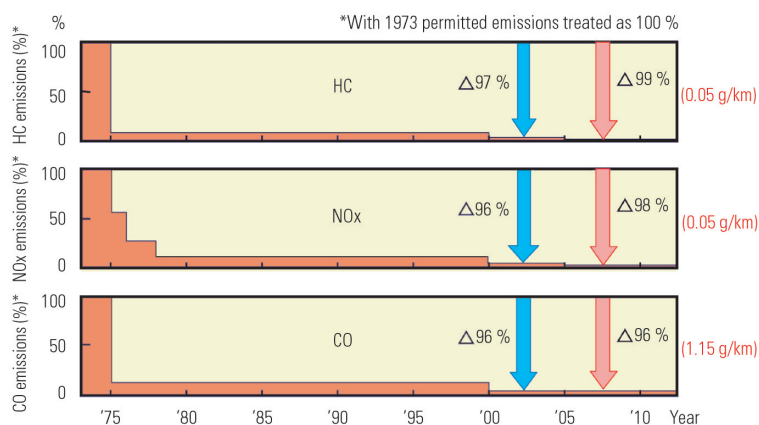


Fig. 8 Circumstance of reduction of emission regulations for gasoline passenger cars in Japan

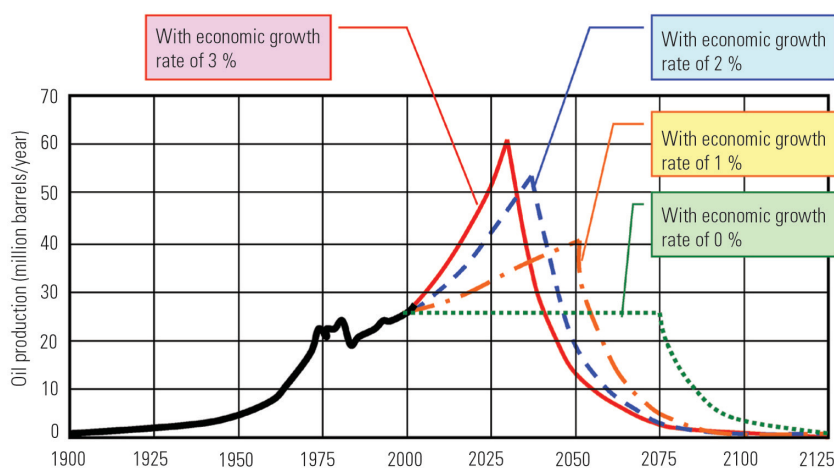


Fig. 9 Predictions for worldwide oil production

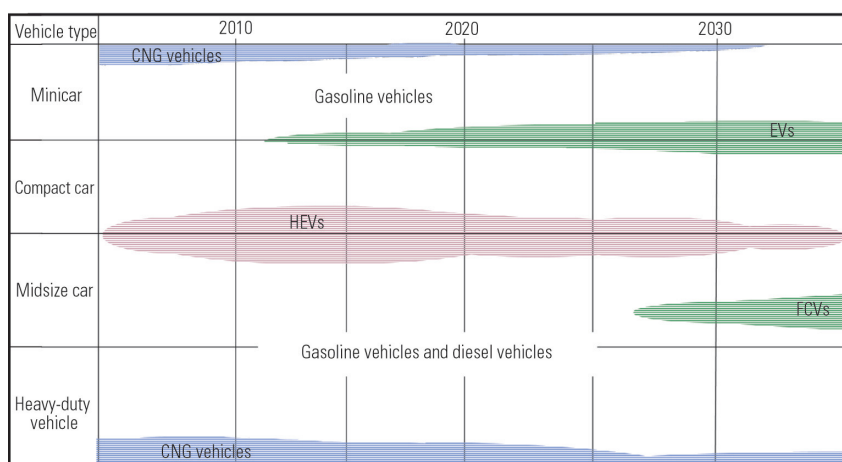


Fig. 10 Forecasts for CEV adoption

technology, an FC stack. Consequently, HEV and FCV technologies will likely be applied to part of compact cars, and midsize or heavy-duty vehicles. **Table 5** summarizes EV and HEV development and sales trends

among automakers. It can be seen here, too, that EV technology is focused on minicars and compact cars and that HEV technology is focused on compact and larger cars. HEV technology has also been applied to certain minicars, but the sales volumes are extremely small.

During the period of growing adoption of HEVs and other low-fuel-consumption vehicles through about 2020, then, it is highly likely that EVs will become prevalent in the minicar and compact-car size categories. And if progress is made in development of smaller, higher-performance batteries and in construction of rapid-charging infrastructure, it is likely that EVs will become prevalent not only in the minicar and compact-car categories but also in the midsize and larger vehicle categories.

Anyway, it is highly likely that EVs will become prevalent mainly in the minicar and compact-car categories from about 2010.

4. Efforts of MMC for LEV

MMC has for many years been working on ways to reduce the exhaust emissions and fuel consumption of gasoline and diesel vehicles, and we have marketed numerous models incorporating the benefits of our efforts. With regard to CEVs, we have marketed CNG vehicles, developed and marketed EVs, developed HEVs, and built prototype FCVs.

Notably, MMC has gained a wealth of technological know-how concerned EV through our development and marketing of EVs over the years. We recognize the importance of making a social contribution by commercializing our proprietary technologies and using them to promote the adoption of EVs.

4.1 MMC's history of EV research and development; and MMC's next-generation EV

Fig. 11 shows history of research and development of EV in MMC. From the 1970s to the mid-1990s, MMC produced previous-generation

EVs with lead-acid batteries and direct-current motors under contract from electric utilities. These previous-generation EVs were far from commercially viable; their ranges were extremely short (60 – 100 km); they

Table 4 Suitability of EV, FCV, and HEV technologies for vehicle size categories

Vehicle type	Attributes	Suitable size category
EV	<ul style="list-style-type: none"> Number of additional onboard parts is small (limited to motor and battery), and engine, fuel tank, and transmission are unnecessary, allowing efficient use of interior space and permitting application to minicar and compact-car categories. Efficiency is higher than that of gasoline vehicles at low speeds but sharply deteriorates at high speeds, making application suitable for low-speed applications. Per-charge driving ranges are short with current technologies, making application suitable for short-distance applications. 	Minicar
		Compact car
HEV/FCV	<ul style="list-style-type: none"> Number of additional onboard parts is large (motor, battery, inverter, etc. are added to gasoline-vehicle configuration), necessitating use of onboard space and thus precluding application to minicar and compact-car categories. HEV technology permits long driving ranges between refueling stops, making application suitable for long-distance applications. 	Midsize cars Heavy-duty vehicles

Table 5 Development and sales trends of major EV and HEV among automakers

Source: Information released by Japan Automobile Research Institute, information released by the automakers, and newspaper items

required long charging periods; the weight of large numbers of onboard secondary batteries detracted from driving performance; and the price of each vehicle was several times that of the base gasoline model.

At the end of the 1990s, MMC began developing next-generation EVs with lithium-ion batteries and high-performance permanent-magnet synchronous motors. A major advantage of the lithium-ion batteries was quick chargeability. In one of the trials conducted by MMC, repeated quick charging enabled a next generation EV to be driven more than 2,000 km in 24 hours. Practical adoption of EVs became a real possibility.

In 2003, MMC began developing a Mitsubishi In-wheel Motor Electric Vehicle (MIEV), which had lithium-ion batteries and in-wheel motors (Fig. 12) as its core technologies. Later, MMC released two experimental EVs with in-wheel motors: the COLT EV in May 2005 and the LANCER EVOLUTION MIEV (Fig. 13) in August 2005. Each of these experimental vehicles has running performance comparable with that of a gasoline vehi-

cle. And the COLT EV has a range of the 150 km, meaning that it is adequately practical for day-to-day short-distance applications such as commuting and shopping. As a further merit, in-wheel motors permit a significantly reduced number of powertrain components, meaning that interior space can be efficiently employed. Consequently, the in-wheel-motor vehicles offer merits that cannot be enjoyed with gasoline vehicles.

MMC has announced a plan to produce and market to the general public a next-generation EV based on the minicar by 2010. In line with this plan, the company is conducting market research, having focus groups perform trial drives, and making preparations for infrastructure construction. These activities will support the future spread of EVs.

4.2 Developments in charging facilities

With the current level of secondary battery technology, the range of EV is about 200 km, meaning that EVs are positioned mainly as a means of mobility over short

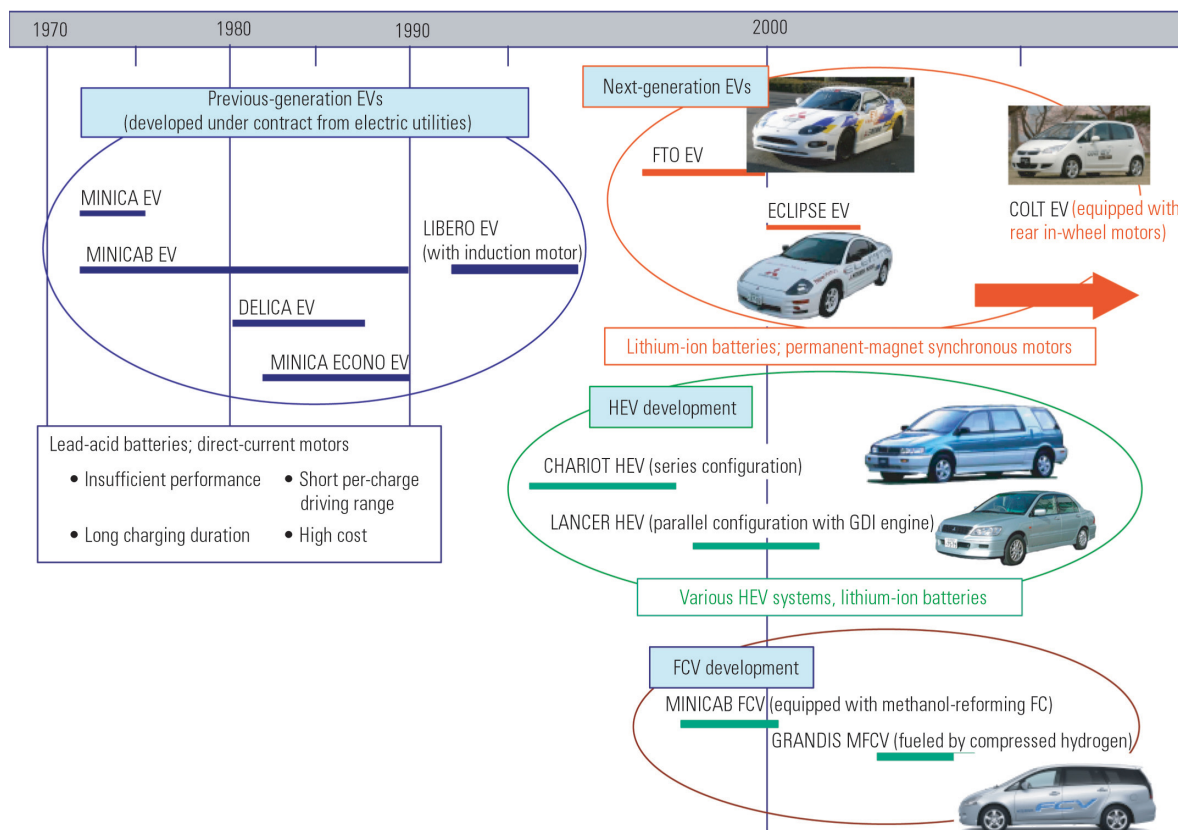
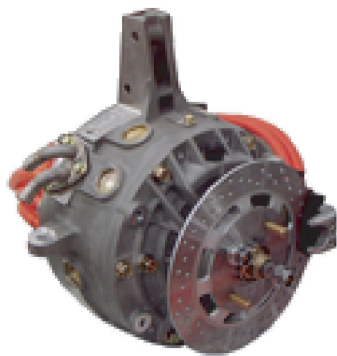


Fig. 11 MMC's history of EV research and development



(a) Inner-rotor in-wheel motor of COLT MIEV



(b) Outer-rotor in-wheel motor of LANCER EVOLUTION MIEV

Fig. 12 In-wheel motors of MIEV experimental vehicles

distances. If quick chargers capable of completing a full charge in 15 – 20 minutes are widely installed for use at highway service areas, convenience stores, supermarkets, public parking lots, and other suitable locations, EVs will become practical for long-distance transportation as well. For EVs to become widespread, therefore, it is essential for EV manufacturers, electric utilities, and businesses in other sectors to form a consortium and work together.

4.3 Possibilities offered by EVs

Owing to their total absence of exhaust emissions, EVs can be used in ways that are not possible with gasoline vehicles and HEVs. For example, EVs can conceivably be brought indoors and used for indoor applications after outdoor operation, used by shoppers as a means of transportation between stores in shopping malls, and taken into areas hit by earthquakes and other natural disasters and used as mobile emergency power supplies. It is essential to promote EV market creation by making the motoring public aware of such



(a) COLT EV



(b) LANCER EVOLUTION MIEV

Fig. 13 MMC's MIEV next-generation experimental EVs

unique possibilities.

5. Summary

It is not easy to accurately predict the types of LEVs that will be accepted and adopted by society over the long term. However, the need to reduce exhaust emissions, the need to reduce fuel consumption, and the need to make a transition away from fossil fuels are inescapable; it is possible to confidently predict that LEVs meeting these needs will be adopted to suit size requirements and user applications.

MMC is committed to environmental preservation in addition to working in line with our core philosophy of providing our customers with driving pleasure and safety. With the MIEVs embodying our flagship technologies, we are working to turn EVs into a market reality. With a keen eye on social trends, we intend to take a broad-ranging approach that encompasses efforts to promote the construction of charging infrastructure and simultaneous efforts to create an EV market.

References

- (1) Outline of measures to combat global warming (19 March 2002 edition), Japanese government task force on measures to combat global warming, pp. 73, 2002
- (2) Rapid Global Warming in the 20th Century: The Crisis Has Already Begun, Japan Center for Climate Change Actions, p. 3, 2001
- (3) Kyoto Target Achievement Plan (28 April 2005 edition and later), Japanese government task force on measures to combat global warming, p. 13, 2005
- (4) Green automobile taxation (measures for 2006), Japanese Ministry of Land, Infrastructure, and Transport website (Road Transport Bureau section on tax system: <http://www.mlit.go.jp/jidosha/roadtransport.html>), p. 3, 2005
- (5) Information on regional measures to combat global warming (project code: P01049), New Energy and Industrial Technology Development Organization website (<http://www.nedo.go.jp>), 2005
- (6) Report on 2005 global economic outlook, spring 2005, website of Cabinet Office, Government of Japan (http://www5.cao.go.jp/j-j/sekai_chouryuu/index.html), 2005



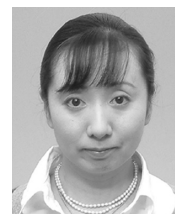
Eizo TABO



Takashi YOSHINA



Yasufumi SEKINE



Reiko SAITO

Left-Right Torque Vectoring Technology as the Core of Super All Wheel Control (S-AWC)

Kaoru SAWASE* Yuichi USHIRODA* Takami MIURA*

Abstract

The Super All Wheel Control (S-AWC) system is an integrated vehicle dynamics control system that maximally exploits the capability of all four tires in a balanced manner to realize predictable handling and high marginal performance. A direct yaw moment control technology that effects left-right torque vectoring (this technology forms the core of S-AWC system) can control cornering maneuvers as desired during acceleration, steady-state driving, and deceleration. Various left-right torque vectoring mechanisms have been proposed for the direct yaw moment control technology. These mechanisms are identical in terms of theoretical efficiency, but each has distinct characteristics owing to the employed elemental technology. It is conceivable that various left-right torque vectoring systems will emerge as various elemental technologies are improved.

Key words: Torque Split, Four Wheel Drive (4WD), Vehicle Dynamics, Integrated Control

1. Introduction

All Wheel Control (AWC) is a Mitsubishi Motors Corporation (MMC) four-wheel dynamic control philosophy for maximally exploiting the capability of all four tires of a vehicle in a balanced manner to realize predictable handling and high marginal performance, which in turn yield the driving pleasure and utmost safety that MMC sees as fundamental in producing vehicles. As shown in Fig. 1, the AWC philosophy is put into practice by means of three forms of control.

The first form of control is control over the four tires' vertical loading, by means of which each tire is kept in firm contact with the road surface for consistently maximal grip. The vehicle's basic specifications and its body and suspension technologies are exploited for this purpose.

The second form of control is control over the four tires' slip ratios and slip angles (control that is effected over the respective slip ratios and slip angles of the four tires such that the longitudinal force and lateral force produced by each of the four tires are maximized in a balanced manner). An Anti-lock Braking System (ABS), a Traction Control (TCL) system, and steering-system control technologies are exploited for this purpose.

The third form of control is control over the four tires' force assignment (control that is effected over the distribution of longitudinal forces and lateral forces among the four tires such that the tires are uniformly loaded for well-balanced utilization). Powertrain and braking-system control technologies are exploited for this purpose.

In line with this development philosophy, MMC in 1987 equipped the Mitsubishi GALANT with a center-differential-type full-time four-wheel drive (4WD) system (this system incorporated a viscous coupling unit),

a four-wheel steering system, four-wheel independent suspension, and a four-wheel ABS (these systems were highly advanced for the time), thereby dramatically improving dynamic performance⁽¹⁾. MMC has since realized various other technologies including a trace-control function that controls engine output for stable cornering⁽²⁾ and an electronically controlled center-differential-type full-time 4WD system that controls the front/rear torque distribution for heightened traction performance and cornering performance⁽³⁾.

Notably, in 1996 MMC led the industry by equipping the world's first production vehicle with an Active Yaw

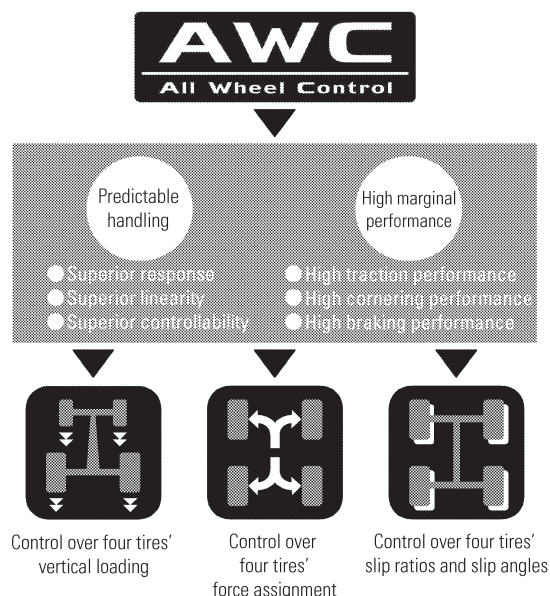


Fig. 1 AWC philosophy

* Drivetrain Engineering Dept., Development Engineering Office

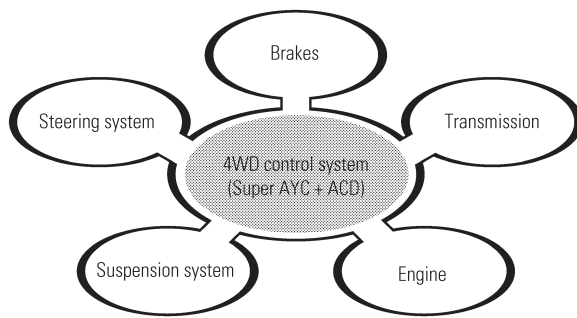


Fig. 2 S-AWC concept

Control (AYC) system that controlled the vehicle's yaw moment by vectoring torque between the left and right wheels in accordance with a totally new concept. Thanks to the appearance of this technology, it became possible for the first time for the load distribution among a vehicle's four tires to be controlled during all vehicle operation. As a result, cornering could be controlled as desired⁽⁴⁾. Since then, MMC has continuously worked on to turn the AWC philosophy into reality by refining and evolving AYC hardware and software and by developing integrated control arrangements that control not only the AYC system but also a center differential, an ABS, and other items. The ultimate embodiment of the AWC philosophy is the S-AWC system, a 4WD-based integrated vehicle dynamics control system that MMC unveiled in the Mitsubishi Concept-X vehicle at the 2005 Tokyo Motor Show. As with earlier embodiments of the AWC philosophy, AYC plays a central role in this system.

Left-right torque vectoring technologies exemplified by MMC's AYC systems are, owing to flexibility they realize in cornering control, a focus of great interest in Europe and North America. In recent years, various left-right torque vectoring mechanisms providing the same function as MMC's AYC systems have been proposed⁽⁵⁾⁽⁶⁾. Most of these mechanisms are based on an arrangement in which a differential is combined with planetary gears and two or more clutches or brakes. Their operation and distinct characteristics are difficult to intuitively ascertain.

The remainder of this paper, then, gives an overview of the S-AWC system and describes the benefits of the direct yaw moment control yielded by this system's left-right torque vectoring technology. It also describes, using the velocity diagram method⁽⁷⁾ (a method used in analysis of the shift control of automatic transmissions), the respective characteristics of various mechanisms that realize left-right torque vectoring. Plus, it discusses possible future developments.

2. The S-AWC system

Various vehicle dynamics control technologies have been developed since the 1980s. From the viewpoint of active safety (safety that it intended to reduce the likelihood of accidents), the main purpose of these technologies has been to stabilize the vehicle by erecting func-

tional barriers that make it difficult for the vehicle to exceed its performance limits. Control over the braking system has been used as the primary means of advancing the practical implementation of the system. In relatively recent years, arrangements have emerged in which control over the braking system is supplemented by control over the steering system for seamless enhancement of driving stability from normal driving conditions right up to the vehicle's performance limits.

Unfortunately, placing the braking system at the heart of integrated control creates a conflict with the driver's desire to exploit the vehicle's running capability (one of the three fundamental vehicle capabilities, the others of which are turning and stopping). Such an arrangement thus represents a handicap with respect to driving pleasure.

On the other hand, a 4WD system offers certain major advantages as the basis of a dynamics control arrangement. By transmitting torque to all four wheels, a 4WD system gives better running stability than a two-wheel drive system. And if a 4WD system's distribution of torque to the wheels is appropriately controlled, enhancement of cornering performance is possible. Notably, cornering control effected by means of a 4WD system brings great merits. It does not conflict with the driver's acceleration and deceleration operations, meaning that it can be exploited not only near the vehicle's performance limits but also in normal driving conditions.

Consequently, MMC focused on the aforementioned merits of 4WD-based control in development of its AYC systems and in development of an Active Center Differential (ACD)⁽⁸⁾. As shown in Fig. 2, MMC used 4WD control as the core of the S-AWC integrated vehicle dynamics control system.

Fig. 3 shows the configuration of the S-AWC system in the Mitsubishi Concept-X. This system is based on 4WD control effected by a combination of a Super AYC system and an ACD. It also incorporates an Active Brake Control system, an Active Steering System, and a Roll Control Suspension system. Integrated control of all system elements ensures that the vehicle gives predictable handling and high marginal performance even when it is operating near its performance limits and with all four tires slipping.

3. Direct yaw moment control yielded by left-right torque vectoring

When control over the distribution of torque to a vehicle's four wheels is considered, the typical approach is to focus on the proportions of torque to be transmitted to the respective wheels and then work out a mechanism and control logic to realize those proportions. With this approach, however, decreases in engine torque (including engine braking force) toward zero are accompanied by decreases toward zero in the potential for control over the vehicle's dynamics. And during constant-speed driving, no control effect can be obtained. Further, appropriate distribution of torque when the engine torque is high requires an unduly large

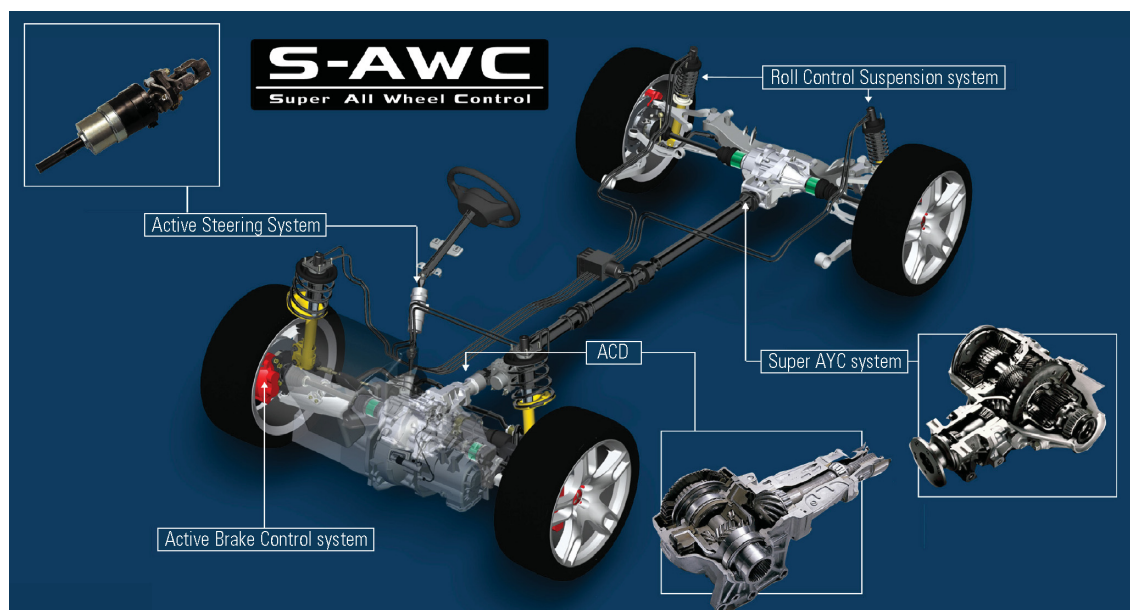


Fig. 3 S-AWC system configuration

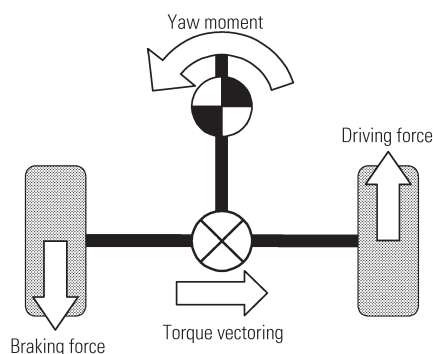


Fig. 4 Left-right torque vectoring concept

mechanism since the torque designated as a control object is large.

In light of the aforementioned factors, MMC realized that the ideal mechanism to enable cornering to be controlled as desired was one capable of controlling the yaw moment (in other words, a mechanism capable of controlling torque differences between wheels, not one that controlled the torque distribution). Based on this realization, MMC devised the concept of left-right torque vectoring and put the concept into practice with an AYC differential.

As shown in Fig. 4, the left-right torque vectoring concept involves vectoring torque between the left and right wheels such that braking force is generated on one side and driving force of the same magnitude is generated on the other. Consequently, it is possible to directly control the yaw moment as desired at any time without the control being dependent upon the level of engine torque and without their being any conflict between the control and the driver's acceleration and deceleration operations.

When left-right torque vectoring is implemented on the rear wheels of a 4WD vehicle, it yields two main benefits. One is enhancement of cornering performance by means of tire load equalization between the left and right rear wheels. The other is enhancement of cornering performance by means of tire load equalization between the front and rear wheels as a result of direct yaw moment control.

An example of tire load equalization between the left and right rear wheels is shown in Fig. 5. While the vehicle is cornering, a load vectoring between the left and right wheels causes the loading on the cornering inside tire to decrease and the loading on the cornering outside tire to increase. Thus, a difference is created between the left and right wheels in terms of capacity to vector force to the road surface. At the same time, however, the differential mechanism located between the left and right wheels' respective drive shafts distributes torque uniformly (discounting the effects of transient conditions and mechanism friction) to the left and right wheels. If the torque increases, therefore, the cornering inside tire, whose capability has decreased, reaches its grip limit and starts to slip, meaning that no further improvement in dynamic performance can be obtained (Fig. 5 (a)). By controlling the torque transmitted to the left and right wheels such that it is optimally apportioned, it is possible to increase the load margin relative to the tire capability, thereby improving cornering performance (Fig. 5 (b)). Fig. 6 shows the results of a simulation conducted for verification of the rear cornering force margin relative to the torque difference between the left and right rear wheels. As the left-right torque difference increases, the cornering force margin increases up to a certain point. Any excessive torque vectoring reduces the benefit. As shown, however, the slope is extremely gentle in the vicinity of the optimal

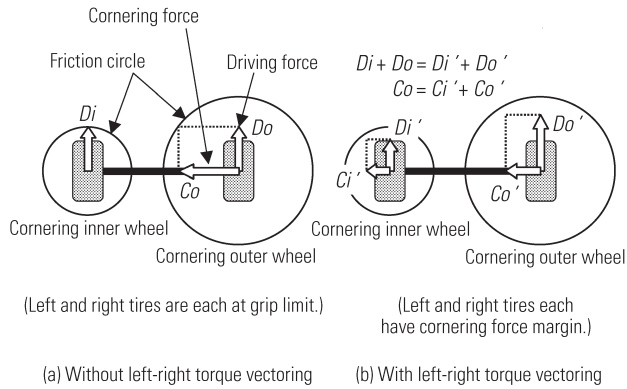


Fig. 5 Tire load equalization between left and right rear wheels

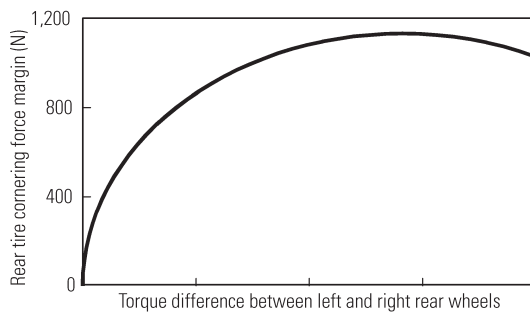


Fig. 6 Cornering force margin of rear tire

value, meaning that an ample benefit can be obtained even if the optimal value is not determined with strict precision.

An example of tire load equalization between the front and rear wheels is shown in **Fig. 7**. **Fig. 7 (a)** indicates understeer where further cornering is not possible. Here, the capability of the front tire is being maximally employed but there is a margin of capability in the rear tire. If the cornering force of only the rear wheel were increased, the moment (yaw moment) balance about the center of gravity would break down such that cornering could not be continued. Notwithstanding the margin in the rear tire, therefore, the capability of the rear tire cannot be more greatly exploited. By imposing a yaw moment by means of a left-right torque vectoring, it is possible to increase the cornering force of the rear tire and reduce the cornering force of the front tire by the same magnitude with no breakdown in the moment balance about the center of gravity such that the load margin of the front tire is increased and cornering performance is improved (**Fig. 7 (b)**). **Fig. 8** shows the results of a simulation conducted for verification of the front tire cornering force margin relative to the torque difference between the left and right rear wheels. As shown, increases in the left-right torque difference are accompanied by increases in the front tire cornering force margin.

From the aforementioned points, it can be seen that

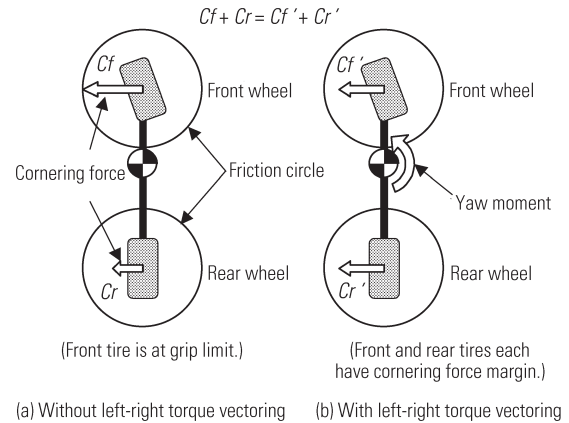


Fig. 7 Tire load equalization between front and rear wheels

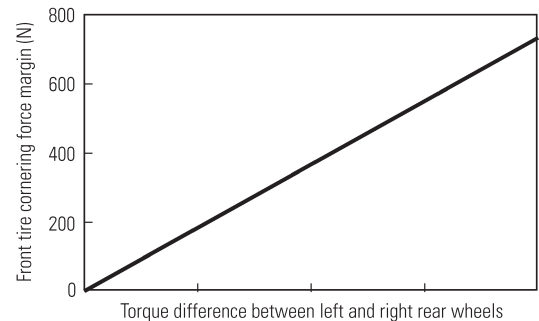


Fig. 8 Cornering force margin of front tire

increasing the left-right torque difference between the rear wheels causes the respective cornering force margins of the front and rear wheels to increase up to a certain point such that the vehicle's cornering performance improves. It can also be seen that increases in the yaw moment yielded by the left-right torque difference between the rear wheels are accompanied by increases in the front tire cornering force margin such that the vehicle's turnability improves. The benefits can be obtained not only during acceleration but also during steady-state driving and during deceleration.

To maximize the benefits, a torque vectoring mechanism such as the AYC differential (a mechanism capable of controlling the left-right torque difference regardless of whether the vehicle is accelerating, moving at a constant speed, or decelerating) is clearly desirable.

4. Analysis of torque vectoring mechanism

The AYC differential and other torque vectoring mechanisms are combinations of multiple gears and clutches, so their operation and distinct characteristics are difficult to understand. MMC employs the velocity diagram method as before, which is also used for analysis of the shift mechanisms of automatic transmissions, as an effective analysis tool for visually ascertaining the operation of such complex mechanisms. With the

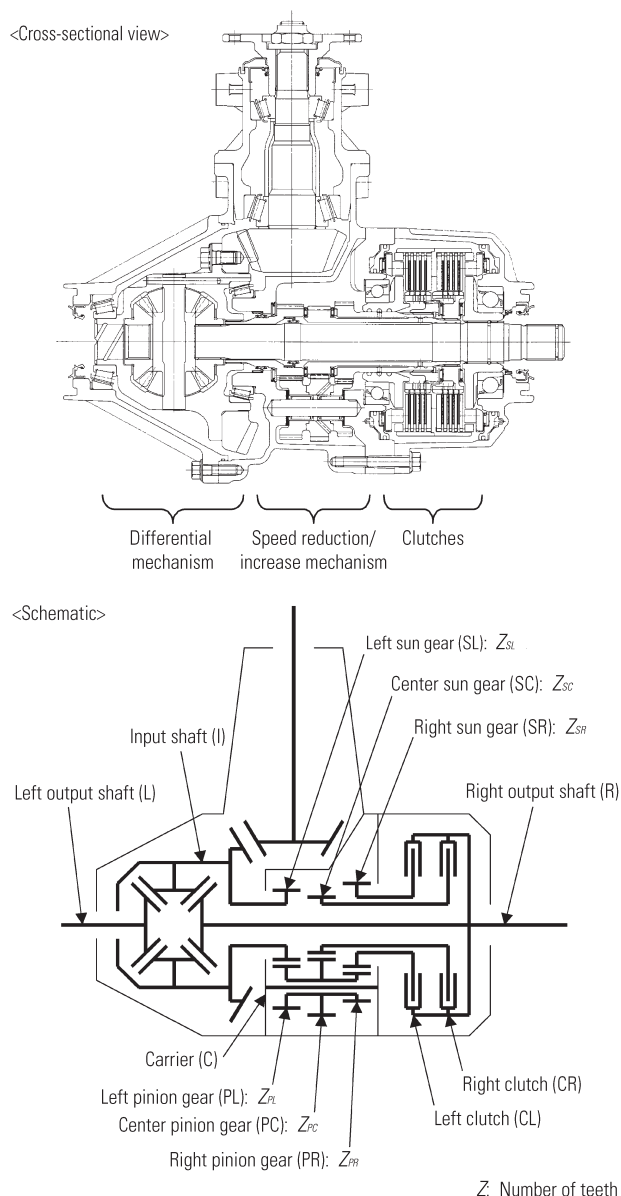


Fig. 9 Structure of AYC differential

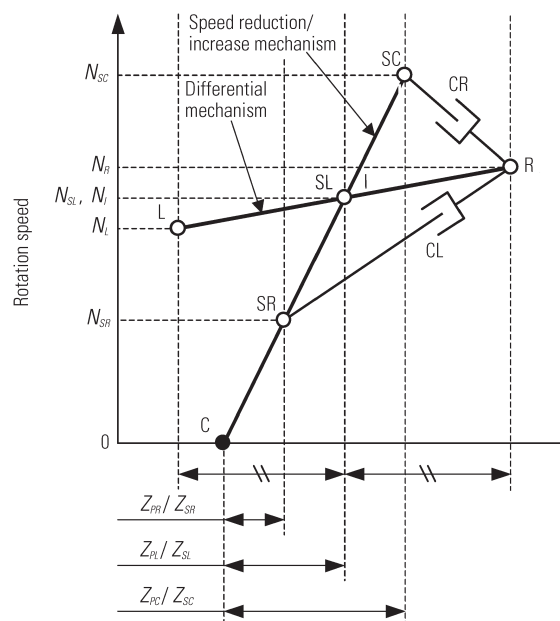


Fig. 10 Velocity diagram of AYC differential

or downward in accordance with their respective rotation conditions. They retain their straight-line relationship. Note that the diagram corresponds to leftward cornering. The speed reduction/increase mechanism consists of three sun gears, three pinion gears (these turn as one body), and a carrier C, which holds the sun gears and pinion gears. The carrier C is held in position, so the speed reduction/increase mechanism has four elements and one degree of freedom. In light of the relationships between the gear ratios, the diagram shows the right sun gear SR, left sun gear SL, and center sun gear SC positioned in that order from left to right along the straight line that begins at the carrier C. The two gear mechanisms (the differential mechanism and speed reduction/increase mechanism) are linked by the differential mechanism's input shaft I and the speed reduction/increase mechanism's left sun gear SL. The left clutch CL is located between the differential mechanism's right output shaft R and the speed reduction/increase mechanism's right sun gear SR. The right clutch CR is located between the differential mechanism's right output shaft R and the speed reduction/increase mechanism's center sun gear SC.

The clutch elements each transmit torque from the faster-turning side to the slower-turning side. In the situation shown in Fig. 10, with the right clutch CR engaged, torque is transmitted from the center sun gear SC to the right output shaft R such that the torque at the right output shaft is increased. With the left clutch CL engaged, conversely, torque is transmitted from the right output shaft R to the right sun gear SR such that torque at the right output shaft R decreases. It can be seen, then, that if the rotation speed of the right output shaft R is between that of the center sun gear SC and that of the right sun gear SR, torque vectoring is possible toward either side (left or right). With the AYC differential, then, the driving conditions in which torque

velocity diagram method, a single gear set is represented by a single straight line; the rotation speed of each rotating element positioned on a straight line can be visually ascertained. In the text hereafter, expansion of this technique for application to a left-right torque vectoring mechanism is explained with reference to the AYC differential.

The AYC differential consists of a differential mechanism, a speed reduction/increase mechanism, and two clutches (Fig. 9). The differential mechanism has three elements and two degrees of freedom. In the velocity diagram in Fig. 10, the AYC differential is represented by the straight line that has the input shaft I positioned in the middle and the left output shaft L and right output shaft R equidistantly positioned on the respective sides. The vertical axis of the diagram indicates rotation speeds, and the relative positions (higher or lower) of items in the lateral axis indicate opposite directions of rotation. The elements can each move only upward

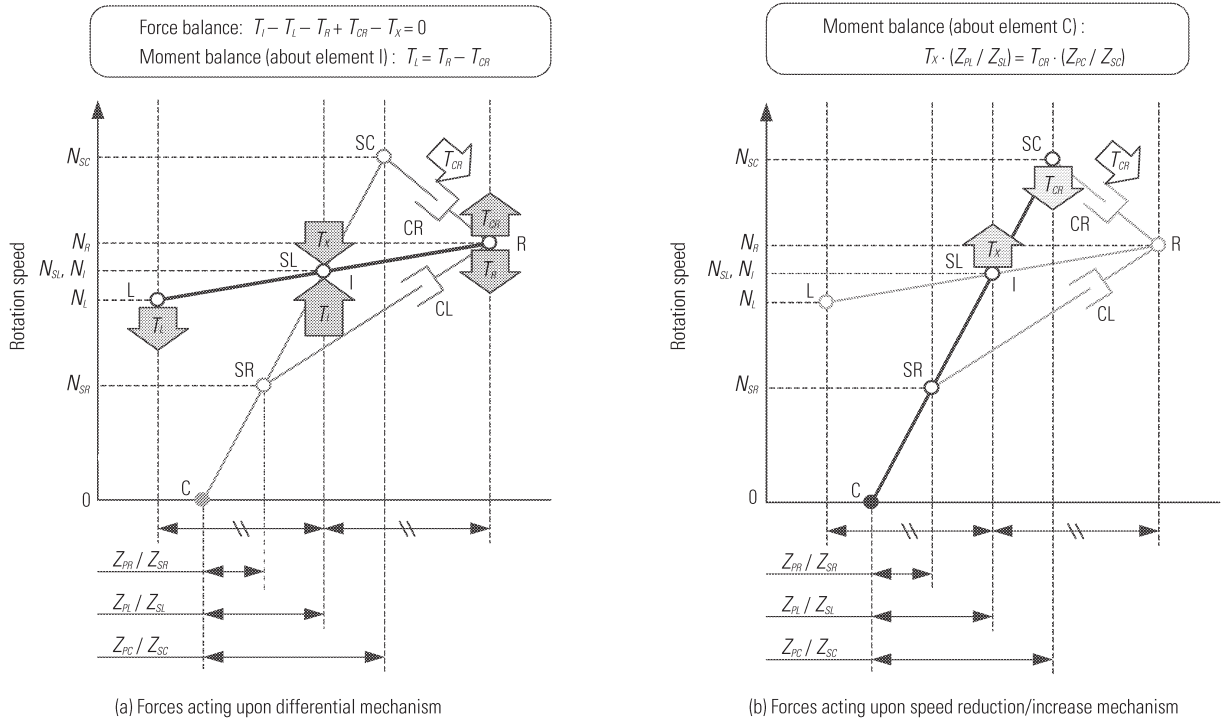


Fig. 11 Force balance during torque vectoring

vectoring is possible are determined by the respective rotation speeds of the center sun gear SC and right sun gear SR, making the gear ratio settings of the speed reduction/increase mechanism crucial with respect to the AYC differential's performance.

The text hereafter describes the torque acting upon each element during torque vectoring. With the velocity diagram method, the straight line corresponding to a gear set is treated as a single lever and the torque at each element is expressed as a vertically acting force(s). It is possible to deduce the torque at each element from the balance of the upward and/or downward direction(s) of the force(s) acting on each element and the balance of moments. By way of example, engage the right clutch CR in a torque vectoring from the left output shaft L to the right output shaft R in a situation where torque T_I is being applied to the differential mechanism's input shaft I (Fig. 11). The torque transmitted by the right clutch CR (this torque is designated T_{CR}) acts upon the right output shaft R in the direction that increases the speed of rotation (upward in the diagram) and upon the center sun gear SC in the direction that reduces the speed of rotation (downward in the diagram). In the speed reduction/increase mechanism, torque T_{CR} acting upon the center sun gear SC is opposed by torque T_X , which acts upon the left sun gear SL such that the moments about the C element balance. Since the left sun gear SL is linked to the differential mechanism's input shaft I, the reaction force caused by T_X acts upon the differential mechanism's input shaft I. At this time, the reaction forces acting upon the left and right output shafts L and R (in other words, the left and right shafts' respective torques T_L and T_R) can be deduced from the balance of forces in

the differential mechanism and the balance of moments as follows.

$$T_L = T_I / 2 - (Z_{PC} / Z_{SC}) / (Z_{PL} / Z_{SL}) / 2 \cdot T_{CR}$$

$$T_R = T_I / 2 - (Z_{PC} / Z_{SC}) / (Z_{PL} / Z_{SL}) / 2 \cdot T_{CR} + T_{CR}$$

where

Z : Number of gear teeth

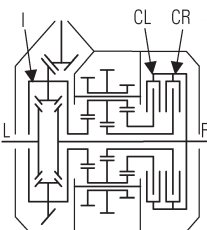
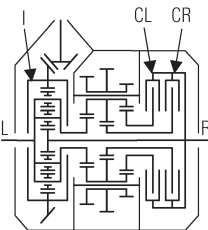
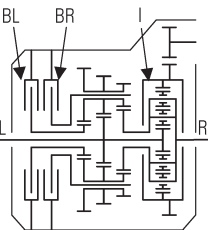
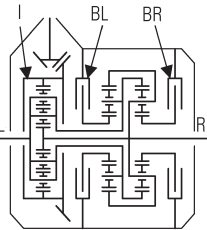
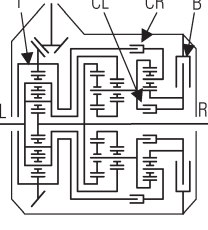
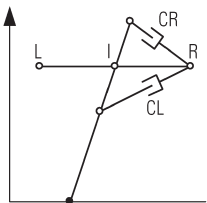
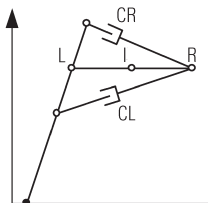
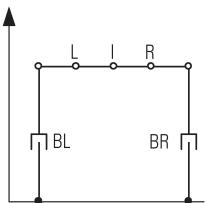
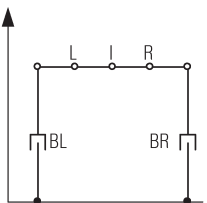
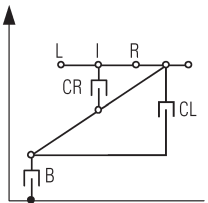
In this way, the velocity diagram method enables the respective rotation speeds of individual elements to be visually ascertained and facilitates deduction of the relationships between the acting torques. Since the velocity diagram method gives a straight-line representation of a gear set, it is possible for gear sets with different structures to be represented in the same way as each other. Once a given mechanism has been expressed in the form of a velocity diagram, therefore, it is easy to find structural variations. It can be seen, then, that the velocity diagram method can be applied not only to shift analysis with automatic transmissions but also to analysis of complex torque distribution mechanisms. Plus, the velocity diagram method is a valuable tool for devising new structures.

5. Distinct characteristics of various torque vectoring systems

The respective characteristics of the AYC differential and other torque vectoring systems that have the same type of functionality are shown in the form of velocity diagrams in Table 1. ② in Table 1 is the Super AYC as the core of the S-AWC.

Assuming (a) the driving conditions in which torque

Table 1 Comparison of various left-right torque vectoring systems

System	① MITSUBISHI AYC	② MITSUBISHI Super AYC ⁽⁹⁾	③ HONDA ATTS ⁽¹⁰⁾	④ MAGNA MDT-II ⁽⁵⁾	⑤ RICARDO Torque Vectoring Differential ⁽⁶⁾
Schematic	 <p>CL: Controlled for torque vectoring to left shaft CR: Controlled for torque vectoring to right shaft</p>	 <p>CL: Controlled for torque vectoring to left shaft CR: Controlled for torque vectoring to right shaft</p>	 <p>BL: Controlled for torque vectoring to right shaft BR: Controlled for torque vectoring to left shaft</p>	 <p>BL: Controlled for torque vectoring to right shaft BR: Controlled for torque vectoring to left shaft</p>	 <p>CL: Engaged for torque vectoring to left shaft CR: Engaged for torque vectoring to right shaft B: Controls vectored torque</p>
Velocity diagram					
Clutch capacity	Large	Medium	Small	Small	Small
Clutch speed difference	Small	Medium	Large	Large	Large
Energy losses	Small	Small	Small	Small	Small
Controllability	High	High	Middle	Middle	Low

vectoring is possible are the same for all of the systems and (b) the magnitude of the creatable left-right torque difference is the same for all of the systems, the energy losses resulting from torque vectoring are the same with all of the systems. In other words, the theoretical system efficiency is the same for all torque vectoring mechanisms that use clutches or brakes regardless of structure; the merits and demerits of each system in practice are determined by the effects of the elemental technology whose employment is dictated by the structure.

An illustration: The AYC differential requires greater clutch capacity than the other systems shown in **Table 1**, but it also has merits. The differences in rotation speeds in its clutches are the smallest, meaning that its clutch clearances can be made small for superior control response without creating any cause for concern about clutch drag. With systems that use brakes (for example, systems ③, ④, and ⑤ in **Table 1**), on the other hand, it is possible to make the brake capacity small and the physical dimensions concomitantly compact but a number of measures to enhance the elemental technologies are needed. For example, large differences in speeds of rotation necessitate measures to prevent drag, and enhancements in control precision are needed to enable large left-right torque differences with small control inputs.

Even though they have the same theoretical efficiency, then, systems that use clutches and systems that use brakes each have distinct merits and demerits. As the

elemental technologies are refined, various systems are likely to be implemented.

If advances are made in efficiency improvements and cost reductions with new elemental technologies, left-right torque vectoring systems employing electric motors or hydraulic pumps (rather than clutches or brakes) as actuators may emerge. Notably, a system employing an electric motor would offer advantages in terms of controllability and efficiency since it could use a single electric motor to effect left-right torque vectoring and to lock the left and right drive shafts together. A number of basic structures have already been proposed. Provided electric vehicles and hybrid electric vehicles become more widespread, higher power supply voltages are adopted, and inverters are made more compact and less costly, the day when an electric-motor-based torque vectoring system is realized may not be far away.

6. Summary

Using AYC left-right torque vectoring technology, MMC added high cornering control potential to 4WD control. By doing so, MMC heightened vehicle dynamics control from a dimension in which 4WD gave a good balance of traction performance and cornering performance to a dimension in which cornering performance and turnability are vastly enhanced. The technology forms the core of the S-AWC system – an integrated vehicle dynamics control system that offers a superla-

tive drive.

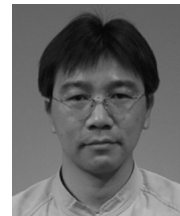
Although various similar technologies are likely to be implemented, MMC intends to continue basing its efforts on AYC, supplementing its extensive know-how with new ideas in pursuit of ever-higher levels of driving pleasure and utmost safety.

References

- (1) Yoshida et al: New Technologies for Advanced Mobility – Future Prospect on Control Technologies of Vehicle Dynamics, Mitsubishi Motors Technical Review, No. 1 (Japanese version), 1988
- (2) Isoda et al: Mitsubishi Traction Control (TCL) and Integrated Chassis Control, Mitsubishi Motors Technical Review, No. 3, 1990
- (3) Sawase et al: Development of 4WD with Integrated Torque Control, Journal of JSAE, Vol. 46, No. 10, pp. 7 – 13, 1992
- (4) Sawase et al: Active Yaw Control Employing Driving Force and Braking Force, JSAE symposium proceedings, No. 9702, 9730894
- (5) Mohan: Torque Vectoring Systems: Architecture, Stability Performance and Efficiency Considerations, 6th All-Wheel Drive Congress Graz, 2005
- (6) Weals et al: SUV Demonstration of a Torque Vectoring Driveline and New Concepts for Practical Actuation Technologies, JSAE Annual Congress, No. 38-05 194, 2005
- (7) Nagayoshi et al: Dynamic Analysis of Automatic Transmission during Gear Shifting through Velocity Diagram on Planetary Gears, Mitsubishi Motors Technical Review, No. 1, 1988
- (8) Sawase et al: Development of Center-Differential Control System for High-Performance Four-Wheel-Drive Vehicles, Mitsubishi Motors Technical Review, No. 13, 2001
- (9) Takahashi et al: Enhancement of Performance of Active Yaw Control System, JSAE SYMPOSIUM, No. 10-03, 2003
- (10) Shibahata et al: Development of Left-Right Torque Distribution System, HONDA R&D Technical Review, Vol. 9, 1997



Kaoru SAWASE



Yuichi USHIRODA



Takami MIURA

Dynamic Scheduling Control for Engine and Gearshifts: Consolidation of Fuel-Economy Optimization and Reserve Power

Kazuhide TOGAI* Miki KOSO**

Abstract

If the power needed for vehicle propulsion is determined, the most fuel-efficient operating point during steady-state driving operation can be determined with complete certainty and in using a continuously variable transmission (CVT), the optimal operating point can be obtained over a wide operating range. During the on-road operation, however, power requirements continuously fluctuate, meaning that the power control system must continuously track and accommodate the changes. Further the power settings matched to the road environment and to the driver's acceleration demands are needed. In setting of the target operating point for the optimal fuel efficiency, the CVT's transmission efficiency is considered in addition to the engine's fuel consumption rate. And since the target operating point varies greatly within short periods of time, dynamic torque and gear ratio trajectory generation that take torque-generation response and shift response into account is also performed. The concept of the reserve power was adopted, and an algorithm was created for changing the operating point from the point of optimal fuel efficiency in accordance with changes in the road environment and to accommodate any preference for sporty driving on the part of the user. By means of the created algorithm, it became possible to consolidate fuel-efficiency enhancement with acceleration enhancement matched to driver behavior.

Key words: CVT, Shift Control, Dynamic Scheduling, Fuel Efficiency, INVECS

1. Introduction

Mitsubishi Motors Corporation (MMC) uses the name "INVECS" for its adaptive shift control technology. It employed INVECS for the first time in 1992 in a GALANT with a four-speed automatic transmission. It subsequently employed an INVECS II arrangement in 1994 in an FTO that had a four-speed automatic transmission with a sports mode and in 1995 in a second-generation DIAMANTE with a five-speed automatic transmission. In 2000, MMC employed its first ever CVT in the LANCER and equipped the CVT with adaptive shift control in the form of an INVECS III arrangement (**Fig. 1**)^{(1) - (3)}. Demand for improvements in fuel economy and ride comfort continue to grow. A number of papers have been published on operational control for minimization of fuel consumption⁽⁴⁾. MMC applied such control in the 2003 and later COLT. In the algorithm for real-time minimization of fuel consumption, the engine, transmission, and human system are interrelated. The reason why such integrated control is difficult to achieve and the technologies used to overcome the difficulty are presented in this paper.

2. Predictive evaluation and minimization of urban-cycle fuel consumption

There are two methods for predicting fuel consumption. One method involves calculation of engine loading from running resistance and prediction of fuel consumption from the engine loading. The other method involves actual simulation of urban-cycle operation.

2.1 Inverse operation from running resistance

The inverse operation from running resistance is a handy method for initial fuel-consumption prediction. The required vehicle power is determined from the vehicle acceleration needed to track the subject vehicle's running resistance and urban-cycle operation (**Fig. 2**). It is taken into account, together with the gear ratio and the transmission's transmission efficiency, in determination of the engine power and engine operating point. Fuel consumption rates (g/kWh) measured during bench test operation can thus be used. Addition thereof enables the fuel consumption to be determined, but the gear ratio must be established. With a transmission that has fixed gear ratios, it is possible to select the gear ratio based on the point of minimal fuel consumption, making it possible to formularize the computation as an optimization problem without a large number of calculations. With this computation, however, dynamic

* Advanced Powertrain Development Dept., Development Engineering Office

** Chassis & Power Train System Designing Department, Office of Development & Engineering, Mitsubishi Automotive Engineering Co., Ltd

Type	Year (model)	TM	Main function
INVECS I	1992 (GALANT)	4 A/T	· Fuzzy ruled shift control
INVECS II	1994 (FTO)	4 A/T	· Sports (manual) mode
	1995 (DIAMANTE)	5 A/T	· Neural network shift control
INVECS III	2000 (LANCER)	CVT	· Learning control
			· Sports (manual) mode
			· Neural network shift control
			· Learning control



INVECS I (GALANT)



INVECS II (FTO)



INVECS II (DIAMANTE)



INVECS III (LANCER)

Fig. 1 Application of INVECS on the market

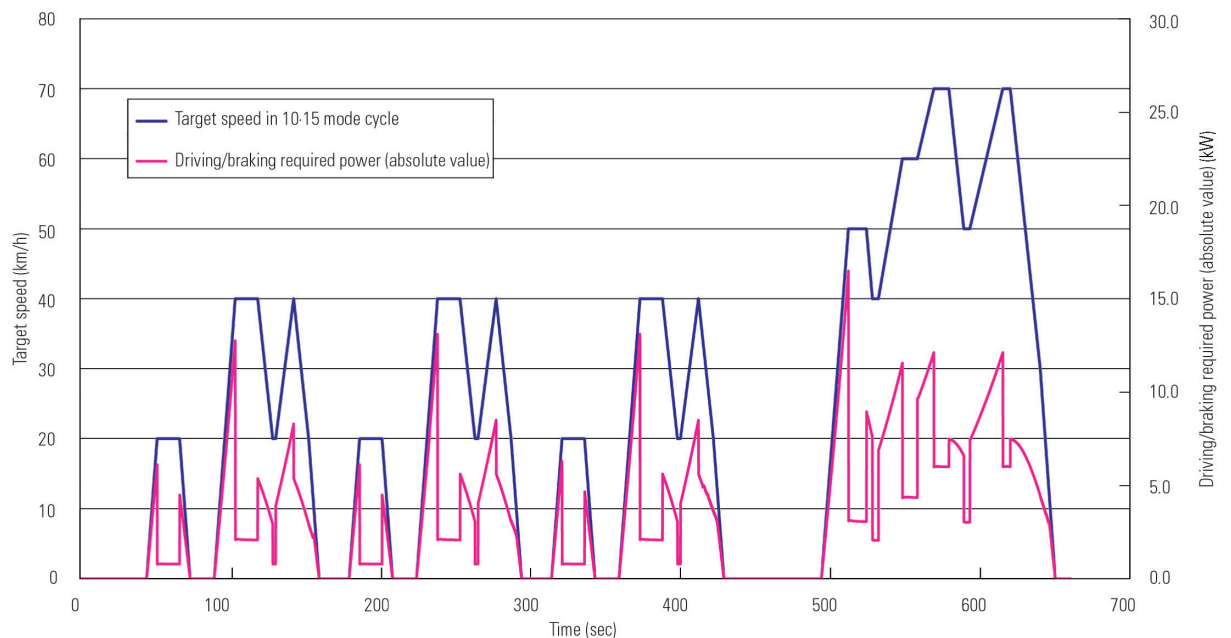


Fig. 2 Target speed and driving/braking required power in 10-15 mode cycle

gearshifts are not taken into account and the synchronizer (with a manual or automated manual transmission) and clutch engagement processes are not included. Also, losses incurred during non-lockup operation of the torque converter (with an automatic transmission or CVT) are not included. Owing to the complexity of the computation, it is not expedient to include them.

2.2 Operation simulation using virtual driving

A driver, an engine, a transmission, a vehicle, and a controller are composed as a simulator, and target speed tracking operation is performed on the simulator. With the Japanese 10-15 mode cycle, legislation requires that the actual speed must be within ± 2 km/h of the target. Making the computation time increments

small causes the computation to take considerable time. But since driving is performed in all ranges, behavior during standing starts employing the clutch or torque converter and behavior during gearshifts can be understood. Also, the accuracy of acceleration fuel consumption improves, meaning that the rates of contribution of deceleration and idling operation to overall fuel consumption can be obtained. The fuel consumption is determined from the fuel consumption volume characteristics, which are based on the engine loading at individual computation times. Alternatively, if the fuel injection volume is calculated, the fuel consumption can be determined from the fuel injection volume. It is assumed that the gear ratios are predetermined. Even so, calibration for optimal fuel economy is possible. It

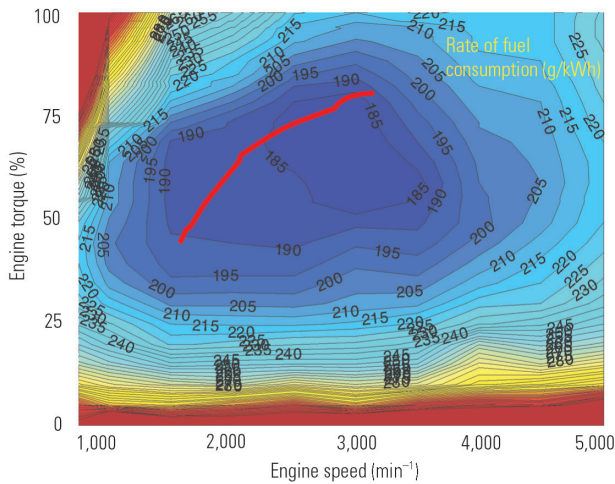


Fig. 3 Operation at point of minimal fuel consumption

is appropriate to treat the fuel consumption and constraints as evaluation functions and to change the gear ratio and lockup range by means of the optimization algorithm (for example, simulated annealing) for each simulation. Consequently, the idea of determining the engine power from the required power and thus establishing the engine's operating point (in other words, the gear ratio and engine torque) in real time (as described in part 2.1 of this paper) is born. The algorithm and constraints for this purpose are studied.

3. Real-time fuel-consumption-minimizing algorithm and related problems

3.1 Basic algorithm

Once the axle power has been established, it can, with the transmission's transmission efficiency taken into account, be converted into the engine's output power. At this stage, only the output has been determined; operation is not possible. If this power is drawn on a graph of the fuel consumption rate characteristics per unit output (with the engine torque plotted against the vertical axis and the engine speed plotted against the horizontal axis) and the point where the isopower line and minimum fuel consumption curve crossing is treated as the operating point, fuel consumption is minimized with steady driving mode (Fig. 3). Given that the transmission's transmission efficiency depends on the gear ratio, the target engine power is not readily determined and repeated computation can be necessary. This computation should be performed in real time (in other words, on each control cycle of the controller). When a robot is caused to perform only urban-cycle driving, the target axle power can be obtained from the vehicle and target speed. If normal driving is considered, however, it is natural to provide the target power from the accelerator.

3.2 Target tracking

With the basic algorithm, there is an implicit prerequisite that the basic algorithm be capable, when the tar-

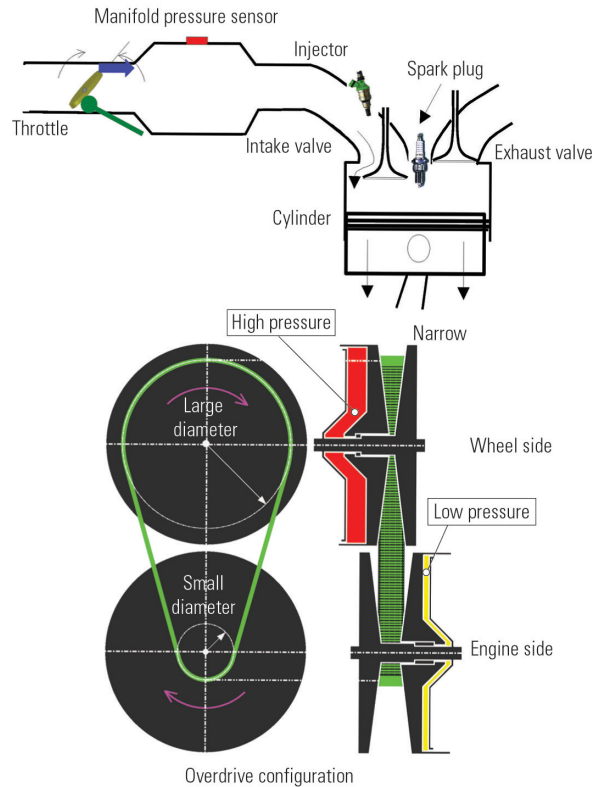


Fig. 4 Engine torque generation and CVT shift

get operating point changes, of instantaneously transitioning to the next target operating point. With an actual power plant, however, this prerequisite is not satisfied. Because of the accumulative effect of a gasoline engine's intake manifold, air corresponding to the throttle does not enter the cylinders when the throttle moves. Further, the stroke lag (intake, compression, expansion) that characterizes reciprocating internal combustion engines has an effect. Also, when oil is supplied to the hydraulic cylinders inside the pulleys of a CVT it takes time for each pulley to move the belt to the target ride diameter. The action is slower than the engine's response; the engine's torque response time is in the order of 0.1 s, but the CVT's shift response time is several times as long (Fig. 4).

3.3 Powertrain's acceleration/deceleration energy

Energy used in acceleration cannot be recovered during deceleration. Consequently, it is desirable to keep the acceleration of the engine and CVT input shaft to a minimum. It is essential to take into account not only the target value generation but also the results (speed increases). The CVT pulleys that hold the belts have large moments of inertia. Plus, gearshifts cause the equivalent moment of inertia to change. If a gearshift is completed in a short time, therefore, torque absorption (caused by the engine speed increase if the vehicle is accelerating) or torque release (if the vehicle is decelerating) occurs, affecting the energy balance and detracting from comfort (Fig. 5).

The torque absorption and release resulting from

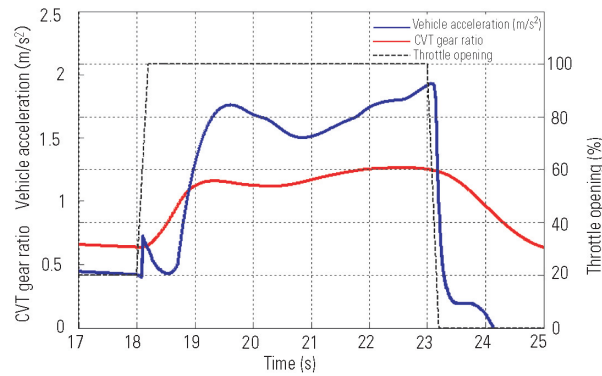


Fig. 5 Torque absorption accompanying CVT gearshifting

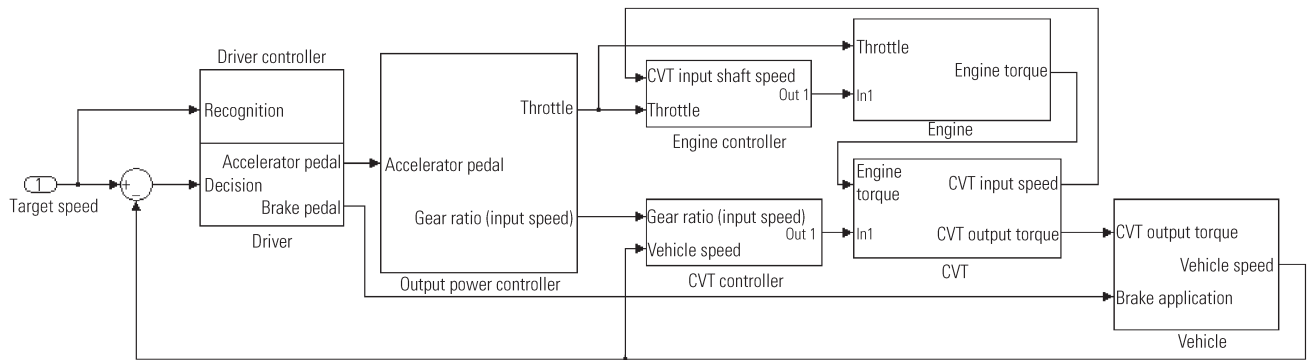


Fig. 6 Stability of control system including driver

gearshifts with a CTV can be determined using the following equation:

$$(I_v + I_e R^2) \dot{\omega} v = -I_e \dot{\omega} e \dot{R} + T_e R - T_{ld} \quad (1)$$

where

I_v : Vehicle's inertia moment

I_e : Engine's inertia moment

R : CVT's gear ratio

ωv : Vehicle speed

ωe : Engine speed

T_{ld} : Running resistance

T_e : Engine torque

4. Conflicts with human's driving operations

4.1 Structure of speed control system

With conventional operation, the driver's inputs to the accelerator pedal cause the throttle (mechanical or electronic) to operate and CVT gearshifts to be performed. With the fuel-consumption-minimizing algorithm, the extent of accelerator pedal movement is the required propulsion power, not the throttle. Inside the controller, it is converted into the target engine torque and gear ratio. Torque inflows and outflows caused by the powerplant's acceleration and deceleration exist as external disturbances. At this stage, the addition of gain variations and response lag can be considered. In certain cases, the driver may move the accelerator pedal

further in response to the powerplant's acceleration/deceleration and the vehicle's behavior. Simply stated, the control system is structured such that the controller superscripts such additional actions in response to the driver's inputs (Fig. 6). In target speed tracking simulations, the speed causes an oscillatory phenomenon depending on parameters.

4.2 Driver response model

The driver's driving operations can be categorized in terms of recognition; determination of extents of control actions based on information processing; and actions. In target speed tracking operation, recognition encompasses future target speeds and directions of speed changes and discrepancies between target and actual speeds; information processing encompasses determination of the extents of accelerator and brake pedal inputs from the difference between the speed t seconds in the future and the current speed (feedforward) and current speed deviation; and actions are foot movements that depress the pedals. Recognition includes response lags, and information processing includes establishment of inappropriate extents of control actions. These factors are inherent to human beings, but with the inclusion of minimal-fuel-operation control that implements driving operations in addition to the driver's actions there is a risk of conflicts between the human and the control system. Simply stated, with a speed feedback system incorporating a human being

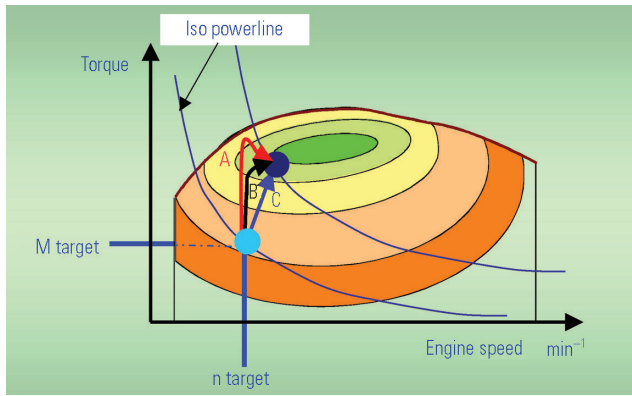


Fig. 7 Target power tracking locus

the gain and phase that integrate the human being and the controller approach the stability limit. In other words, attempts to track the target speed can cause accelerator inputs (with frequent depression and release, brake inputs also) to become oscillatory.

4.3 Elimination of conflicts

Inside a speed control system incorporating a driver, simplifying the driving action transmission characteristics by means of the speed deviation gain, first-order lag (low-pass characteristics), and dead time does not cause a large error. If the transmission characteristics of the fuel-consumption-minimizing controller, powertrain, and vehicle are approximated as the transmission characteristics from an accelerator input to the vehicle speed response, they can be expressed as dead time + second- and higher-order transfer functions. If, with a system combining the driver's driving response characteristics and this vehicle transmission system, the gain exceeds 0 while the phase is greater than 180° , the system becomes unstable. Elimination of structures that expand response lags and correction of the gain from the accelerator to the throttle and gearshift are necessary, and in certain cases it is effective to perform local feedback between the fuel-consumption-minimizing control and throttle control. The viewpoint of a human-machine system with which the driver's speed feedback gain does not become large (with which unfamiliar responses are not caused) is also necessary.

5. Target operating point tracking

Even if the accelerator changes in a stepped manner and the target power changes instantaneously, the torque and speed (gear ratio) cannot accurately follow them. The response is dictated by the transmission's gearshift response.

5.1 Target power trajectory generation

The target power changes in a stepped manner during a transition from steady-state vehicle operation to acceleration. Power target following takes place as shown in Fig. 7. Here, if the torque and gearshift are

independently controlled the path B is followed. If the change in the power target is matched to the gearshift, path C is followed. If gearshift response compensation is performed using the torque, path A is followed. In the trajectory line drawing the path looks long, but it is a short-time response. Performing this trajectory generation from the power target is not easy. But if, at the target power stage, the power is broken down into the torque and the gear ratio (target engine speed) and the transfer function of the gearshift response is corrected into a torque target, torque and gear ratio trajectory generation is easy to perform.

The transfer function of the gearshift response can be expressed as the first-order lag $1/(1 + T_{gr}S)$ (reverse responses proportional to the shift speed are not included), so the torque target can be corrected. The transmission characteristics of the torque response are, from the transfer function of the intake system, $1/(1 + T_{ce}S)$. Note that stroke lags and fuel transport lags are not included.

Compensator to torque target value is shown as equation (2).

$$T_{et} = \frac{1 + T_{gr}S}{1 + T_{new}} T_{et0} \quad (2)$$

where

- T_{et} : Target torque (with shift correction)
- T_{gr} : Shift response time constant
- T_{new} : Appropriate low-pass filter (added)
- T_{et0} : Demanded torque
- T_{ce} : Intake system time constant

5.2 Torque and gear ratio control

With a CVT, the maximum gear shift speed that does not cause belt slip is treated as an absolute constraint. This constraint exists also because fast gear shifts lead to a feeling of deceleration (a feeling of freewheeling) and a feeling of acceleration (Fig. 5, equation 1) yielded by the acceleration and deceleration of the engine and CVT input portion's inertia moments. The time constant is a low-pass characteristic in the order of seconds. With regard to the engine's torque generation, there is a first-order lag and a stroke lag with a time constant related to the volume of the intake manifold; and the amount of air passing through the throttle depends not only on the throttle opening area but also on the intake manifold's internal pressure, meaning that it is not easy to match the generated torque to continuously issued torque commands. Throttle opening feedforward and intake air volume feedback based on a steady-state condition must be jointly used (However, the intake manifold pressure includes pulsations, meaning that only stroke-average values can be used; a dead time system occurs such that high-gain feedback cannot be expected. It is better to concurrently use estimated values provided by an observer.).

Notably, when there is a significant error in the torque control the gain of the closed-loop system containing the driver deviates, affecting the stability of the

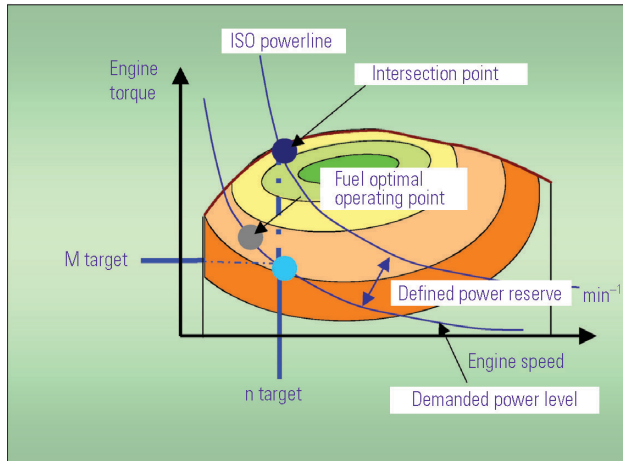


Fig. 8 Concept of reserve power

entire system containing the driver. Further, rapid torque changes act as stepped inputs, causing torsional vibration in the drive axle. This vibration becomes an input from the mounts and suspension system such that ride comfort suffers.^{(5) (7)}

5.3 Improved control

The required propulsion power when the vehicle starts moving from a standstill is 0, but this value is meaningless so the target engine power cannot be calculated. Also, even when power is generated after the vehicle has started moving the torque converter's efficiency affects the transmission's efficiency such that computation becomes more complex and numerical stability deteriorates. Consequently, the engine power is calculated from the target power with the gear ratio as full low (the efficiency corresponds to full low) then the CVT input torque is calculated with that gear ratio and speed control is effected with the calculated CVT input torque as the target. The torque transmission equation for the torque passing through a torque converter (a well-known equation) is shown below. The required engine speed can be determined from here.

Torque converter output torque

$$T_{tc} = \tau(e)C(e)Ne^2 \quad (3)$$

where

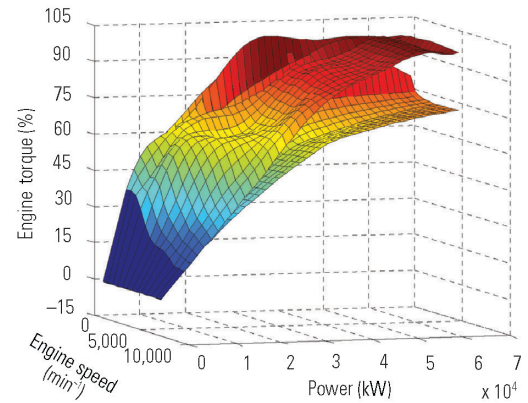
τ : Torque ratio

e : Speed ratio

C : Volume coefficient

Ne : Engine speed

After lockup of the torque converter, the aforementioned searching for the fuel-efficiency-optimal operating point is performed. The engine torque target is subjected to gear ratio response correction. Further, feedback (with an observer additionally employed) is performed for engine intake system non-linear correction. The response and stability of target torque tracking are thus assured.



Given that control of the gear ratio does not increase the acceleration/deceleration energy and that it suppresses the reverse response amount yielded by the CVT gear shift speed, a control system that increases responsiveness is not composed.

6. Gearshift timing scheduling

A real-time operating point changing algorithm that accommodates the fuel-consumption-minimizing algorithm, the surrounding environment, and the driver's preferences is described hereafter.

6.1 Concept of reserve power

Typically, driving with a high gear ratio causes the engine speed to be high but permits good acceleration when the accelerator pedal is depressed. For example, compared with driving with a four-speed automatic transmission in fourth gear and with an engine speed of 1,500 min⁻¹, driving with the same transmission in third gear and with an engine speed of 2,000 min⁻¹ permits a higher rate of acceleration for a given extent of depression of the accelerator pedal and yields a greater engine torque increase reserve. For application of these factors to a CVT, the concept of reserve power is adopted. The reserve power is the distance from a given point on a given power curve to the maximum torque curve with the engine speed kept constant (Fig. 8). At the point of intersection between the maximum torque curve and a given power curve, there is no reserve power; if the speed is increased, reserve power is created.

A control method for dynamically changing this reserve power in accordance with driving conditions and the surrounding environment is considered.

6.2 Realization of dynamic scheduling

With an automatic transmission or CVT, a gear shift mode in which the gear ratios are all relatively high (this mode is called a power mode or a sports mode) is typically provided in addition to the normal driving mode. With this mode selected, the gear ratios are fixed. The gear ratios do not change even when the vehicle is dri-

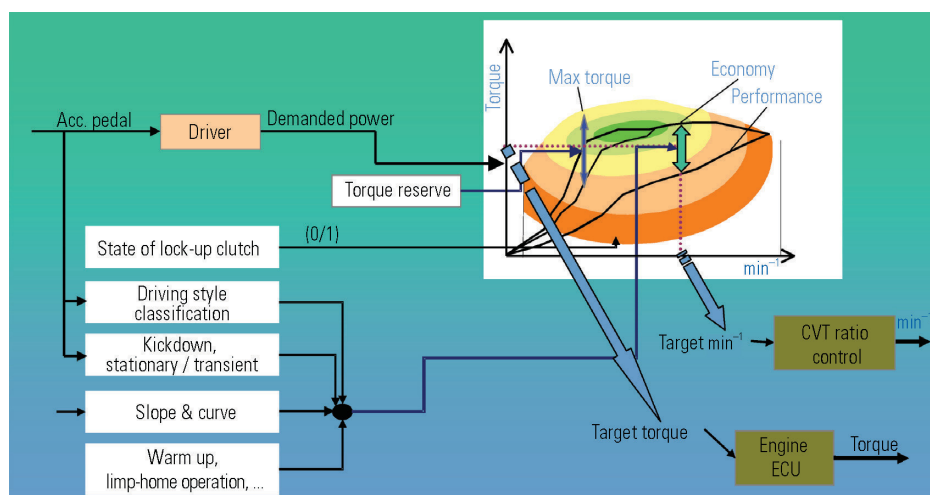


Fig. 9 Dynamic gear shift scheduling

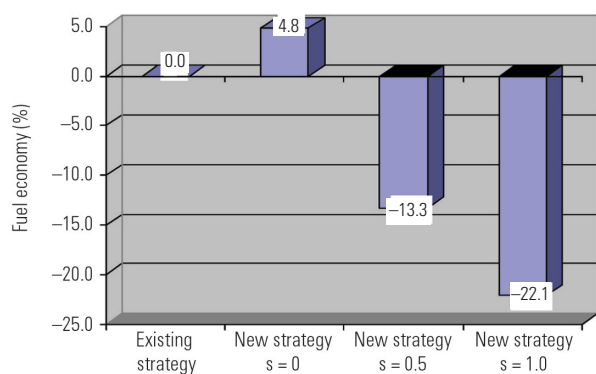


Fig. 10 Fuel-economy performance

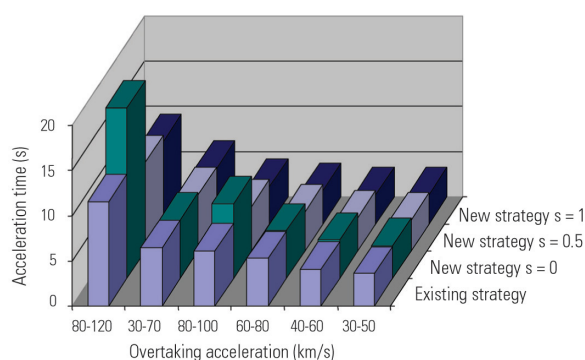


Fig. 11 Acceleration performance

ven on a slope. Neither do they change regardless of whether the vehicle is driven gently or in a manner that causes frequent kickdown.

An algorithm that allows the vehicle's acceleration response to change in accordance with the road environment and the user's driving preferences while fundamentally optimizing fuel efficiency can be composed using the aforementioned concept of reserve power. The algorithm consists of two parts: changing the operating point in accordance with the level of reserve power and changing the reserve power in accordance with the road conditions and driver behavior. The former part was added to the target value generation portion, and the latter part was newly created (Fig. 9).

There are various conceivable reasons for changing the reserve power: the road gradient; the road's curve radius; the kickdown frequency; promotion of warmup for emissions performance; and driving characteristics.

On a slope, it is possible, as with systems introduced earlier by MMC, to predict the road gradient from the torque and acceleration and, if the gradient is greater than a certain angle, to increase the reserve power as necessary. Also, the reserve power is increased in situations where kickdown is frequent, i.e., situations where kickdown occurs repeatedly in a short period of time.

If, when the reserve power has been increased, there is a continued period of gentle driving, the reserve power decreases and the fuel-consumption-minimizing mode is implemented. In other words, fuel efficiency is improved provided the driver takes care to drive in a fuel-efficient manner (for example, stopping the engine when the vehicle is stationary).

6.3 Effects of dynamic scheduling

The effects upon fuel consumption and acceleration performance were investigated by means of simulations. A comparison was made of the effects with fuel efficiency prioritized (with reserve power of 0) and those with sportier driving (with the reserve power changed). Here, a reserve power coefficient of $S = 0$ corresponds to the fuel-efficiency-prioritizing mode and $S = 1.0$ corresponds to the power-prioritizing mode. Urban-cycle fuel consumption was predicted with various values of S (Fig. 10). With $S = 0$, fuel efficiency is better than with the current shift control. Fuel efficiency deteriorates with increases in S . With $S = 1.0$, it decreases by 25%. Off-the-line acceleration and overtaking acceleration are shown in the form of a graph in Fig. 11. $S = 0$ corresponds to the fuel-efficiency-prioritizing mode. With increases in the reserve power and a transition to sporti-

er driving, fuel economy deteriorates but acceleration performance is improved.

7. Summary

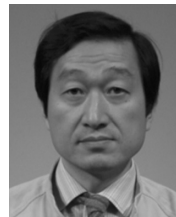
Operation at the point of optimal fuel efficiency can be realized under steady-state conditions. When the loading changes and the required power changes with it, however, reconstruction is necessary from the viewpoint of target following. Consequently, a fuel-consumption-minimizing algorithm that takes response into account was created and operating stability was studied with a feedback system. Using the concept of reserve power, a form of dynamic gear shift scheduling whereby real-time correction is applied to the fuel-consumption-minimizing operation in accordance with the road environment and driver behavior was proposed. Simulations showed that the proposed method significantly improves acceleration for sporty driving with only a slight sacrifice in fuel economy.

8. Thanks

The authors were instructed on the concept of driver models by the staff of the Tamaki Laboratory at Kobe University. The concept and results of dynamic gear shift scheduling came about through joint research conducted with Dr. Shinkel and Dr. Halfmeier of DaimlerChrysler Research and Technology. The authors wish to express their gratitude.

References

- (1) Tani, Magoshi, Tanaka, Shimizu, and Tanimoto: Development of New Active Safety System (INVECS) Incorporating Fuzzy Control Concepts, Mitsubishi Motors Technical Review, No. 6, 1994
- (2) Fujita, Asano, Onishi, and Nakamura: Development of INVECS-II Sports Mode Automatic Transmission, Mitsubishi Motors Technical Review, No. 7, 1995
- (3) Kondo, Ikushima, Sato, Notani, Ikeda, et al: Development of Power-Train System Combining Gasoline Direct Injection Engine and Continuously Variable Transmission, Mitsubishi Motors Technical Review, No. 12, 2000
- (4) Nakamura, Ashizawa, Sugawara, and Kanai: Design of Multi-Input, Multi-Output Acceleration Feedback Control System for Improvement of Driveability and Fuel Economy, JSAE symposium proceedings 2003, 20035005
- (5) Togai, Takeuchi, et al: CVT Drive Train Vibration Analysis and Active Control System Design, Mitsubishi Motors Technical Review, No. 17, 2005
- (6) Allen, Fancher, Levison, Maurant, Schnell, and Srinivasan: Simulation and Measurement of Driver and Vehicle Performance, Transportation Research Board Millennium Papers
- (7) K. Choi and K. Togai: Passenger car acceleration vibration suppression strategy with constraint control, SICE annual conference, 2003
- (8) Ide, Udagawa, Kataoka, and Uchiyama: Shift Response of a CVT with a Metallic V-Belt, Subaru Technical Review, No. 22



Kazuhide TOGAI



Miki KOSO

Enhancement of Combustion by Means of Squish Pistons

Katsuhiko MIYAMOTO* Yoshiyuki HOSHIBA*
Kiyotaka HOSONO* Syunichi HIRAO*

Abstract

Knowledge gained through studies aimed at enhancing combustion by means of changes in piston shapes is presented in this paper.

Attention was first focused on tumble and squish in the context of in-cylinder flows, and the characteristics of combustion patterns and effects on partial-load fuel consumption were investigated. Squish is characterized by invigoration of combustion in the middle and late stages, which is desirable for combustion pattern. For reduction of fuel consumption, it was confirmed that improved in thermal efficiency yielded by squish-enabled increase in combustion speed is beneficial with low engine loading and that squish-enabled suppression of knock is beneficial with high engine loading. During full load operation, it was confirmed that not only knock suppression but also piston-shape-yielded improvements in volumetric efficiency are beneficial. The benefits were evaluated experimentally and through the analysis of in-cylinder flows. These findings and particularly influential design factors are discussed in this paper.

Key words: Gasoline Engine, Combustion, Knocking, Piston

1. Introduction

Amid the growing problem of global warming, about 20 % of carbon-dioxide emissions are attributable to transportation and about 90 % of this amount is attributable to automobiles. Since improvements in fuel efficiency are vital, there is much ongoing research into ways to enhance the thermal efficiency of engines. There are various techniques for improving thermal efficiency. Some techniques (exhaust-gas recirculation and lean combustion, for example) work primarily by reducing pumping losses. Others (suppression of high-load knock and optimization of in-cylinder flows, for example) work primarily by enhancing combustion. Efforts to enhance combustion by optimizing in-cylinder flows fall into two broad categories: ① those that invigorate combustion by promoting tumble, swirl, and other in-cylinder flows throughout the engine's intake and compression strokes; and ② those that use squish to create turbulence mainly in the vicinity of Top Dead Center (TDC) on the compression stroke. At the time of writing, slanted squish areas, which are suitable for pentroof combustion chambers, are widely used. The study described in this paper was focused on comparing the effects of slanted-squish pistons with those of flat pistons with respect to combustion and performance. The effects of slanted-squish pistons on knock suppression and intake air amounts during high-load operation and their effects on fuel consumption during partial-load operation were investigated.

2. Piston shapes and general characteristics

Table 1 shows three main piston-crown shapes and

their respective merits and demerits⁽¹⁾. A flat piston has a small crown surface area and consequently has the merits of small heat losses and low weight. A horizontal-squish piston is effective at promoting combustion, but small valve diameters are necessary to provide a squish area. During high-speed operation, therefore, there is a tendency for air volumes to decrease and for performance to be concomitantly limited. A slanted-squish piston is well suited to a pentroof combustion chamber in which ignition takes place at a central point between the four valves (the typical combustion-chamber configuration in recent engines), and it has the merit of providing a squish area without requiring any reduction in valve diameter. However, it has the demerits of a relatively large piston-crown surface area and relatively high weight. It has been reported that slanted-squish pistons suppress knock by accelerating combustion toward the end of the combustion process⁽²⁾.

The shapes of the cylinder head and piston that form the combustion chamber are shown in Fig. 1. Squish areas are formed between the pentroof portions, which run in the intake-exhaust direction, and the piston, but no squish areas are formed in the engine's front-rear direction. This combustion chamber was used as the basis for various tests.




3. In-cylinder flows and combustion characteristics

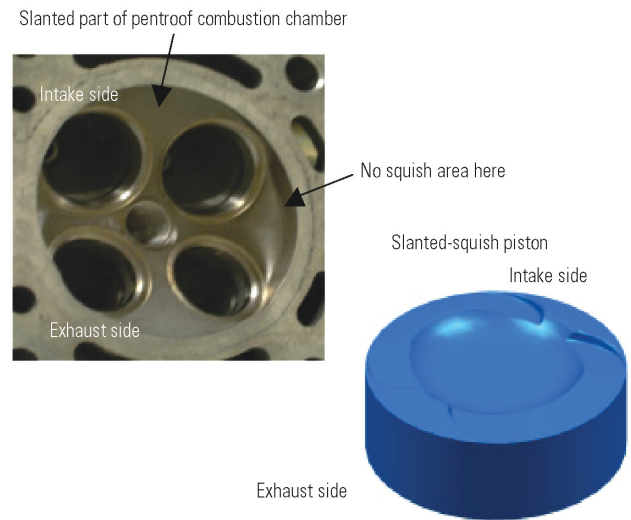
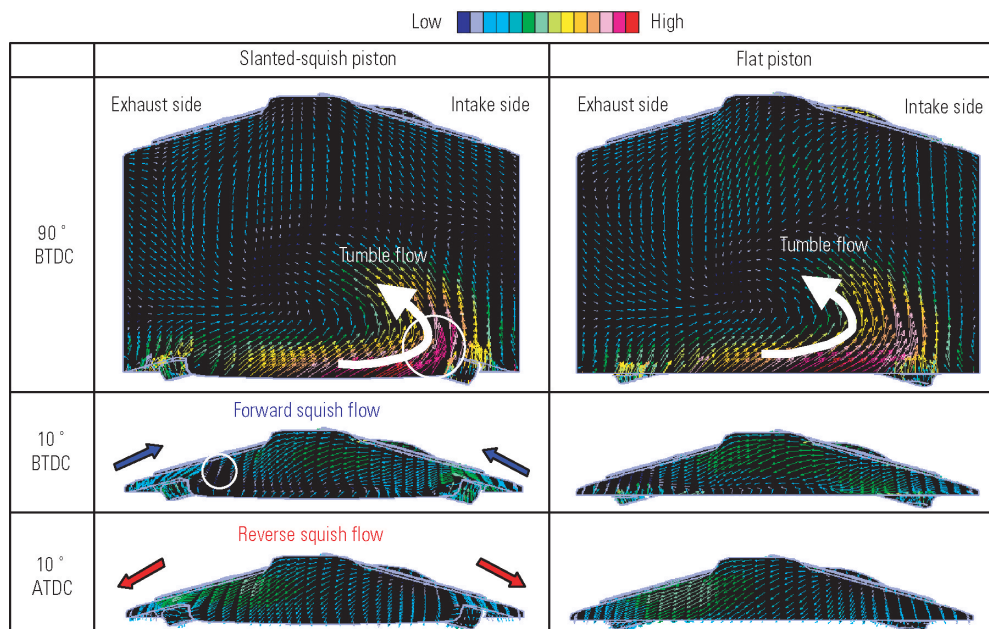
3.1 Computational Fluid Dynamics (CFD) comparison of flat piston and slanted-squish piston

The results of CFD calculation with a flat piston and a slanted-squish piston are shown in Fig. 2. The software used was STAR-CD and es-ice. In the tumble flow

* Advanced Powertrain Development Dept., Development Engineering Office

Table 1 Merits and demerits of piston shapes

Item	Combustion chamber with squish areas		Flat piston
	Slanted squish	Horizontal squish	
Shape			
Surface/volume ratio	×	×	○
Combustion duration	○	○	×
Knock resistance	○	○	×
Intake air resistance	○	×	○
Piston	Weight	×	△
	Size	×	△
	Heat losses	×	△

**Fig. 1 Shape of combustion chamber and shape of typical slanted-squish piston****Fig. 2 CFD computation for flat piston and slanted-squish piston (Flow velocity vector chart)**

on the compression stroke, the flow velocity in area A tends, with the slanted-squish piston, to be slightly increased by the influence of the squish entrance of piston, but there is no great difference from the results for the flat piston. At 10° BTDC on the compression stroke, there is an intense forward squish flow on the slanted-squish piston. Owing to collisions between this flow and the tumble flow, sluggishness in the flow occurs in the vicinity of the exhaust-side squish exit. Also, the flow in the vicinity of the spark plug is weaker than it is with the flat piston. Fluctuations in initial combustion are concomitantly limited⁽³⁾.

At 10° ATDC, a strong reverse squish flow is formed on the slanted-squish piston. The area where sluggishness occurred before TDC (the area circled in the figure)

is drawn into the reverse squish flow and is simultaneously pushed by residual tumble, resulting in the generation of a flow there. To this extent, the reverse squish flow is stronger on the exhaust side than it is on the intake side.

3.2 CFD comparison of tumble ports and base ports

Promoting in-cylinder flows is an effective means of invigorating combustion, but CFD computation was performed with regard to various combinations of tumble flow caused by the collapse of the eddy in the vicinity of TDC from bulk flow and squish (slanted) that causes turbulence only in the vicinity of TDC.

The shape differences between tumble and base ports and the tumble characteristics of each of port type

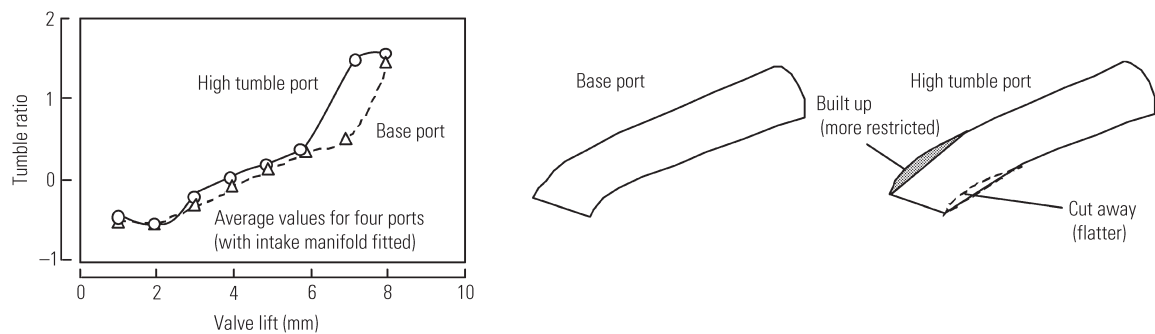


Fig. 3 Port shapes and their tumble characteristics

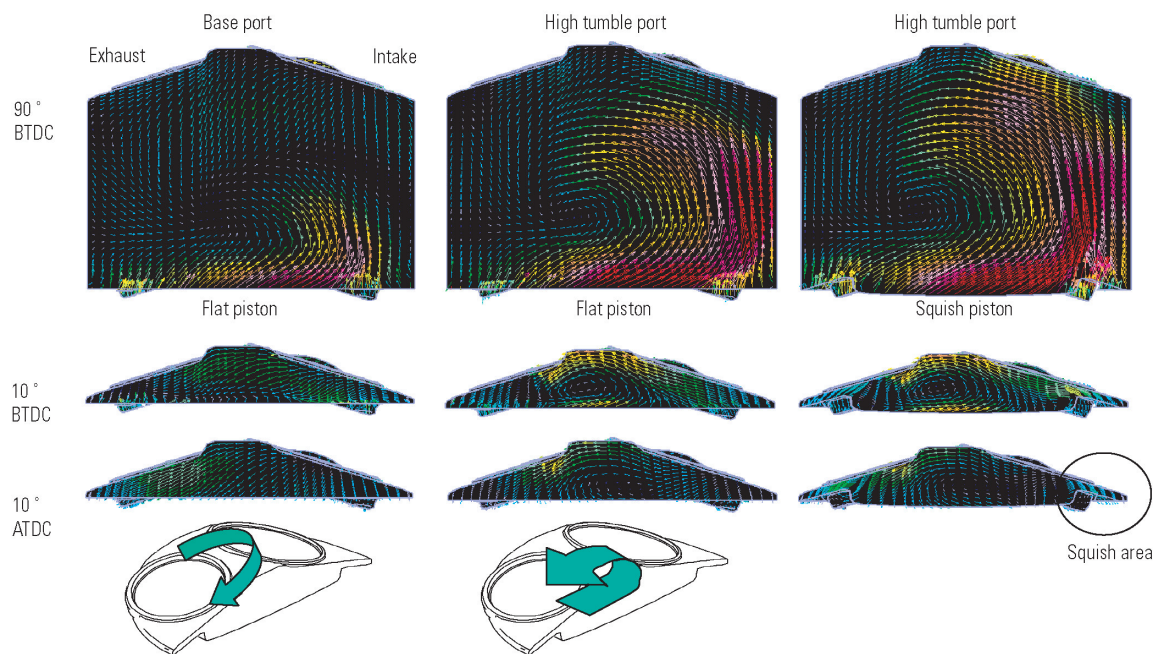


Fig. 4 CFD computation for tumble port and base port (Flow velocity vector chart)

in steady-flow tests are shown in Fig. 3. Compared with the base port, the tumble port is more built-up (more restricted) above the intake valve and more cut-away (flatter) at the bottom. Its shape directs the main intake flow toward the spark plug, thereby intensifying the tumble. As shown in Fig. 3, the tumble port makes flows more intense with a valve lift of 6 mm and more. As this port was modified by hand, three-dimensional measurements were taken, the results were dropped into CAD data, and a simulation model was made.

CFD calculation results for the model and the base port (with a flat piston crown) are shown in Fig. 4. It can be seen that the upstream flow on the intake side with the tumble port is relatively strong on the compression stroke (at 90° BTDC) in comparison with the flat piston, meaning that the port modifications led to intensification of in-cylinder flows. At 10° BTDC, there is a strong flow from the intake side toward the center of the spark plug. In the vicinity of TDC, tumble is maintained with the high tumble port. With the base port, by contrast, tumble is weak; vertical flows cannot be maintained, so the flow rotates at a slant. (See the bottom-left part of

Fig. 4.)

The right-hand parts of Fig. 4 correspond to a combination of a squish piston and the tumble port. With the squish piston, the tumble flow is thrown upward by the slanted face of the squish entrance on the intake side of the piston so that the tumble at middle of the liner is made stronger than it does with the flat piston. Consequently, an area of high velocity extends as far as the vicinity of the spark plug.

3.3 Partial-load combustion with combination of squish and tumble

Heat release rate under partial loading with various combinations of piston and port is shown in Fig. 5. With regard to the average high tumble ratio, it is 0.77 with the base port and 1.08 with the high tumble port. In Fig. 5, the broken red line corresponds to a combination of base port and flat piston. It can be seen that only changing the port to the tumble port (see the solid red line) and only changing the piston to the squish piston (see the broken blue line) both make combustion faster. With these two combustion-promoting arrangements

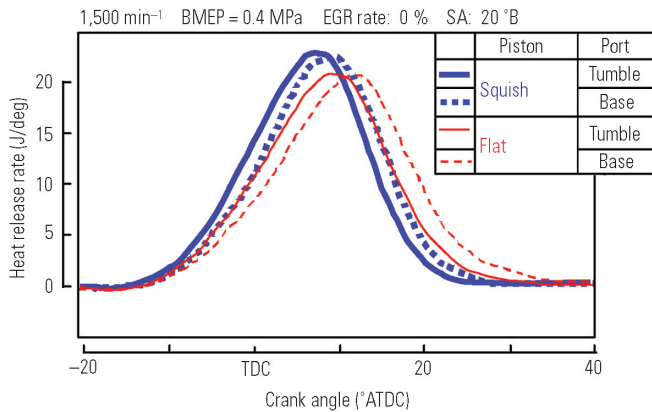


Fig. 5 Heat release under partial loading with various combinations of piston and port

(see the solid red line and broken blue line), the lines corresponding to initial combustion areas in this study happen to more or less coincide.

With the squish piston used, the rise in heat release is rapid after TDC and the absolute values are also high (evidence of the combustion-promoting arrangements of the reverse squish flow that was confirmed by CFD calculation). The sharp increase in combustion acceleration after TDC shows that the cylinder pressure increases during the piston's descent and that the combustion energy is efficiently converted into work.

With the tumble port combined with the squish piston (see the solid blue line), the late-stage combustion acceleration that characterizes squish exists but, in addition, early- and middle-stage combustion occurs earlier; the combustion pattern shows a shift in the heat release toward the advance-angle side. This combustion pattern has most of the heat release occurring too far toward the advance-angle side, which conceived as not desirable with respect to heat losses and cycle efficiency.

Fig. 6 shows the turbulence energy in the vicinity of the spark plug as shown by CFD computation. With the combination of tumble port and squish piston, the turbulence energy is high from BTDC and is the reason that combustion is fast in the early and middle stages. This phenomenon is connected to the intensification of tumble by the squish piston shape as shown by the CFD calculation results in **Fig. 4**.

By contrast, combining the squish piston with the base port does not increase the turbulence energy in the vicinity of the plug.

The slanted-squish piston tends to preserve tumble easily due to its squish inlet shape (rise from the cavity). Therefore, care must be taken to combine it with a port which does not intensify turbulence⁽³⁾.

3.4 Partial-load fuel consumption with combination of squish and tumble

Fig. 7 shows partial-load fuel consumption with the aforementioned flow intensification implemented. Average tumble ratios by steady-flow are plotted

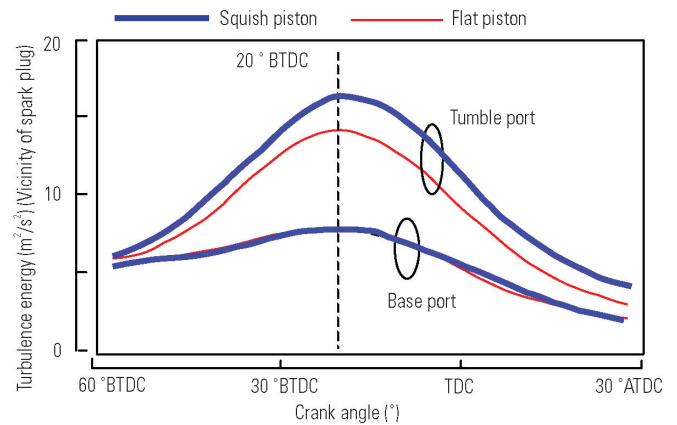


Fig. 6 Turbulence energy in vicinity of spark plug

against the horizontal axis, and fuel consumption and combustion durations are shown against the vertical axes. As the tumble rate increases, the flow coefficient decreases. With the base port, changing from the flat piston to the squish piston enables a reduction in fuel consumption without a change in the tumble ratio, i.e., without a decrease in the flow coefficient (see part ① of **Fig. 7**). With the flat piston, changing from the base port to the tumble port enables a reduction in fuel consumption (see part ② of **Fig. 7**). If the tumble port and squish piston are combined, however, fuel consumption becomes higher than it is with the base port and squish piston.

As stated in the discussion of combustion analysis, a combination of squish piston and tumble port makes combustion occur early and is thus unfavorable with regard to thermal efficiency and heat losses. **Fig. 8** shows the calculation results for heat losses with the conditions used for combustion analysis. (For the calculation equations, reference was made to reference document (4). It was not possible to make reference to differences between in-cylinder flows caused by differences between heat transfer rates.) The faster the combustion, the greater the heat losses shown. It can be inferred that the heat losses are particularly high with the squish piston partly because the combustion-acceleration position is close to TDC and the temperature in the cylinder is concomitantly high and partly because the surface area of the piston crown is relatively large.

4. Effects of squish-area shape on knock and combustion

4.1 Effects of squish-area clearance height and shape

With regard to effects of clearance shape (a squish-area design parameter), a study was made of partial-load combustion and knock. Two types of clearance were evaluated. Their heights were 0.8 mm and 2.0 mm. The other clearance was wedge shaped, having a height of 1.4 mm at the widest point at the squish entrance and a height of 0.8 mm at the narrowest point of the liner side (**Fig. 9**).

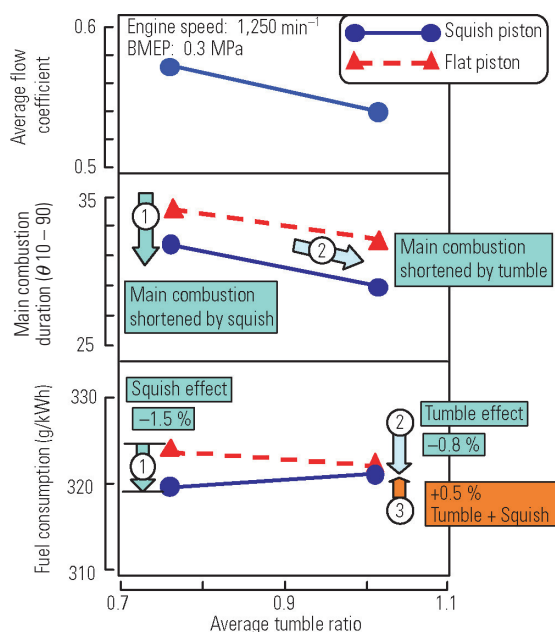


Fig. 7 Partial-load fuel consumption with flow-intensifying measures implemented

Fig. 10 shows test results for partial-load combustion and full load knock characteristics. The testing for partial-load combustion was conducted at $1,250 \text{ min}^{-1}$ with a constant fuel amount. The higher the indicated mean effective pressure (P_{mi}), the more efficient the combustion. With the 0.8 mm clearance, the 10 – 90 % combustion duration is short and the P_{mi} values are high. With the wedge shape, by contrast, the P_{mi} values are the lowest and the 10 – 90 % combustion duration is the longest. Apparently, ample forward or reverse squish flow is not generated with a shape that widens toward the squish entrance like this.

With regard to full load knock, with the 0.8 mm clearance and the wedge shape the knock ignition timing is, relative to the knock ignition timing with the 2.0 mm clearance, advanced by 2° at $3,000 \text{ min}^{-1}$ and by 1° at $1,000 \text{ min}^{-1}$. With the 2.0 mm clearance, the knock ignition timing is almost the same as with the flat piston and no knock-suppressing effect is obtained. Considering the common features of the aforementioned test result and the results for the wedge shape and 0.8 mm clearance, it is supposed that a small clearance in the end gas area leads to knock suppression. One reason for the knock suppression is apparently that the 0.8 mm clearance and the wedge shape, with both of which the end gas area has a high surface-to-volume (S/V) ratio, yield large amounts of heat transfer to the wall such that the end gases are cool.

4.2 Effects of squish in cylinder-head front-rear direction

This paper has thus far discussed evaluation performed with combustion chambers that have squish areas aligned only in the engine's intake-exhaust direction. Subsequently, the effects on full load per-

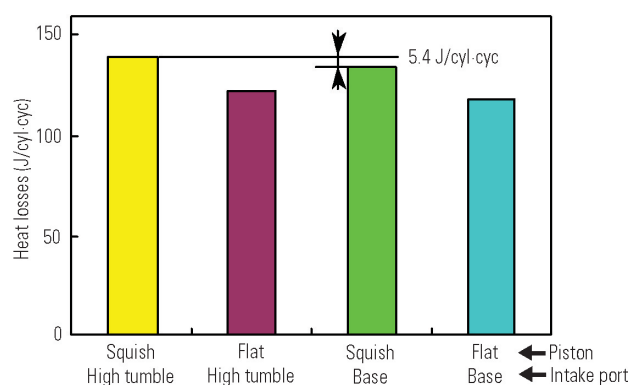


Fig. 8 Partial-load heat losses with flow-intensifying measures implemented

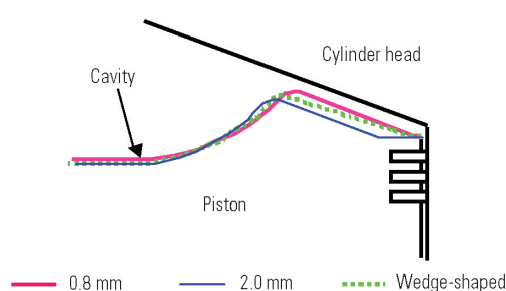


Fig. 9 Shapes of squish-area clearances

formance and combustion of squish areas provided in the engine's front-rear direction (on the cylinder head) in addition to squish areas aligned in the intake-exhaust direction were investigated. A photograph of the cylinder head is shown in **Fig. 11**. The front-rear-aligned squish areas on the cylinder head are each approximately 7 mm wide. The clearance between the piston and cylinder head is 1.4 mm in the squish area on the exhaust side and 1.2 mm in each other squish area.

Fig. 12 shows heat release rate with each of two squish-area patterns and with a flat piston. Combustion is fastest with the four squish areas (intake, exhaust, front, and rear). The difference between combustion with the four squish areas and combustion characteristics with squish areas aligned in only the intake-exhaust direction are small, but there is a marked difference from combustion characteristics with the flat piston. Full load operation is fastest with the four squish areas at any given ignition timing, meaning that torque is concomitantly high and the knock ignition timing is retarded, meaning that output of the knocking point is superior to that with squish areas aligned in only the intake-exhaust direction (**Fig. 13**). A possible reason is that cooling of the squish areas aligned in the cylinder head's front-rear direction is inadequate.

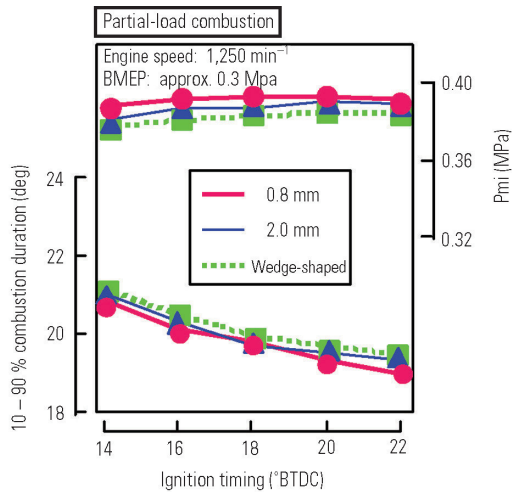


Fig. 10 Effects of squish-area shape on partial-load combustion and full load knock

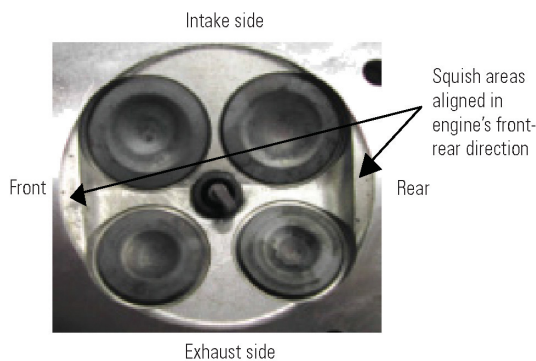


Fig. 11 Cylinder head with squish areas aligned in engine's front-rear direction

5. Intake performance and piston shapes during full load operation

Fig. 14 shows the full load performance of the squish piston and flat piston. At nearly all engine speeds, the squish piston yields superior torque and suppresses knock such that the ignition timing is advanced. In addition at engine speeds of 4,500 min⁻¹

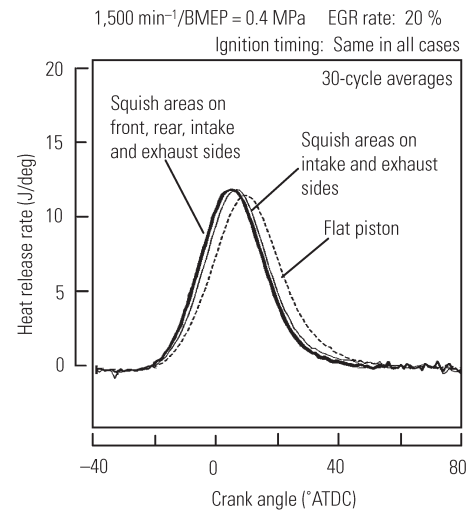


Fig. 12 Heat release rate with each of two squish-area patterns and with flat piston

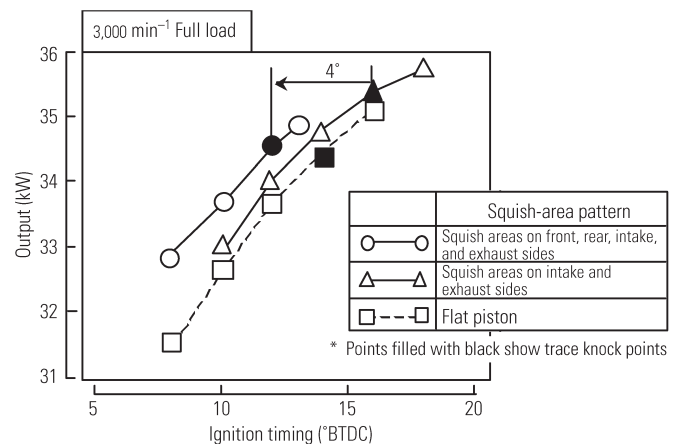


Fig. 13 Full load performance with various squish-area pistons

and lower, it can be seen that volumetric efficiency is better with the squish piston than it is with the flat piston. In line with these benefits, the squish piston realizes 1.4 % higher maximum torque than the flat piston and 1.2 % higher maximum output than the flat piston.

Generally speaking, a squish piston is inferior to a flat piston in terms of intake performance since it does not readily permit large valve surface areas. On the other hand, it has been reported that a slanted-squish piston is better than a horizontal-squish piston in terms of intake performance owing to a smaller masked area in the cylinder head⁽²⁾. However, there are no study results indicating superiority of a slanted-squish piston over a flat piston.

A study was performed based on two hypotheses regarding the superiority of a slanted-squish piston in terms of volumetric efficiency: ① Fast combustion and concomitantly low exhaust temperatures and low exhaust pressure reduce the internal exhaust recirculation amount. ② Creating the slanted squish areas

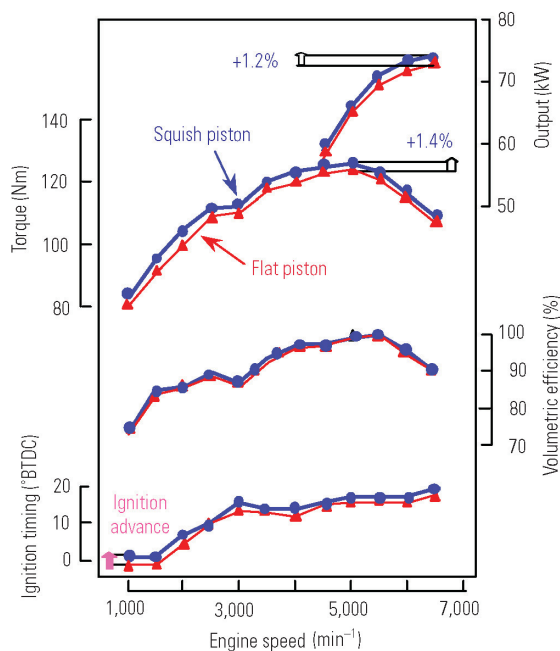


Fig. 14 Full load performance

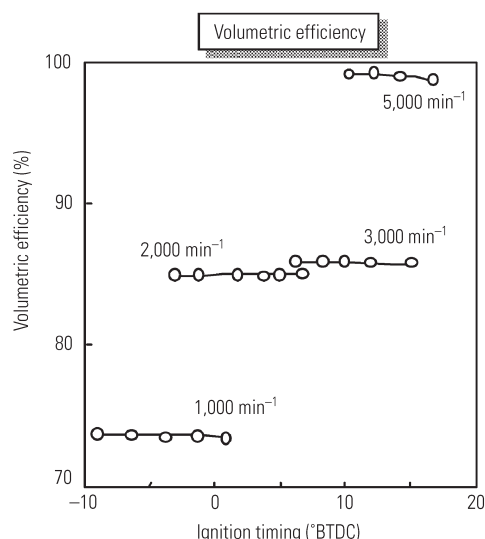


Fig. 15 Full load volumetric efficiency relative to ignition timing at various engine speeds

necessitates thickening of the material at the periphery of the piston crown, so a cavity is provided in the center to ensure ample volume; the cavity promotes intake flows. With regard to hypothesis ①, volumetric efficiency with various ignition timing was studied. If hypothesis ① were correct, a change in the ignition timing would change the combustion speed; retarding the ignition timing would raise the exhaust temperature, and the volumetric efficiency would decrease. As shown in Fig. 15, however, there is hardly any change in volumetric efficiency when the ignition timing is changed; volumetric efficiency does not decrease as the ignition timing is retarded.

Next the effects of the elements mentioned in

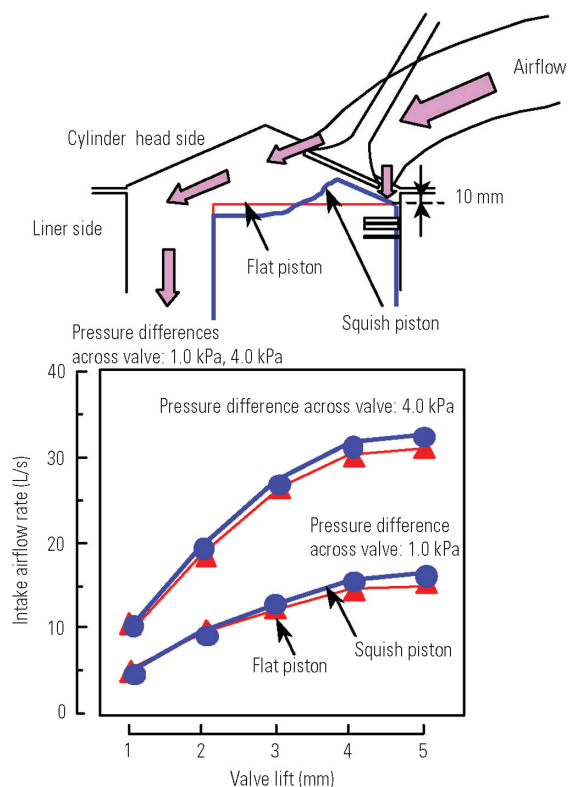


Fig. 16 Outline of test stand and results of steady-flow tests

hypothesis ② were studied using a test stand. An outline of the test stand and the results of steady-flow tests are shown in Fig. 16. In the test stand, one third of the piston is cut away for air suction. With each of two piston types (the flat piston and the slanted-squish piston), tests were performed with the pressure difference between the upstream side of the valve and the liner area constant at 1.0 kPa and constant at 4.0 kPa. The airflow was compared. Differences between the two pistons' results are evident with valve-lift values of 1.5 mm and greater. The greater the valve lift, the greater the difference in intake airflow between the two piston shapes. And the higher the airflow, the more marked the difference between the respective effects of the piston shapes. In actual engine operation, large valve lift does not occur near TDC. Nevertheless, the results of the tests performed with the test stand clearly show that the piston shape affects intake performance.

The effects with an actual engine were next studied. Two test pistons (both of the slanted-squish type) were used. One of the pistons (designated piston B) has large squish areas around its periphery. The other piston (designated piston A) is similar except that its squish area in the vicinity of the intake valve is smaller (Fig. 17). Fig. 18 shows volumetric efficiency during full load operation. Although the shape difference is small, there is a clear difference in volumetric efficiency. It was thus verified with a real engine, too, that piston shape influences volumetric efficiency. From these findings, it can be said that providing a space under the intake valve (particularly in the direction of the main

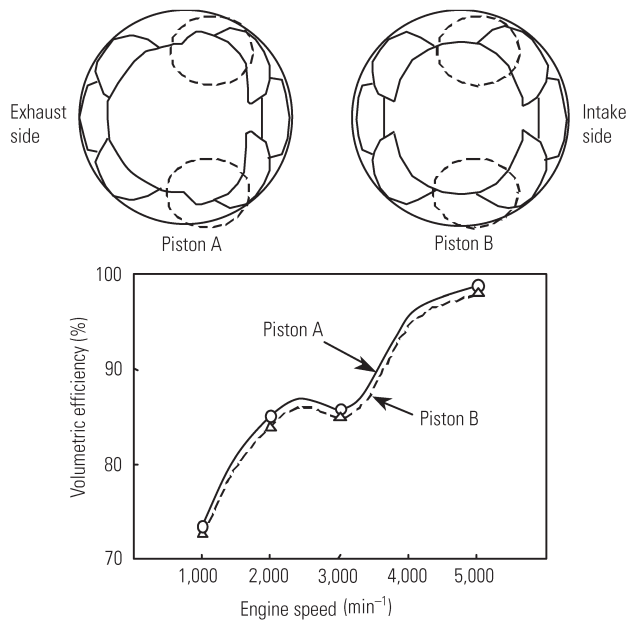


Fig. 17 Effect on full load volumetric efficiency of reduction in size of squish area in vicinity of intake valve

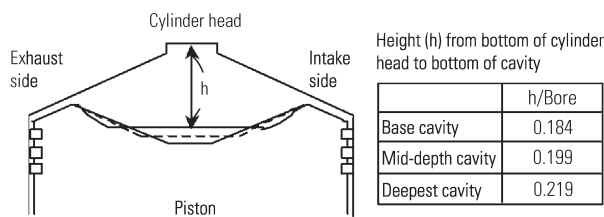


Fig. 18 Piston for evaluation of cavity depth

intake flow) is a key factor of the piston design for improvement of volumetric efficiency.

6. Effects on combustion of piston shape outside squish areas

To enable a slanted-squish piston to be used at a desired compression ratio, it is common practice to form a cavity in the middle of the piston crown such that the configuration of the cavity yields the desired compression ratio. The influence of the cavity on combustion was studied. For the cavity itself, the cavity depth was used as the main evaluation parameter. For the portion running from the cavity to each squish area, the angle of the slope was used as the main evaluation parameter.

Fig. 18 shows the respective shapes of evaluated pistons with different cavity depths. The index indicating the depth was designated " h " and taken as the distance from the bottom of the thread on the spark plug to the center of the piston crown. The h/Bore ratio is 0.18 – 0.22. It has been reported that the h/Bore ratio controls the timing of the collapse of tumble; the larger the h/Bore ratio, the later the collapse of tumble⁽⁵⁾.

Fig. 19 shows full load heat release rate and initial

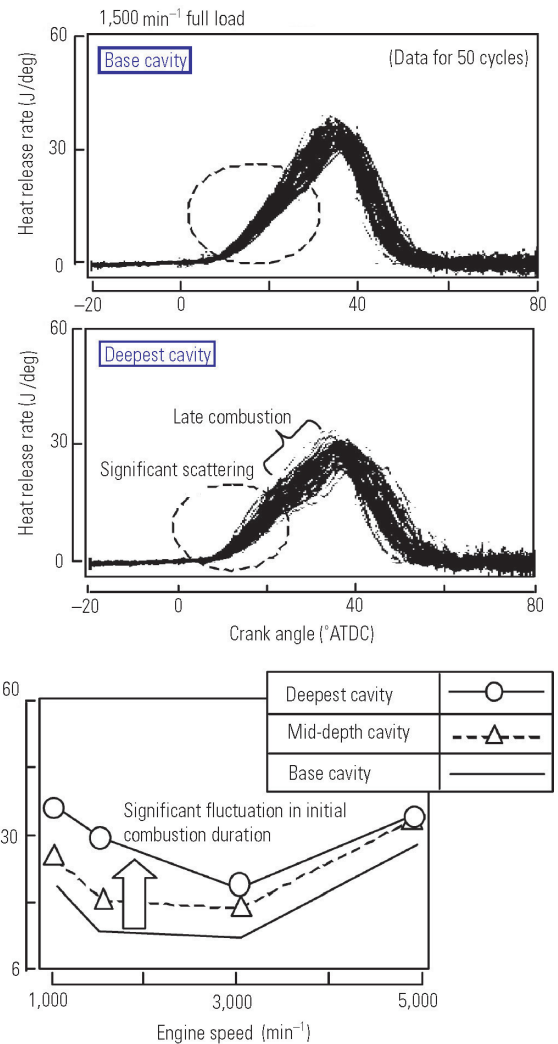


Fig. 19 Influence of cavity depth on combustion

combustion duration (0 – 10 %) variation (standard deviation / average value). With the piston containing the deepest cavity, there is significant scattering in the data for initial combustion. And it can be seen from comparison with data for the base piston that mid-period combustion with the piston containing the deepest cavity is sluggish. With a deep cavity and a concomitantly high h/Bore ratio, the tumble-collapse delay and the collapse itself are insufficient, apparently meaning that a bulk strong flow remains in the vicinity of the spark plug at the time of ignition such that initial combustion is unstable. With regard to the slowness of mid-period combustion, it can be inferred that the deep cavity makes the bulk flow-squashing effect weak such that the transformation into turbulence is insufficient.

Investigative comparisons of slanted-squish pistons and conventional-squish (horizontal-squish) pistons have yielded the view that reverse squish flow from the cavity separates on the sharply angled part of the piston at the squish entrance, thereby intensifying turbulence, with the result that knock is suppressed by acceleration of late-stage combustion⁽⁶⁾. In the study described in this paper, the influence of a slanted-squish piston was studied with three angles of the slope

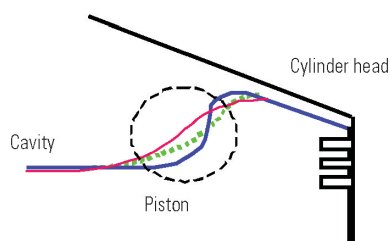


Fig. 20 Shape of slope from cavity to squish area

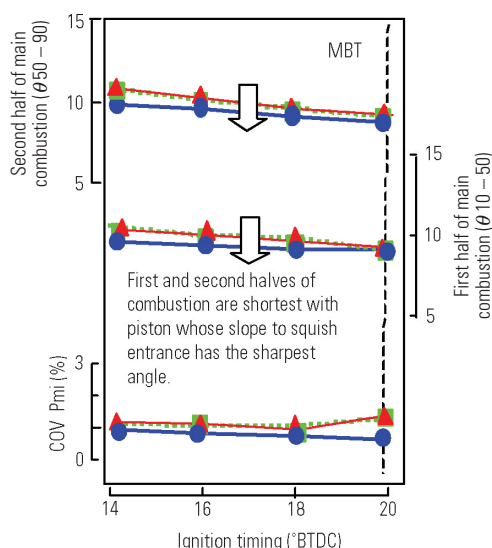


Fig. 21 Partial-load combustion durations

from the cavity.

Fig. 20 shows the respective shapes of the three evaluated pistons. The figure shows only the slope shapes in the intake-exhaust direction, but the slope shapes are the same in the engine's front-rear direction.

Fig. 21 shows the respective combustion durations of the three pistons under partial loading. With the piston whose slope to the squish entrance has the sharpest angle, the first half of the main combustion (10 – 50 % combustion) and the second half of the main combustion (50 – 90 % combustion) are both shorter than they are with the other pistons. Full load heat release rate is shown in Fig. 22. The most notable characteristic is that acceleration of combustion can be seen ATDC at 1,000 min⁻¹. (See the circled part of the figure.) This shows that it is possible to influence turbulence with a given slanted-squish piston by means of the design of the angle of the slope from the cavity. At 3,000 min⁻¹, however, in-cylinder turbulence is increased such that the difference in heat release between the evaluated pistons is smaller than at 1,000 min⁻¹. It can be said that the squish-area entrance angle is a crucial design factor.

7. Heat losses

Forming slanted squish and providing a cavity in the piston crown to achieve a suitable compression ratio

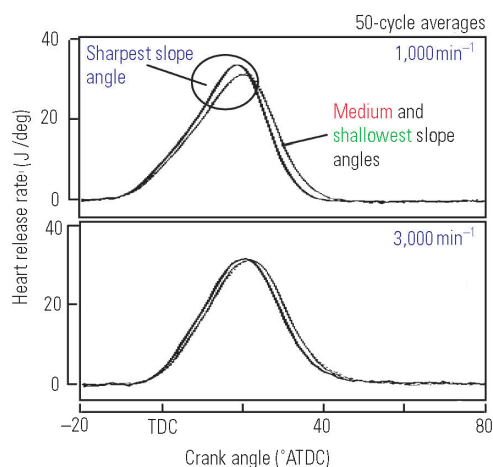


Fig. 22 Full load heat release

increase the surface area and thus they are disadvantageous against heat loss. Since combustion is promoted under partial loading with a slanted-squish piston, however, the minimum advance for best torque (MBT) is retarded such that the period in which the piston crown receives heat is shortened. At this point in the study, heat losses at MBT with a flat piston and with a slanted-squish were verified.

Fig. 23 shows indicated thermal efficiency against ignition timing. The ignition timing at which combustion is fastest and thermal efficiency is highest is later with the squish piston than it is with the flat piston. For each piston, the measured cylinder pressure at the point with maximum thermal efficiency was used in calculation of heat losses⁽⁴⁾. The results are shown in Fig. 24. With the flat piston, the ignition timing at which thermal efficiency is highest is relatively advanced so heat release starts relatively soon and heat losses are concomitantly high. For the squish piston, the calculations indicate heat losses almost the same as those for the flat piston, notwithstanding the squish piston's larger surface area. Even though a squish piston is inferior to a flat piston in terms of geometric surface area, then, the demerits of a squish piston in terms of heat losses can be minimized if ample consideration is given to combustion characteristics.

8. Summary

Squish area was studied mainly with respect to the influence of piston shape on combustion and volumetric efficiency. An understanding of the effects of the heights and shapes of squish areas and of the effects of the parts of a squish piston's crown outside the squish areas was gained. It was found that the angle of the slope from the cavity to the squish area and the cavity depth are crucial design factors and that the space formed by the piston below the intake valve influences volumetric efficiency.

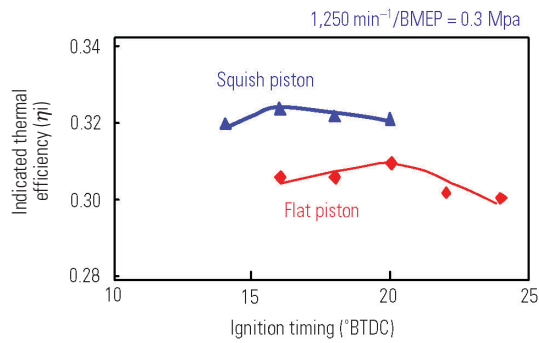


Fig. 23 Indicated thermal efficiency relative to ignition timing

References

- (1) Yoshikazu Ishikawa: "Key Factors in Gasoline Engine Design", Sankaido Publishing Co., Ltd., 2002
- (2) Takanori Ueda et al: "Effects of Squish Area Shape on Knocking", JSAE symposium proceedings, Vol. 982, p. 99, 1998
- (3) Michihiko Tabata, Masahiko Fujimoto, and Kohei Iwai: "Improvement of Knocking by Means of Tumble Flow and Reverse Squish Flow", Mazda Giho, No. 21, p. 192, 2003
- (4) Toshio Shudo and Hiroyuki Suzuki: "Research into Wall Heat Transmission Formulae with Hydrogen Engine", JSME transactions, Vol. 68, No. 673, p. 200, 2002
- (5) Makoto Kaneko, Susumu Kato, and Yohei Saishu: "Control of Spark-Ignition Engine by Means of Control over Tumble Generation and Collapse", Subaru Technical Review, Vol. 30, p. 117, 2003
- (6) Shinji Kojima: "Elucidation of Knock-Suppression Mechanism by Means of Combustion Simulation", Toyota Central R&D Labs R&D Review, Vol. 33, No. 3, p. 114, 1998

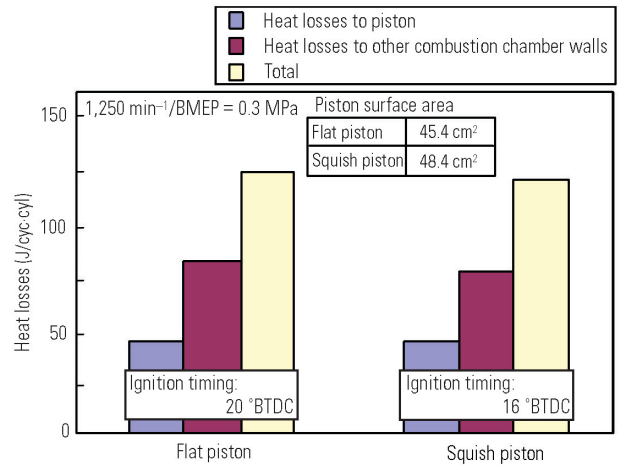


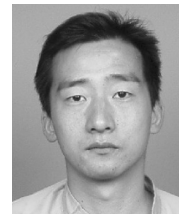
Fig. 24 Heat losses (approximate) with each piston type



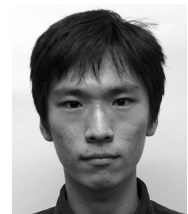
Katsuhiko MIYAMOTO



Yoshiyuki HOSHIBA



Kiyotaka HOSONO



Syunichi HIRAO

Development of Optimizing System for Engine Performance Simulator

Taizo KITADA* Masato KUCHITA* Shinji HAYASHI*

Abstract

With the recent advances in computer performance enabling massive calculations to be performed with ease, an optimization system was developed for our engine performance simulator. Multi-objective optimization with a genetic algorithm in iSIGHT™ was used for our system. In-house software using the Monte Carlo method and the response surface analysis was also developed. It was discovered that multi-objective optimization can produce a Pareto curve with fewer calculations, and the Monte Carlo method with the response surface analysis can show maps for visualizing the effect of control parameters on the objectives. Additionally, our developed optimization software has a dispersed processing function for sharing piled up calculation jobs among several personal computers. An overview of this function is also introduced.

Key words: CAE, Optimization, Genetic Algorithm, Monte Carlo Method, Response Surface Analysis

1. Introduction

Tremendous progress in computers has made it possible to calculate a massive volume of 0- and 1-dimensional calculations without difficulty. To date, effort has focused on obtaining optimum values by the smallest number of calculation trials using our accumulated experience. Recent progress has changed this: the computer can provide optimized values after a suitable algorithm was chosen for the target objectives. A term “paradigm shift”, which means that a current norm is changing, is often heard. There is now a paradigm shift in the field of CAE.

An engine performance simulator⁽¹⁾ with one-dimensional gas dynamics calculation and a vehicle fuel consumption and exhaust gas simulator⁽²⁾ have been developed in our company and have been widely used for developing new engines and refining production engines. An example of multi-objective optimization with a genetic algorithm in iSIGHT™ combined with in-house codes is introduced in this paper. Since in-house optimization software consisting of the Monte Carlo method and the response surface analysis has also been developed, its outline and some calculation results are also introduced.

2. Optimization calculation for engine performance simulator

2.1 Multi-objective optimization in iSIGHT™

The commercially available software iSIGHT™ has excellent functions for composing a series of processes in a GUI environment. Furthermore, this software automatically produces the optimal values after an optimizing algorithm is selected. Two genetic algorithms, NSGA-II⁽³⁾ and NCGA⁽⁴⁾, have been provided since

Version 8 of iSIGHT™. iSIGHT™ repeatedly performs the following processes: (1) partially changes the descriptions in input files; (2) runs the calculation code; (3) gathers objective values from the calculation results; and (4) revises the next input parameters from the objective values. At the end of sequential calculations, a Pareto curve (a set of Pareto solutions) can be produced. The user has to set an algorithm that manipulates the control parameters, taking the calculation category into consideration. **Fig. 1** shows an example of applying iSIGHT™ to our engine performance simulator. The series of the engine simulation is packed in a batch file.

Fig. 2 shows an example of optimizing maximum power and maximum torque for a 1.6-L engine by using the NSGA-II algorithm. The intake manifold length and diameter are defined as the control parameters.

The upper right figure shows the calculation results including 192 calculation points up to the 5th generation whose parent population is 32. A complete Pareto curve was generated. It can be seen in the Pareto solutions that three portions (A, B, and C groups) stand out. The A-group has torque advantage, the C-group has power advantage, and the B-group is concave between the other two groups in the Pareto curve. This means that the B-group is inefficient where the trade-off relationship between maximum torque and maximum power is distorted. This result suggests that the intake layout be redesigned from scratch in order to achieve maximum power or maximum torque around this area. Furthermore, it is not sufficient to revise only the intake manifold length and diameter.

Fig. 2 also shows many curves whose y-axis is engine torque or power and x-axis is engine speed. These curves are from ten Pareto solutions selected in increments along the Pareto curve. It can be seen that

* Advanced Powertrain Development Dept., Development Engineering Office

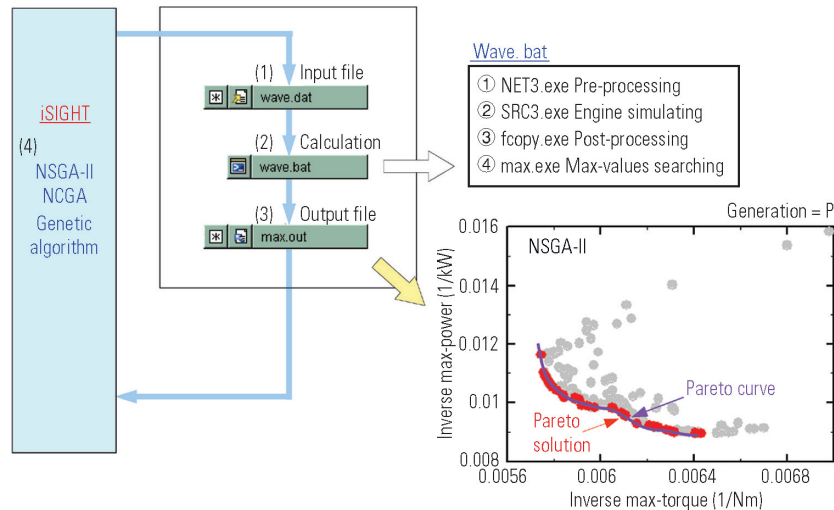


Fig. 1 Multi-objective optimization with iSIGHT™

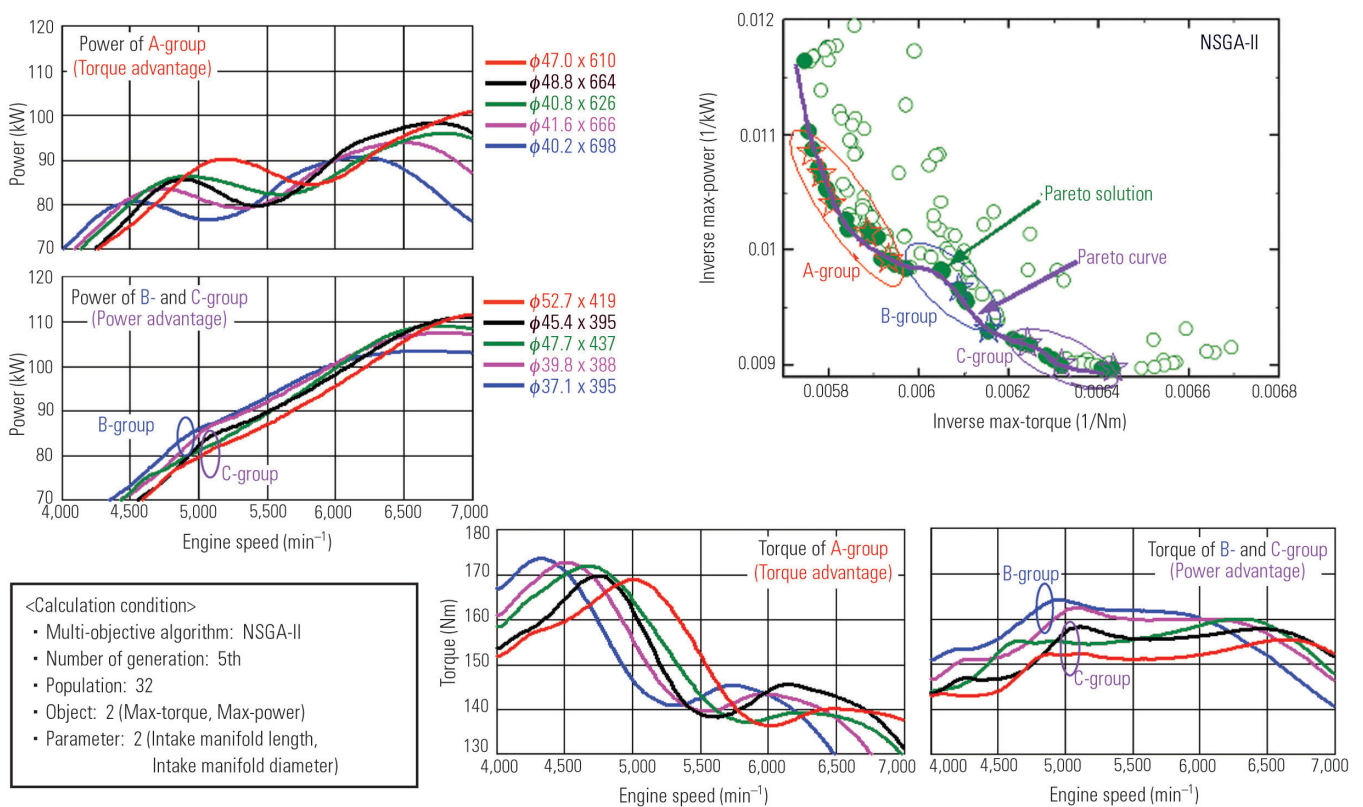


Fig. 2 Example of multi-objective optimization as engine maximum power and maximum torque (between intake manifold length and diameter)

the group of torque and power curves change in a cascading manner.

The control parameters, the intake manifold length and diameter, at each Pareto solution are written beside the power curves. These figures show that the longer intake manifold length brings the higher maximum torque because the length of the A-group is always longer than that of the C-group. On the other hand,

varying the intake manifold diameter does not produce any clear tendency in this analysis.

2.2 Searching optimum solutions with Monte Carlo method

2.2.1 Comparison with multi-objective optimization

The Monte Carlo method without any optimization

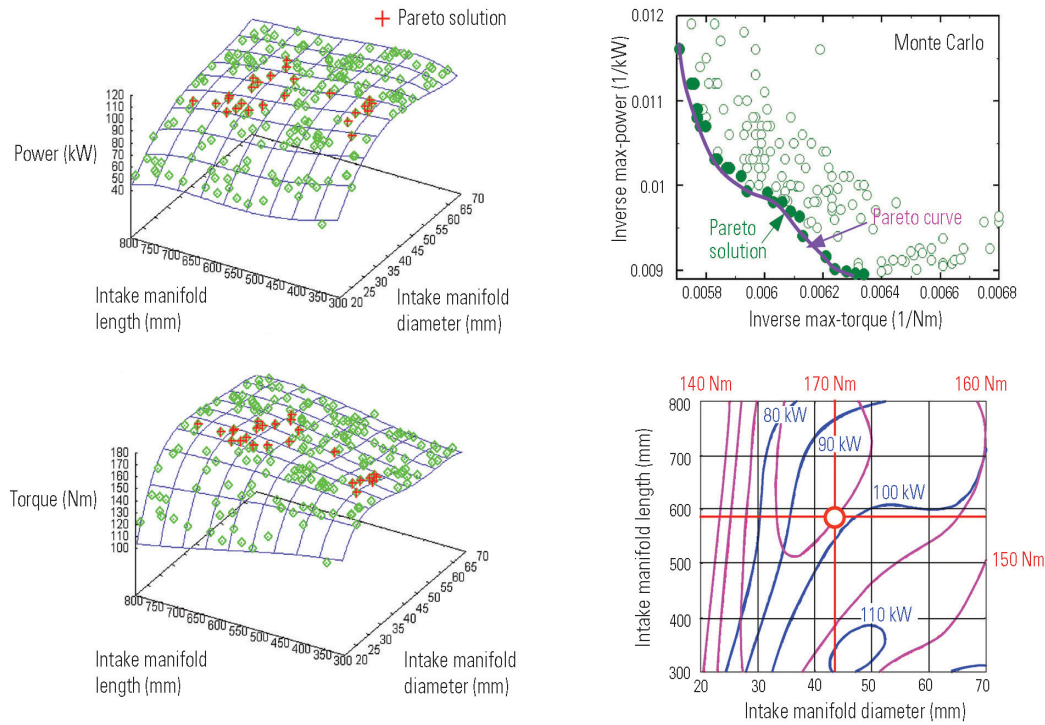


Fig. 3 Optimization by Monte Carlo method with response surface analysis

loops only yields the control parameters in random order. However, as shown in **Fig. 3**, a Pareto curve can be obtained similar to that of the multi-objective optimization using iSIGHTTM. Compared to **Fig. 2**, the Monte Carlo method allows many calculation points far from the Pareto curve.

2.2.2 Response surface analysis

Response surfaces⁽⁵⁾ of maximum torque and maximum power were acquired from the calculation results using the Monte Carlo method. The left graph in **Fig. 3** confirms that the majority of calculation points are on response surfaces.

The deviation between the calculation points and the response surface is no greater than 5 % even on the boundary of the calculation area both of the maximum torque and the maximum power, signifying good correlation. The figures are the plotted maximum torque or maximum power points. The + mark indicates a Pareto optimum solution.

As the calculation points are randomly scattered within a defined region in the Monte Carlo method, numerous excess calculations far from the optimal values are accidentally computed. However, these excess calculations can be used to depict a contour map, which helps us visually understand how the control parameters affect the objects. The chart in the lower right of **Fig. 3** shows the maximum torque contour lines superimposed on the maximum power contour lines. This helps us envision the preferred optimum dimensions. For instance, the answer for a proposal to take the utmost maximum power and keep the maximum torque around 170 Nm can be solved at a glance: the intake manifold length should be 590 mm and the diameter

should be 43 mm. This type of explanation can be very persuasive.

In addition, the map shows how the diameter of the intake manifold affects the maximum torque and maximum power, which cannot be understood in the prior multi-objective optimization. It is a general idea that the amount of airflow into a cylinder decreases as the intake manifold diameter is reduced. However, increasing beyond the optimal diameter is also undesirable because the squeezing of airflow into a cylinder, so called intake inertia effect, weakens due to the reduction of intake flow velocity.

2.2.3 Numeration of response surface

The response surface⁽⁵⁾ here is solved using multiple regression analysis, which regresses the calculated solutions to a curved surface expressed using the fourth function by minimizing the sum of the square of differences.

In concrete terms, when intake manifold length and diameter are expressed by x and y , and maximum torque or power is expressed by z , the surface is formalized as equation (1). Then the response surface can be defined with fifteen coefficients, a_0 to a_{14} .

$$z = a_0 + a_1x + a_2y + a_3x^2 + a_4xy + a_5y^2 + a_6x^3 + a_7x^2y + a_8xy^2 + a_9y^3 + a_{10}x^4 + a_{11}x^3y + a_{12}x^2y^2 + a_{13}xy^3 + a_{14}y^4 \quad (1)$$

Equation (2) is described for n calculation points.

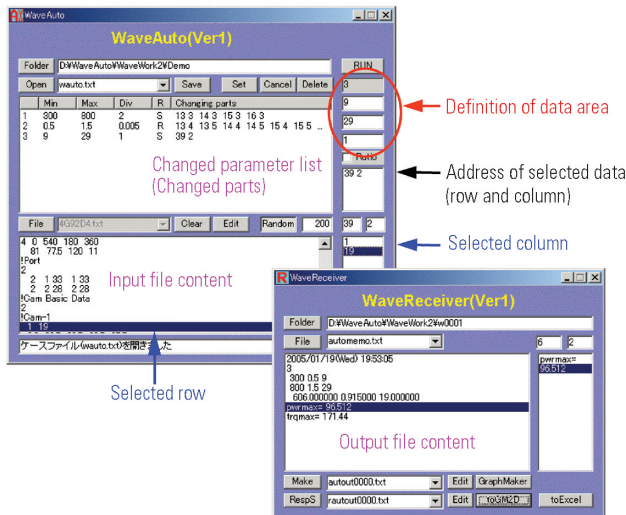


Fig. 4 In-house software WaveAuto and WaveReceiver

$$\begin{Bmatrix} Z_1 \\ Z_2 \\ \vdots \\ Z_n \end{Bmatrix} = \begin{Bmatrix} 1 & x_1 & y_1 & x_1^2 & x_1 y_1 & y_1^2 & x_1^3 & x_1^2 y_1 \\ 1 & x_2 & y_2 & x_2^2 & x_2 y_2 & y_2^2 & x_2^3 & x_2^2 y_2 \\ \vdots & \vdots & \vdots & \vdots & \vdots & \vdots & \vdots & \vdots \\ 1 & x_n & y_n & x_n^2 & x_n y_n & y_n^2 & x_n^3 & x_n^2 y_n \end{Bmatrix} \begin{Bmatrix} a_0 \\ a_1 \\ \vdots \\ a_{14} \end{Bmatrix} \quad (2)$$

$$\{Z\} = \{X\} \{A\} \quad (2')$$

The fifteen coefficients are obtained from the following equation (3):

$$\{A\} = (\{X\}^T \{X\})^{-1} \{X\}^T \{Z\} \quad (3)$$

3. In-house software (WaveAuto)

3.1 Overview of calculation system

It is not so difficult to make a kind of software that overwrites some figures with random digits in text-format input files and drives calculation codes. And iSIGHT™ has a license limitation. Taking into account the facts, in-house software seemed preferable. Then WaveAuto was developed for the optimization system combining the Monte Carlo method and the response surface analysis with an expectation that there would be many users in our company.

This software enables us to perform jobs using the Windows™ application shown in Fig. 4. A list describing the changed parameters is made by clicking the rows and columns of an input file. The software drives a predesignated calculation code the predefined number of times according to the list. Although WaveAuto was developed for our engine performance simulator,

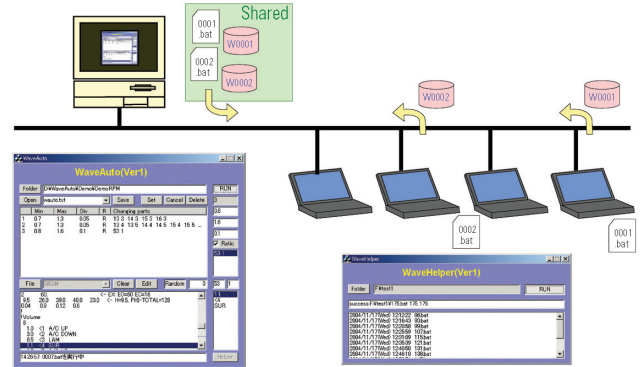


Fig. 5 Dispersed processing for optimization

its flexibility makes it possible to run any calculation code simply by changing the calculation code name and description of the procedures.

Because WaveAuto outputs are stored in separate files, another in-house code, WaveReceiver, was also developed for gathering the target data and packing them into one file. It computes the response surface analysis from the packed file. It is also possible to nominate gathered data by clicking rows and columns like WaveAuto.

3.2 Dispersed processing system

Our engine simulator consumes several tens of minutes even on the latest-model Personal Computer (PC) because the code has to solve one-dimensional gas dynamics calculation. Therefore, an in-house code named WaveHelper was developed to enable many calculations without stress. This software makes it possible to disperse the piled up jobs to several PCs. The system becomes available after a local PC with WaveHelper installed mounts a shared folder of the parent PC with WaveAuto installed, as shown in Fig. 5. WaveHelper repeatedly works the following jobs: brings back an operation sheet (batch file) issued by WaveAuto and a folder packed with input files and sends back the calculation results after finishing the job on a local PC according to the operation sheet. No software installation is required because the job uses the calculation codes in the parent PC. Also, no data remains on the local PC. These features make it possible for users to access idle PCs readily at home.

3.3 Example of using WaveAuto and WaveHelper

This system virtually eliminates time constraints and achieves large-scale calculations within a short time.

Fig. 6 shows example calculation results in the case of adding intake valve timing as a new control parameter to intake manifold length and diameter. Since the response surface, including valve timing, can be obtained in this method, a map at the specified valve timing can be depicted instantaneously. The map can express how the intake manifold length and diameter relate to maximum torque or maximum power at this valve timing.

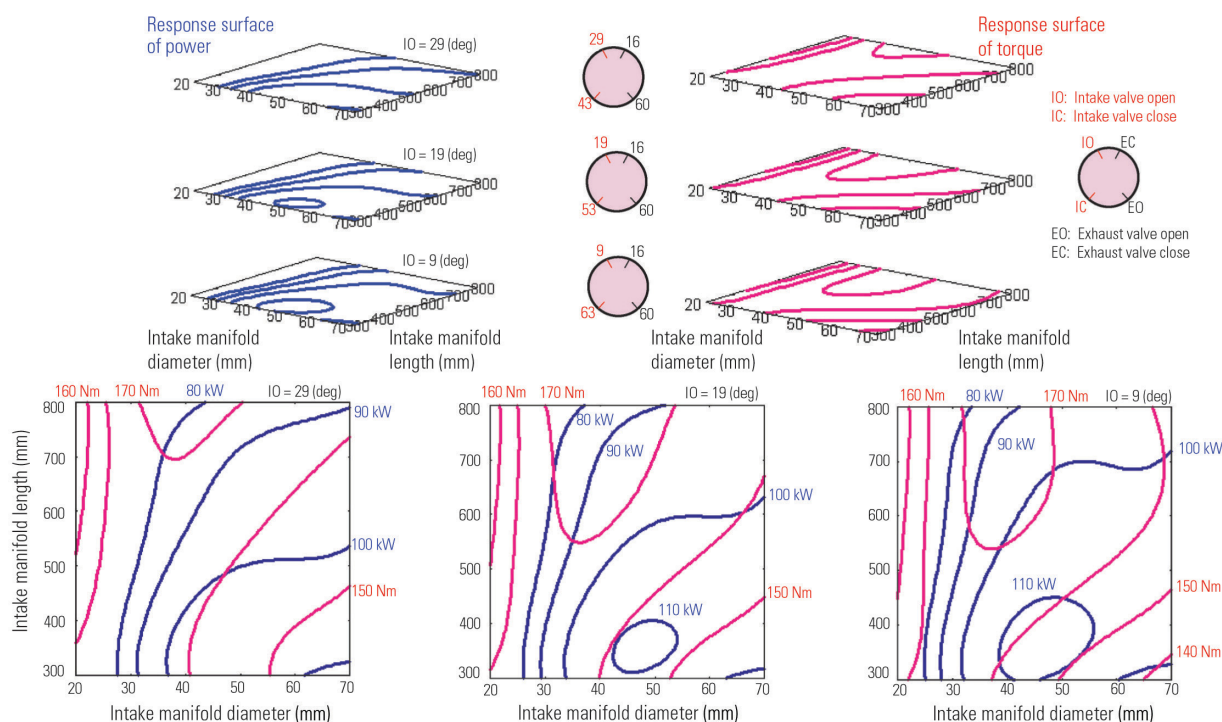


Fig. 6 Example of multi-objective optimization as engine maximum power and maximum torque (among intake manifold length, diameter and intake valve timing)

Fig. 7 shows how many calculation points are required to evaluate calculation results using a response surface. Maximum torque maps are drawn at each engine speed as the intake and exhaust valve timings are its control parameters. The maximum error in the upper graph is very small, up to 1.5 % (average error is 0.16 %), even in the case of 25 calculation points. No differences in features are found between the contour lines of 25 calculation points and those of 200 points.

The fourth function is applied to our response surface analysis; therefore, it is not possible to use it for multimodal solutions. Because our parameters affect simply engine performance, the fourth functional analysis can be applied to our target. Even a small number of calculation points can produce an accurate response surface.

Different types of variable valve timing devices are now generally equipped on passenger car engines. Intake and exhaust valve timings can be set for each engine speed. Therefore, when developing new engines, it would be advantageous to determine the best points beforehand using this kind of calculation. In addition, the maps enable us to set the design dimensions in the center of the circle for best performance. The red portion in the contour maps in **Fig. 7** indicates the high torque zone, which shifts according to engine speed.

3.4 Application to vehicle fuel consumption and exhaust emission simulator

WaveAuto was developed for our engine performance simulator, but it can also be applied to our vehi-

cle fuel consumption and exhaust emission simulator⁽²⁾. Mouse operation changes the operation panel as shown in **Fig. 8**.

Fig. 9 is an example of optimizing the results using this simulator. Japanese 10-15 mode fuel economy and 0 – 100 km/h acceleration performance are calculated for a manual transmission car, using three control parameters: vehicle weight, engine displacement and differential gear ratio.

The two lower cubes painted with the contour maps enable us to observe how the control parameters affect fuel consumption and acceleration time. The engine displacement, differential gear ratio and vehicle weight parameters correspond to the x, y and z axes, respectively. 150 calculation points are plotted in the upper left figure. The upper right is a map for observing at a vehicle weight of 1,150 kg. Lowering the differential gear ratio from 5.0 to 3.8 improves fuel economy provided that the acceleration time is the same, but lowering the ratio to less than 3.8 does not make any improvement.

For instance, as the differential gear ratio point is lowered from 5.0 along the 12.0 sec acceleration line, it continuously improves the fuel economy because of cutting across the 17.0 and 17.5 km/L fuel economy lines. However, it can be seen that the fuel economy does not improve below 3.8 because the fuel economy lines become parallel with the acceleration time lines.

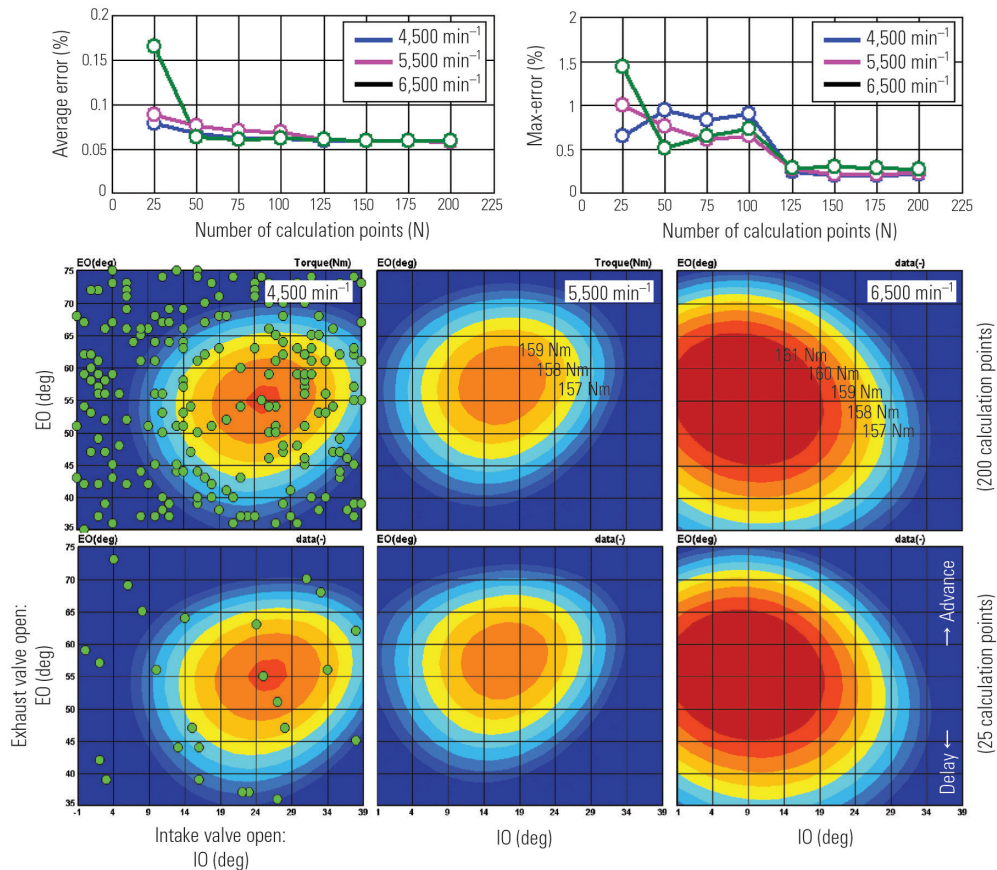


Fig. 7 Example of intake/exhaust valve timing optimization at each engine speed

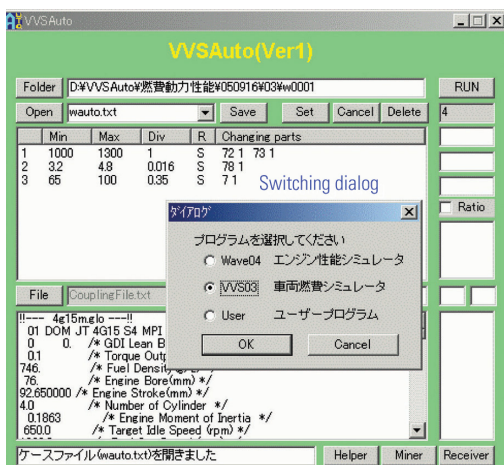


Fig. 8 Operation panel for vehicle fuel consumption and exhaust emission simulator

4. Summary

The multi-objective optimization with a genetic algorithm in iSIGHT™ seems suitable for heavy calculations such as 3-dimensional CFD because it is possible to obtain a Pareto curve with a smaller number of calculations. On the other hand, the Monte Carlo method with the response

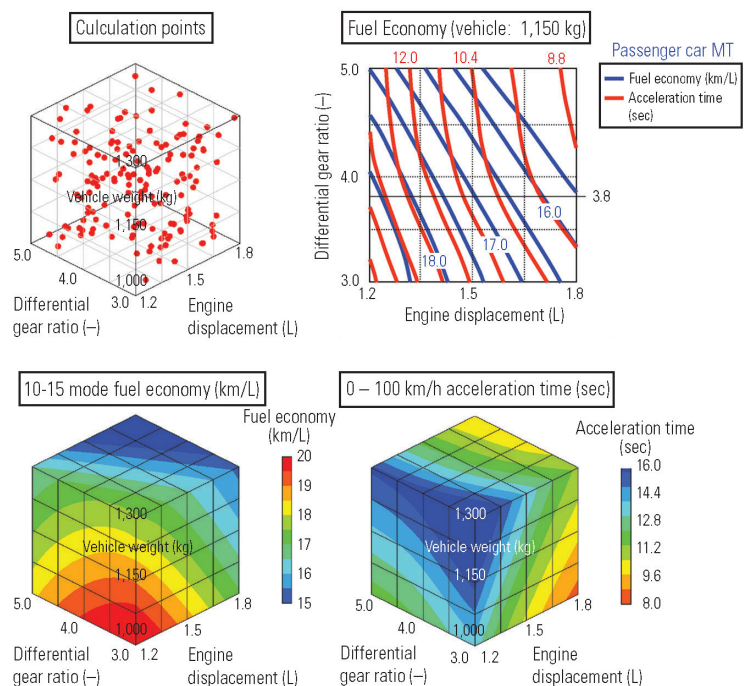


Fig. 9 Example of optimization for vehicle fuel consumption and exhaust emission simulator

surface analysis, at first glance, calculates unnecessary points scattered over the predefined area. However,

these excess calculation points can be used to depict a map providing a broad overview, which allows us to visually understand how control parameters affect the objectives. Therefore, this method seems to be appropriate for light calculations.

Since both methods are applied not only to CAE but also to experiments, availability would have to be verified.

5. Afterword

The near future vision with expectation of computer's progress, "our engine performance simulator can be running in a pocket during commuting", was mentioned in the Technical Review No. 11 seven years ago. Then nowadays it can run in a small pouch. The advent of the new age surprises us again. Since computer simulation becomes familiar and the cost has been reducing, a sort of the computer calculation maintaining adequate precision should be shifted to simulation from experiment. The shift gives us a big improvement on developments. And that comes to an authorized idea. On the other hand, introducing an optimization system enables everyone to get the best designing dimensions without any mistakes. But it looks like a double-edged sword because it includes a risk which robs engineers of chances to brush up their sensitivity. From here on,

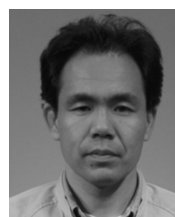
the way of searching the best dimensions efficiently as well as of improving engineers' sensitivity is needed and should be groped continuously.

References

- (1) T. Kitada, M. Kuchita, T. Ohashi: Mitsubishi Motors Technical Review No. 11, p. 29, 1999
- (2) M. Kuchita, T. Kitada, K. Kido: Mitsubishi Motors Technical Review No. 14, p. 16, 2002
- (3) K. Deb: KanGAL report 200001, Indian Institute of Technology, Kanpur, 2000
- (4) S. Watanabe, T. Hiroyasu, M. Miki: Late-Breaking Papers (GECCO), p. 458, 2002
- (5) S. Yamada: DOE (Methodology Edition) Nikka-Giren, p. 185, 2004 (in Japanese)



Taizo KITADA



Masato KUCHITA



Shinji HAYASHI

Development of Technique for Predicting Parts Temperatures Using Radiation Analysis

Tsuyoshi HAYASHI* Tetsuji UKITA*
Hiroki SETO* Masaki YANASE*

Abstract

The parts in a vehicle's engine compartment are exposed to a high-temperature environment. Among them, the parts positioned in the vicinity of the exhaust system become particularly high temperature owing to the effects of thermal radiation and convection⁽¹⁾. The amount of radiant heat transfer depends on geometrical conditions such as shapes and positional relationships of parts. It has recently become possible to calculate the amount of radiant heat transfer using computers. This paper describes a study of a technique for predicting parts temperatures using numerical analysis of the thermal radiation in the structurally complex area around the exhaust system.

Key words: Thermal Radiation, Exhaust System, Temperature Prediction, Numerical Analysis

1. Introduction

The thermal management needed to prevent occurrence of heat damage (deformation, deterioration, and melting) from being inflicted on a vehicle's parts is a crucial element for ensuring that the vehicle is reliable. In recent years, the need to quickly meet market requirements has created a need for the durations of development schedule to be shortened. In the early stage of development, therefore, design engineers must identify parts which have a risk of heat damage and consider effective countermeasures. To facilitate this work, it is necessary to devise techniques that enable part temperatures to be predicted at a stage of the development when a prototype vehicle has not yet to be built.

To predict part temperatures, it is necessary to accurately determine the amount of heat transfer from the vehicle's heat sources (the engine and exhaust system). In parts of the exhaust system, the surface temperature becomes particularly high (in excess of 600 °C) (Fig. 1). It is known that the amount of radiant heat emitted by a part's surface is proportional to the fourth power of the temperature⁽²⁾, so it is easy to imagine that the radiation from the surface of the exhaust system has a huge influence on the temperatures of nearby parts.

The amount of radiant heat transfer is determined by the surface temperature, the thermal emissivity, and the view factor (the positional relationship between the relevant parts). The thermal emissivity varies according to the coating and finish on the surface of each relevant part, so it needs to be determined by means of measurement. With regard to the view factor, values for complex shapes are extremely difficult to determine by manual calculation. However, it has recently become possible to calculate them using computers.

We are constructing a technique for predicting the temperatures of parts in the vicinity of the exhaust sys-

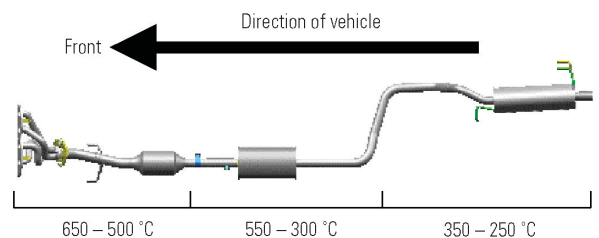


Fig. 1 Distribution of surface temperatures on exhaust system

tem from the results of numerical analysis of the radiant heat between the exhaust system and the nearby parts. The study is described in this paper.

2. Calculation of radiant heat flux

When the distribution of the surface temperatures on exhaust system is stable at a certain condition, the effect of radiation on nearby parts is determined by the parts' thermal emissivities and positional relationships with exhaust system parts. For evaluation of the effect of radiant heat on the surface of nearby parts, a technique was adopted whereby the shape of exhaust system parts and nearby parts was modeled, and the radiant heat flux on the part surfaces was calculated from the numerical analysis with the surface temperature and thermal emissivity used as boundary conditions. For convenience, the analysis is hereafter called "radiation analysis". The following text describes the method used to measure the thermal emissivity (needed as a boundary condition for the radiation analysis) and the radiation analysis itself.

* Performance Testing Dept., Development Engineering Office

Table 1 Thermal emissivity

Measurement point	Thermal emissivity	Reference material	Reference thermal emissivity
Heat protector	0.18 – 0.38	Polished metal surface	0.1 – 0.2
Engine block	0.45 – 0.69	Oxidized cast iron	0.5 – 0.7
Hanger rubber	0.95 – 1	Rubber	0.95

2.1 Measurement of thermal emissivity

The thermal emissivity was measured with the radiation thermometer and the contact-type thermometer. A radiation thermometer converts the radiant heat flux incident upon the measurement area into a temperature value in accordance with a preset value of thermal emissivity. If the preset thermal emissivity differs from the thermal emissivity of the part surface under measurement, the measurement value differs from the actual temperature. A decision was made to take advantage of this characteristic of radiation thermometers; a contact-type thermometer was used to take temperature measurements at the same time as temperature measurements were being taken using a radiation thermometer; comparison of the measurement values enabled estimation of the thermal emissivity.

The temperature of a part and the radiant heat flux radiated from the part have the following relationship:

$$q_{emi} = \varepsilon_{part} \cdot \sigma \cdot T_{part}^4 \quad (1)$$

where

q_{emi} : Radiant heat flux emitted from the part surface [W/m²]

ε_{part} : Thermal emissivity of the part surface [–]

σ : Stefan · Boltzmann constant [5.67 × 10^{–8} W/(m²·K⁴)]

T_{part} : Part temperature [K]

If, when the preset thermal emissivity of the radiation thermometer is 1, the measured temperature is T_{rad} , the relationship between the radiant heat flux incident upon the radiation thermometer q_{sensor} and the measured temperature is expressed by the following equation:

$$q_{sensor} = \sigma \cdot T_{rad}^4 \quad (2)$$

To prevent nearby parts from affecting the measurement performed using the radiation thermometer, the measurement was performed with the thermometer positioned as close as possible to the measurement area. Radiant heat emitted by the measuring instrument itself was reflected off the measurement area and came back to the measuring instrument. It is necessary to take this reflected heat into account. If thermal emissivity of the measuring part of the radiation thermometer is assumed to be 1, q_{sensor} is expressed by the following equation:

$$q_{sensor} = \varepsilon_{part} \cdot \sigma \cdot T_{part}^4 + (1 - \varepsilon_{part}) \cdot \sigma \cdot T_{sensor}^4 \quad (3)$$

where

T_{part} : Part temperature measured with the contact-type thermometer [K]

T_{sensor} : Temperature of the radiation thermometer itself [K]

Thus, the thermal emissivity of the part surface ε_{part} is, based on equations (2) and (3), expressed by the following equation:

$$\varepsilon_{part} = (T_{rad}^4 - T_{sensor}^4) / (T_{part}^4 - T_{sensor}^4) \quad (4)$$

As can be seen from equation (4), when the temperature of the part and the temperature of the radiation thermometer itself are equal, it is not possible to calculate the thermal emissivity. When measurements are taken, therefore, it is essential to keep the part temperature sufficiently higher than the temperature of the radiation thermometer itself. In this study, an actual vehicle was used; thermal emissivity was measured with the engine running and the exhaust system parts concomitantly hot. The results of measurements taken using this technique and typical values obtained from reference documentation⁽²⁾ are shown in **Table 1**. The measurement results show slight dispersion owing to differing extents of contamination and rust on part surfaces, but the values are more or less equivalent to the values in the reference documentation. Consequently, the validity of the technique was confirmed.

2.2 Radiation analysis

The analysis was performed using STAR-CD. To shorten the computational time with the radiation analysis, the flow field was not solved; computation was performed with respect to the radiant heat transfer only. The thermal emissivity obtained by means of measurement was set for the exhaust system and individual part surfaces; by inputting the exhaust system surface temperature, it was possible to determine the radiant heat flux of nearby parts. The radiation-analysis model addressed the radiant heat transfer between the exhaust system and part surfaces, so the Discrete Beam Method (DBM)⁽³⁾, which is advantageous for surface-to-surface analysis, was used. With the computation, the radiant heat flux incident upon part surfaces and the radiant heat flux emitted from part surfaces could be obtained. Through determination of the difference between them, the amount of net radiant heat flux on the part surfaces was calculated. Example results of radiation analysis are shown in **Fig. 2**. The red coloring indicates heating resulting from radiation, and the blue coloring indicates cooling resulting from radiation. The exhaust system mainly emits heat, so it is shown in blue. Nearby parts receive that heat, so they are shown in red.

3. Relationship between radiation and part temperatures

Employment of radiation analysis made it possible to calculate radiant heat flux on part surfaces. In actual vehicle development, however, the thermal reliability of parts is managed by allowable temperatures. With plastic and

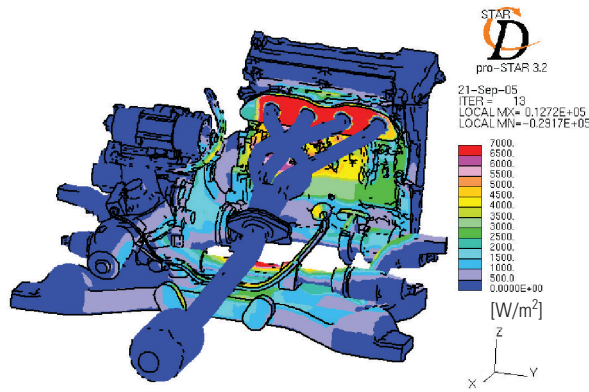


Fig. 2 Calculation example of radiant heat flux

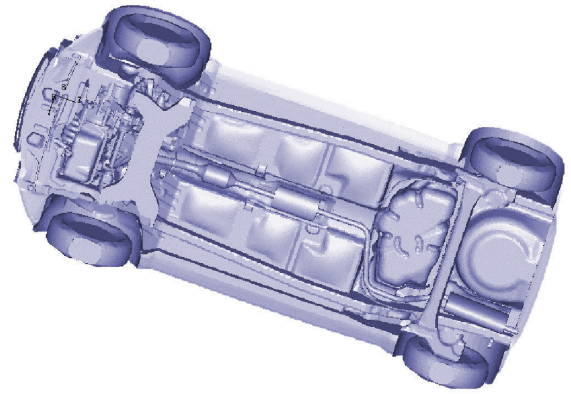


Fig. 3 Validation model

rubber parts (among the parts located near the exhaust system, these have relatively low allowable temperatures) used as study subjects, the following parts of this paper describe the thinking that forms the basis of the technique for predicting part temperatures. They also describe the outcome of an effort to verify the validity of the technique.

3.1 Derivation of theoretical equations

Parts in the vicinity of the exhaust system are influenced by radiation from the exhaust system surface, which is always extremely hot while the engine is running, so their temperatures are higher than the ambient temperature. If there were a complete absence of the effects of radiation and heat conduction, the part temperatures would be equal to the ambient temperature. With the extremely hot exhaust system nearby, however, the part temperatures rise owing to radiation from the exhaust system; the resulting differences between the part temperature and ambient temperature cause heat release from the part to the atmosphere. The extent of the increase in each part temperature at this time is determined by the balance between the amount of radiant-heat and the amount of heat released to the atmosphere.

If it is assumed that the effects of intra-part heat generation and heat conduction can be ignored with a plastic or rubber component, the balance of heat flux on the part surface is, with the radiation-caused heat flux designated q_{rad} and the convection-caused heat flux designated q_{con} , expressed by the following equation:

$$q_{rad} + q_{con} = 0 \quad (5)$$

Here, q_{con} is given by the following equation:

$$q_{con} = \alpha_{air} \cdot (T_{amb} - T_{part}) \quad (6)$$

α_{air} is the heat transfer coefficient; T_{part} is the part surface temperature; and T_{amb} is the ambient temperature. If the difference between the part temperature and the ambient temperature is treated as the radiant-heat-caused part temperature increase (hereafter designated ΔT), ΔT is, in accordance with equations (5) and (6), expressed by the following equation:

$$\Delta T (= T_{part} - T_{amb}) = q_{rad} / \alpha_{air} \quad (7)$$

From equation (7), it can be seen that the part temperature increase caused by radiant heat flux is proportional to the radiant heat flux and inversely proportional to the heat transfer coefficient.

The relationship between radiation and part temperatures was thus clarified by means of theoretical equations. To verify the validity of equation (7), radiation analysis and a test involving measurement of part temperatures in an actual vehicle were performed. The verification method and results are described hereafter.

3.2 Verification method and results

For verification purposes, the correlation between the results of temperature measurements performed on an actual vehicle and the radiant heat flux indicated by radiation analysis was investigated. The test subject was an MMC compact passenger car with a 1.5-liter gasoline engine.

The actual-vehicle test was performed in a wind tunnel; the surface temperature of the exhaust system T_{exh} , the surface temperature of a part T_{part} , and the ambient temperature T_{amb} were measured in under constant conditions, and the radiation-caused temperature increase ΔT was determined from them. The wind tunnel permitted the outside air temperature, the wind speed, the humidity, and the running load to be controlled independently of each other, so it permits various running conditions to be simulated.

The analysis model used in the radiation analysis is shown in Fig. 3. The model simulates the engine compartment and underfloor area in detail; it faithfully reproduces the shapes of the engine, exhaust system parts, and heat insulators and the shapes of wiring harnesses, hanger rubbers, and other parts near the exhaust system. The temperature boundary conditions were given to match those in the actual-vehicle test to enable analysis corresponding to the actual vehicle. With a front-pipe hanger rubber (a parts located near the exhaust system; mentioned hereafter as the "hanger rubber") treated as the subject, the text hereafter describes the verification process and the results thereof. In the verification process, the surface tem-

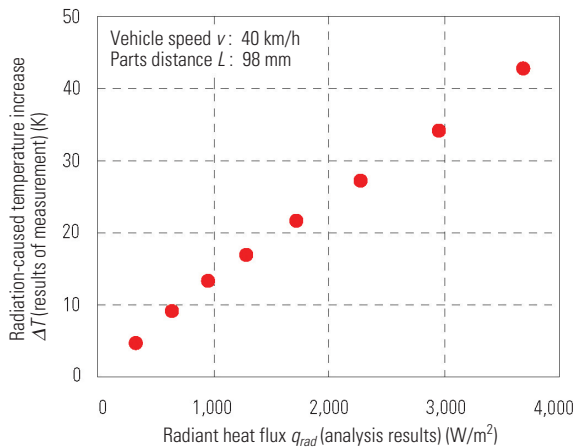


Fig. 4 Relationship between radiant heat flux and increased amount of parts temperature

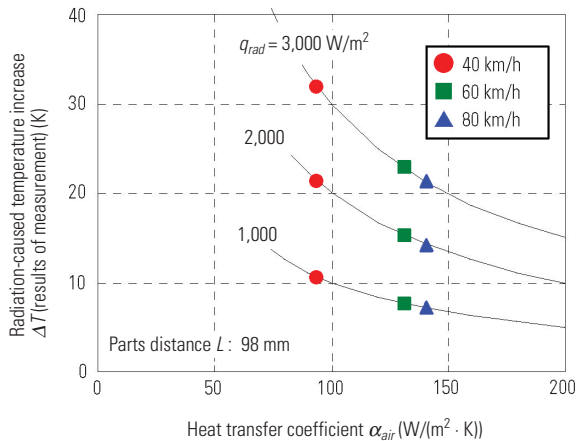


Fig. 5 Influence of vehicle speed v

perature of the exhaust system T_{exh} , the distance between the exhaust system and hanger rubber L , and the vehicle speed v were used as parameters.

(1) Influence of surface temperature of exhaust system

Fig. 4 shows the relationship between the ΔT values obtained in an actual-vehicle test and the radiant heat flux obtained using radiation analysis with respect to a vehicle speed v of 40 km/h, a distance between the exhaust system and hanger rubber of $L = 98$ mm, and various exhaust system surface temperatures. Each point corresponds to a different exhaust system surface temperature; the higher the temperature, the higher the radiant heat flux q_{rad} . From the high degree of correlation between ΔT and the radiant heat flux, it can be seen that ΔT and the radiant heat flux have a proportional relationship and that they are consistent with the trend indicated by equation (7).

(2) Influence of vehicle speed

For verification of the influence of the heat transfer coefficient, a study in which the vehicle speed was varied was performed. **Fig. 5** shows the relationship between ΔT and the coefficient of heat transfer α_{air} with a distance between the exhaust system and hanger rub-

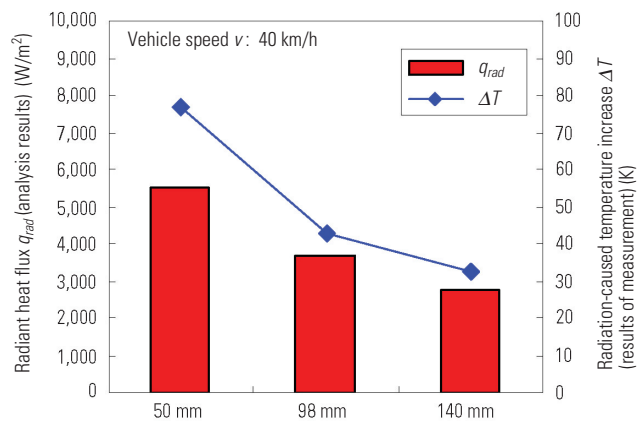


Fig. 6 Influence of parts distance L

ber of $L = 98$ mm and various values of vehicle speed v in the 40 – 80 km/h range. As shown, when the vehicle speed increased, the heat transfer coefficient increased and ΔT decreased. It means that increasing the wind speed around the part promoted the heat release from the part surface. It can be seen, therefore, that the heat transfer coefficient and ΔT have an inversely proportional relationship. The proportional relationship between ΔT and the radiant heat flux is maintained at each vehicle speed, substantiating the relationship indicated by equation (7).

(3) Influence of distance

Fig. 6 shows the relationship between ΔT and the radiant heat flux with a vehicle speed of $v = 40$ km/h and various distances between the exhaust system and hanger rubber L . Increases in the distance made the radiant heat flux weaker, and the same results were obtained by means of radiation analysis. Also, the correlation between the radiant heat flux and ΔT was maintained, indicating that equation (7) could, even with respect to changes in the distance, be used for approximate evaluation.

(4) Influence of location

As explained thus far, it was verified, with only the hanger rubber treated as the subject, that radiation analysis could be used to evaluate ΔT . Hereafter, an example of application to other parts is described. **Fig. 7** shows the results of radiation analysis of parts A, B, and C located in the engine compartment near the exhaust system, and **Fig. 8** shows the correlative relationship between the radiant heat flux and ΔT at each measurement point. From these figures, it can be seen that the heat transfer coefficient was approximately the same at parts B and C and that it had a lower value at part A. It can be assumed that these results occurred because of the different positions of the parts: Whereas part A was positioned behind the engine, parts B and C were positioned under the floor and were thus more exposed to air flow. When the technique for predicting part temperatures using radiation analysis is used, then, the air flow inside the engine compartment must be taken into account in estimation of the coefficient of heat transfer.

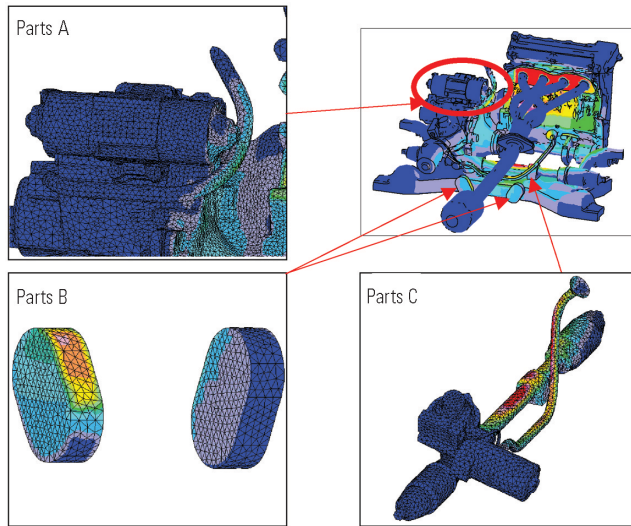


Fig. 7 Radiant heat flux distribution on parts near exhaust system

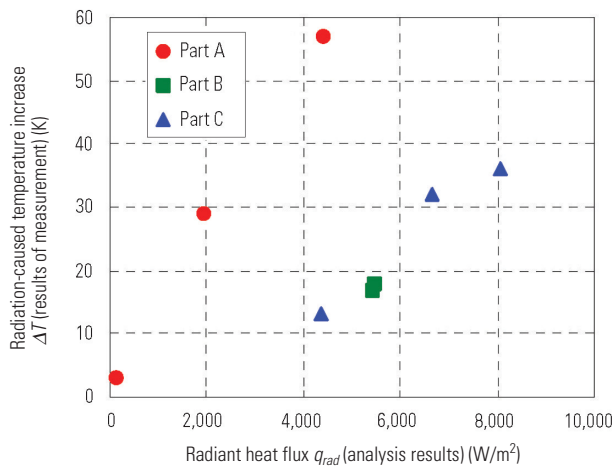


Fig. 8 Influence of parts location

4. Study of technique for predicting temperatures using radiation analysis

In the study described thus far, the relationship between the radiant heat flux and part temperatures was investigated and it was verified that the radiation-caused increase in part temperature ΔT was proportional to the radiant heat flux q_{rad} and that it could be evaluated using analysis of the radiant heat flux. In actual vehicle development, however, part temperatures are not managed using ΔT alone; it is ultimately necessary to predict the part temperatures themselves. In the next part of the study, therefore, a technique for predicting part temperatures using the results of radiation analysis was studied. An overview of this technique and an example of the technique's application are given hereafter.

4.1 Overview of prediction technique

If equation (7) is rearranged with respect to the part

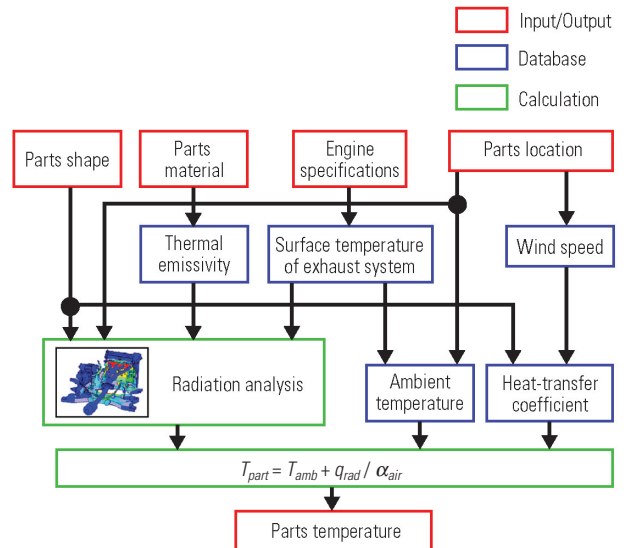


Fig. 9 Process for parts temperature prediction

temperature T_{part} , it is possible to obtain the following equation:

$$T_{part} = T_{amb} + q_{rad} / \alpha_{air} \quad (8)$$

Prediction of part temperatures was performed using this equation. Fig. 9 shows an outline of the prediction technique. The part shape, part location, part material, and engine specifications are inputted. The ambient temperature around the part, the radiant heat flux, and the heat-transfer coefficient of the air around the part are then calculated for running conditions assumed by means of a database and analysis. Finally, the obtained values are substituted into equation (8) for prediction of the part temperature.

4.2 Example of application of temperature-prediction technique

The database used for deduction of the ambient temperature and heat-transfer coefficient was constructed from basic data measured on the compact car (equipped with a 1.5-liter gasoline engine) that was used in the part of the study described in the previous section of this paper. This database was used in prediction of part temperatures in a car of the same class as the aforementioned compact car but was completely different from it in terms of upper body, platform, and engine (a 1.5-liter turbocharged gasoline engine). The subject car had two hanger rubbers in approximately symmetrical positions on the left and right of the exhaust system (Fig. 10). Radiation analysis was performed with respect to each of the hanger rubbers, and the part temperatures were then predicted. For running conditions, uphill driving at a speed of 40 km/h was assumed. Part temperatures under constant conditions were assumed. The prediction results and the results of an actual-vehicle test are shown in Table 2. With regard to ΔT , the predicted temperatures are almost the same with measured temperature (with prediction

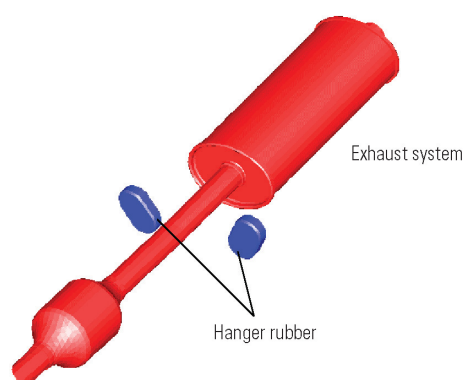


Fig. 10 Computational model for study of technique for predicting parts temperatures

errors not exceeding about 2 °C). With regard to the ambient temperature, however, there were prediction errors of about 10 °C, meaning that problems remained to be overcome for accurate component-temperature prediction.

4.3 Discussion

In the verification process, ambient temperatures established using a database based on actual-vehicle values contained large errors, indicating that, even with cars that have the same dimensions as each other, the temperatures and wind distribution in the engine compartment and under the floor differ greatly between models. For greater prediction accuracy, it is necessary to create a prediction technique that takes airflow fields into account.

With regard to ΔT , by contrast, good prediction results were obtained using radiation analysis. Consequently, it can be assumed that prediction of ΔT using radiation analysis is effective with various plastic components, rubber components, and vehicle models and that the influence of radiation can be approximately evaluated using this technique.

5. Summary

A part temperature prediction method using radiation analysis was studied to predict the part temperature at the early development stage.

The part temperature heated by radiation becomes higher than the ambient temperature. The increase (designated ΔT in the study) is proportional to the radiant heat flux. It was found that, with parts made of plastic or rubber (such parts have no heat generation in itself), this relationship generally exists and can be employed regardless of the vehicle model. Consequently, it was verified that radiation analysis could be used to predict ΔT .

6. Afterword

With regard to prediction of the ambient temperature, which is, together with radiation, a critical factor

Table 2 Results of parts temperature prediction

	Ambient temperature		ΔT		Parts temperature	
	Left	Right	Left	Right	Left	Right
Predicted temperature	80 °C		11 °C		91 °C	
Measured temperature	70 °C	72 °C	9 °C	12 °C	79 °C	84 °C
Error	+10 °C	+8 °C	+2 °C	-1 °C	+12 °C	+7 °C

determining the temperatures of parts near the exhaust system, three-dimensional heat-flow analysis and system analysis of the cooling and exhaust systems are under study. Ultimately, combining radiation analysis with these forms of analysis can be expected to enable further improvements in the accuracy of part temperature prediction.

The study described in this paper dealt with part temperatures in constant conditions, but other challenges (for example, handling of transient temperature characteristics and prediction of the temperature of the exhaust system surface itself) remain to be addressed. We will continue studying techniques for prediction of part temperatures with a view to shortening development periods and improving reliability.

References

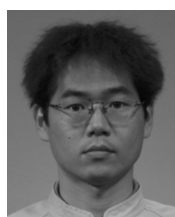
- (1) T. Hayashi, et al: A Study of Prediction Method of Thermal Radiation from an Exhaust System with CAE, JSAE 2005 Annual Congress (Autumn) Proceedings No. 115-05, p. 11-16, 2005
- (2) JSME Data Book: Heat Transfer, 4th Edition, pp. 156-189, published by Maruzen Co., Ltd., Tokyo, 1986
- (3) STAR-CD version 3.22, Radiation Computation Settings, p. 2, published by CD-adapco Japan Co., Ltd., 2004



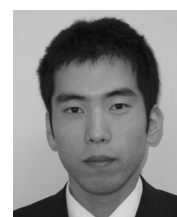
Tsuyoshi HAYASHI



Tetsuji UKITA



Hiroki SETO



Masaki YANASE

Basic Study for Reducing Noise in a Vehicle Cavity (Experimental and Theoretical Analyses of Structural – Acoustic Coupling Problems in a Rectangular Parallelepiped Space)

Hiroyuki SEINO*

Abstract

In this study, low frequency booming noise of wagon and minivan-type vehicles is clarified from a dynamics perspective and an effective reduction method is proposed according to some experimental and theoretical analyses. First, the phenomena of low frequency booming noise are discussed dynamically as structural – acoustic coupling system by using rectangular parallelepiped test rig and one-dimensional theoretical model. Second, the unique optimum method that reduces booming noise at structural – acoustic coupling system with a dynamic vibration absorber is proposed based on a one-dimensional theoretical model. Finally, the proposed method is examined in an actual vehicle and it is confirmed to be satisfactory for reducing low frequency booming noise.

Key words: *Vibration, Noise, Optimum Design*

1. Introduction

In vehicle development, cabin quietness is a crucial performance attribute for which there is a high level of demand. The study described in this paper was performed for elucidation and reduction of low frequency booming noise (a phenomenon that detracts from quietness) in wagon and minivan-type vehicles. In this context, low frequency booming noise is defined as the phenomena caused by the engine force and road-surface inputs during vehicle operation and excited by the low-order longitudinal modes of the system composed of the panel sections – windshield, tailgate, etc. – that surround the cabin coupled with the cabin space.

As a means of analyzing low frequency booming noise, structural – acoustic coupling analysis using large-scale finite-element models has thus far been widely used. For analysis with this method, however the model creation requires the production of detailed drawings, meaning that the method is hard to use effectively at early stages of development. To ensure a high level of quietness, effective structural proposals are required at early stages of development. For that purpose, it is essential to have a dynamic understanding of the phenomena of low frequency booming noise.

Consequently, the authors sought to ascertain the phenomena of low frequency booming noise in wagon and minivan-type vehicles from a dynamic perspective and, in accordance with these results, proposed a method for reducing low frequency booming noise. The authors also applied their proposed method to an actual vehicle and summarized the results. The abstract of this paper is introduced here. For details, please refer

to reference documents (1) through (4).

2. Analysis of a vehicle's low frequency booming noise

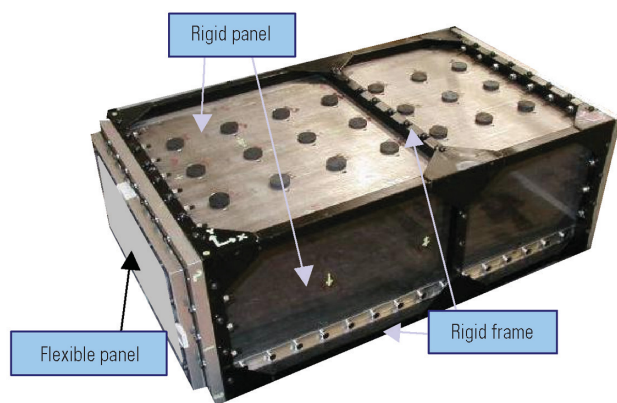
Firstly, an actual vehicle was subjected to an excitation test and its low frequency booming noise was experimentally investigated. The results were compared with results of analysis performed using the finite-element method. Consequently, with the coupling of the acoustic system and structural system taken into account, it was deemed that the analysis results closely matched the experimental results. It was thus deemed necessary to treat the phenomena of low frequency booming noise as a structural – acoustic coupling problem.

3. Experimental analysis and theoretical consideration of rectangular parallelepiped space

In accordance with the aforementioned results, a rectangular parallelepiped test rig replicating a vehicle cabin (**Fig. 1**) was created and the structural – acoustic coupling problems were experimentally investigated to detailed study. This model was designed so that the primary eigen frequencies of the panel and acoustic system came close to each other.

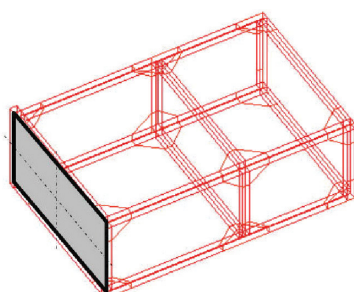
There are various types of problem for the low frequency booming noise of wagon and minivan-type vehicle. Classified with respect to the basic model, they are as follows: a rectangular parallelepiped closed space where one side is a flexible panel (**Fig. 2 ①**); a rec-

* FF Vehicle Testing Department, Development Engineering Office

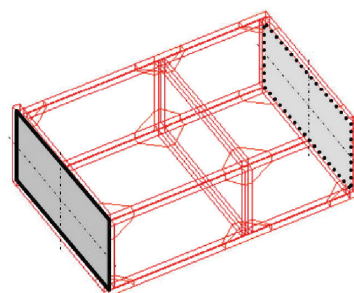


- Rectangular parallelepiped test rig: 800 mm x 400 mm x 200 mm
- Eigen frequency of acoustic system: 1,344.6 rad/s
- Flexible panels attachable to opposite sides
- Eigen frequency of frames: above 2,500 rad/s

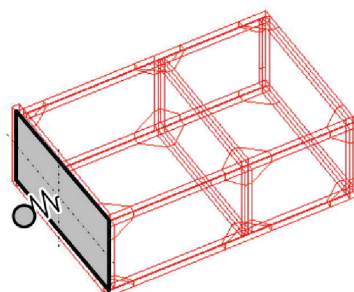
Fig. 1 Test rig



① One side coupled



② Two sides coupled



③ One side coupled with spring-mass system

Fig. 2 Modeling of booming noise problem

tangular parallelepiped closed space where two opposing sides are flexible panels (Fig. 2 ②); and a rectangular parallelepiped closed space where one side is a flex-

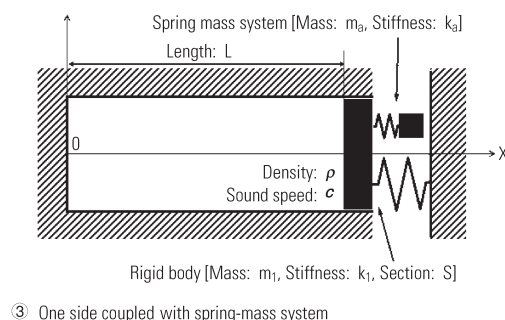
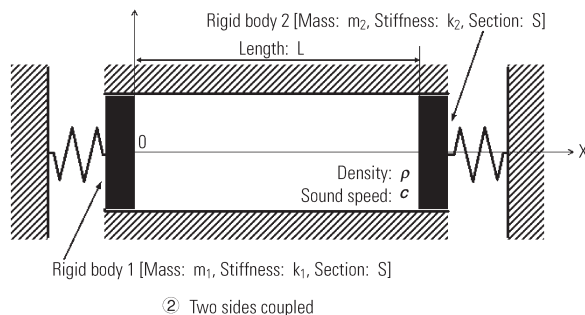
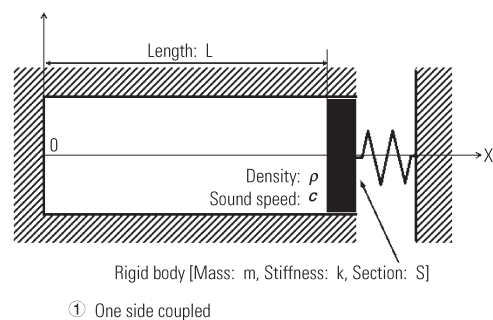


Fig. 3 One-dimensional model

ible panel with spring-mass system (Fig. 2 ③). Problem ① is based on the assumption that the tailgate makes a significant contribution to low frequency booming noise. Problem ② is based on the assumption that the tailgate and windshield make a significant contribution to low frequency booming noise. And problem ③ is based on the assumption that accessories are mounted on the tailgate.

With respect to these cases, characteristics related to eigen frequency, mode shape, and frequency response function were summarized from experimental data. For details, refer to the referenced documents.

Next, for theoretical analysis of these characteristics, the structural – acoustic coupling system was modeled by means of the one-dimensional physical models shown in Fig. 3 and Lagrange equation was applied. The theoretical analysis of this equation proved that the experimentally obtained characteristics could all be described using the model.

Through this work, it is considered that a basic theory that is effective at early stages of vehicle development was derived. The basic characteristics of prob-

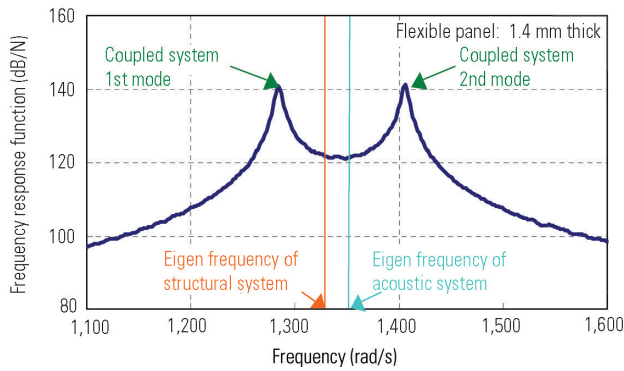


Fig. 4 Frequency response function of sound pressure

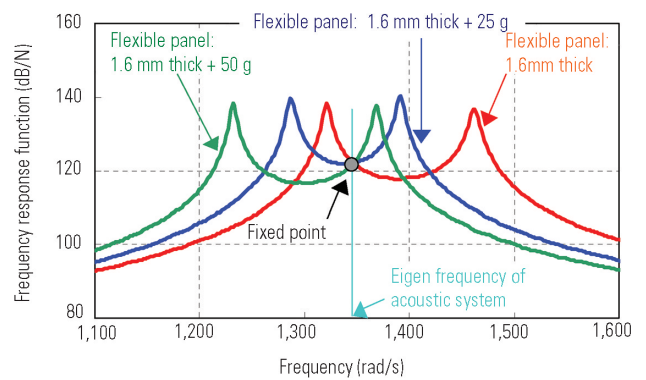


Fig. 6 Fixed point of frequency response function

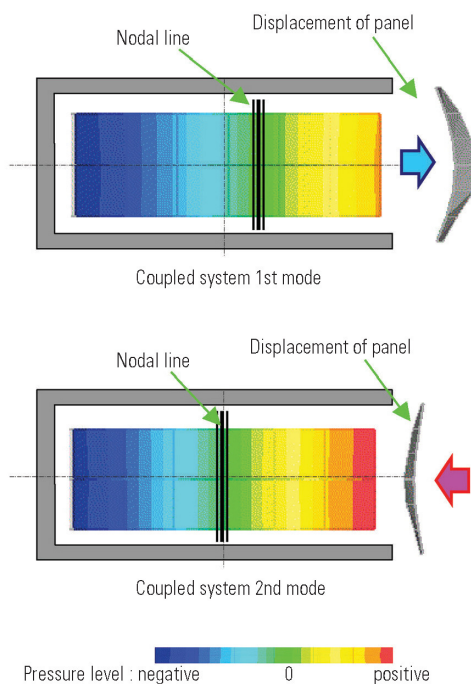


Fig. 5 Mode shapes of test rig with flexible panel at one side

lems ① – ③ are described hereafter.

3.1 A rectangular parallelepiped closed space where one side is a flexible panel⁽¹⁾

- Since the structural system and acoustic system are coupled, the coupling system's eigen frequency is different from the respective eigen frequencies of the individual systems (Fig. 4).
- In accordance with the positive and negative values of the sound pressure neighboring the structural system, the phase relationship of the structural system with respect to the acoustic system is always inside-outside with the coupling system 1st mode and outside-inside with the 2nd mode as seen from the inside of the acoustic system (Fig. 5).
- Regardless of the characteristics of the structural system, the frequency response function of the sound pressure when the structural system is vibrat-

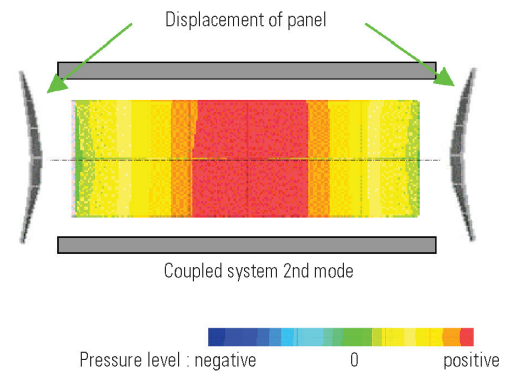


Fig. 7 Mode shape of test rig with flexible panels at opposite sides

ed is always a constant value at the eigen frequency of the acoustic system. In other words, a fixed point exists (Fig. 6).

3.2 A rectangular parallelepiped closed space where two opposing sides are flexible panels⁽²⁾

- The kind of sound-pressure mode shape – center of the rectangular parallelepiped is the thickest – seen with an acoustic system that has both ends open is evident (Fig. 7).
- Regardless of the characteristics of the vibrated structural system, two fixed points exist in the frequency response function of the sound pressure.

3.3 A rectangular parallelepiped closed space where one side is a flexible panel with spring-mass system⁽³⁾

- Owing to the characteristics of the spring-mass system, it is possible to avoid the frequency response function fixed point that was confirmed with one coupled side (Fig. 8).

4. Minimization of acoustic pressure by means of dynamic vibration absorber⁽⁴⁾

With a focus on the effects of the spring-mass system upon the sound pressure, a study was made with regard to the utilization and optimal design method of a

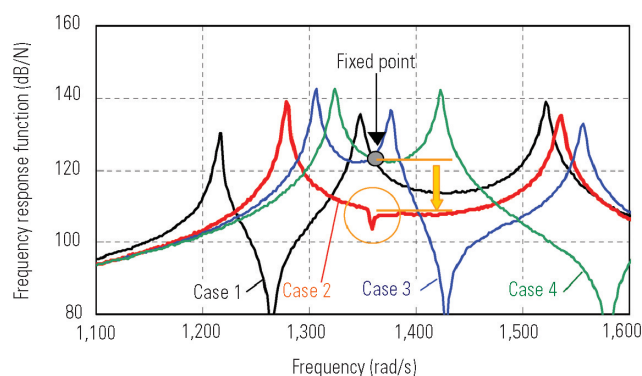


Fig. 8 Avoidance of a fixed point

dynamic vibration absorber from the viewpoint of making active use for reducing low frequency booming noise. The conventional design optimization method, using fixed point theory, could not be applied, so a new method, whereby the successive approximation method is employed such that a one-dimensional model can be used for optimal design of the structural – acoustic coupling system, was proposed. (The guideline for design optimization is to make the sound pressure level the same at the two eigen frequencies derived from the structural system.) The test rig was used to verify the results of theoretical analysis, and the theory was confirmed to be valid.

5. Application to vehicle

The validity of all of the obtained results was studied using an actual vehicle. The eigen frequency and mode shape characteristics were reproduced, so the theory was confirmed to be valid. Also, it was verified that the dynamic vibration absorber adopted in line with the proposed design optimization method was an effective means of reducing low frequency booming noise (Fig. 9).

6. Postscript

Due to the limitation on the number of pages, the author regrets that specific details had to be omitted, but it would be the author's greatest pleasure if any of the readers have become interested. The author recommends reference to the four aforementioned documents.

The author wishes to take this opportunity to express gratitude to Professor Kimihiko Yasuda of Aichi Institute of Technology for considerate, long-term guidance that enabled the study to be brought to conclusion as well as to the staff of Vehicle Providing Department for valuable advice about experiments.

The author received a Doctor of Engineering with this dissertation.

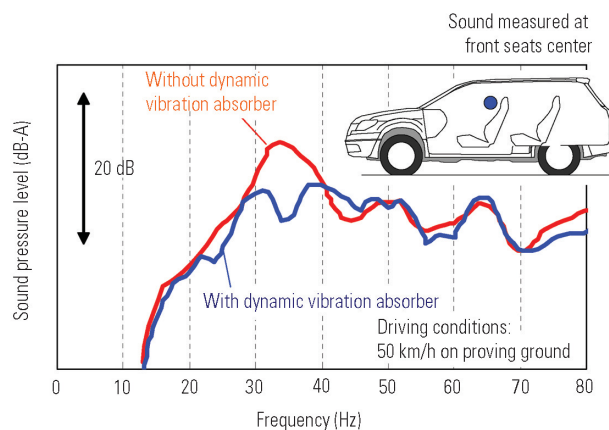


Fig. 9 Reduction of booming noise

References

- (1) Hiroshi Yamauchi, Hiroyuki Seino, and Kimihiko Yasuda: Experimental and Theoretical Study of a Structural – Acoustic Coupling System (Acoustic Tube with a Flexible Panel at One End), Japan Society of Mechanical Engineers journal (C), Vol. 69, No. 685 (2003), pp. 2256 – 2261
- (2) Hiroshi Yamauchi, Hiroyuki Seino, and Kimihiko Yasuda: Experimental and Theoretical Study of a Structural – Acoustic Coupling System (Acoustic Tube with Two Flexible Panels in Opposite Sides), Japan Society of Mechanical Engineers journal (C), Vol. 69, No. 686 (2003), pp. 2533 – 2540
- (3) Hiroyuki Seino, Hiroshi Yamauchi, and Kimihiko Yasuda: Experimental and Theoretical Study of a Structural – Acoustic Coupling System (Acoustic Tube Coupled at One End with a Flexible Panel with a Spring-Mass System Attached), Japan Society of Mechanical Engineers journal (C), Vol. 70, No. 691 (2004), pp. 671 – 677
- (4) Hiroyuki Seino, Hiroshi Yamauchi, and Kimihiko Yasuda: Experimental and Theoretical Study of a Structural – Acoustic Coupling System (Minimization of Sound Pressure Level of Acoustic Tube by Dynamic Vibration Absorber), Japan Society of Mechanical Engineers journal (C), Vol. 71, No. 708 (2005), pp. 2469 – 2476



Hiroyuki SEINO

Newly Developed Four-Cylinder MIVEC Engine

Masato TOJO* Akihito KUBO*

Abstract

This paper gives an overview of a newly developed four-cylinder engine used for the new Mitsubishi OUTLANDER Sports Utility Vehicle (SUV).

The new engine is one of the results of the World Engine project conducted by Mitsubishi Motors Corporation (MMC), DaimlerChrysler Corporation, and Hyundai Motor Company. The cylinder block and other basic structural parts of the engine were jointly developed by the three companies, but the intake and exhaust manifolds, the cylinder head's intake and exhaust ports, and other elements related to engine tuning were independently developed by MMC. For high quality and reliability, MMC adopted a rigorous development process conforming to the Mitsubishi Motors Development System (MMDS), which is also applied to vehicle development.

Production of the new engine began in September 2005 on a newly installed, state-of-the-art production line at the MMC's powertrain plant in Shiga, Japan. MMC sees the new engine as one of the mainstays of its engine lineup and intends to employ it in an increasing number of new vehicle models.

Key words: Engine General, Gasoline Engine, Spark Ignition Engine

1. Targets

New engines must deliver a number of attributes: They must offer high performance that translates into genuine driving pleasure; they must offer fuel efficiency that realizes superior levels of economy; they must run cleanly enough to comply with increasingly stringent regulations on exhaust emissions; they must be light and compact enough to permit good acceleration and fuel economy; and they must operate with sufficiently low vibration and noise to permit comfortable driving.

MMC adopted state-of-the-art technologies in every part of the newly developed engine to enable the engine to deliver all of the aforementioned attributes (Fig. 1).

2. Features

The new technologies adopted by MMC to enable the engine to deliver all of the aforementioned attributes are described hereafter. Many of the adopted technologies contribute to more than one of the demanded attributes, so the technologies and their purposes are summarized in Table 1.

2.1 High output and low fuel consumption

The engine is the first to have the continuously variable valve timing Mitsubishi Innovative Valve timing Electronic Control system (MIVEC) applied not only to its intake valves but also to its exhaust valves, and its cylinder-head intake and exhaust ports and intake and exhaust manifolds are shape-optimized for superior volumetric efficiency. At the same time, friction is suppressed by measures including elastic grinding of the valve stems, adoption of a high-efficiency shroud-



Fig. 1 Newly developed four-cylinder MIVEC engine (4B12)

equipped plastic impeller in the water pump, and adoption of 0W-20 low-viscosity oil. Consequently, the engine offers class-topping output performance and fuel economy. The engine's performance curves are shown in Fig. 2, the operation of its intake and exhaust MIVEC system is shown in Fig. 3, and the effects of the system is shown in Fig. 4.

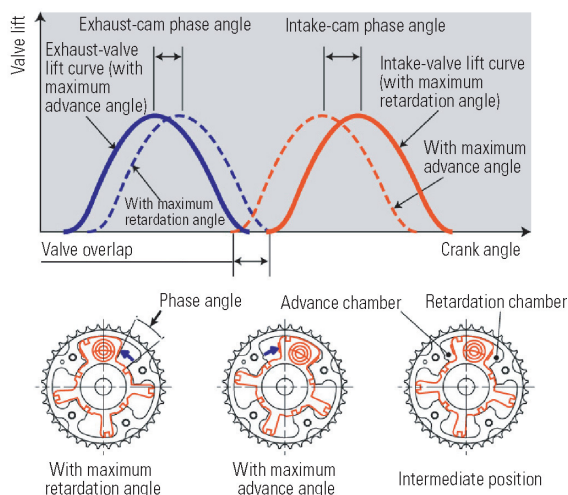
2.2 Low exhaust emissions

Combustion efficiency is promoted by the optimized design of the cylinder-head intake and exhaust ports, by intake-airflow control yielded by the intake and exhaust MIVEC system, and by injectors that give an ultra micro-droplet fuel spray. At the same time, a double-layered stainless-steel exhaust manifold is posi-

* Engine Designing Dept., Development Engineering Office

Table 1 Technologies and purposes thereof

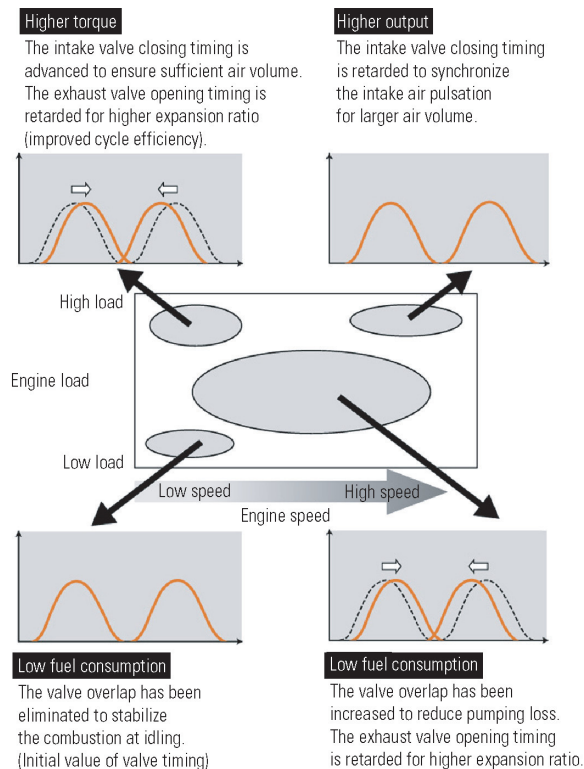
Item	Purpose	High performance and low fuel consumption	Low exhaust emissions	Compactness and lightness	Low vibration and noise	High reliability
Die-cast aluminum cylinder block				○		
Plastic cylinder-head cover				○		
Direct DOHC valve actuation		○		○		○
Intake and exhaust continuously variable valve timing MIVEC system		○	○		○	
Timing chain used to drive camshafts				○		○
Compact balancer module with integrated oil pump				○	○	
Serpentine drive belt used to drive auxiliaries				○		
Plastic long-port intake manifold with equal-length passages		○		○		
Stainless-steel exhaust manifold		○	○	○		
Rear exhaust layout			○	○		
Low-viscosity engine oil (0W-20)		○				
Ultra micro-droplet spray injectors				○		
Exhaust-gas recirculation system		○	○			
Water pump with shroud-equipped plastic impeller		○				
Returnless fuel system			○			
Iridium spark plugs			○			○

**Fig. 2 Engine performance curves****Fig. 3 Operation of intake and exhaust continuously variable valve timing MIVEC system**

tioned at the rear of the engine to suppress the heat capacity of the exhaust system upstream of the catalytic converter, thereby realizing quick activation of the catalytic converter. Concomitantly low exhaust emissions enable the OUTLANDER to qualify for a Japanese 4☆ low-emission-vehicle (LEV) rating (given to vehicles whose exhaust emissions are 75% lower than those permitted by Japan's 2005 LEV regulations).

2.3 Lightness and compactness

For lightness, MMC made new material choices in the form of die-cast aluminum for the cylinder block, plastic for the cylinder-head cover and intake manifold, and stainless steel for the exhaust manifold. Also for lightness, MMC adopted a compact balancer module with an integrated oil pump. Notwithstanding a DOHC configuration and the intake and exhaust MIVEC sys-

**Fig. 4 Effects of intake and exhaust continuously variable valve timing MIVEC system**

tem, therefore, the new engine is 16 kg lighter than a previously used 2.4-liter SOHC MIVEC engine.

With regard to compactness, the rear exhaust layout helps limit the engine's overall width by permitting auxiliaries to be located mainly on the intake side of the engine. A concomitantly large crushable zone between the engine and body promotes collision safety and greatly contributes to design freedom in the front of the

Table 2 Major specifications

Item \ Engine model	4B12	<cf.> 4G69
Vehicle model in which used	OUTLANDER	AIRTREK
Displacement (L)	2.359	2.378
Bore (mm)	88	87
Stroke (mm)	97	100
Bore/stroke ratio (S/B)	1.10	1.15
Cylinder pitch (mm)	96	93
Connecting-rod length (mm)	143.75	150
Compression ratio	10.5	9.5
Cylinder-block material	Die-cast aluminum	Cast iron
Camshaft drive	Silent chain	Timing belt
Valve mechanism	Directly actuated, DOHC, 16 valves + continuously variable valve timing MIVEC system for intake and exhaust valves	SOHC, 16 valves with roller rocker arms + valve lift & timing control MIVEC system for intake valves
Balancer shaft	Balancer module with integrated oil pump	Balancer shaft (independent)
Engine alignment	Rear exhaust	Front exhaust
Max. output (kW/min ⁻¹)	125/6,000	118/5,750
Max. torque (Nm/min ⁻¹)	226/4,100	215/4,000
10-15-mode fuel economy/equivalent inertia mass (km/L)/(kg)	11.6/1,750	10.6/1,750 ^{*1}
Emission compliance	Japanese 4☆ LEV rating (for emissions 75 % lower than those permitted by Japan's 2005 LEV regulations)	Japanese 3☆ LEV rating (for emissions 50 % lower than those permitted by Japan's 2005 LEV regulations)

*1: With four-wheel drive

vehicle.

In addition, the use of a silent chain to drive the camshafts and the use of a serpentine drive belt to drive the auxiliaries allow the engine to be 37 mm shorter overall than the previously used one.

2.4 Low vibration and noise

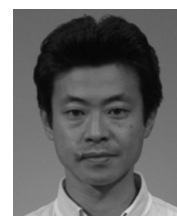
The compact balancer module, the silent chain, the stable combustion yielded by the intake and exhaust MIVEC system, and high-rigidity designs for the cylinder head and cylinder block realize low vibration and noise.

3. Major specifications

Major specifications of the newly developed engine are shown in **Table 2**.



Masato TOJO



Akihito KUBO

Overview of the Newly Developed Front Engine Front Drive Platform

Yasuhiro INOUE* Hideyuki YAJIMA** Takayuki KUROSU**
Ichiro TAKANO** Kenji HAYASHI** Koji SATO**
Junichi YANASE** Eiichi KOBAYASHI** Toshiyuki MATSUMI**
Shinichi KONDO**

Abstract

With the OUTLANDER new-generation Sports Utility Vehicle (SUV), Mitsubishi Motors Corporation (MMC) aimed to surpass the conventional SUVs in terms of user confidence and driving pleasure. To achieve this goal, MMC newly designed not only the engine and transmission but also the platform that forms the foundation of the vehicle. As the first step in developing the platform, MMC established high targets with respect to handling stability, ride comfort, all-direction collision safety, strength, lightness (essential for environmentally compatible fuel economy and exhaust emissions), and quietness (essential for a comfortable cabin environment). To realize these targets, MMC determined the optimal measures using computer-aided-engineering (CAE) analysis techniques and reflected them in an actual vehicle in a process of repeated analysis and refinement.

Key words: SUV, Platform

1. Introduction

As SUVs have become more prevalent in recent years, performance demands placed on them have become more diverse and exacting. Amid these demands, MMC began development of the OUTLANDER (a new-generation on-road SUV) by returning to its fundamental carmaking priority of delivering user confidence and driving pleasure that can be experienced even in ordinary, day-to-day driving environments. To turn this ideal into reality, MMC established performance targets for the platform that would form the foundation of the vehicle and worked without compromise to achieve the targets at the highest possible levels. The text hereafter describes the outline of the CAE analysis techniques and physical technologies used by MMC to achieve the performance targets.

2. Performance requirements for the newly developed platform

(1) All-direction collision safety

To protect vehicle occupants from impact forces applied to the vehicle from any conceivable direction, it was necessary to establish crushable zones that could effectively absorb the impact energy and to provide a sturdy cabin within the crushable zones. It was also essential to minimize the damage inflicted on any other vehicle involved in a collision. MMC sought to meet these demands (thereby promoting user confidence) by adopting an evolution of its Reinforced Impact Safety Evolution (RISE) body structure.

(2) Low weight, high rigidity, and high reliability

To handle the output of a newly developed, high-performance powerplant and realize performance capably delivered through large-diameter, low-profile tires, it was essential to confer high rigidity and reliability on the body frame and suspension mountings. At the same time, environmental considerations made it essential for the platform to be light.

(3) Predictable handling stability and a steady, comfortable ride

MMC aimed to deliver driving pleasure by realizing controllability characterized by precise, faithful responses to the driver's steering inputs, by realizing superior stability, and by realizing a well-damped, steady ride. A low center of gravity and high rigidity in the frame members supporting the suspension system were thus required to the body. In the suspension system, it was essential to realize high rigidity to securely keep the wheel alignment and ample stroke lengths for superior roadholding.

(4) Quietness for occupant comfort

To ensure cabin quietness for occupant comfort, it was necessary not only to make the body highly rigid but also to optimally position damping material and sound-insulating material for effective suppression of unpleasant vibration and transmitted sound from the engine, other powertrain parts, and wheels.

* Body Design Department, Development Engineering Office

** Digital Engineering Office, Development Engineering Office

*** Safety Testing Dept., Development Engineering Office

** Chassis Design Department, Development Engineering Office

** FF Vehicle Testing Department, Development Engineering Office

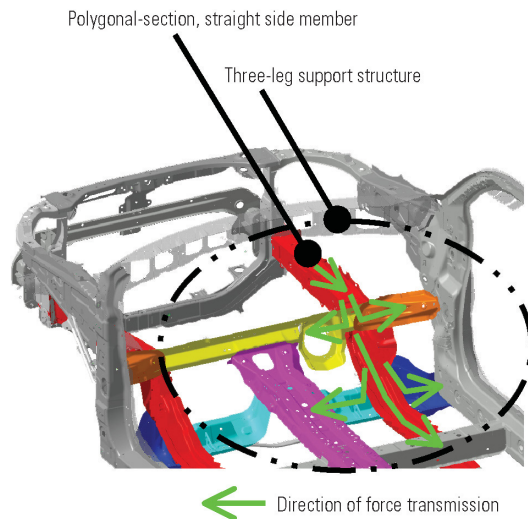


Fig. 1 Polygonal-section, straight side members and three-leg support structure

3. Overview of analysis techniques and adopted technologies

(1) Collision safety

Making maximal use of impact CAE analysis, MMC introduced various innovations (described hereafter) to realize an evolution of its RISE body structure.

First, the rear ends of straight side members that have a carefully considered polygonal cross section are each solidly joined to three major members (the dash center crossmember, the dash side crossmember, and the floor side member) to form a three-leg support structure that can efficiently disperse the energy of a full-wrap frontal impact (**Fig. 1**). Also, a crush-box is positioned at the front end of each side member to help minimize the extent of body damage in the event of a low-intensity frontal impact (**Fig. 2**).

The cabin is surrounded by reinforcing members that are linked to form a solid cage structure that can disperse impact forces applied from any direction (**Fig. 3**).

In MMC tests conducted using methods and criteria identical to those of the Japan New Car Assessment Program (JNCAP) (a key index of passive-safety performance), the new OUTLANDER earned a 6★ rating (the highest possible rating). This result reflects not only the role played by airbags and other occupant-protection devices but also a significant role played the technologies applied to the platform.

For pedestrian protection, ample shock-absorbing space is provided between the front deck and the underlying structures and between the fenders and the underlying structures (**Fig. 4**). Also, ample clearance is provided between the hood and the underlying engine and accessories. And the cross-sectional shapes and positions of the hood's reinforcements are optimized to realize strength and rigidity together with the load control and energy absorption needed for pedestrian protection. At the front of the body, the bumper incorporates

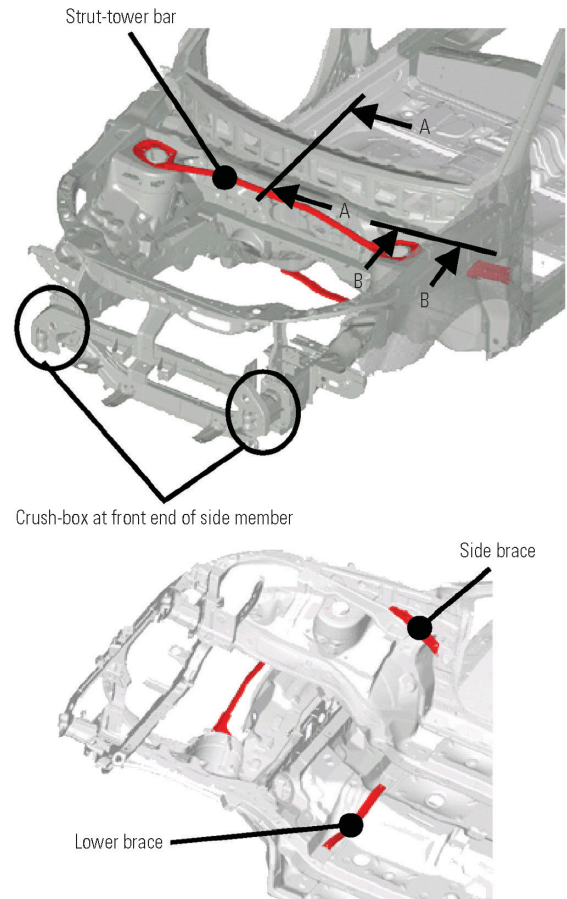


Fig. 2 Crush-box structure and body reinforcements

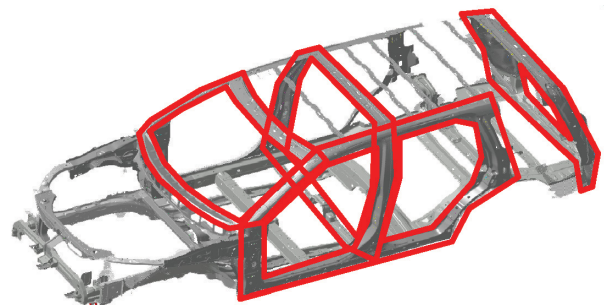


Fig. 3 Protective structure around cabin

shock-absorbing materials that promote leg protection in the event of a collision with a pedestrian. **Figs. 5 and 6** show examples of CAE analysis of the hood and bumper, respectively. By proactively using CAE analysis techniques for the body structure and engine-compartment layout from the initial planning stages, MMC was able to conduct development in an efficient manner.

With regard to the compatibility needed to minimize the extent of damage suffered by a smaller, lighter vehicle involved in a collision with the OUTLANDER, MMC achieved compliance with its self-imposed crashworthiness standards by optimizing the structure and materials of the OUTLANDER using the analysis technique

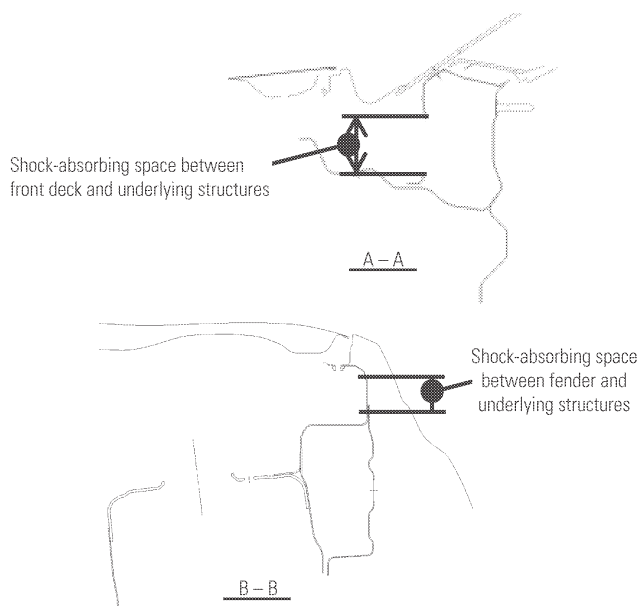


Fig. 4 Shock-absorbing structures of front deck and fenders

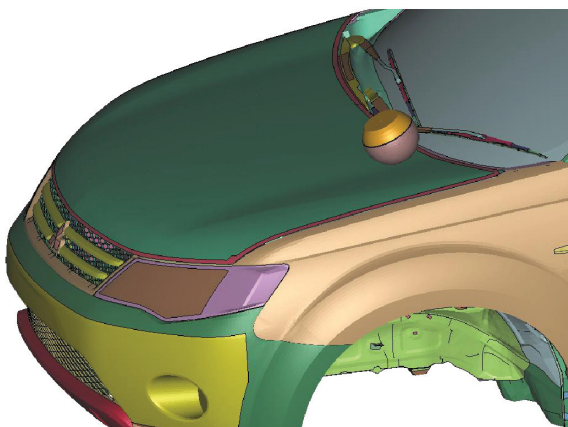


Fig. 5 CAE analysis for pedestrian protection (bonnet)

shown in **Fig. 7** and by conducting repeated tests using actual vehicles.

(2) Low weight, high rigidity, and high reliability

To achieve ample strength, durability, and reliability together with low weight, MMC painstakingly optimized the locations of members incorporating high-strength materials and the structures of joints. MMC pursued the desired combination of attributes using the aforementioned cage structure around the cabin and by making extensive use of 590 MPa-class and 980 MPa-class high-tensile steel (**Fig. 8**).

By test-running a model of the vehicle on an MMC test track with a rough surface in a virtual environment (**Fig. 9**), MMC was able to predict inputs applied to various parts of the body at an early stage of the development program (before the construction of a prototype). Using the results, MMC was able to apply effective countermeasures to the weakest parts of the structure.

By increasing the proportion of rustproofed sheet steel and the underfloor areas of sealant application

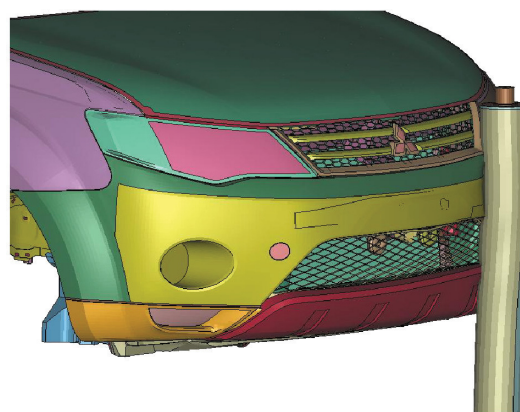


Fig. 6 CAE analysis for pedestrian protection (bumper)

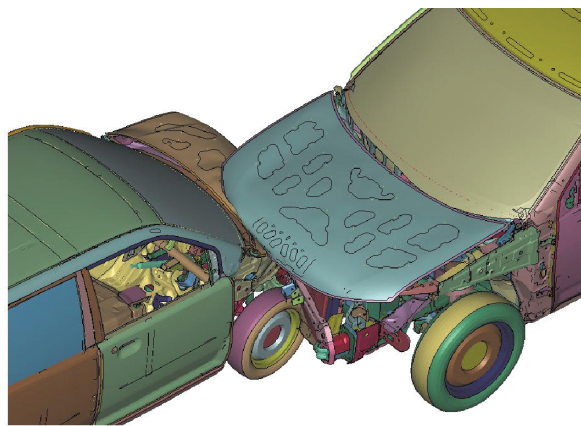


Fig. 7 CAE analysis of effects of collision with smaller vehicle

over earlier vehicles, MMC ensured that the platform would perform consistently during operation over a long period.

(3) Predictable handling stability and a steady, comfortable ride

The body-related measures described thus far make a significant contribution to the vehicle's ability to deliver predictable handling and a steady, comfortable ride.

Fig. 10 shows an example of the distribution of body distortion during vehicle operation. Although body rigidity was heightened by the innovations described in "(1) Collision safety" and "(2) Low weight, high rigidity, and high reliability", MMC was not sufficiently satisfied with it; MMC used the kind of analysis shown in **Fig. 10** to identify body areas prone to significant distortion during vehicle operation and then took countermeasures by adopting reinforcements in the form a strut-tower bar, side braces, and lower braces (all shown in **Fig. 2**). MMC carefully tuned the effectiveness of each reinforcement to a satisfactory level by means of running tests. As a result, the OUTLANDER has class-topping levels of torsional rigidity (a key index of the body's overall rigidity) and flexural rigidity. Compared with the Mitsubishi AIRTREK (its predecessor), it has 18 % more torsional rigidity and 39 % more torsional rigidity.

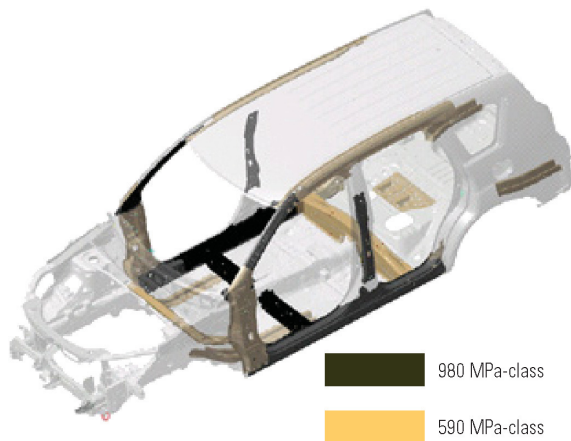


Fig. 8 Locations of 590 MPa-class and 980 MPa-class high-tensile steel

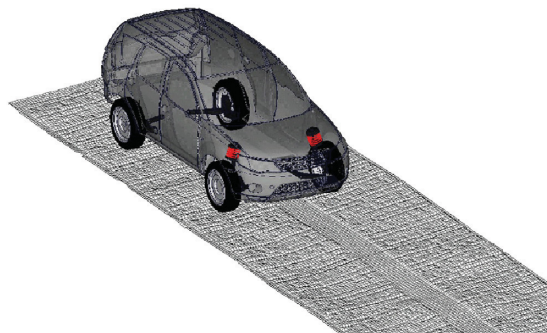


Fig. 9 Rough-road operation of vehicle model in virtual environment

For a combination of low weight and a low centre of gravity, MMC adopted an aluminum roof – a reflection of the know-how gained by the company with the LANCER EVOLUTION. (The aluminum roof is not part of the platform, but it is mentioned here as an example of related innovations.) The aluminum roof is approximately 5 kg lighter than a conventional steel roof. And given that the roof is the highest part of the vehicle, adoption of aluminum for the roof was approximately three times as effective as adoption of aluminum for the bonnet in terms of lowering the vehicle's center of gravity. The minimized center-of-gravity height and concomitantly minimized roll inertia help preclude delays in response to steering inputs and suppress roll, dive, squat, and other superfluous body movements, thereby promoting handling stability with no sacrifice in ride comfort.

The suspension configuration is the same as that of the AIRTREK: MacPherson struts at the front; trailing arms and multiple links at the rear. To enable relatively wide treads, a relatively low center of gravity, lower weight, and higher rigidity, however, MMC newly designed most of the major suspension components for the OUTLANDER. The maximum wheel strokes are longer (15 mm longer at the front; 20 mm longer at the rear). Longer arms permit wider treads (45 mm wider

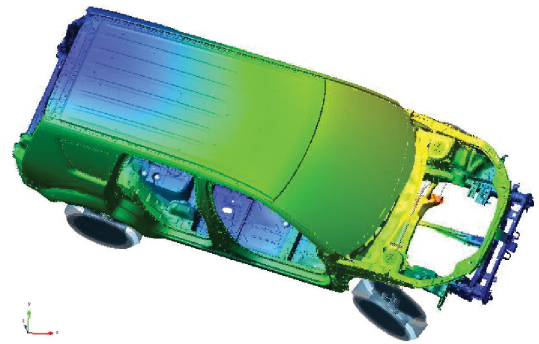


Fig. 10 Results of analysis of body distortion during vehicle operation

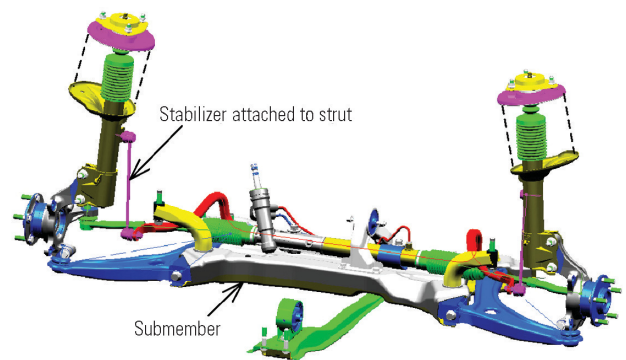


Fig. 11 Front suspension

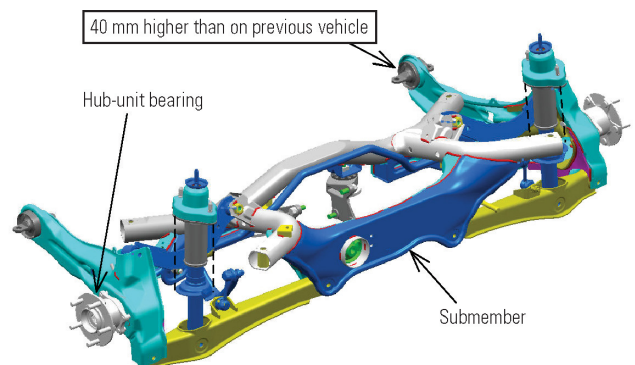


Fig. 12 Rear suspension

at the front and rear). And the front stabilizers are attached to the struts for maximal efficiency. Together, these features significantly reduce roll angles and enable suspension performance that conveys an unmistakably well-planted, stable feeling to vehicle occupants.

Comprehensively shape-optimized submembers are positioned at the front (**Fig. 11**) and rear (**Fig. 12**). The rear submember works with third-generation hub-unit bearings to promote wheel-positioning rigidity while saving weight. The front submember is completely flat. (Its shape is permitted by an engine layout in which the exhaust system is positioned at the rear of the engine.) By adopting it, MMC achieved increases in the rigidity

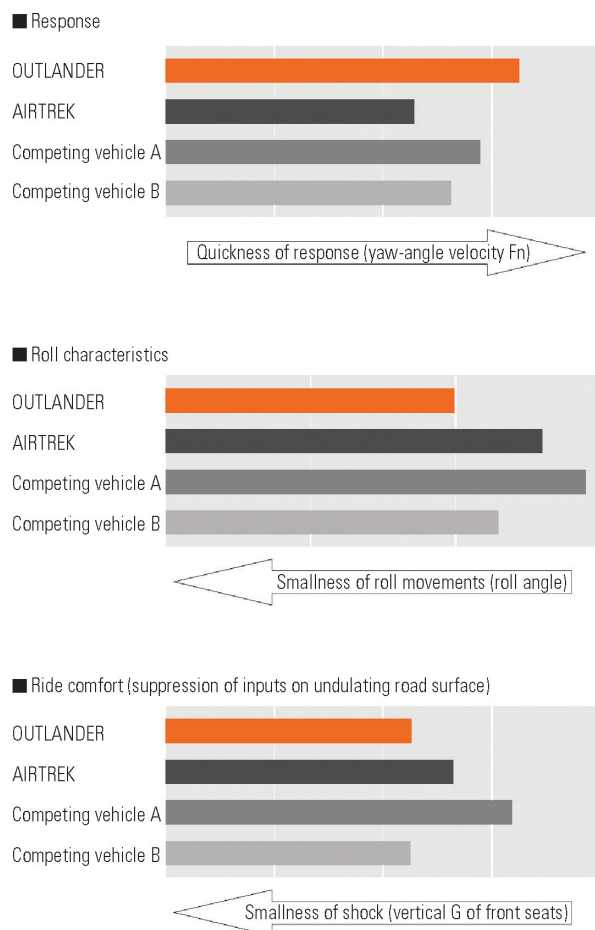


Fig. 13 Examples of characteristics on handling stability and ride comfort

of the lower-arm mounting points (a two-fold increase at the front; a 4.3-fold increase at the rear). It makes a significant contribution to the vehicle's ability to respond precisely and faithfully to the driver's steering inputs. The optimally positioned rear submember has a grid shape. By adopting it, MMC achieved significant increases in suspension mounting rigidity and precision. Further, MMC moved the trailing arms' front mounting points upward to create a layout that promotes the wheels' ability to ride over bumps in a way that realizes a refined, steady ride (Figs. 12 and 13).

Other notable features include monotube rear shock absorbers (Fig. 14). Previously used by MMC on the LANCER EVOLUTION, the monotube shock absorbers have relatively large pressure-application surfaces on their pistons and give concomitantly superior response and ample damping force even on extremely slow strokes. During vehicle operation, therefore, they respond to all suspension movements instantly and with damping force that is neither excessive nor insufficient. The resulting suspension performance meets the development goal of superior roadholding.

(4) Quietness for occupant comfort

The comprehensively maximized rigidity and durability of the platform play a significant role in suppressing the transmission of vibration from the engine, other

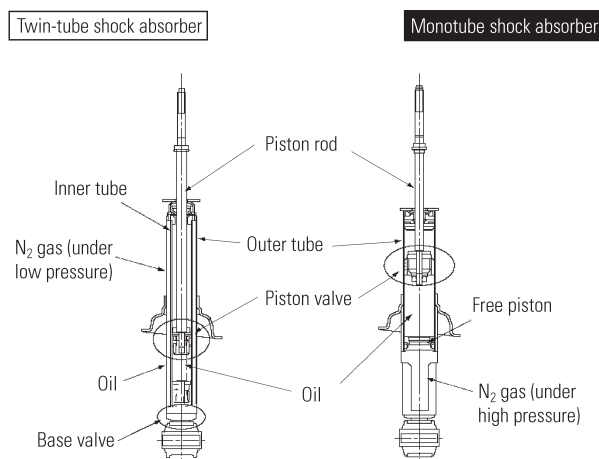


Fig. 14 Monotube shock absorber

powertrain parts, and wheels. The vibration-suppressing benefits of the platform are complemented by optimally positioned damping material for almost total isolation of unpleasant vibration.

Transmitted sound is damped by liquid-type foam filler inside frame members. Compared with application of conventional sheet-type damping material, application of foam filler can be performed with greater positional appropriateness and with concomitantly greater sound-insulating effect since it is less restricted by platform layout and production considerations. The foam filler consequently plays an important role in meeting the development goal of cabin quietness for occupant comfort.

4. Closing comments

In addition to the technologies and techniques described in general terms in this paper, MMC applied various other technologies and techniques to the platform in order to meet its performance requirements, thereby achieving a highly appealing product. MMC initially employed the new developed platform in the OUTLANDER, but it also plans to use it for various other C-segment vehicles. The new vehicles will take various forms to meet customers' diverse needs, but they will all depend on the new platform to underpin their performance. All of the MMC personnel involved with the development of the new platform are determined to continue refining the platform with a view to developing products that attract and delight an ever-growing number of customers.



Yasuhiro INOUE



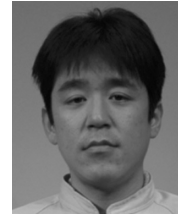
Hideyuki YAJIMA



Takayuki KUROSU



Ichiro TAKANO



Kenji HAYASHI



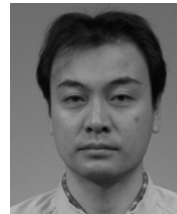
Koji SATO



Junichi YANASE



Eiichi KOBAYASHI



Toshiyuki MATSUMI



Shinichi KONDO

Development of Application Technology of Aluminum Roof

Yoshinobu MATSUMURA* Toshitsugu MISAKI** Tomomi YOSHIDA**
Takayoshi KONDO** Atsuo SAKUMA*** Masayuki MAEDA***
Yasumasa YOSHIHARA**** Koji FUKUMOTO**** Yutaka SUGIURA****
Akitoshi OKUMURA****

Abstract

To maximize the beneficial effect of weight reduction on drive performance, an aluminum roof panel was adopted for LANCER EVOLUTION VIII MR – the first Japanese-made steel body with aluminum-roof vehicle. Subsequently, a development project was carried out to achieve high drive performance comparable with that of sedan models for the tall SUV by introducing an aluminum roof panel into OUTLANDER. As a result, the accuracy of the thermal deformation analysis method developed for LANCER EVOLUTION could be upgraded, and the SPR joining mechanism was elucidated. The present paper describes these two aspects.

Key words: Body, Aluminum, Weight Reduction, Thermal Deformation, Self-Piercing Rivet

1. Introduction

To advance the technology of Mitsubishi, a manufacturer noted for the excellent performance of its vehicles, an aluminum roof, in addition to an aluminum hood and an aluminum fender, was adopted for its LANCER EVOLUTION VIII MR (hereafter called “EVO”), Japan’s first-ever car with an aluminum roof, to realize a low center of gravity, low roll inertia moment and high motion performance⁽¹⁾⁽²⁾.

This renovation is especially beneficial to the tall SUV. The aluminum roof was introduced into the OUTLANDER, which was released for sale in October 2005 (Fig. 1).

Aluminum, which differs in properties from steel, presents problems in terms of:

- (1) Shaping
- (2) Joining
- (3) Galvanic corrosion
- (4) Thermal deformation of the outer panel due to heat treatment during the painting process (hereafter called “thermal deformation”).

The CAE analysis technique was used to solve the shaping problem. Self-piercing rivets (hereafter called “SPR”) were used for joining purposes. An adhesive was used against galvanic corrosion. The thermal deformation was analyzed by the upgraded method.

How the accuracy of thermal deformation analysis was upgraded will be explained here. The SPR joining mechanism and the technique for joining to 590-MPa

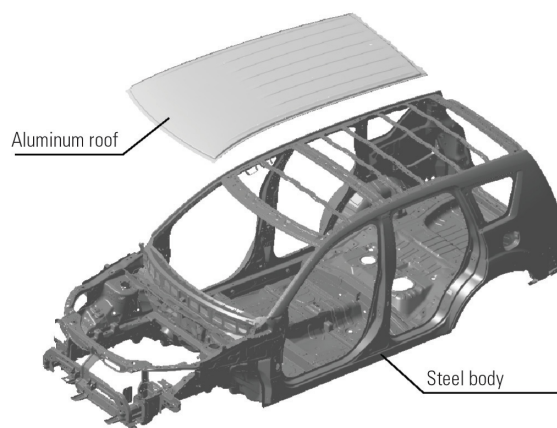


Fig. 1 Structure of aluminum roof

class ultra high tensile strength steel sheet for the new high-rigidity light body will also be described.

2. Outline of aluminum roof structure

The OUTLANDER, like EVO, is roofed over with Series 6XXX aluminum sheets that provide the proofing against dents and strength against snow load required of the roof panel of a car. This aluminum roof is approx. 5 kg lighter than a steel roof.

The rear end of the OUTLANDER’s roof is the split

* Advanced Vehicle Engineering Dept., Development Engineering Office

** Digital Engineering Office, Development Engineering Office

*** Mini & Commercial Car Assembling Production Dept., Mizushima Plant

**** Office of Mizushima Production Engineering, Mitsubishi Automotive Engineering Co., Ltd.

***** Chemical Business HQ., Sunstar Engineering Inc.

** Body Design Dept., Development Engineering Office

** Production Engineering Body Dept., Production Engineering Office

*** Mizushima Quality Control Dept., Quality Affairs Office

**** Technical Dept., Aluminum & Copper Company, Kobe Steel, Ltd.

***** Tokyo Boeki Techno-system Ltd.

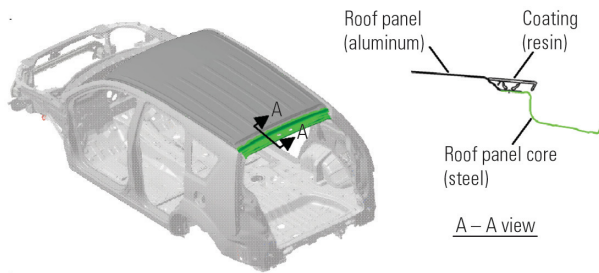


Fig. 2 Structure of rear end of roof

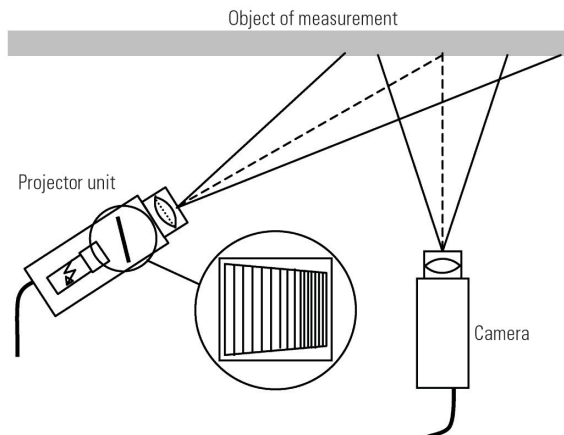


Fig. 3 How ABIS works

type, as shown in Fig. 2, to facilitate shaping. It is provided with a resin coating of the same color as the roof panel to improve the appearance.

3. Improved thermal deformation analysis

Deformation (thermal deformation) caused by heat during the heat treatment necessary for painting, which mars the outward appearance, was noticed on the roof side of EVO. Thermal deformation analysis⁽³⁾ was conducted, and a large design bead that had proven effective through testing with a real car was incorporated into the model.

Attempts to improve the analysis technique, associated with the following aspects, were made to ensure satisfaction of the requirements of the OUTLANDER by CAE thermal deformation analysis alone, without testing a real car:

- (1) Establishment of criteria for evaluating thermal deformation figures
- (2) Better analysis technique that allows for the characteristics of a mastic sealer

3.1 Establishment of criteria for evaluating thermal deformation figures

An attempt was made to quantify the extent of deformation of finished cars, which had been determined by human sense in the past.

- (1) Quantification of extent of deformation

First, the extent of deformation determined by a

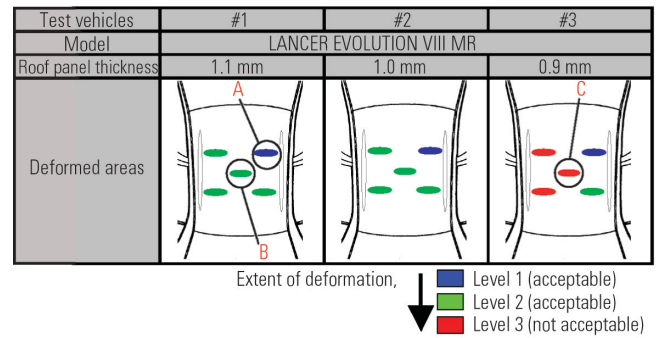


Fig. 4 Results of evaluation of test vehicles by human sense

skilled technician's visual inspection had to be quantified before establishing criteria for evaluating thermal deformation analysis figures. The Automatic Body Inspection System (hereafter called "ABIS"), a Steinbichler deformation measuring instrument, was used for this purpose. ABIS can measure deformation with an accuracy of 10 μm . Relevant knowledge accumulated in the past reveals that deformation can vary by dozens of μm or so, so ABIS can measure thermal deformation. How ABIS works is shown in Fig. 3.

(2) Measurement of deformation of real cars

EVO was chosen as the car model for the evaluation. We thought a thicker roof panel would be the primary solution to the deformation problem, so we fabricated a test vehicle with an aluminum roof 1.1-mm-thick, which is equal to the thickness of EVO's roof, another test vehicle with a 1.0-mm-thick aluminum roof and the third one with a 0.9-mm-thick aluminum roof. An evaluation was conducted with these three test vehicles. The results of evaluation by human sense are shown in Fig. 4, showing that the extent of deformation is in inverse proportion to the panel thickness. This evidences the effectiveness of a thicker roof panel against thermal deformation. The thermal deformation of the 0.9-mm-thick roof is at Level 3, which is not acceptable for a car.

The results of the evaluation by human sense and the measurements taken by ABIS were then compared. Fig. 5 shows the ABIS deformation measurements at Levels 1, 2 and 3 as evaluated by human sense. These deformation gradations are justifiable in view of the measurement figures. A specific value based on the pertinent ABIS measurement could be assigned to Level 3, which is classified as unacceptable.

3.2 Better thermal deformation analysis technique allowing for characteristics of mastic sealer

Generally, the roof of an SUV, such as the OUTLANDER, is larger than the roof of a sedan, and the panel rigidity at the center of the former is lower than that of the latter. Accordingly, thermal deformation due to heat shrinkage at the mastic sealer (hereafter called "mastic") deposited between the roof bow and the roof panel poses a serious problem in some cases. Thermal deformation was detected at the center of a thin, low-panel-rigidity roof like the roof of a sedan similar to the EVO's fabricated for the test purpose mentioned in sec-

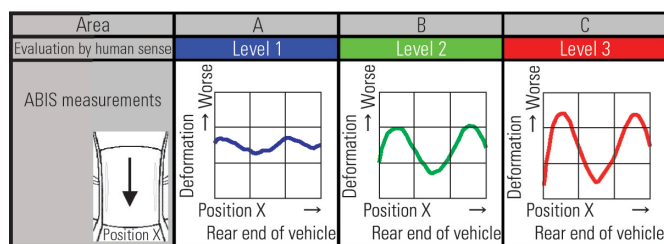


Fig. 5 Deformation measurements by ABIS

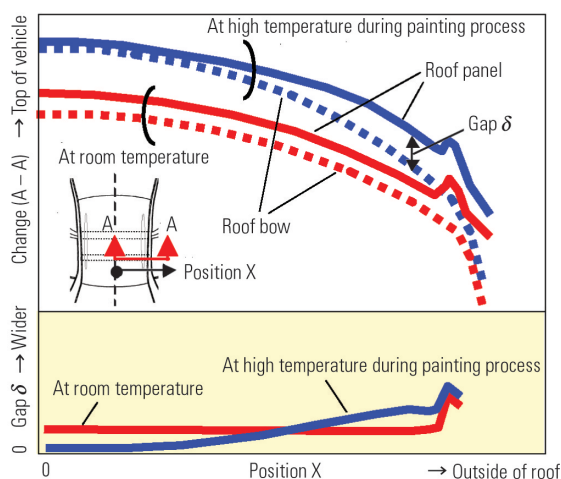


Fig. 6 How the gap between roof panel and roof bow is changed by heat during painting process

tion 3.1. A new analysis technique that allows for thermal deformation at the mastic was developed for the OUTLANDER.

(1) How thermal deformation occurs at mastic

The gap between the roof panel and the roof bow at normal temperature and the one at a hot temperature differ due to the thermal deformation caused by the heat treatment as shown in Fig. 6. If the mastic hardens at the high temperature, thermal deformation presumably occurs to a low-rigidity roof panel when the temperature drops back to the normal level at the end of the heat treatment.

(2) Model mastic

The properties of the mastic are dependent on the thickness per unit area. A peeling strength test with test pieces of various thicknesses was conducted to verify the validity of a mastic model. As can be seen from Fig. 7, there is a close correlation between the test results and the analysis results.

(3) Analysis of thermal deformation of EVO's roof

Thermal deformation analysis was conducted using the model shown in Fig. 8. The thermal deformation due to the heat treatment and the properties of the mastic were taken into account. It was presupposed for the analysis that the properties of the mastic do not change sharply after its hardening. The analysis results and the evaluation by human sense for the real car were closely correlated with each other, as shown in Fig. 9. The Level 3 value based on the ABIS measurements serves

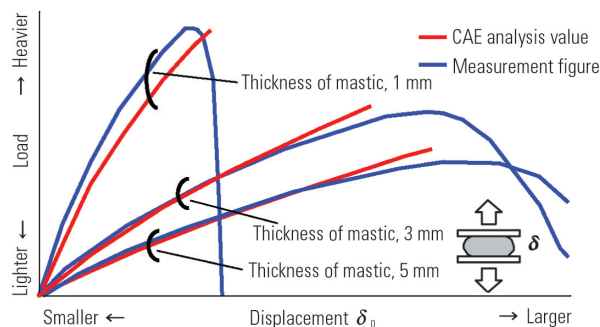


Fig. 7 Model mastic proven to be correct

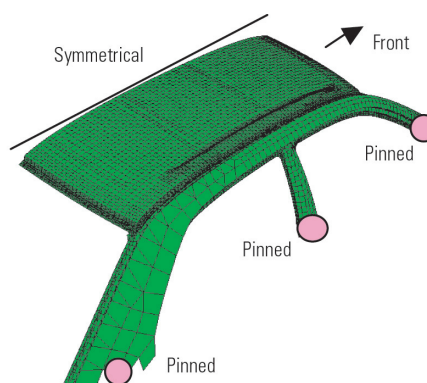


Fig. 8 Analysis model matched with EVO's shape

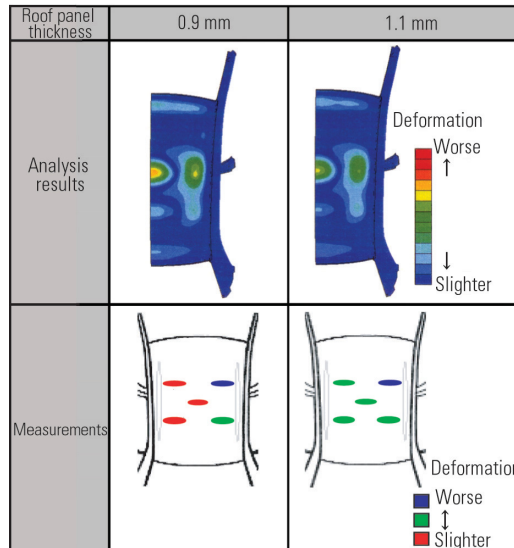


Fig. 9 Analysis results and evaluation by human sense of real car – EVO

as a criterion for deformation judgment based on the CAE analysis.

3.3 Application to OUTLANDER

The thermal deformation was examined with the mastic model mentioned in section 3.2 reflected in the shape of the OUTLANDER's roof. The design bead in EVO was found to be effective against the thermal

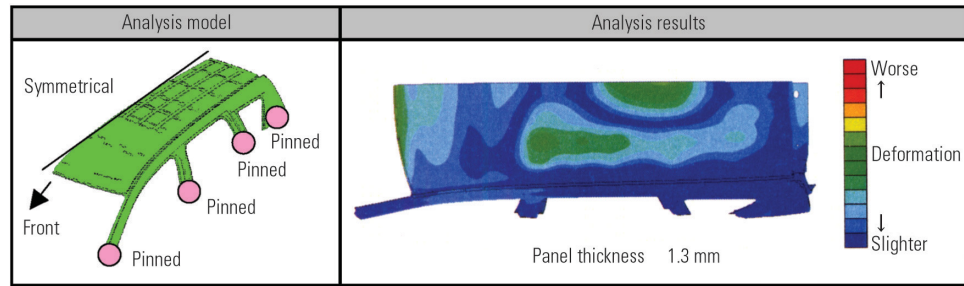


Fig. 10 Analysis result – OUTLANDER

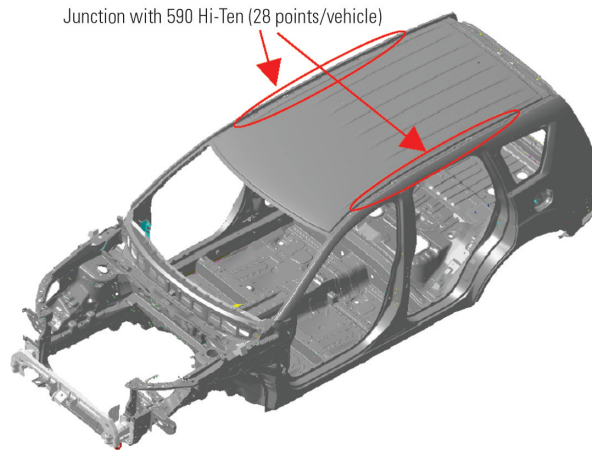


Fig. 11 Junction with 590 Hi-Ten

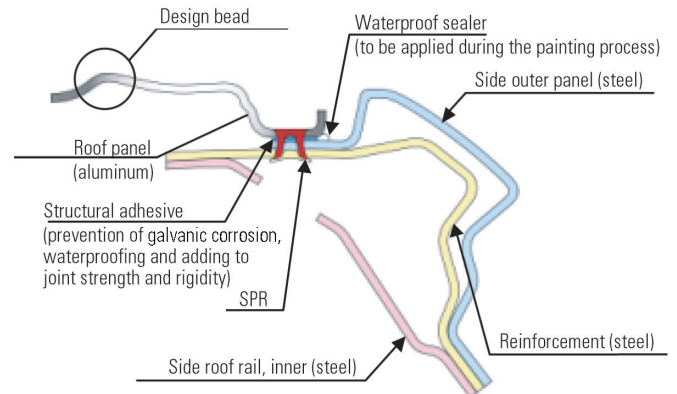


Fig. 12 Sectional view of SPR joint for OUTLANDER

deformation on the roof side and that the thermal deformation at the center of the roof, which is attributable to the mastic, does not occur on a 1.3-mm-thick panel (Fig. 10).

4. Joining technique

As in the case of EVO, SPRs were adopted for joining the aluminum roof to the steel monocoque body. The joining mechanism, which will be outlined here, was elucidated as a preliminary step before setting an SPR control index.

For the OUTLANDER, those areas of the newly developed light and highly rigid body that are to be joined to the roof panel (shown in Fig. 11) are made of a 590-MPa class high tensile strength steel sheet (hereafter called "590 Hi-Ten"). As few instances of SPR joining to 590 Hi-Ten have been reported in the past^{(4)–(7)}, the technique will be outlined here. The SPR joint for the OUTLANDER is shown in Fig. 12.

4.1 Setting control index

Two sheets joined together by SPRs and subjected to a peeling strength test are torn apart in two different ways. As shown in Fig. 13 (a), SPR is disengaged from the top sheet or from the lower one. The depth to which the rivet legs penetrate and the extent to which the rivet head pokes out from the surface, as shown in Fig. 13 (b), as well as the strength of the material and the sheet

thickness are significant factors in determining the SPR joint strength⁽⁴⁾. Let " F_{head} " be the peeling load in the case where SPR is disengaged from the top sheet and let " F_{leg} " be the peeling load in the case where it is disengaged from the bottom sheet. We suspected a correlation between F_{head} and the extent to which the rivet head pokes out from the surface and also between F_{leg} and the depth to which the rivet legs penetrate. A correlation was found between the extent to which the rivet head pokes out and the depth to which the rivet legs penetrate, as shown in Fig. 13 (c). Hence, the extent to which the rivet head pokes out, which is easier to control on the production line, was chosen as a control index.

Peeling load F is either F_{head} or F_{leg} , whichever is smaller, as indicated by Eq. (1) below.

$$F = \min (F_{head}, F_{leg}) \quad (1)$$

where

F : Peeling load

F_{head} : The peeling load when SPR is disengaged from the top sheet

F_{leg} : The peeling load when SPR is disengaged from the bottom sheet

F_{leg} is in inverse proportion to the extent to which the rivet head pokes out whereas F_{head} is proportional to it as shown in Fig. 13 (d). Presumably, if a rivet is driven deep into the parent material, the thickness of that

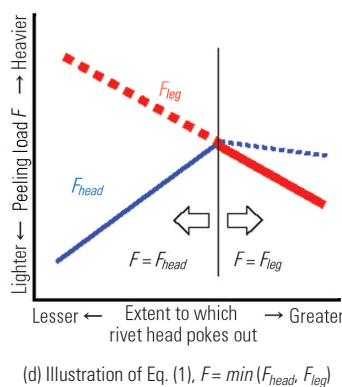
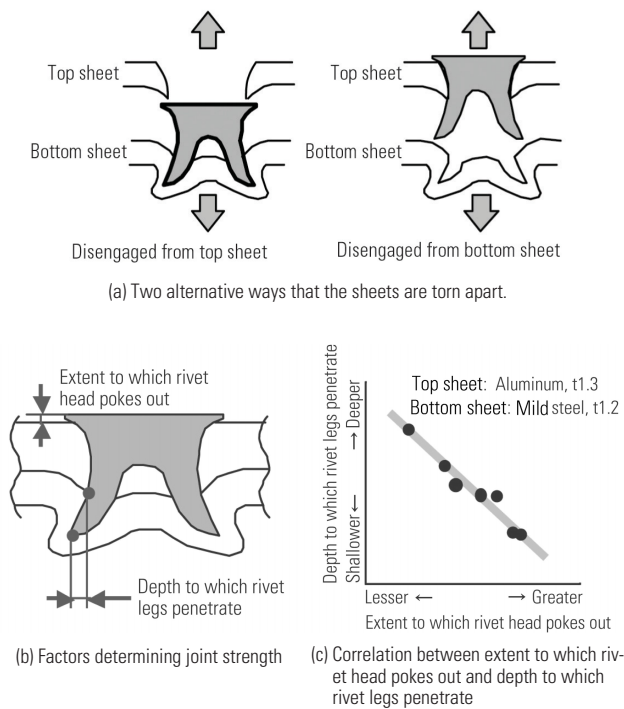


Fig. 13 SPR joint strength

material is reduced accordingly, with a resultant decline of the peeling load. Correlation between the extent to which the rivet head pokes out, which was chosen as a control index, and the result of the peeling strength test will be graphically presented later.

4.2 Evaluation control index validity

An aluminum roof is composed of two sheets as shown in Fig. 14 or of three sheets. In the latter case, the three-sheet composition is torn apart in four ways. The peeling load is placed on the top sheet with the middle and bottom sheets paired off (hereafter called "top/middle"), or it is placed on the bottom sheet with the top and middle sheets paired off (hereafter called "middle/bottom"). The results of a peeling strength test of a three-layer composition with a top sheet (aluminum, 1.3 mm), middle sheet (soft steel, 0.65 mm) and bottom sheet (soft steel, 1.2 mm) is presented in Fig. 15. In the case of "middle/bottom", only F_{leg} is imposed. In the case of "top/middle", Eq. (1) holds true. Peeling load F is graphically presented in Fig. 13 (d). As can be

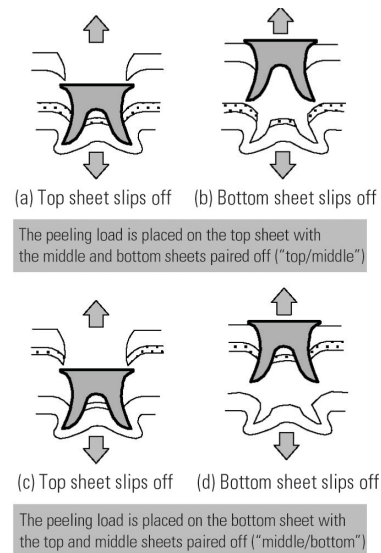


Fig. 14 Two alternative ways that the three sheets are torn apart

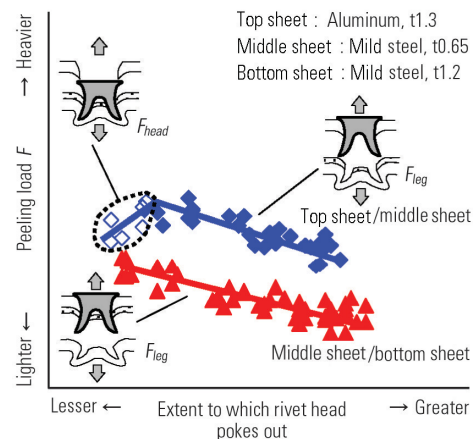


Fig. 15 Correlation between peeling strength and extent to which rivet head pokes out

seen from the foregoing, the peeling strength can be determined from the extent to which the rivet head pokes out regardless of the way the three-sheet composition is torn apart.

4.3 Joining to 590 Hi-Ten

The joining strength of a three-layer composition with a 590 Hi-Ten bottom sheet will be analyzed here. Fig. 16 shows the results of a peeling strength test of a three-layer composition with a 1.3-mm aluminum top sheet, 0.65-mm soft steel middle sheet and 1.2-mm 590 Hi-Ten bottom sheet. The relationship between top/middle and middle/bottom differs from the corresponding relationship in the case discussed in 4.2 where a soft steel bottom sheet is used. This is attributable to the fact that the peeling load increases in proportion to the depth to which the rivet legs penetrate if a 590 Hi-Ten bottom sheet is used. Consequently, the aluminum peeled off from the top sheet. A process of

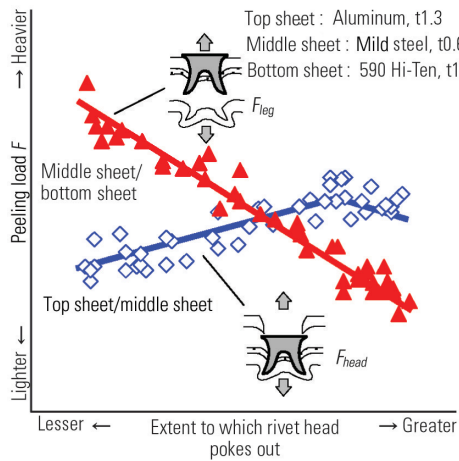


Fig. 16 Correlation between peeling strength and extent to which rivet head pokes out (590 Hi-Ten)

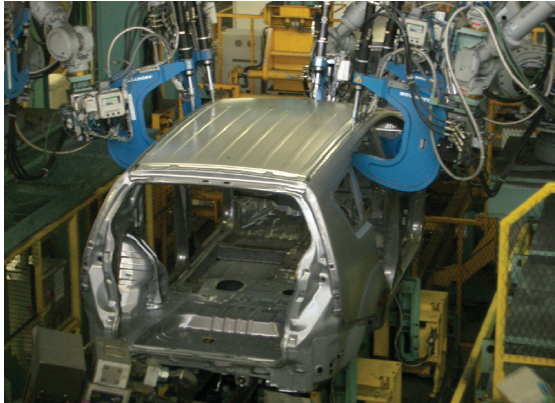


Fig. 17 SPR joining along OUTLANDER main line

joining with SPRs along the main line is shown in Fig. 17.

5. Benefit of aluminum roof

Contributions to the motion performance by an aluminum roof and a steel roof fitted to the OUTLANDER were assessed through a real-car test. As shown in Fig. 18, the OUTLANDER with an aluminum roof is superior to that with a steel roof by 4 % in the yaw rate, 9 % in the roll rate and 14 % in the roll angle. Thus, the body behavior of the tall OUTLANDER when the steering wheel is being turned is quite stable.

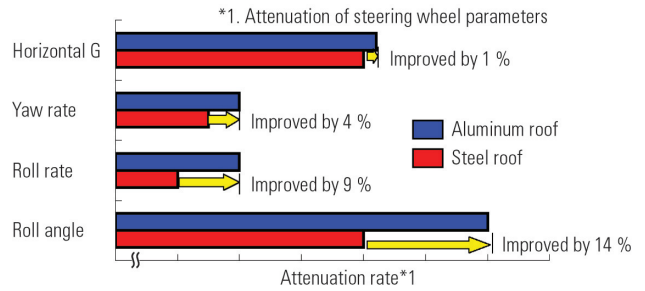


Fig. 18 Verification of OUTLANDER driving performance

6. Concluding remarks

We attempted to upgrade the thermal deformation analysis technique and the joining technique described in this paper, in order to pave the way for using an aluminum roof for the OUTLANDER. As a result, we proposed a product that gives users the true feel of Mitsubishi technology. The present technique for joining to a material stronger than 590 Hi-Ten leaves room for improvement. In view of the keen demand for Hi-Ten material for reducing the weight of new models, we recognize the need for further technological developments and will continue our research efforts.

We sincerely thank Kobe Steel, Ltd., Sunstar Engineering Inc., Tokyo Boeki Techno-system Ltd. and all those concerned inside and outside the company for their cooperation with our development work.

References

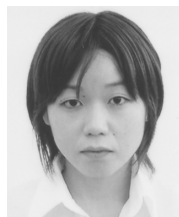
- (1) Yoshinobu Matsumura, Shinichi Ogawa et al.: Weight Reduction Technology for Improved Handling Performance of LANCER EVOLUTION, Mitsubishi Motors Technical Review, No. 16, 2004, p. 79 – 87
- (2) Toru Hashimoto et al.: Technology DNA of MMC, Mitsubishi Motors Technical Review, No. 17, 2005, p. 6 – 10
- (3) Koji Fukumoto et al.: Evaluation of Thermal Deformation on Panel By Applying Effective-width Theory, Preview of Automotive Technology Lectures, No. 72 – 05, 2005, pp. 15 – 20
- (4) Tetsu Iwase and Seiji Sasabe: Use of Self-piercing Rivets on Aluminum Alloys, Preview of Automotive Technology Lectures, No. 83 – 99, 1999, pp. 1 – 4
- (5) Haruo Ishikawa et al.: Reduction of Environmental Load Imposed by Automobiles and Hybrid-material Body (II), Light Metal Welding, Vol. 41, 2003, No. 8, pp. 345 – 355
- (6) Hidefumi Fujimura and Takao Mori: Tensile Shearing Strength Evaluation for Aluminum-High-Tensile-Steel SPR Couplings, Preview of Automotive Technology Lectures, No. 90 – 03, 2003, pp. 1 – 4



Yoshinobu MATSUMURA



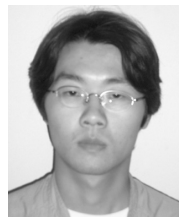
Toshitsugu MISAKI



Tomomi YOSHIDA



Takayoshi KONDO



Atsuo SAKUMA



Masayuki MAEDA



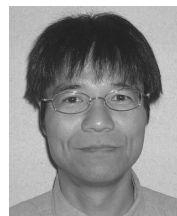
Yasumasa YOSHIHARA



Koji FUKUMOTO



Yutaka SUGIURA



Akitoshi OKUMURA

Development of a Next Generation Electronics Platform

Hiroki FUKATSU* Hiroshi KANEDA* Kunihiro SAKAI*
Akitoshi TOKUNAGA* Satoshi OGAWA*

Abstract

As part of the new OUTLANDER project, we have upgraded the electronics platform in order to realize a foundation for answering the needs of ever-evolving electrical components.

Through the enhancement of the ECU communication network and introduction of cutting-edge failure diagnosis technologies, variant coding, and other advanced infrastructure technologies, we have realized greater functionality in electrical components, the reduced number and increased combined usage of ECUs, and the reduced number and lengths of harnesses.

Key words: Electronics Platform, Communication, E/E Architecture, Diagnosis, Gateway

1. Foreword

Following the launch of the COLT in 2002, we at Mitsubishi Motors Corporation (MMC) have provided support⁽¹⁾ for the reduction of harness numbers and lengths, and the enhancement of the functionality of electrical equipment through the introduction of communication systems based on the CAN protocol to new vehicles; however, as a result of recent increasing demand for an even higher level of functionality and enhanced failure diagnostic functions, there has been rapid growth in the number of ECUs connected to the communication network, and the current communication system is now at the limit of its support capabilities.

In order, therefore, to support expected further intensification of the above-mentioned demand, it is absolutely necessary not only to reinforce the communication network itself, but also to develop infrastructure that supports the needs of electrical equipment, such as fundamental failure diagnostic technologies and software technologies – in other words, an electronics platform.

As part of the new OUTLANDER project, we have developed a next generation electronics platform that incorporates a wide range of advanced technologies and that will become the standard for all other such platforms at MMC. Described hereinafter, this has allowed the realization of greater functionality in electrical components, reduced numbers and increased combined usage of ECUs, and reduced the numbers and lengths of harnesses.

2. Overview of the new electronics platform

During the course of the OUTLANDER platform's lifecycle, the key issues that needed to be addressed in order to provide an electronics platform capable of supporting ever-evolving, advanced ECUs were as follows:

- Construction of a communication network system

which could support increasing numbers of ECUs

- Enhancement of the quality of communication software as the communication network increases in complexity
- Improvement of failure diagnostic functionality
- For the purpose of lowering costs, reduction of the number of ECUs, increasing the degree of combined usage thereof, and streamlining of the power supply system
- Adoption of supplier standard ECUs

None of these issues could be resolved using the technologies that had been in use at MMC. Accordingly, the electronics platform was upgraded through the introduction of new technologies to the communication network, the ECU infrastructure, and the power supply system. The characteristics of these technologies are described below.

3. Technological characteristics

3.1 Communication network

In order to provide support for growth in the number of ECUs in line with continuing enhancement of the functionality of electrical components, we developed a communication network featuring four communication busses matched to the characteristics of ECUs. Through the action of a gateway ECU, these four busses can exchange data with the network. The following section will provide a description of the network architecture and gateway.

3.1.1 Network architecture

As shown in Fig. 1, the network comprises four communication busses classified in accordance with the functionality of on-board ECUs – namely, a powertrain and chassis communication bus (CAN-C: 500 kbps), a mid-speed body and AV communication bus (CAN-B: 83.3 kbps), a low-speed body communication bus (LIN: 19.2 kbps), and a dedicated failure-diagnosis communication bus (CAN-C: 500 kbps); furthermore, these busses are all interconnected via an Electronic Time &

* Electronics Engineering Dept., Development Engineering Office

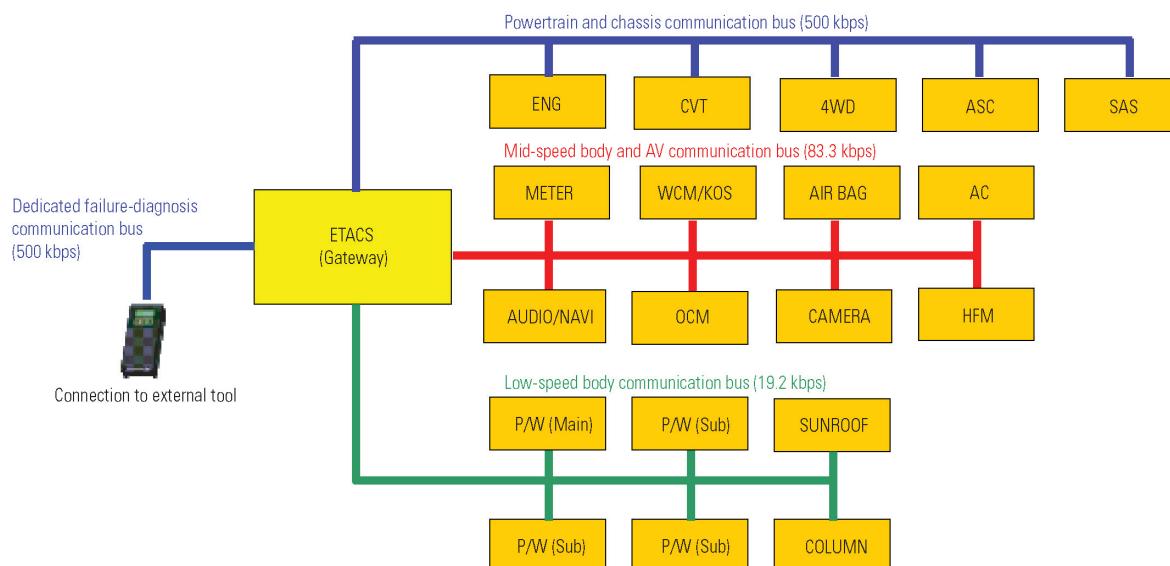


Fig. 1 OUTLANDER's network architecture

Alarm Control System (ETACS), which features integrated gateway functionality.

The engine, CVT, 4WD, Active Stability Control (ASC), and steering angle sensor are connected to the powertrain and chassis communication bus, while ECUs for the instrument panel, wireless controls, the airbags, the air conditioner, the audio system, and the like are connected to the mid-speed body and AV communication bus. Meanwhile, the low-speed body communication bus is connected to the ECUs for the power windows, sun-roof, and column switches; furthermore, when connected to a diagnostic tester, the dedicated failure-diagnosis communication bus relays information relating to ECU failure diagnosis. The infrastructure has been designed such that direct access to the vehicle's internal communication network is not possible via the diagnostic connector, thus improving the security of the other three busses (i.e., the on-board busses).

3.1.2 Gateway

In order to facilitate the connection of multiple communication busses, the ETACS has been provided with the gateway functionality that constitutes the heart of the network. Here, the term "gateway" refers to the function of receiving data from the various busses and forwarding said data to the other busses; accordingly, the ETACS performs data relay between the above-mentioned three communication busses (Fig. 2).

In terms of routing processing methods, the architecture uses message routing, where each received frame is forwarded to a different bus, and signal routing, where designated signals from multiple frames are grouped together in a single frame and then forwarded (Fig. 3). Meanwhile, functionality is broadly classified into three different types – namely, On-Board Data Transfer (OBDT), Diagnostic Message Routing (DMR), and Network Message Mirroring (NMM). OBDT carries out two-way relaying of data between the on-board powertrain and chassis communication bus, mid-speed

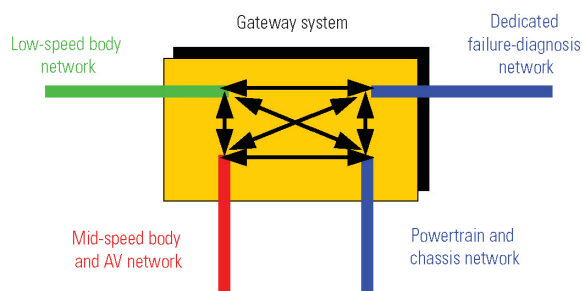


Fig. 2 Gateway system functionality

body and AV communication bus, and low-speed body communication bus. Furthermore, message routing and signal routing techniques are applied by this functionality. DMR constitutes the routing of information between the dedicated failure-diagnosis communication bus and the on-board busses, while NMM constitutes the routing of all data from the on-board busses to the dedicated failure-diagnosis communication bus. Both DMR and NMM use only the message routing technique.

In addition, the gateway has been designed in such a way that it constantly monitors the communication network and performs failure diagnosis. If a physical failure (i.e., open or short circuit) is detected in a communication bus, it stores the result thereof as a Diagnosis Trouble Code (DTC). Furthermore, the gateway also monitors the transmission messages of data-transmitting ECUs, and if the messages are lost, it stores the corresponding DTC.

3.2 ECU infrastructure technologies

The new electronics platform integrates all of the ECU infrastructure technologies described below into ECUs, thus contributing to reduction of ECU numbers and enhancement of failure diagnosis functions.

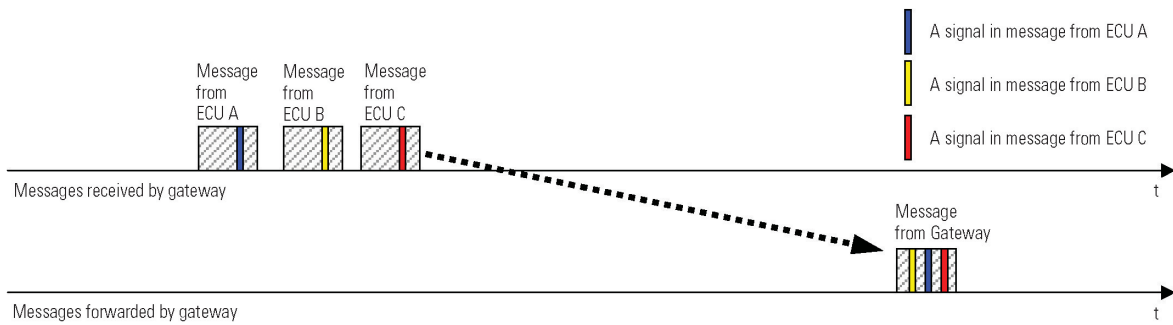


Fig. 3 Signal routing process

(1) Software modules

In the past, a software module featuring CAN receipt and transmission was used, and by incorporating this module into all ECUs, it was possible to achieve the required levels of quality. However, the new platform uses a group of modules combining schedule management functionality for receive and transmit messages, network management functionality, diagnosis functionality, and communication data flow control functionality. By incorporating these modules into ECUs, therefore, it is possible to achieve a greater level of quality (Fig. 4).

(2) Diagnosis

Previously, the messages of transmission from transmitting ECUs were monitored by the receiving ECU, which was also provided with functionality (loss of ECU) for recording the results of monitoring as a DTC; however, major improvements were made to failure diagnostic functionality as part of this project. The principal new functional elements are as follows:

- Freeze-frame data

In order to confirm vehicle conditions immediately before and after the detection of a failure, the ODO value upon the issuance of a DTC, the integrated failure time, and the like are recorded. The term "freeze frame data" is used to describe this data.

- Chronostack

An area called as the chronostack is used to store DTCs and freeze frame data that may be deleted in accordance with commands from a tester. Accordingly, this area stores the ODO value upon the issuance of a DTC, the integrated failure time, and the like. DTCs that can be monitored by, for example, a dealer using a diagnosis tester, are those DTCs stored in the chronostack.

- Tell-tale retention stack

The area that cannot be cleared based on commands from a dealer's tester is known as the tell-tale retention stack. The same data as the chronostack is stored. This area makes it possible for the development department to investigate the cause of problems even after deletion of data at a dealership.

(3) Variant coding

Variant coding is a parameter writing function that is used to change software implementation, and it allows ECUs to switch their functionality in accordance with country-specific information, parameters for spe-

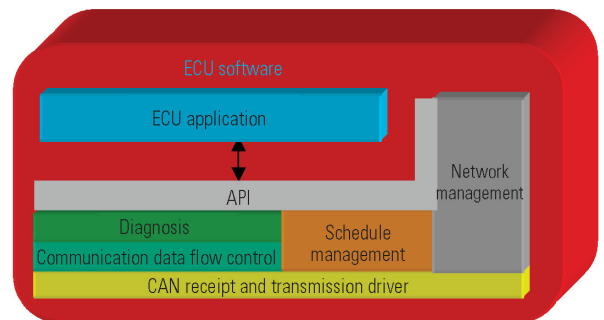


Fig. 4 Software module configuration

cific engine types, and other written data. The writing of variant coding data is carried out in-house, and therefore, it is possible to reduce the range of different ECUs that must be installed in a vehicle, thus contributing to the reduction of production, component control, and other related costs. For more details, please refer to the separate report, "ECU Variant Coding System".

(4) Reprogramming

The overwriting of software (i.e., reprogramming) is possible in the case of ECUs that incorporate flash memory. Reprogramming specifications have been standardized in the new electronics platform, and this facilitates high-speed reprogramming via the CAN.

(5) Security access

A diagnosis tester can be used to retrieve various items of information stored in ECUs, but since certain information is strictly for in-house purposes, it was necessary to prevent easy access from non-company personnel. Accordingly, access restriction levels called as "security levels" were assigned to various items of data based on the importance thereof, and the platform was designed such that restricted information could be monitored only using a diagnosis tester at an equal or higher security level.

3.3 Power supply system

The power supply system has been streamlined by a significant degree. Previously, supplied under the direct control of the ignition switch, power source is now centralized-controlled by the relay control in the ETACS integrated with the junction box. The ETACS detects the

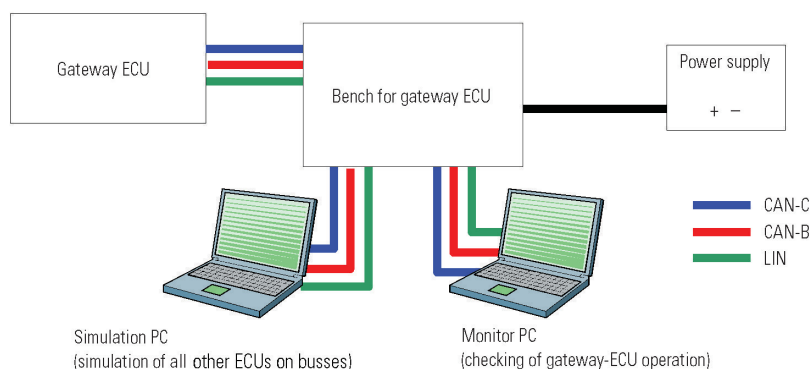


Fig. 5 Gateway bench test equipment

condition of the ignition key, and based on the position thereof, controls the relays for power to the ACC and IG systems. By supplying power to electrical components in this way, without passing through the ignition switch, it has been possible to streamline the power-system wiring. For more details, please refer to the separate report, "ETACS Functionality Development for the OUTLANDER".

4. Evaluation of reliability

As described above, the next generation electronics platform represents a significant advancement from the current system in the form of its four communication busses, a gateway which connects said busses, ECU variant coding functionality, and other improvements. The following describes a portion of the testing undertaken in order to ensure the reliability of the new system.

4.1 Network communication confirmation test

(1) Table testing and in-vehicle testing

Table testing of network communication involved the placement of vehicle harnesses on a table, connecting each ECU, and testing the equipment. This testing mainly-focused on the functionality of software; the content of communicated data, communication bus load, recovery processing on communication error, and the like. In terms of the confirmation of communicated-data content, we examined for problems in data consistency among the transmitting and receiving ECUs. In addition, the gateway testing of item 4.2 was undertaken principally through bench testing.

In-vehicle testing focused on the examination of communication lines for open or short circuits (power-supply or ground shorting) and other hardware-related issues. Although unlikely, harness open-circuit problems can occur in actual-vehicle situations; accordingly, we carried out the above-mentioned testing in actual-vehicle conditions, confirming vehicle behavior, network communication conditions, and the failure codes recorded in each ECU. In addition, electrical noise tests, transient surge tests, static electricity tests, and the like were also carried out in order to confirm that the communication system was free of abnormalities.

(2) HILS-based network failure testing

Open-circuit and short-circuit failure modes can combine in hundreds of different patterns throughout the entire network; accordingly, we employed Hardware In the Loop Simulator (HILS) in order to create failure environments and automatically confirm the DTCs stored by each ECU. In this way, it was possible to greatly reduce the number of manhours required for testing.

4.2 Gateway testing

Failure of the gateway affects those ECUs transmitting and receiving data via it, and depending on the level of importance of the corresponding signals, this can lead to problems in the operation of the overall vehicle. Accordingly, all gateway-related data was carefully examined to confirm correct operation in accordance with specifications. Fig. 5 illustrates the configuration of equipment used during testing. In terms of specific items under test, we focused on the operation of routing processes, routing processing time, and communication-bus diagnosis functionality.

4.3 Testing of variant coding

As a result of failure to correctly write variant coding information, a state arises where ECUs are not correctly matched to the vehicle in which they are installed, and this can have an adverse effect on vehicle behavior. For this reason, error handling and all other aspects of the writing process were tested in detail to confirm compliance with specifications. Testing involved the writing of parameters under various different writing conditions and confirmation of the correct writing thereof using a diagnosis monitor.

5. Conclusion

During the course of this project, we achieved wide-ranging benefits through the development of a next-generation electronics platform, the improvement of control and diagnosis functionalities, and the reduction of costs. Specifically, we expanded the number of communication busses in order to support the ever-evolving functionality of electrical components; furthermore, we introduced freeze frame data in order to boost the

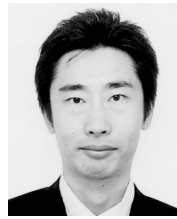
convenience of diagnosis processes, variant coding and reprogramming in order to reduce costs, and standardized communication protocols in order to facilitate the usage of supplier-standard ECUs.

Continuing to introduce new communication technologies going forward, it is our aim to optimize electrical and electronic architecture throughout the vehicle.

To conclude, we would like to express our gratitude to all parties, both internal and external, who contributed so much during the course of this development project.

Reference

- (1) Yoshiaki Sano et al: "Development of New In-Vehicle Communications System", Mitsubishi Motors Technical Review, No. 16, 2004



Hiroki FUKATSU



Hiroshi KANEDA



Kunihiro SAKAI



Akitoshi TOKUNAGA



Satoshi OGAWA

ECU Variant Coding System

Hiroki TAKIMIZU* Toshiki FUKAYA**

Yoshiaki ITO** Nobuhiko SAKANO**

Abstract

Mitsubishi Motors Corporation (MMC) has developed and introduced the new integrated system allowing design, production, and after-sales sections to support Electronic Control Unit (ECU) variant coding, and this system was first installed in the new OUTLANDER. The said system makes it possible to create and manage variant coding data within an existing list system through specifications of model and equipment information; furthermore, this data can be supplied to vehicle assembly lines and after-sales departments without the need for manual input.

Key words: Electronics, Information System, Production Engineering, Service

1. Introduction

In certain cases in the past, ECUs installed into vehicles were assigned different part numbers in accordance with the model or specification of the vehicle in question, even in situations where the electronic control system was identical. However, the differences between these ECUs were limited to slight changes in specifications at the software level, and the resultant setting of individual part numbers generated a large amount of administration expense. Meanwhile, when compared with a little over ten years ago, the number of ECUs installed into vehicles has increased significantly, and these control units are connected via a Controller Area Network (CAN) bus, making it possible for them to communicate with tools outside the vehicle.

Against this backdrop, a technology known as "ECU variant coding" is spreading in the industry, particularly amongst US and European auto makers and ECU manufacturers.

At MMC, we began to adopt the technology related to ECU variant coding with the 2004 European COLT. However, as a large number of variant coding items are required for the new OUTLANDER, the need arose for a full-fledged data management system.

Accordingly, we established the in-house ECU Data Coding System (e-DaCS) project, with design, production, and after-sales cooperating as one in its execution.

In accordance with the realization of this data management system, evaluation of the system and its operation processes was carried out with respect to the following four core issues.

- Capability for seamlessly handling variant coding data through the various stages of design, production, and after-sales operations
- Ability for permitting variant coding data set in an upstream process to be used in downstream

processes without the need for manual editing

- Capability for management and tracing of variant coding data, which is unique to individual vehicles, based on the vehicle identification number (VIN)
- Provision of production and after-sales with the ability to process changes in variant coding data in accordance with design change

This report gives an overview of the technology related to ECU variant coding, and describes the system development and application methods employed at design, production, and after-sales.

2. Overview of ECU variant coding

The term "ECU variant coding" refers to a process where common ECUs, for which initial setting is carried out by the manufacturer thereof, are delivered with a single part number, and are set to appropriate control specification on the vehicle assembly line or by the dealerships based on information classifying the vehicle or equipment specification (i.e., variant coding items).

3. Design application

3.1 Overview

A vast number of variant coding items exist for the new OUTLANDER, and these are managed within a variant-coding data list based on vehicle model, destination, and type. This list is created and managed in accordance with an existing MMC design management system.

Without the need for manual processing, the information defined in the variant-coding data list is delivered to vehicle assembly lines and after-sales departments via the internal LAN established within the company.

* Electronics Engineering Dept., Development Engineering Office

** Distributor Business Support & CS Promotion Dept., Global After sales Office

** Production Engineering Final Assembly Dept., Production Engineering Office

** SCM IT Dept., Corporate Affairs Office

3.2 Converting variant coding data to component lists

Since the list containing the model, destination, and equipment information which forms the basis of variant coding data is managed in accordance with an existing in-house design management system, it is desirable that the variant-coding data list also be managed based on the same system.

For the purpose of management, variant coding data is linked with information specific to the model or vehicle in question, and also with equipment specification information that determines vehicle settings and options for each customer (Fig. 1).

The variant coding data for each individual vehicle is determined uniquely based on this information.

3.3 Management and administration of variant coding data

As described above, variant coding data is managed in the form of a list and based on an existing design management system; however, relative importance in terms of management is set to the same level as the list that regulates design information for the variant coding ECU. In other words, variant coding data is treated as a component assembled within the vehicle. Accordingly, if a modification or addition is required to be made with respect to the content of the variant coding data list, notification is provided to the relevant departments through the issuance of a design change notice by the design department in question, in the same way as would be done in the case of a so-called "design change".

4. Production application

4.1 Overview

The Pro-METS* Runtime Server (PRS) was newly developed in order to manage the ECU variant coding (Fig. 2).

*Pro-METS: Mitsubishi ECU Test System for Production

The main functions of PRS are as follows:

- Automatic creation of the variant coding data based on the production planning information and design specific information.
- Creation and adoption of the proper variant coding data by using the design change notification with effective date.

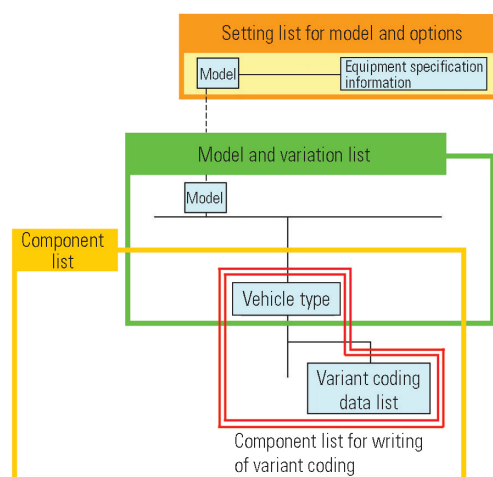


Fig. 1 Interlinking of design data

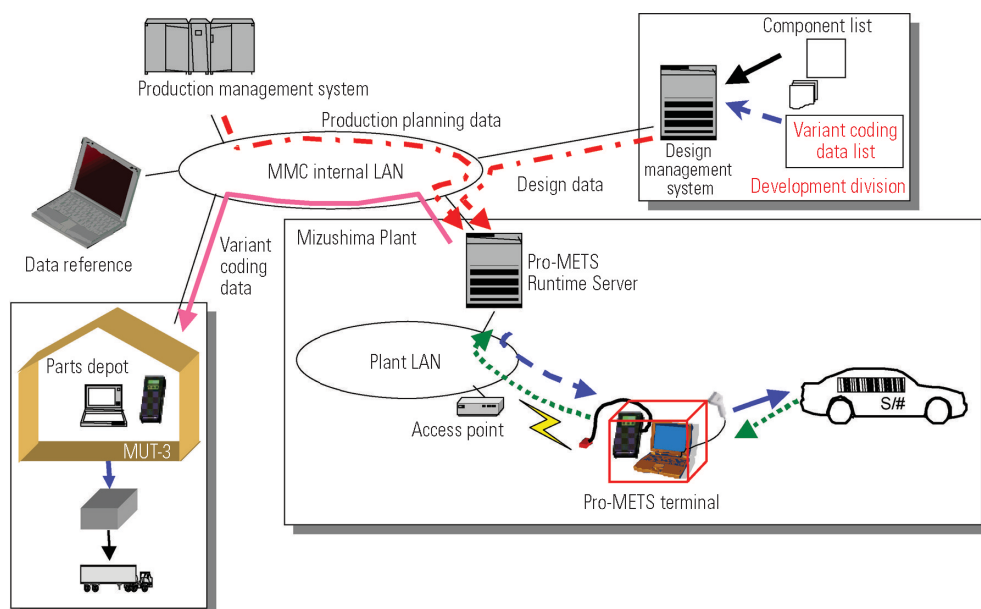


Fig. 2 e-DaCS overview

- Storage the variant coding data written in the ECU as a historical information by using Pro-METS.

4.2 Creation of variant coding data

Variant coding data based on equipment specification information for each vehicle is created by the PRS on a daily basis from production plan data for each mass-production vehicle, which is managed in accordance with the production management system, and design data, which is created by the design division (Fig. 3).

4.3 Application of design change to mass-production vehicles

In situations where variant coding information is changed, there is a possibility that the corresponding design changes will be applied using design change notification prepared by the design division.

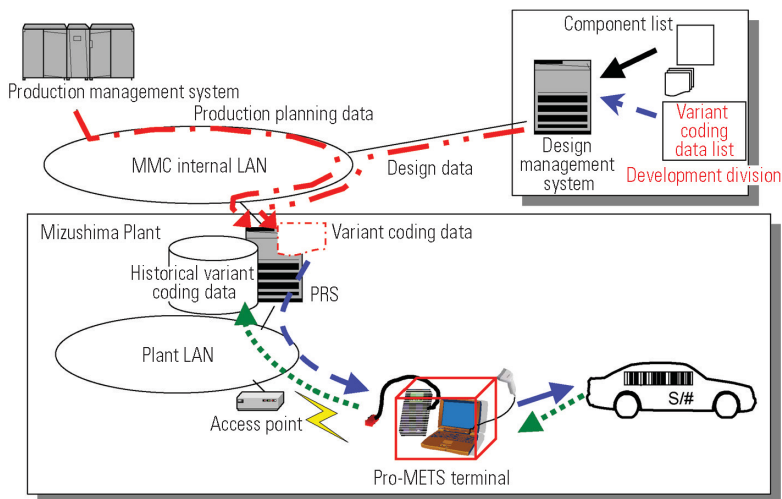


Fig. 3 Variant coding information and flow of data

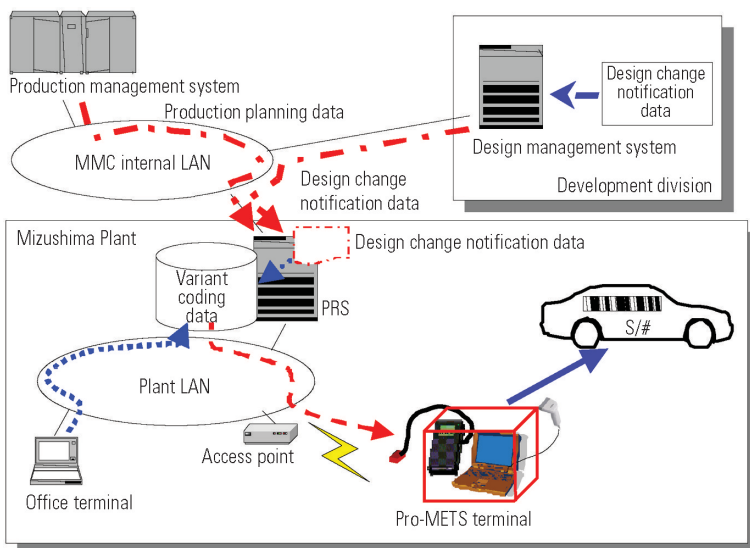


Fig. 4 Support for design changes

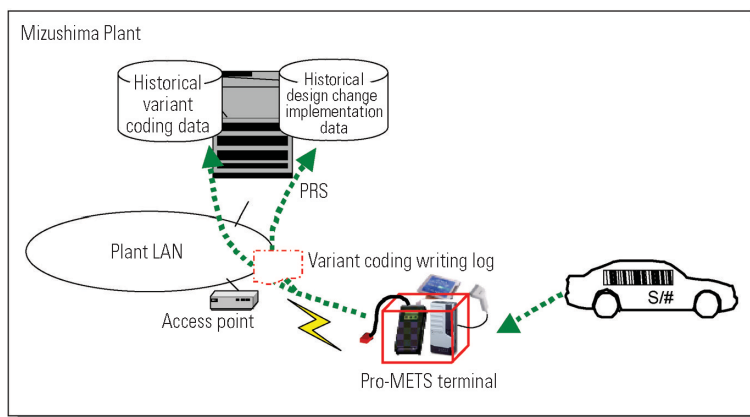


Fig. 5 Flow of data during the recording of logs

When design change is being used to update mass-production vehicles, the corresponding model and implementation timing must be specified from the Web screen of an office terminal (Fig. 4).

4.4 Storage of variant coding logs

The diagram of keeping the log data flow is shown as Fig. 5. Variant coding log data from a Pro-METS terminal is forwarded to the PRS via the plant LAN, and this is stored together with design change implementation logs. Furthermore, this log data is reused as writing data when replacing an ECU in the market.

5. After-sales application

5.1 Overview

When performing the replacement of the ECU should be done variant coding at a dealership, it is necessary to install an ECU in which the correct variant coding data for the vehicle in question has been recorded.

Accordingly, the MUT-3 breakdown diagnosis tool has been provided with functionality for the writing of variant coding data. The fundamental concepts of

- Usage of variant coding data, which is downloaded from the PRS, without modification, and
 - Implementation of variant coding data with complete correlation with the VIN and the ECU part number
- were adopted as preconditions during the development of this functionality.

5.2 MUT-3 variant coding process

The method for writing variant coding data using an MUT-3 requires that, first of all, the variant coding data file corresponding to the vehicle in question be downloaded from the PRS using the VIN and the ECU part number as keys, and that it then be written to the MUT-3.

Using the VIN that was input and the part number read from the ECU, the MUT-3 performs a comparison with the VINs and ECU part numbers in the variant coding data file and displays a list of the matching files (Fig. 6).

Next, the data to be actually written to the ECU is extracted from the matching variant coding data file, and a CRC operation is carried out. The results of this CRC operation are compared with CRC operation result data already contained in the data file, and if they match, actual writing of data to the ECU takes place.

Finally, the content read from the variant coding data file (b) and the content read from the data written in the ECU (a) are dis-



Fig. 6 Searching variant coding data

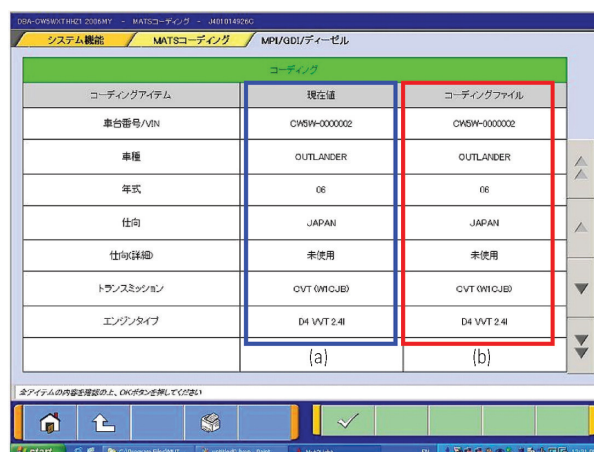


Fig. 7 Data verification

played simultaneously in order to allow visual confirmation of the match between them (Fig. 7).

5.3 Issues to be addressed

At the domestic startup of the new OUTLANDER, support for the replacement of the ECU should be done variant coding at dealerships has been provided by writing of variant coding data using an MUT-3 at the Spare Parts Supply Division, and by then sending the fully-written ECU to the dealerships in question.

Although this process will be employed for the present, a study is currently underway to evaluate the feasibility of having the writing of variant coding data performed at domestic and overseas dealerships as soon as possible.

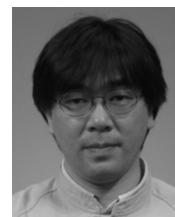
6. Conclusion

In order to provide support for the writing of variant coding data to ECUs, an integrated system for development, production, and after-sales servicing was developed and implemented. In this way, it has been possible to limit the amount of ECU part numbers and reduce the associated administration costs.

To conclude, we would like to express our heartfelt thanks to all who contributed to the development of this system.



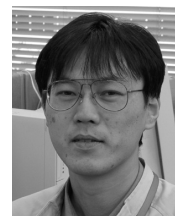
Hiroki TAKIMIZU



Toshiki FUKAYA



Yoshiaki ITO



Nobuhiko SAKANO

ETACS Functionality Development for the OUTLANDER

Takeo NAGAMORI* Takashi INOUE* Yasuyuki MIZUTANI*
Yukihiro NISSATO* Hiroshi HYODO* Naoki KAWASHIMA*

Abstract

Mitsubishi Motors Corporation's (MMC's) unique body-system electronic controller, Electronic Time & Alarm Control System (ETACS) has been advanced in order to take on the role of core ECU for the entire electronics system in vehicles from the conventional body control system⁽¹⁾. In the new OUTLANDER, ETACS performs a gateway for vehicle communications. Also it distributes power, and switches electronic component's variations to establish proper Controller Area Network (CAN) bus communication structure. With the integration of these significant functions, ETACS achieves considerable advantages for development, production, and retail processes.

Key words: Electronic Equipment, Electronics Control, Multiplexing, Diagnosis

1. Foreword

The vehicle mounted ECUs are desired to achieve development-related "Seeds", such as wiring minimization or performance enhancement, through using communication network. At the same time, it has to satisfy production or retail process "Needs". For example, ECU is being required to reduce its number of variations, and to implement full diagnosis function or assurance of traceability. In the new OUTLANDER, a new-generation platform⁽²⁾ for electronics has been adopted with the ETACS that designated as a core ECU thereof. This infrastructure has made possible to satisfy "Seeds" and "Needs" above, including to apply switching variation of ECUs (variant coding)⁽³⁾ with this network communication. These systems will be described hereinafter.

2. ETACS system configuration

The appearance of the ETACS is illustrated in Fig. 1, and the overview of the system is provided in Fig. 2. Approximately thirty different switches, auto-light sensor, and external temperature sensor are connected directly to the ETACS. In terms of networks, the communication system comprises four CAN and LIN, and as the central unit thereof, the ETACS exchanges signals with the various networks. Furthermore, based on the various numbers of data obtained from switches and communication network, the ETACS controls most of body electronics components such as power door locks, exterior lights, and windshield wipers.

3. Overview of the evolution of ETACS functionality

3.1 Junction-block unification

Although reduced wiring is an inevitable consequence of the practical implementation of communica-

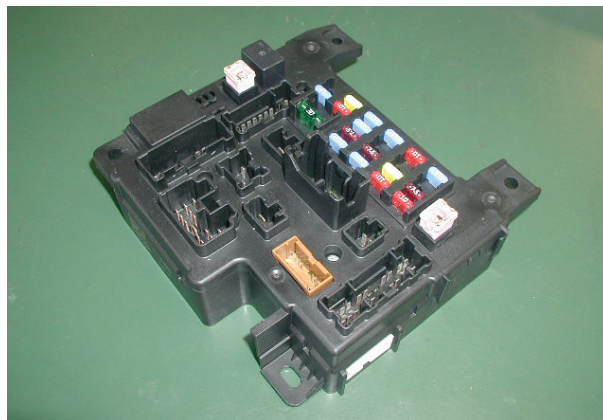


Fig. 1 Outer appearance of ETACS

tion networks, this project has achieved optimum harness routes through the integration of junction blocks and fuse boxes, which had traditionally been separate components. Furthermore, by integrating the wire-to-wire joints into ETACS, this development has also given rise to further harness reduction.

3.2 Power control

This implementation of the ETACS is provided with functionality for the control of all vehicle power using relays and based on data from the ignition switch (Fig. 3). This adds a high level of convenience when, for example, post-fitting remote-control engine starters, which are in high demand in colder regions. If this type of post-fitting operation were to be performed in a standard vehicle, it would be necessary to insert bypass circuit into the ignition switch, and furthermore, special modification would also have to be performed on the immobilizer. In the new OUTLANDER, however, since the ETACS is capable of controlling the vehicle's entire power system, there is no need to insert bypass circuit

* Electronics Engineering Dept., Development Engineering Office

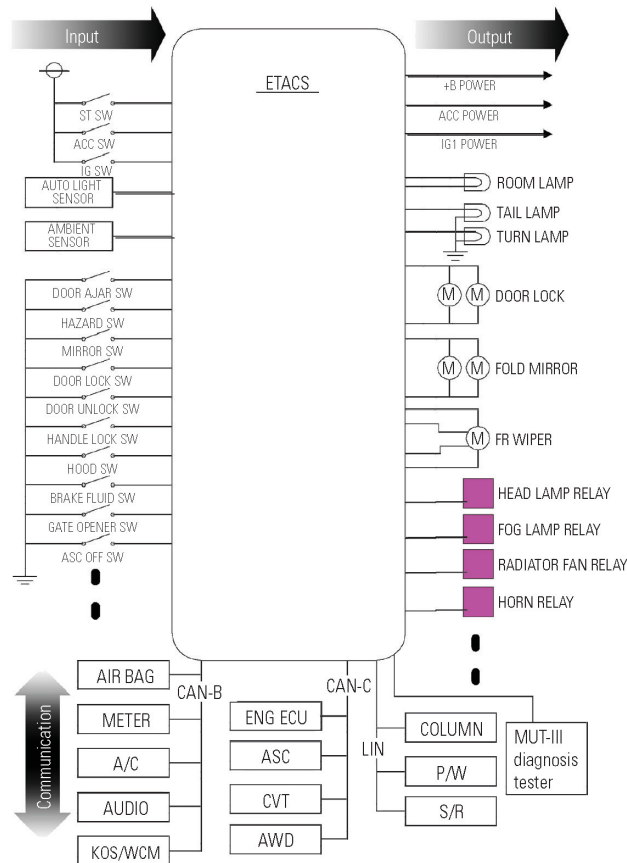


Fig. 2 Overview of the system

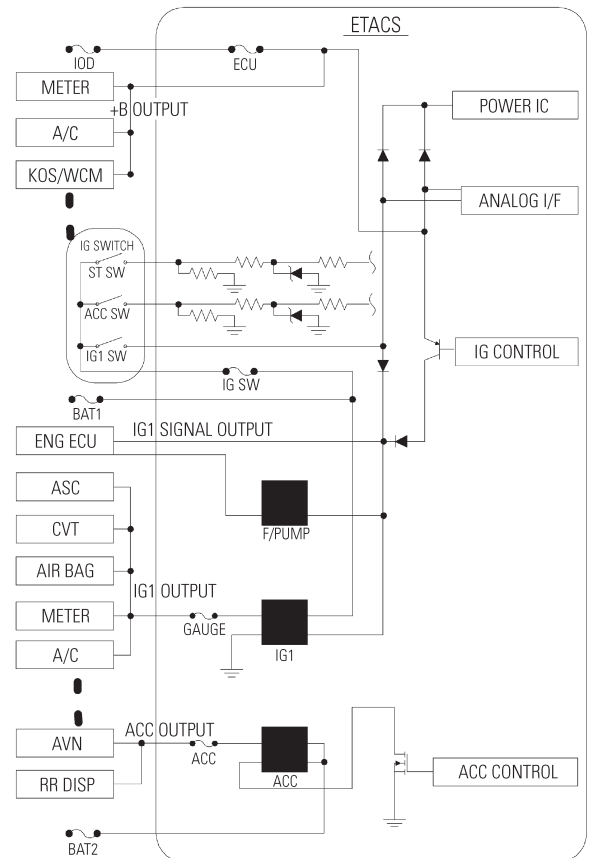


Fig. 3 Ignition control

into the ignition switch, and also since the CAN already incorporates the functionality of the immobilizer, making this available through the action of the ETACS simplifies the post-fitting of a remote-control engine starter.

3.3 Gateway

The conventional ETACS featured gateway functions between a pair of communications busses (CAN and SWS); however, this project provided functions for four such busses – namely, CAN for the powertrain & chassis, CAN for the mid-speed body & AV, LIN for the low-speed body, and CAN for diagnosis – and made it possible for ECUs to be deployed on the corresponding communications busses. Furthermore, CAN for diagnosis is dedicated to the communication with a diagnostic tester, and the ETACS acts as a firewall in order to realize physical isolation and security protection. (For more details, refer to the separate report, Development of a Next Generation Electronics Platform).

3.4 Data coding

The major distinguishing characteristic of the new OUTLANDER's ETACS is data coding, which is classified into the following three types. In order to respond suitably to the needs of production plants, dealerships, and customers, the functionality of ETACS can be switched without the need for parts replacement.

(1) Variant coding

Performed at the final stage of a production plant's assembling line, variant coding is a process whereby data pertaining to a vehicle's equipment specification is written to ECUs and the functionality thereof is switched. In this way, it is possible to significantly curtail the increase in part numbers that had come about in line with the recent trend for increased ECU functionality. **Fig. 4** presents an overview of the variant coding process. In said final stage of a production plant's assembling line, equipment specification data required for the switching of functions in the ETACS and other ECUs (hereinafter "coding data") is written using an inspection tool known as Pro-METS. In addition to switching its own functions based on coding data, the ETACS also forwards this data to the CANs and LIN. Accordingly, the ECUs connected to these networks perform function switching based on the coding data.

Up to 100 different items of coding data are used, and this comprises both the basic equipment information pertaining to vehicle type, destination market, and engine and transmission models, as well as unique specification-related information for the detailed switching of functions in the ETACS and in ECUs for the combination meter, the air conditioner ECU, and other similar components.

(2) Option coding

Coding data also contains information relating to the specifications of additional equipment fitted at deal-

An example of coding items

Vehicle line	LANCER	General coding items
	LANCER EVO	
	MIRAGE	
	LANCER WAGON	
	OUTLANDER	
	DELICA	
Destination	JAPAN	General coding items
	GENERAL EXPORT	
	USA	
	EUROPE	
	AUSTRALIA	
	GCC	
Engine type	3.0L 54	General coding items
	2.0L DIESEL	
	1.8L D4	
	2.0L D4	
	2.4L D4	
	1.5L D4	
	2.0L D4 T/C	
	2.2L D4	
DRL	DRL not present	ETACS coding items
	Normal DRL	
	Dimming DRL	
	Independent DRL	
	Dimming DRL with P	
	Independent DRL with P	
Turn signal bulb	21W + 21W + 5W	ETACS coding items
	21W + 16W + 5W	
	21W + 21W	
	21W + 16W	
Security alarm	Not present	ETACS coding items
	A-spec.	
	B-spec.	
	C-spec.	
Vehicle Language	No request	Combination meter coding items
	Japanese	
	English	
	French	
	Spanish	
	German	
	Portuguese	
	Dutch	
	Italian	
	Swedish	
	Danish	

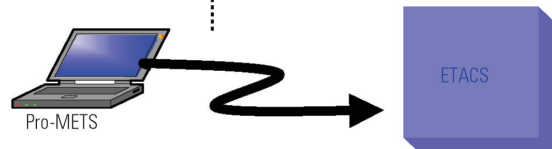


Fig. 4 Example of variant coding items

erships. For example, a specific item of coding data is used to indicate whether or not the vehicle is fitted with fog lamps; however, it is often the case that this component is an optional extra that is fitted at the dealership. Overwriting of such items of coding data can be carried out at the dealership in question using a diagnostic tester. However, only certain items of data can be overwritten at dealerships and all others are protected from accidental overwriting. For example, the lighting mode of fog lamps varies from country to country, and another coding item is used to identify the relevant mode. Since a country's fog-lamp lighting mode is defined by law, overwriting of the corresponding coding item at a dealership is not possible.

(3) Customization

The term "customization" is used to describe the modification of detailed functions by the individual user. For example, the ETACS facilitates the setting of theft alarm, adjustment of the lighting threshold of

An example of customizing items

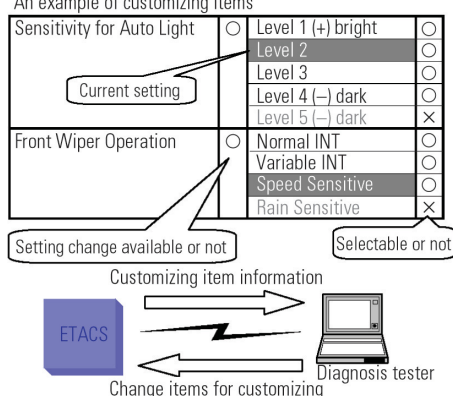


Fig. 5 Example of customizing items

auto-lights, and other similar customization actions through the use of a diagnostic tester at the dealership in question. The conventional ETACS also has the customizing function but it is limited. Although customizable items will depend on the equipment specification of the vehicle in question (for example, it will only be possible to modify the lighting threshold of auto-light for vehicles fitted with this component), it is not possible for the diagnostic tester to determine those that are customizable and those that are not; accordingly, it was required that all menu items be displayed. In the case of this OUTLANDER, however, customizable items are sent to the diagnostic tester based on coding data, and only those which can be modified are displayed on the tester's screen (Fig. 5).

3.5 Vehicle number correlation

As the ETACS records the coding data specific to the vehicle, installation on a vehicle with different equipment will result in the ECUs becoming unable to function correctly. A process for preventing this outcome is described below. In the production plant, variant coding is performed on the ETACS after the vehicle identification number (VIN) has been written to the engine ECU. At this time, the ETACS independently obtains the VIN sent from the engine ECU to CAN bus and stores it internally. In other words, this ensures that the VIN stored in the engine ECU and the ETACS are identical. In the unlikely event that, in the marketplace, an ETACS were to be removed from one vehicle and installed in another, it would identify non-conformity between its internally stored VIN and that in the new vehicle's engine ECU, and would send an error message on the combination meter. Upon receipt of this message, the combination meter would display "SYSTEM ERROR" to inform the owner that a non-genuine part had been installed.

3.6 Network diagnosis

In the case of conventional vehicles, diagnosis of optional functionality (i.e., whether this was due to failure or non-fitting) was required to be left to the discretion of the service technician in question. For example,

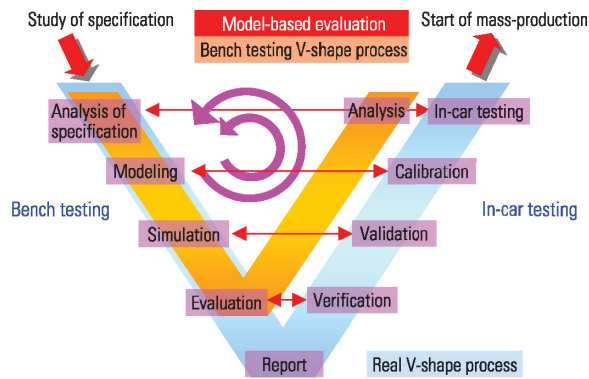


Fig. 6 Model-based evaluation

since the sunroof ECU and the audio-system ECU are linked via a network, even if one of these systems were not present in the vehicle, it would be determined that a communication error had occurred. Nevertheless, diagnosis is carried out based on regulated coding data in the new OUTLANDER, and this improvement ensures that failure is not diagnosed with respect to the functionality of a non-fitted item of equipment. Furthermore, by functioning as a gateway, the ETACS can monitor the communication status of all ECUs, record distance traveled or time elapsed since the occurrence of a failure, and collect a wide range of diagnosis-related information in this way. (For more details, refer to the separate report, Development of a Next Generation Electronics Platform.)

3.7 Reprogramming

In accordance with increasing ROM capacity and functional complexity in recent ECUs, it has become more common to use flash ROM as a means of reducing lead time and eliminating risk. Although flash ROM is also being used in the ETACS of the OUTLANDER, this has been further advanced in order to enable a diagnostic tester to reprogram via the CAN bus without the need to remove the ETACS from the vehicle. Flash ROM was traditionally used at the development stage in order to allow reprogramming; however, by making this possible without the need for removal from the vehicle, the efficiency of development operations has been significantly enhanced. Furthermore, flash ROM is continuously used in post-production as the gateway and variant coding functionality provides support for situations where specification changes must be executed in short periods of time. This is advantageous in that old-part inventory is reduced to zero for changes in specifications.

4. Evaluation of reliability

4.1 Bench testing

The ETACS control volume can rise to the equivalent of hundreds of thousands of microprocessor commands. Furthermore, the increased number of man-hour at testing stages now required to evaluate more advanced, complex systems has become a serious

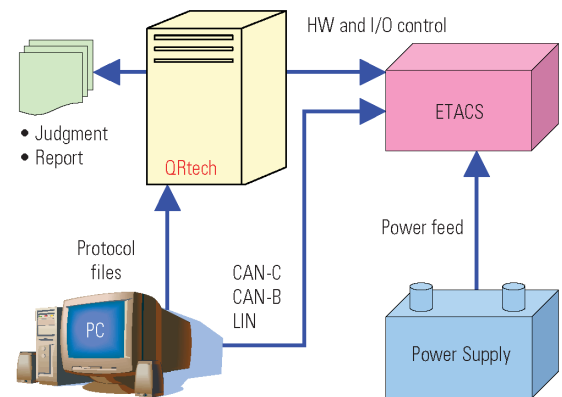


Fig. 7 Bench testing tool

problem. As a countermeasure, the focus has been shifted to model-based evaluation wherein loading conditions equivalent to those in an actual vehicle are recreated in a bench-test simulator, and operation is examined in a hypothetical manner, thus reducing the extent of evaluation required of subsequent in-car testing (Fig. 6).

QRtech® (from Qualified Real-time Technologies) is used as the simulation tool for model-base evaluation. In accordance with the input of special protocol created as a text file, this fully-automatic bench testing tool can simulate conditions equivalent to those in an actual vehicle operation, evaluate with respect to pass/fail criteria, and output the corresponding reports (Fig. 7).

As many as 42,000 different functional test patterns can be implemented using this model-base evaluation, and by also examining for software bugs, setting errors in microprocessor control resistors, and other design mistakes, it is possible to determine whether the ETACS is operating in accordance with design parameters.

4.2 In-car testing

For the ETACS that is a core of the new-generation electronic platform, it is difficult to reveal all the malfunctions by the bench testing of ECU only. It must be verified as a vehicle system formed by many components to evaluate its reliability. Therefore, a vast in-car testing hours of totally 2,400 hours were spent to confirm the system while placing stress on the following points:

- Operation check with respect to switch operation timing, transient input, and simultaneous operation of multiple functions
- Check of software filter with respect to communication data receive timings
- Operation check with respect to the power voltage fluctuation due to cranking
- Check of failsafe with respect to the switch input and erroneous data receipt that are not possible in real working conditions
- Operation confirmation and interference confirmation with respect to the data coding

5. Conclusion

In conjunction with a major system change to apply new generation electronic platform, the critical responsibility as core network component was assigned to the OUTLANDER ETACS. Thus, corresponding man-hours in the development have been taken, compare than typical conventional ETACS developments. The action was taken with the aim of realizing not only design-related benefits, but also significant advantages in terms of production, retail process and service. We are sure that these technologies become more common because of the convenience afforded by switching function by ECU variant coding, diagnosis and reprogramming functionality on many occasions. Of course, based on the system established for the OUTLANDER, it is our desire to continue development of unique MMC ETACS.

In concluding, we would like to express our sincere gratitude to our ETACS supplier, who have made great effort for design review of up to 4,000 hours, and to all others who contributed to this project.

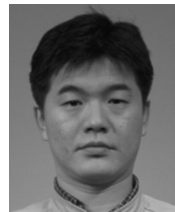
References

- (1) Naoki Kawashima et al.: Multiplex Communication System for Column Switch and Instrument Panel Switches, Mitsubishi Motors Technical Review No. 10, 1998 (Japanese edition)

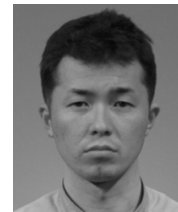
- (2) Hiroki Fukatsu et al.: Development of a Next Generation Electronics Platform, Mitsubishi Motors Technical Review No. 18, 2006
- (3) Hiroki Takimizu et al.: ECU Variant Coding System, Mitsubishi Motors Technical Review No. 18, 2006



Takeo NAGAMORI



Takashi INOUE



Yasuyuki MIZUTANI



Yukihiro NISSATO



Hiroshi HYODO



Naoki KAWASHIMA

Development of High Quality Premium Sound System

Taizo NAKAMURA* Atsushi GOMI* Hidekazu ISHIWATA*
Takahiro UMEMURA* Shigeaki ASANO* Yuji KAMIYA*

Abstract

The new OUTLANDER features the first application of the Rockford Fosgate premium sound system in Japan. In the realization of its aim of achieving audio quality beyond that expected of manufacturer's genuine-part systems, this sound system not only improves the individual performance characteristics of speakers, power amplifiers and other system components, but also optimizes the speaker mounting conditions, in order to maximize the performance levels thereof.

Key words: Premium Sound System, High Quality Sound, Speaker Installation Condition, DSP (Digital Signal Processor)

1. Introduction

We targeted the following in order to achieve audio quality beyond that expected of manufacturer's genuine-part systems and surpassing the customer's expectations.

- (1) Clarity
- (2) Strong, punchy ultra-low sounds
- (3) Atmospheric sound field

In order to realize the above, it is insufficient to simply improve the individual performance characteristics of speakers, amplifiers, and other system components; rather, it is critical to optimize the speaker mounting conditions expanded to the level of the vehicle structure and to also match the power amplifier's output characteristics to the sound qualities of the new OUTLANDER's passenger compartment. We would now like to present the results achieved through optimization of speaker mounting conditions, and through sound matching using a digital signal processor (DSP) integrated into the power amplifier.

2. System configuration

We have adopted a 9-speaker / 7-position configuration for the Rockford Fosgate premium audio system used in the new OUTLANDER (Fig. 1).

- Passenger-compartment side of door mirrors: 3.5-cm soft dome tweeter (sound only high-frequency band)
- Front doors: 16-cm mid/bass speaker (sound only mid-low frequency band)
- Rear doors: 16-cm coaxial 2-way full-range speaker (sound full-range frequency band)
- Left side of cargo room: 25-cm subwoofer (sound only ultra-low frequency band)

Furthermore, in order to provide these speakers with ample input, a 650-W (max output) power amplifier has been mounted underneath the driver's seat.

In this way, clear audio without the feel of distortion

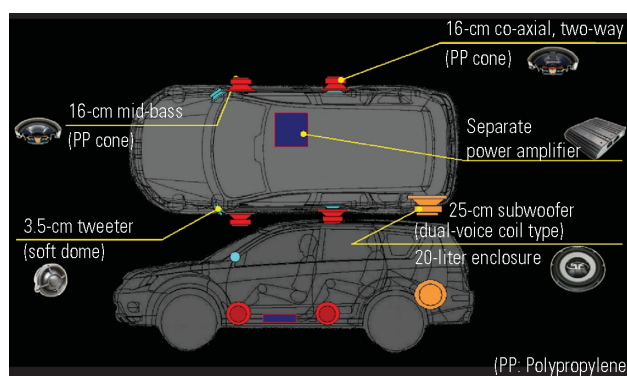


Fig. 1 Speaker layout of the new OUTLANDER

can be output from front- and rear-door speakers and tweeters, with punchy ultra-low sounds reproduced by the 25-cm subwoofer. Furthermore, the output characteristics of the power amplifier are matched to the sound qualities of the new OUTLANDER's passenger compartment by the DSP contained therein, thus realizing an audio system capable of generating a high-quality sound field.

3. Technical characteristics

3.1 Optimization of door-speaker mounting conditions

In order to output high-quality audio from speakers mounted on vehicle doors,

- (1) Rigidity of the speaker mounting surface, and
 - (2) Doors with a speaker-box structure
- must both be achieved. If the mounting surface is insufficiently rigid, the energy of the output sound will be converted into energy of vibration in the door panels, and in addition to reducing the sound-generation efficiency of the speakers, this has the added effect of reproducing unwanted distortion when the mounting surface itself begins to vibrate. Furthermore, if the door

* Electronics Engineering Dept., Development Engineering Office

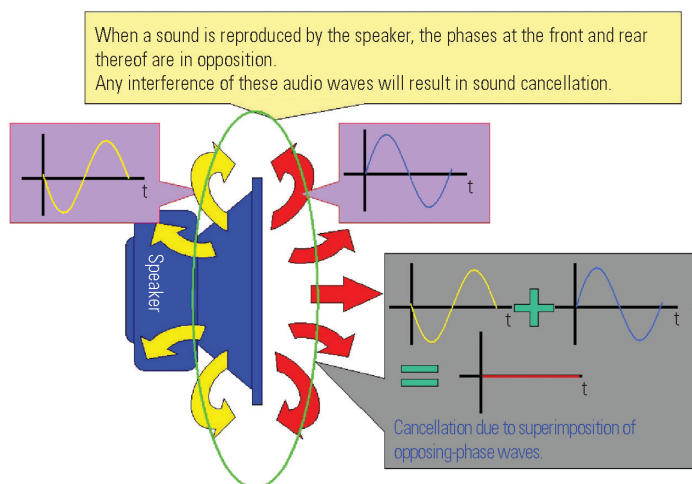


Fig. 2 Leakage of sound from the rear of the speakers

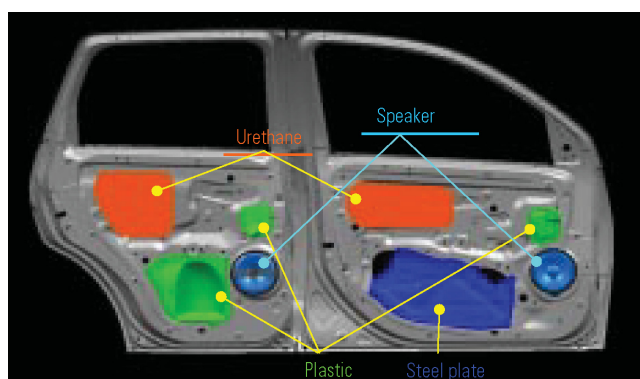


Fig. 3 Door structure of the new OUTLANDER (speaker-box structure)

does not have a speaker-box structure and if holes provided in the inner panels for assembly work are not closed off, sound from the rear of the speakers will leak in via these holes, will interfere with the sound being output from the front, and will result in audio-wave cancellation (Fig. 2). In order to eliminate such sound deteriorating factors, this premium sound system reinforces the doors while at the same time giving them a speaker-box structure (with work holes closed over) (Fig. 3). The following will describe the effects of these improvements. Specifically, the results of measurement carried out in doors with and without a speaker-box structure will be compared.

Fig. 4 presents the results of measurement of the sound pressure level that causes total harmonic distortion (THD) of greater than 10 % when sine waves with frequencies ranging from 40 to 100 Hz are input to a right-front door speaker.

Generally speaking, as the volume rises, sound pressure increases and distortion increases.

As can be seen from the figure, when the door has a speaker-box structure, the sound pressure corresponding to 10 % distortion is higher. In other words, the clarity of sound output is enhanced since distortion is elim-

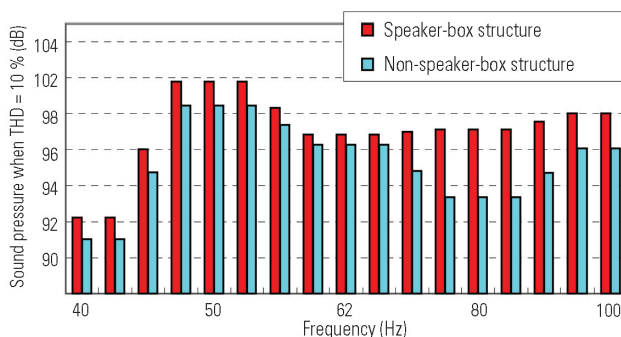


Fig. 4 Results of sound pressure characteristics measurement at 10 % total harmonic distortion

inated. In the case of large output, furthermore, sound with little distortion can also be achieved.

Fig. 5 presents the results of measurement of reverberation when an impulse is input into the right front-door speaker.

As can be seen from the figure, response in the ultra-low frequency band is better in the case of speaker-box structure, and in addition, the sound also attenuates smoothly. In other words, audio signals can be regenerated definitely as a result of superior responsiveness to the input signal.

Fig. 6 presents the results of the measurement of frequency characteristics when an 80-Hz sine wave is input with a uniform input level into the right front-door speaker.

As can be seen from the figure, a speaker-box structure gives an 80-Hz sound pressure level that is approximately 2.5 dB higher, even though the level of the signal input into the speaker is unchanged. In other words, less energy need be input in order to reproduce sound at the same volume, thus improving the efficiency of sound generation.

In the new OUTLANDER, therefore, responsiveness can be improved, and clear, distortion-free sound can be reproduced by providing the mounting surface for the speakers on the doors with sufficient rigidity, and

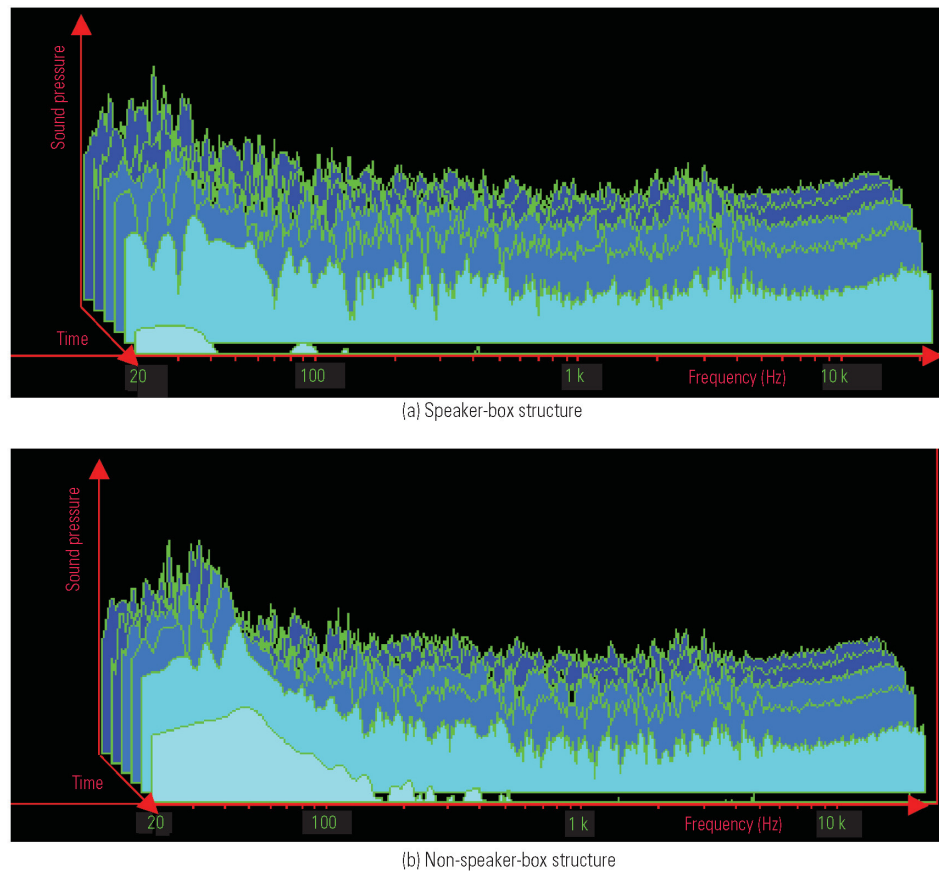


Fig. 5 Results of impulse response measurement

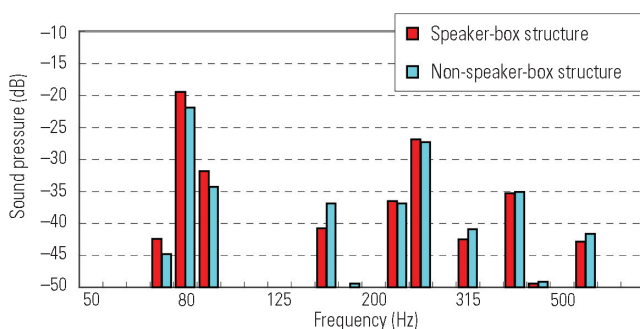


Fig. 6 Results of harmonic distortion measurement with 80-Hz input

by also giving the doors a speaker-box structure.

3.2 Optimization of the 25-cm subwoofer mounting

In order to achieve high-quality sound reproduction, it is necessary to faithfully reproduce the entire 20 Hz to 20 kHz spectrum that is recorded on CDs. However, the reproduction of ultra-low sound is particularly difficult inside a vehicle's passenger compartment, and very few companies have been able to reproduce a sound system with sufficient low-frequency punch. In order to fully reproduce sound in these frequencies,

- (1) a subwoofer with large diameter, and
- (2) a large, closed speaker-box structure

must both be achieved. Generally speaking, the larger the diameter of the subwoofer, the greater the ability to reproduce the ultra-low sounds; however, the subwoofer's mounting conditions and the capacity of the speaker-box also have a considerable effect on its performance. Since the speaker-box is completely sealed, when its capacity is excessively small, the air that it contains can obstruct movement of the subwoofer's cone, and consequently, the lowest reproduction frequency in the ultra-low band is raised, and the efficiency of the speaker is reduced. Conversely, if the capacity of the speaker-box is excessively large, movement of the cone is completely unrestricted, and it becomes impossible to achieve tightness in the ultra-low sounds. In order to achieve accurate reproduction of ultra-low sounds in tandem with high-quality sound overall, this premium sound system has made use of 20-liter speaker-boxes. The following will describe the results achieved.

Fig. 7 shows the sound pressure results obtained with identical $\phi 25$ -cm subwoofers and a speaker input level of 128-W when the capacity of the speaker-box was varied (between 20, 15, 10, and 5 liters).

As can be seen from the figure, the greater the capacity of the speaker-box, the higher the sound pressure reproduced in the frequency band of 100 Hz and lower, wherein the subwoofer is effective. For example, a difference of approximately 3 dB is present between 10-liter and 20-liter boxes at 50-Hz, and when converted back, this difference corresponds to a dou-

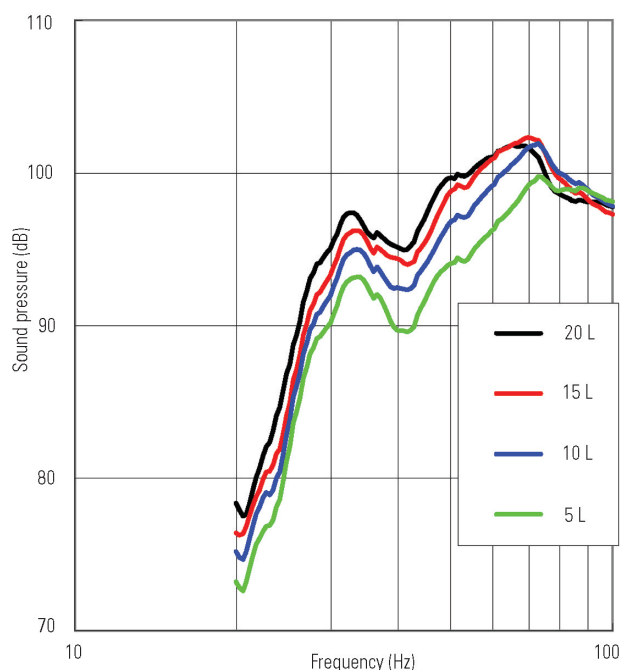


Fig. 7 Results of sound pressure measurement with 128-W subwoofer input

bling of the amplifier output. Accordingly, it can be seen that increasing the capacity of the speaker-box increases the reproduction efficiency of the woofer.

Fig. 8 shows the results obtained when measuring subwoofer impedance in similar test conditions to those described above.

The lowest resonance frequency F_0 is an indicator of a subwoofer's lowest reproduction frequency, and as can be seen from the figure, a comparison of speaker-box capacities indicates that larger capacities give lower F_0 frequencies. In other words, the larger the speaker-box, the greater the ability to reproduce sound in the ultra-low frequency band. In addition, this implies that the lowest reproduction frequency can be further lower to make possible regeneration at frequencies close to 20 Hz (**Fig. 7**).

By installing the above-described large, $\phi 25$ -cm subwoofer with a large, 20-liter capacity in the new OUTLANDER, it has been possible to reproduce ultra-low sounds at large volumes.

3.3 Audio quality tuning using a DSP

In order to reproduce high-quality sound within a vehicle's passenger compartment,

- (1) tuning of the frequency characteristics of power-amplifier output (i.e., matching to passenger-compartment sound environment characteristics), and
- (2) tuning of the timing of each speaker's output (i.e., compensating for differences in distance from listener to speaker)

must both be achieved. When reproducing audio inside a vehicle, certain frequency bands become emphasized and certain others become attenuated due to the influence of unique shape and material characteristics within

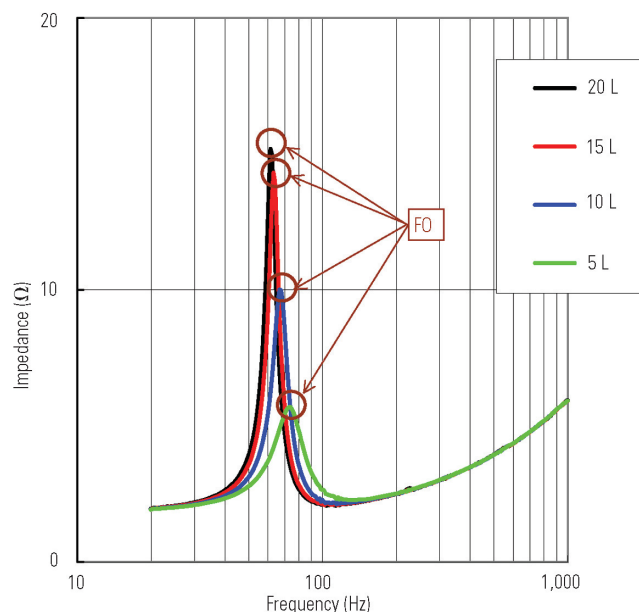


Fig. 8 Results of subwoofer impedance measurement

the passenger-compartment environment in question. A parametric equalizer is used to compensate for these differences. Through the use of such a device, the over-emphasized frequency bands can be attenuated, and the weak bands can be amplified, thus tuning to a flat and smooth frequency response overall. In this way, the listener can enjoy natural and clear sound reproduction.

Furthermore, each speaker is positioned at a different distance from the listener, and if this condition were not compensated for, the audio actually being heard would be closest in terms of sound quality to that reproduced by the nearest speaker. Compensation is therefore achieved through the use of time alignment functionality. In this way, the differences in the distance to the left and right speakers are compensated for by adjusting the output timing of said speakers, thus tuning the overall sound in order to achieve a pleasing stereo balance and acoustic image. The following will describe the results achieved by these processes.

Fig. 9 presents comparative data corresponding to the use and non-use of parametric-equalizer compensation.

As can be seen from the figure, sound reproduction is enhanced with regard to the following through the use of this technique.

- Improved tightness in ultra-low sounds in the vicinity of 100 Hz
- Reduced muffled sound in the mid-lows in the vicinity of 200 Hz
- Reduced muffled sound in the vocals in the vicinity of 1 kHz
- Reduced distortion in vocals in the vicinity of 2 kHz
- Attenuation of unpleasant frequencies in the high-band in the vicinity of 10 kHz

In the data corresponding to non-use of the parametric-equalizer compensating technique, unpleasant muffled sound and/or distortion can be seen in each of

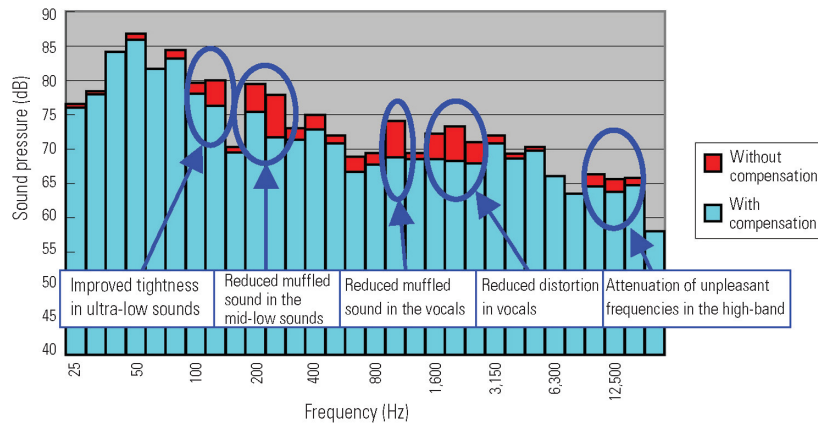


Fig. 9 Effectiveness of parametric equalization

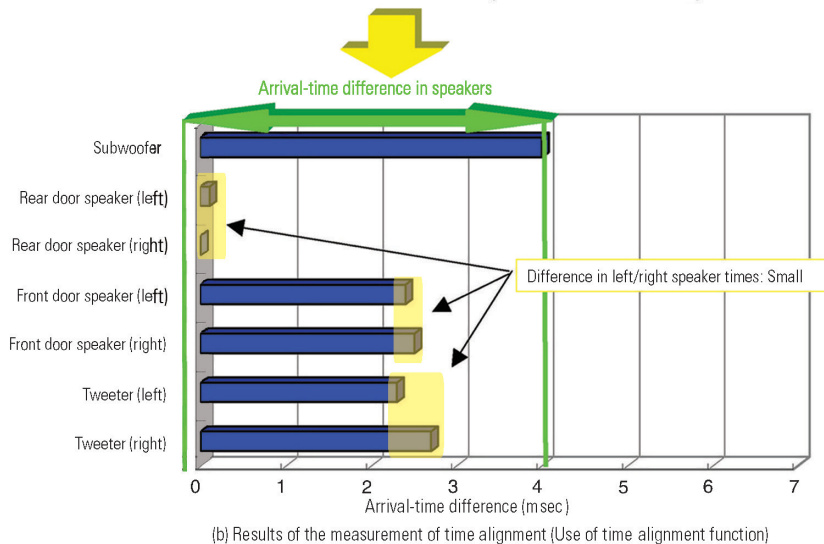
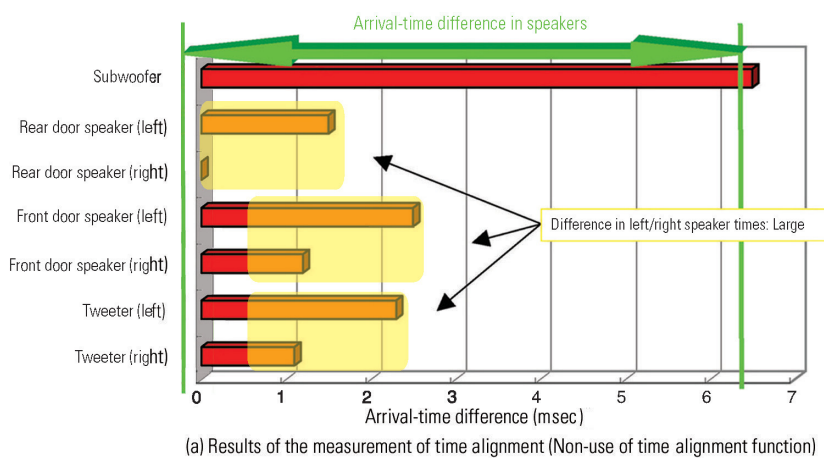


Fig. 10 Effectiveness of time alignment function

the frequency bands. These factors are brought about by speaker mounting conditions and the acoustic environment within the passenger compartment, and for this reason, they can be assumed to constitute an acoustic footprint unique to the new OUTLANDER. As a result of compensation using a parametric equalizer, however, it is possible to reproduce music that is both clear and free of distortion.

Fig. 10 presents the results of the measurement of time lag taken for sound to reach the driver from each speaker in situations where time alignment function is and is not used.

This is a time lag elapsed from output of sound signal by generator to receipt of that signal by microphone on driver's seat. The base time is the time microphone received the sound firstly (the sound from rear door speaker (left)).

As shown in Fig. 10 (a), there is considerable disparity in the times at which sound from the various speakers reaches the driver when time alignment function is not used, and this is particularly so in the case of the left and right speakers of the vehicle. Since the driver hears the sound from the right speaker first, the acoustic image tends to lean toward the right side. Furthermore, since the sound from the subwoofer arrives late considerably, there is a concern that the acoustic image may be dim. By using the time alignment function to adjust the arrival times of sound from the various speakers to suitable levels, the characteristic shown in Fig. 10 (b) can be achieved. When compared with that of Fig. 10 (a), it can be seen that the disparity in arrival times has been reduced, and that the time lag between left and right speakers is also lower. Furthermore, the delay in sound arriving from the subwoofer has been almost eliminated. In this way, the driver can enjoy a clear acoustic image with excellent stereo qualities.

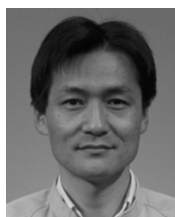
4. Conclusion

Through the use of high performance speakers mounted on a chassis optimized for this purpose, and matching of the acoustic characteristics of the new OUTLANDER's passenger compartment using a DSP tuning technique, it has been possible to achieve the development target – namely, audio quality beyond the customer's expectations.

Furthermore, specialist magazines have also lauded the system for its "audio quality beyond that expected of genuine-part systems and an extremely punchy

sound”.

Going forward, we will strive for more improvements in audio quality through further research into the enhancement of audio quality, the creation of body structure that allow speakers to perform to their maximum potential, and other such activities.



Taizo NAKAMURA



Atsushi GOMI



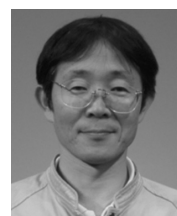
Hidekazu ISHIWATA



Takahiro UMEMURA



Shigeaki ASANO



Yuji KAMIYA

Newly Developed Three-Cylinder MIVEC Engine

Yukihiro RYUGO* Hiroaki MIWA*

Abstract

This report introduces the newly developed three-cylinder engine for "i", the new-concept minicar.

This engine was developed to be the optimum match for the mid engine rear drive (MR) platform of "i"; and during the course of this development, the focus was placed firmly on achievement of a lightweight, compact, high performance, fuel efficient, and low cost design.

As one of the core engines for the Mitsubishi Motor's future fleet of minicars, production began in December 2005 at our Mizushima Powertrain Plant, and cutting-edge manufacturing equipment was newly added for this purpose.

Key words: Gasoline Engine, Development/Mini Car, Basic Structure, Technical Feature

1. Development target

"The revolutionary mini car for a new generation" is the keyword of "i". And following items were required for its new engine; more compact contributing to "both innovative style and interior comfort", higher performance and more lightweight for admiring "fun to drive", lower fuel consumption for enabling better economical efficiency, lower noise for more delightful driving feeling than that of the same class cars, and cleaner exhaust emissions.

To meet these requests, this engine was harmonized with performance, fuel economy, quietness and reliability by newly considering its dimensions and structures, integrating our basic technology accumulated from our long experience and adopting the technologies exceeding the same class engines to make drivers aware the quality completely different from conventional mini cars.

2. Basic structure and technical features

All the dimensions, structures and specifications were considered from scratch for attaining the targets described above, so this engine's all elements; basic dimensions like bore and stroke, body structure, components, material and so on, were completely innovated. In addition, future promising variations were also considered. Its core technologies and achievements are introduced below. And the engine overview, the section view, the major specifications and the applied principal technologies are shown in **Fig. 1, 2** and **Table 1, 2** respectively.

2.1 Lightweight and compact design

The engine was downsized for mounting just in front of the rear drive shafts and for no harming the cabin and cargo space. Furthermore the engine was also

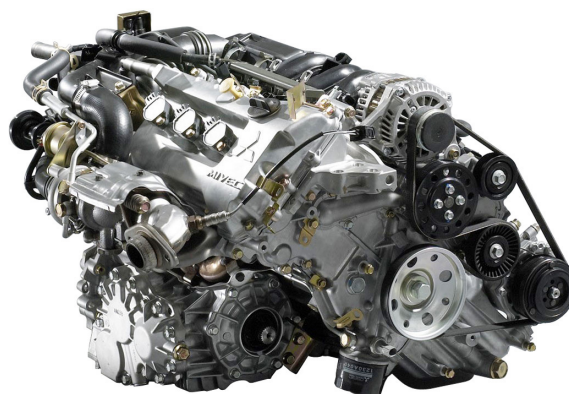


Fig. 1 External view of 3B20 engine

lightened to improve the driving performance.

The principal ingenious points for downsizing are the selection of the basic dimensions which reduce the height, simplification of the cylinder block structure, the adoptions of a timing chain for driving cams, a direct drive valve train system, modularized chain case, oil pump, water pump and engine mount and modularized intake and fuel system parts. The engine is mounted at 45 degrees slant back angle so that both dimensions of vehicle length direction and height direction can be settled with good balance. And the intake system and the auxiliary parts are placed efficiently.

The principal ingenious points for weight saving are the adoptions of lightweight materials like aluminum for the cylinder block and nylon resin for the intake manifold, the adoptions of thin plate parts like SUS plates for the exhaust manifold, the simplified structural elements, the modularized structure for integrating some parts and so on. Although it is equipped with DOHC MIVEC™, eventually the weight is shed by about 20 % against our conventional 3G83 SOHC 4-valve

* Engine Designing Dept., Development Engineering Office

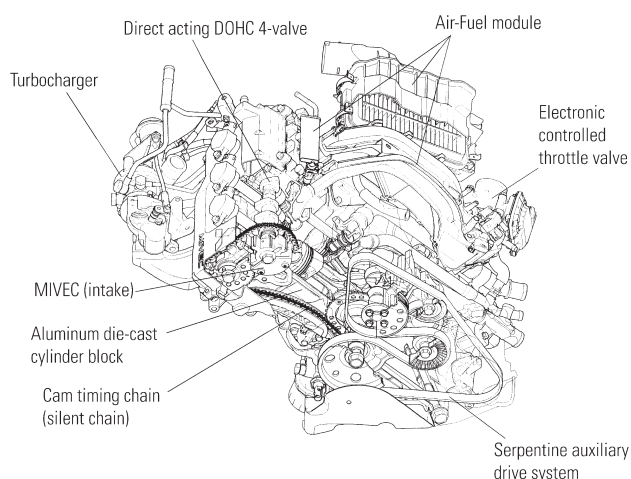


Fig. 2 Sectional view of 3B20 engine

Table 1 Major specifications

Item	Model	3B20	<cf.> 3G83
Vehicle model		i	ek-SPORT
Displacement	(L)	0.659	0.657
Cylinder bore diameter	(mm)	65.4	65
Stroke	(mm)	65.4	66
Stroke to bore ratio (S/B)		1.00	1.02
Cylinder bore pitch	(mm)	80	72
Compression ratio		8.8	8.5
Cylinder block material		Aluminum die-cast	Cast iron
Camshaft drive system		Silent chain	Timing belt
Valve train		Direct acting DOHC, 12 valves, with continuously variable valve timing MIVEC (intake)	SOHC, 12 valves, with roller rocker arms
Engine alignment		Rear exhaust	Front exhaust
Max. output	(kW/min ⁻¹)	47/6,000	
Max. torque	(Nm/min ⁻¹)	94/3,000	93/3,500
10-15-mode fuel consumption/ Equivalent inertia weight	(km/L)/(kg)	18.4/1,000	16.0/1,000
Emission control		Exhaust emissions 50 % lower than those specified by Japan's 2005 emission regulations (3☆)	

Table 2 Technologies and purposes thereof

Technology	Purpose	High performance/ low fuel consumption	Low exhaust emission	Lightness and compactness	Low vibration and noise	High reliability
Aluminum die-cast cylinder block		○		○	○	○
Mitsubishi Innovative Valve timing Electronic Control system (MIVEC)		○	○		○	
Direct acting DOHC valve drive		○		○		○
Cam timing chain (silent chain)		○		○	○	○
Squish piston for improved combustion		○	○			
Low friction main moving parts		○	○		○	
Modular design: chain case				○		○
Modular design: intake (resin manifold) and fuel systems			○	○	○	○
Optimum engine cooling specification		○	○			
Long-reach iridium spark plugs		○	○			○
Serpentine auxiliary drive system		○		○	○	○
High-response turbocharger		○				
Stainless steel pipe exhaust manifold		○	○	○		
Rear exhaust engine layout			○	○		
Electronic controlled throttle valve		○	○			○
Low-viscosity engine oil (5W-20)		○				

engine. The air-fuel module is shown in Fig. 3.

2.2 High performance and low fuel consumption

High performance, 47 kW (64PS), is attained by using the turbocharger with the intercooler.

The Mitsubishi Innovative Valve timing Electric Control (MIVEC) system and the high response turbocharger, which can act from low engine speed, enable to generate high torque from 2,000 min⁻¹. And 8 % gain of torque in low speed range is obtained against 3G83. The engine performance is posted in Fig. 4.

In addition to MIVEC system, raising the compression ratio, adopting squish pistons and the optimizing engine cooling system with the cylinder head oriented cooling, improving combustion with the resin intake manifold, reducing piston ring tension and other friction of engine elements enable the top level low fuel consumption in the class.

2.3 Low vibration and low noise

The technical concept to reduce vibration and noise had been tackled with a target to enhance the engine

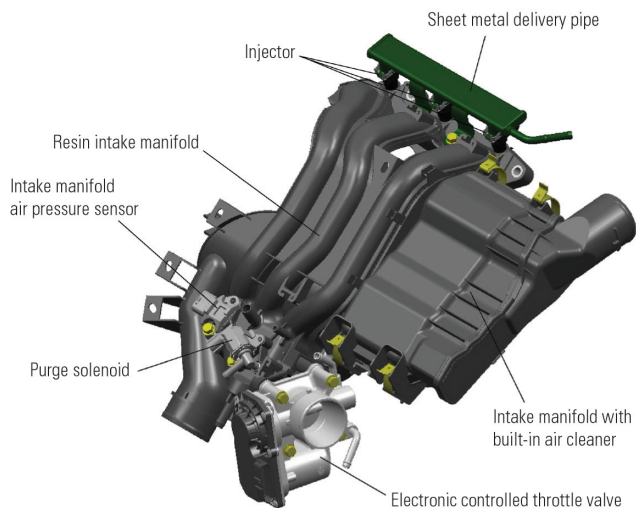


Fig. 3 External view of Air-Fuel module

body stiffness and diminish the noise from the moving parts.

The basic dimensions and structures of the cylinder block and the crankshaft were thought out. And high quality parts like an aluminum oil pan and an aluminum head cover are used for overcoming the same class engines.

The noise from moving parts was reduced by adopting a silent timing chain, improving the rigidity around the valve train and adopting an auto-tensioner for the auxiliary belt train. These improvements brought smooth sound and vibration from the lowest engine speed to the highest.

2.4 Environmental friendly

Accelerating activation of the catalysts was achieved by optimizing the intake port design, using MIVEC, implementing the double-pipe exhaust manifold, optimizing the fuel injector atomization and using newly developed catalysts. Therefore the emission level is extremely reduced. It eventually meets 50 % lower than the Japanese 2005 emission regulation level (3☆).

And the oil consumption and deterioration are managed to improve so that the oil change interval can be extended 1.5 times longer than usual.

2.5 Functions

The adoption of an electric control throttle valve improves engine controllability and can make a smooth relation between engine output and accelerator pedal

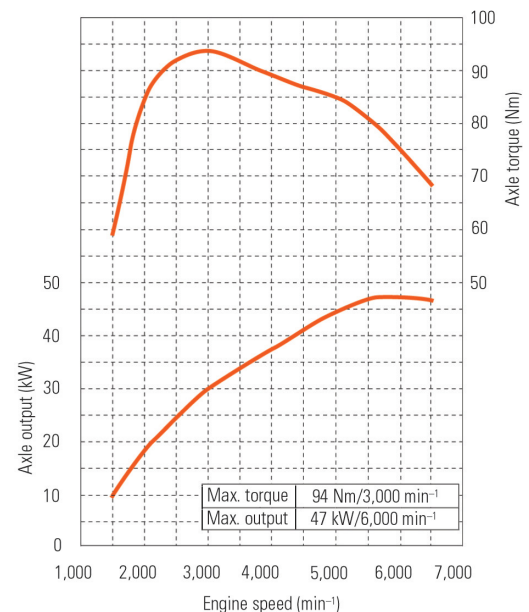


Fig. 4 Performance curve of the engine

operation, so it contributes good driving feeling which exceeds the same class cars'.

Furthermore, the latest ECU including a high performance and high capacity 32-bit microprocessor and the sophisticated software provide the optimum control in any driving conditions.

2.6 Others

The quality of this engine was extremely improved by means of wide variety of analyses using the latest simulation technology, implementation of digital modeling, collaboration with suppliers, application of our strict development process regulated by the Mitsubishi Motors Development System (MMDS), front loaded certain preparation for the production and installation of the latest production facilities.



Yukihiro RYUGO



Hiroaki MIWA

Overview of the Newly Developed Mid Engine Rear Drive Platform

Akinobu IWAO* Shinsuke KAWAMURA*

Abstract

The "i" platform development project was undertaken with the aim of achieving high targets which were not possible to achieve with conventional designs within the regulated subcompact automobile category – namely, highly-modern styling in tandem with interior comfort, light handling, a high level of riding comfort, and 360 ° collision safety. By relocating the power plant normally found under the front bonnet to the beneath the floor in the luggage compartment, it became possible to simultaneously achieve a one-motion silhouette profile, interior comfort, light handling, consistently high-quality driving comfort, a longer passenger compartment, safety under collision from all directions, long wheelbase, large wheels, small turning radius, and many other high-level elements that would traditionally have had to be traded off against each other.

Key words: MR, Platform, Subcompact Automobile

1. Foreword

The market for subcompact automobiles, which accounts for approximately one third of all automobile demand in Japan, is an extremely important business segment for Mitsubishi Motors Corporation (MMC), and over many years, we have introduced a range of new subcompact automobile products. The subcompact automobile – originally intended to become a simple means of transport for the masses – is nowadays seeing a wide diversification in customer requirements; against this background, we have embarked on the development of a new concept subcompact automobile, different to all others currently on the market, and as a means of generating new product value, we have designed a new layout platform. By removing the engine from the front of the vehicle, this new-development Mid Engine Rear Drive (MR) platform not only allows us to realize designs not previously possible as shown in **Fig. 1**, but also makes possible an extended passenger compartment through the application of technologies such as a long wheelbase equivalent to that of a small car, large wheels, and a longitudinal weight distribution of approximately 45:55, and it also delivers consistently high driving comfort, light handling, safety in the case of collisions from any angle, and low levels of road noise. This report will provide an overview of the MR platform.



Fig. 1 External view of "i"

2. Packaging

Fig. 2 shows an overview of the MR platform. In the MR layout, with the engine no longer situated at the front of the vehicle, the position of the front wheels can be determined with a much higher degree of freedom than conventional Front Engine Front Drive (FF) vehicles, and by placing the front wheels nearer to the front of the vehicle, the distance between the front and rear

axles can be increased to give a long wheelbase. With this change, the position of the passengers in the "i" has been moved forward to extend the usable longitudinal space within the passenger compartment. Even with an apparently short front nose, it retains a sufficient crash length to absorb frontal collision impact energy as the engine is not at the front. Although restrictions apply to the full length of subcompact vehicles, the intelligent MR layout makes it possible to achieve a long passenger compartment in tandem with collision safety. Furthermore, when large wheels are introduced in order to improve driving performance, the length restriction of the FF variation of subcompact vehicles can lead to larger tires interfering with side members when making the tightest possible turn, and in order to avoid this phenomenon, it is often the case that the minimum turning radius must be made larger by restricting the steering angle. With the MR layout, however, the fact that the engine has been moved from the front means that the side members can be shifted towards the middle of the vehicle, thus eliminating the possibility of interference with tires as shown in **Fig. 3**. In this way, a long wheelbase and large wheels can be achieved without having to sacrifice the standard turn-

* Mini Car Product Development Project, Product Development & Environment Affairs Group Headquarters

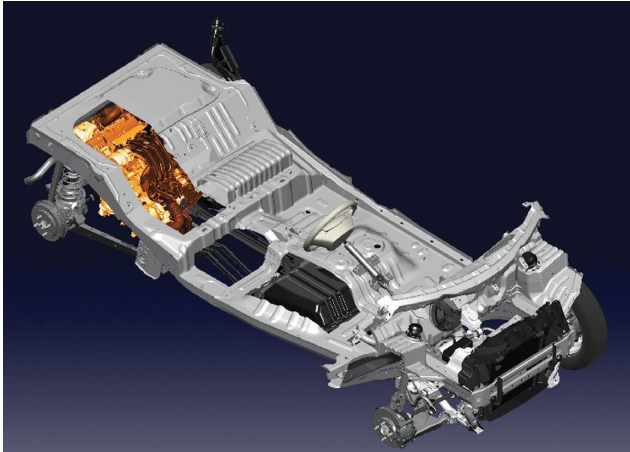


Fig. 2 MR platform

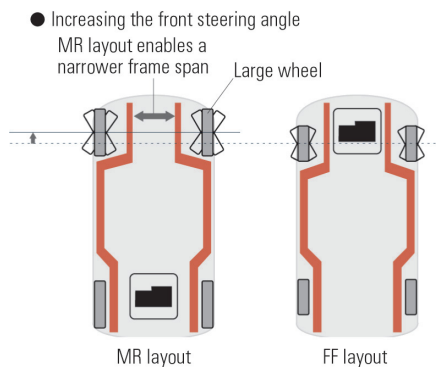


Fig. 3 Front wheel steering angle

ing radius of the subcompact vehicle. Furthermore, the long wheelbase and larger wheels also has a beneficial effect in terms of the exterior design, interior comfort, steering performance, and driving comfort.

3. Body

3.1 Body structure overview

The body structure is the core component of the platform. It must have high levels of strength and rigidity, and it must also be as light as possible while still maintaining the ability to absorb energy in a collision situation. As shown in **Fig. 4**, the body structure of the “i” features frames with large cross-sectional areas extending straightly from front to rear, and with cross members located at the ideal positions to connect with the left and right members, it has been possible to achieve a level of body stiffness under bending and torsion that is almost twice that of conventional vehicles. In light of its excellent energy-absorption efficiency, a hexagonal section has been adopted for the front side members, thus improving the absorption of energy in the case of a collision. The level of freedom in layout design is also enhanced by the relocation of the engine; furthermore, a trapezoidal cross member joining the



Fig. 4 Body structure of “i”

front side member to the A-pillar has been newly added, and thus the upper body is supported when collision energy is input and the rearward displacement of the toe board at this time is also minimized. In terms of protection from side impact, the position of the cross members linking to the left and right frames has been optimized so that deformation of the body can be controlled, the integrity of the passenger compartment can be maintained, and the level of any injury can be kept at a minimum. In the case of rear impact, furthermore, collision energy is input to the frame via the engine and the engine mount, and this together with the frame’s large cross-section ensures that the integrity of the passenger compartment can be maintained. High body stiffness achieved in this way also benefits steering stability, driving comfort, and NVH characteristics.

3.2 Body weight reduction

Our approach to weight reduction involved the optimization of cross sections and panel thickness using CAE techniques and the expansion of the areas of usage of high-tension steel. In addition to the 590 MPa high-tension steel typical of conventional vehicles, certain sections of the front-end cross member and roof bow utilize 980 MPa high-tension steel, thus enabling further weight reductions.

4. Chassis

4.1 Front suspension

For the front suspension, we have selected a McPherson Strut design in accordance with its light weight, compact size, and proven track record as shown in **Fig. 5**. The lower arm features an A-type design and has also been configured to minimize nose-dive during braking. With the engine no longer located at the front of the vehicle, it was possible to move the shock absorbers’ upper connection points further towards the interior of the vehicle than in FF models, and this allowed the inclination of the struts to be made larger when viewed from the front. Accordingly, the strut bending force can be reduced from that of FF vehicles



Fig. 5 Front suspension



Fig. 6 Rear suspension

using the spring reaction when the suspension is compressed, and this contributes to a more comfortable ride through smoother operation of the suspension. Thanks to this construction, the front hood has also been lowered as part of efforts to achieve the one-motion silhouette of the “i”.

4.2 Square configuration frame

The square configuration frame joined to the front frame supports the lower arms, steering gear box, and 4WD front differential. Direct connection of the highly stiff square configuration frame to the front side member has made it possible to maintain suspension stiffness and to achieve a steering feel that reflects the vehicle's excellent driving performance. In the case of front impact, furthermore, the square configuration frame – which supports the steering gear box – bends towards the bottom of the vehicle, disconnecting the steering shaft from the gear box, and in this way, increases the degree of steering contraction and reduces the level of occupant injury. The vehicle's power steering features an electric motor mounted on the pinion shaft, and this design realizes excellent steering performance at any

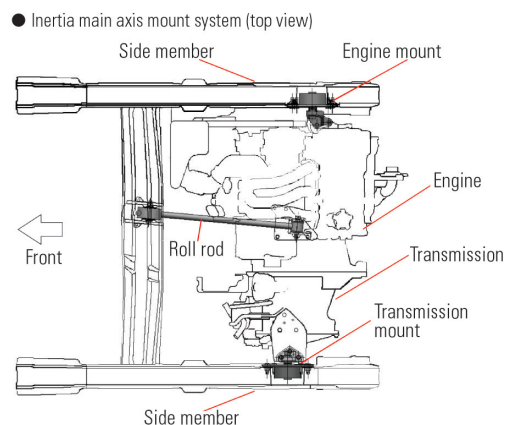


Fig. 7 Construction of engine mount system

speed in combination with low fuel consumption. Furthermore, since the front wheels are not driven in the 2WD version, it has been possible to achieve a natural steering feel, free of the torque steering typical of FF vehicles.

4.3 Rear suspension

Maintaining a simple construction for the rear suspension, the degree of camber accompanying roll of the body has been reduced through the use of a 3-link, de Dion type design, which is also highly effective in terms of safety (Fig. 6). The body connection points of the main suspension components have all been directly set-up on the body side member, making it possible to realize a high degree of steering stability and high quality ride while also maintaining suspension stiffness; furthermore, input from the wheels is transferred to body components with low sensitivity to resonance, and this also improves road-noise characteristics.

4.4 Engine mount

The construction of the engine mount system is shown in Fig. 7. A three-point pendulum-type engine mount system has been adopted for the inertia main axis. Movement of the engine in the roll direction is restrained by the roll rods, which are supported by the left and right main mounts disposed within the power plant's side members and joined to the body cross members with the bottom of the transmission. In the three-point pendulum-type mount, vertical vibration of the power plant is prevented by the left and right main mounts, while rotational vibration is prevented by the roll rods; accordingly, vibration-prevention countermeasures can be more easily achieved than with the center-of-gravity support method, which mixes the prevention of vertical and rotational vibration. Furthermore, the engine and transmission mounts are embedded into the cross-section of the side members in order to make effective use of space in the transverse direction.

5. Flexibility

In addition to a high degree of freedom in terms of design, another significant advantage of the MR platform is excellent flexibility that can support a wide range of formats from sports car to off-roader.

Furthermore, with no engine in the front, the specifications of the power plant are largely unaffected by front collision characteristics, and this helps to increase the level of efficiency in power-plant development.

6. Conclusion

Although we have faced and tackled a succession of unexpected challenges as part of MMC's first MR platform development project, the strenuous effort of all involved has lead to a successful conclusion in the

achievement of a platform with the desired characteristics and strengths. Going forward, we aim to make more efficient use of one of these characteristics in particular – namely, the platform's high level of flexibility – and to extend the MR platform to other vehicle models.



Akinobu IWAOKI



Shinsuke KAWAMURA

Door Keyless Operation System Using Piezoelectric Cable Sensor

Yoji NAKAMORI* Yutaka FUJIWARA* Akira TAKAHASHI**
Masatake HYODO** Hirofumi INUI** Yukio ABE**
Isao KASAI**

Abstract

We have developed a piezo cable sensor and incorporated it into a compact car model for the first time in the car manufacturing industry as a slim door unlock sensor which fits into the currently predominant paddle-type door handle, in order to expand the scope of application of the highly useful keyless operation system (KOS) even to minicars. The piezo cable sensor, which emits a voltage signal generated by piezoelectric effect in response to the initial vibration from a door handle, is smaller and easier to accommodate than the conventional capacitance-type sensor and is superior in detection performance.

Key words: Keyless Entry, Keyless Operation System, Piezo Cable Sensor, Door Handle

1. Introduction

A notable trend in automotive door locking systems in recent years has been the shift from keyless entry to the higher-utility KOS, which locks and unlocks the door without operating the key fob. The conventional KOS uses an unlock sensor which is too large to build into the paddle-type door handle of a minicar. A compact unlock sensor was therefore required in order to expand the scope of its application to minicars. We have developed a slim and easy to accommodate unlock piezo cable sensor ("PC sensor") for the first time in the car manufacturing industry for incorporation into the new-concept minicar "i". This paper describes the PC sensor.

2. Development objective

At present, most unlock sensors built into a door handle for KOS are the capacitance type at present. The dielectric constant when the handle is touched with a gloved hand is lower than that when it is touched with a bare hand, and the charge does not change sufficiently in some cases, which makes detection of the initial operation difficult. Water drops may also cause a change in charge, making this sensor vulnerable to disturbance by rain or a car wash. Furthermore, the handle body must be made thicker to accommodate the sensor electrode in the handle lever, but there is hardly space for it in the thin door of a minicar.

We focused on the system for detecting the initial vibration caused by when the handle is operated to open the door. We adopted the PC sensor, which has fine detection ability that is not affected by the environment and is a cable and so can be fitted into a narrow

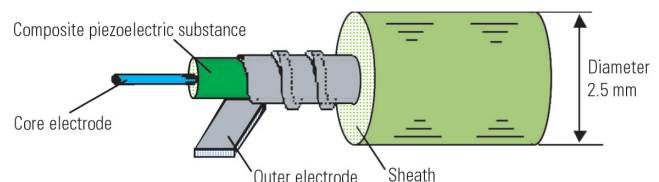


Fig. 1 Appearance of PC sensor

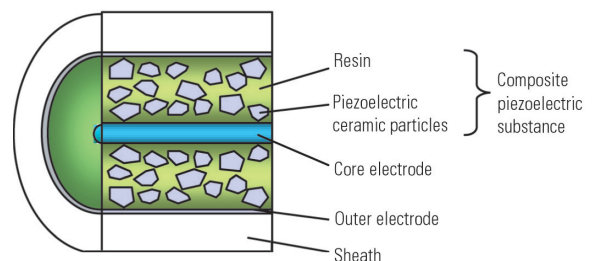


Fig. 2 Inside of PC sensor

space.

3. Structure and operation of PC sensor

3.1 Structure

The newly developed PC sensor is a flexible piezoelectric coaxial cable. With a diameter of 2.5 mm, this sensor is composed of a core electrode, composite piezoelectric substance (a resin and piezoelectric ceramic particles), outer electrode and sheath in coaxial layers as shown in Fig. 1. The inner composition of this sensor (a sectional view) is shown in Fig. 2, and its specifications are given in Table 1.

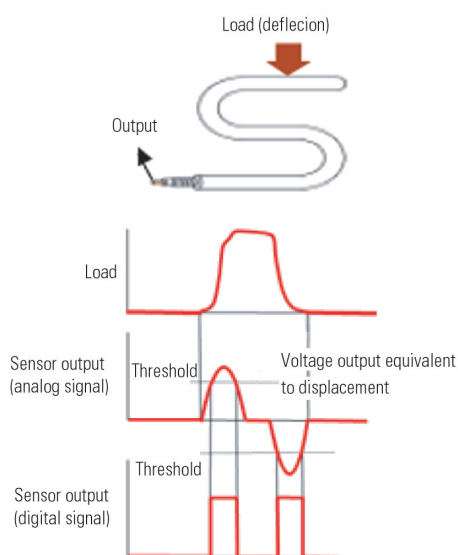
* Advanced Vehicle Engineering Dept., Development Engineering Office

** Matsushita Home Appliances Company, Matsushita Electric Industrial Co., Ltd.

** Office of Development & Engineering, Mitsubishi Automotive Engineering Co., Ltd.

Table 1 Specifications of PC sensor

Component	Specification
Composite piezoelectric substance	Piezoelectric ceramic particles, Resin (polyethylene resin), Others
Core electrode	Cu – Ag alloy coil
Outer electrode	Three-layer laminate film (Al – PET – Al)
Sheath	Elastomer, ϕ 2.5 mm

**Fig. 3 Piezoelectric effect**

3.2 Principle of operation

A voltage proportional to a vibration or deformation acceleration rate is generated in the sensor by piezoelectric effect (Fig. 3).

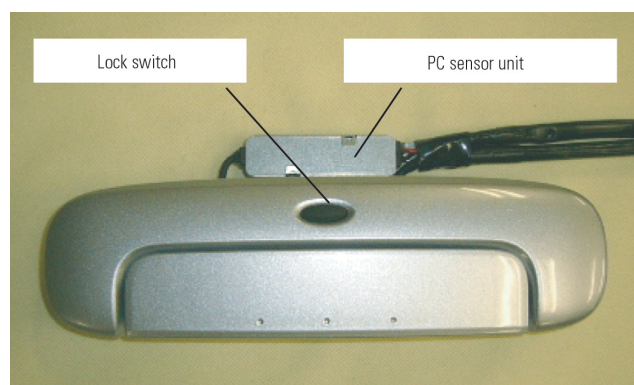
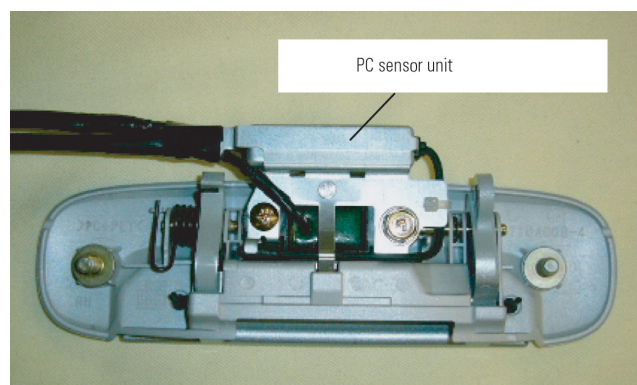
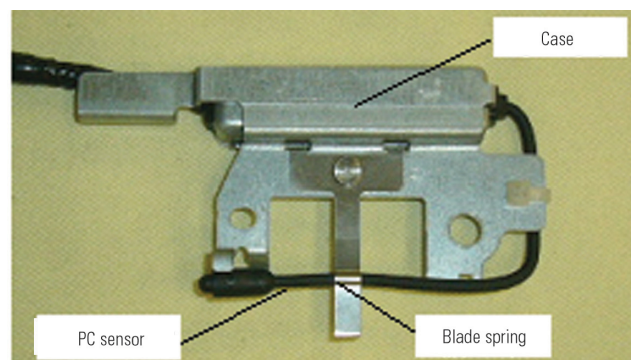
A suitable composite piezoelectric substance was selected, and a unique polarizer with excellent piezoelectric effect and other items were newly developed in the course of developing the PC sensor. All of these were combined to create a highly sensitive and slim piezo sensor which can be accommodated in a confined space.

4. PC sensor as built into a door handle

The PC sensor as built into a door handle is shown in Figs 4 and 5.

The PC sensor and its case are in a one-piece arrangement for quick incorporation into the door handle (Fig. 6).

Operating the lever of the door handle causes displacement of a blade spring and consequently displacement of the PC sensor, which detects the initial vibration (Fig. 7). The detected signal is transmitted to the ECU for KOS to unlock the door. A door locking switch is provided on top of the door handle.

**Fig. 4 Door handle (front view)****Fig. 5 Door handle (rear view)****Fig. 6 PC sensor unit**

5. Composition and performance of detector circuit

5.1 PC sensor unit

The composition of the detector circuit is shown in Fig. 8. The PC sensor unit processes the output signal from the PC sensor and emits a door handle operation recognition signal.

Operating the lever of the door handle applies a vibration or deformation acceleration to the PC sensor, and a voltage signal proportional to it, generated by

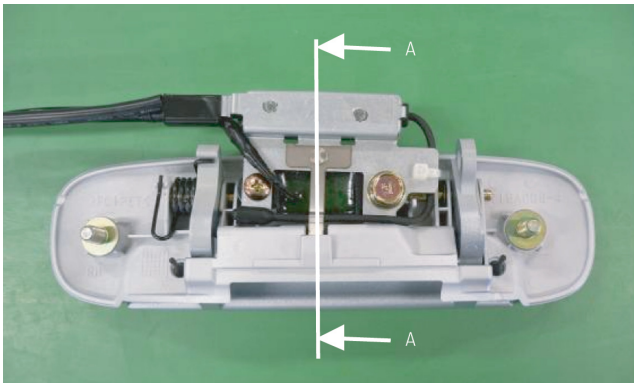
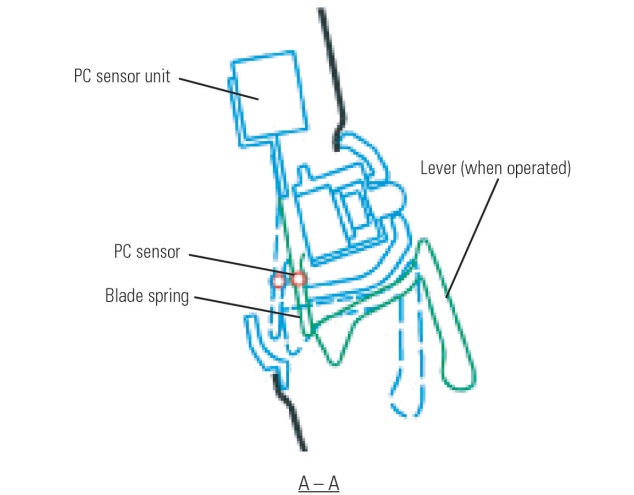


Fig. 7 Door handle and section

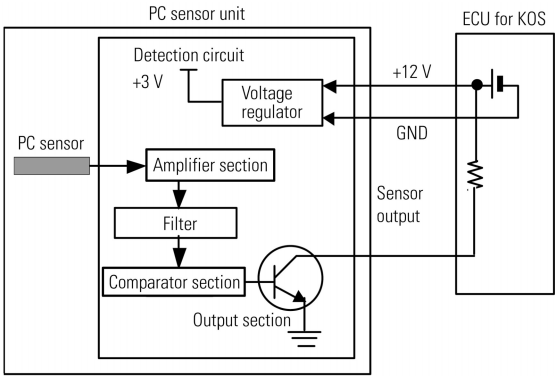


Fig.8 Circuit block in PC sensor unit

Table 2 Specifications of PC sensor

Item	Range
Operational power supply voltage	DC 8 to 16 V
Consumption current	0.8 mA or less (at judgment output)
Output signal	Open-collector type
Output ON time	25 ms or more
Operating temperature range	−30 to +80 °C
Standby temperature range	−40 to +85 °C
Operating humidity range	95 % or less

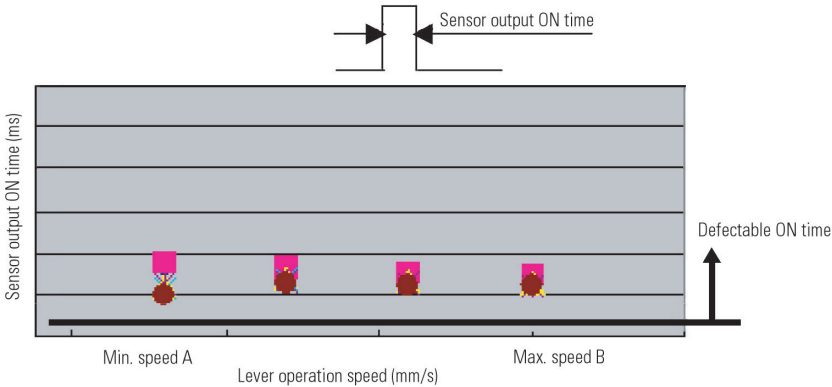


Fig. 9 Handle lever operation speed and output ON time sensor (n = 5)

piezoelectric effect, is emitted by the PC sensor. This signal is amplified approximately 200 times by an amplifier and transmitted to a comparator. The weak signal generated by the operation of the lever is detected as a disturbance of electromagnetic waves reduced through an optimum filter circuit formed in the amplifier. The comparator converts the analog signal from the amplifier into a digital signal (ON/OFF). The effect of voltage fluctuation of the power source is reduced in a voltage regulator by using +3 V power. The specifica-

tions of the PC sensor unit are given in Table 2.

5.2 Detection performance

Under any possible lever operation speed when a door is opened, the initial vibration at the time the handle lever is operated is detected without fail (Fig. 9). It is also verified that it causes no malfunction under various malicious vibration input to the door and that it can detect the signal in various situations.

6. Concluding remark

We have developed a compact PC sensor with high detection performance. The sensitivity of the detection system has a great effect on the feel of the KOS unlocking action on the door handle. The user will immediately receive a favorable impression of the system upon touching the handle. Further improvements of the PC sensor will be made in future to upgrade the sense of touch of the handle and to meet users' needs. We also intend to explore the possibility of using the PC sensor for other types of door handle.

Finally, we thank all those concerned inside and outside the company for their cooperation.

References

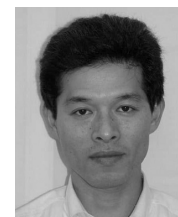
- (1) Y. Fujii, N. Kanazawa, I. Masahiko and T. Nagai: A Piezoelectric Coaxial Cable, Technical Digest of the 18th Sensor Symposium, pp. 269 – 272, 2001
- (2) Y. Fujii, N. Kanazawa, I. Masahiko and T. Nagai: Collection of Papers for the 10th Polymer Material Forum of the Pressure-sensitive Cord and High Polymer Academic Society, 2001



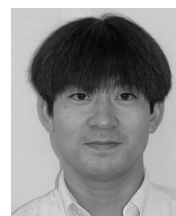
Yoji NAKAMORI



Yutaka FUJIWARA



Akira TAKAHASHI



Masatake HYODO



Hirofumi INUI



Yukio ABE



Isao KASAI

Improvement of Vehicle Dynamic Performance by Means of In-Wheel Electric Motors

Makoto KAMACHI* Kevin WALTERS* Hiroaki YOSHIDA*

Abstract

With an electric vehicle that has in-wheel motors in its driving wheels, each wheel's motor torque can be controlled independently, meaning that a yaw moment created by means of motor-torque differences between the left and right wheels can be used for dynamic control. Without requiring any additional actuators, such an arrangement permits dynamic control to be realized using only software and delivers the benefits of the motors' inherently rapid, precise torque controllability. As part of an effort to verify the potential of in-wheel motors, this paper describes the control method devised to enhance a vehicle's dynamic performance (particularly the transient-response characteristics of the yaw rate and the lateral acceleration relative to the steering angle). The control method was proved effective by means of experiments conducted using a COLT EV prototype vehicle with two rear in-wheel motors.

Key words: *Electric Vehicle, Vehicle Dynamics, Active Control*

1. Introduction

Amid growing concern about degradation of the environment and depletion of oil resources, it is expected that vehicles with internal-combustion engines will be superseded by electric vehicles (including hybrid vehicles and fuel-cell vehicles).

Among electric vehicles, those that have in-wheel motors (IWMs) are attracting attention owing to the advantages with respect to interior spaciousness and design freedom. A further merit of an IWM vehicle is that, since each wheel's motor torque can be controlled independently, dynamic yaw-moment control (DYC) – a means of controlling the vehicle's dynamics using a yaw moment resulting from the creation of torque differences between the left and right wheels – is possible⁽¹⁾. Given these merits, Mitsubishi Motors Corporation (MMC) is conducting research and development for next-generation electric vehicles in line with a Mitsubishi In-wheel motor Electric Vehicle (MIEV) concept that calls for an IWM platform to be employed in hybrid vehicles, fuel-cell vehicles, and other electric vehicles.

This paper discusses work performed to verify whether it is possible to apply DYC to an IWM-equipped vehicle in order to enhance the vehicle's dynamic performance (particularly the transient-response characteristics of the yaw rate and the lateral acceleration relative to the steering angle). The test vehicle used in an experimental investigation into the effects of DYC was a COLT EV (a prototype electric vehicle) with two rear IWMs (Fig. 1).

2. COLT EV

An overview of the COLT EV test vehicle and its sys-



Fig. 1 COLT EV

tem configuration is given hereafter. The COLT EV is an electric vehicle based on a production Mitsubishi COLT. The engine, transmission, and fuel tank were removed from the production COLT, and the vehicle was then fitted with two rear IWMs and with a propulsion battery, which is located in the space originally occupied by the fuel tank. An inverter (the motor control unit) is located under the luggage area (Fig. 2). The inverter and IWMs were developed by MMC. The propulsion battery (a high-performance lithium-ion type) was made by Litcel co., Ltd. The vehicle's specifications are shown in Table 1.

The COLT EV's system configuration is shown in Fig. 3. Data from the accelerator position sensor (APS), brake position sensor (BPS), battery management unit (BMU), and various sensors (vehicle speed, steering angle, yaw rate, and acceleration) are input to the torque control unit (TCU), which calculates the required torque for the left and right motors and issues the necessary commands.

* Advanced Vehicle Engineering Dept., Development Engineering Office

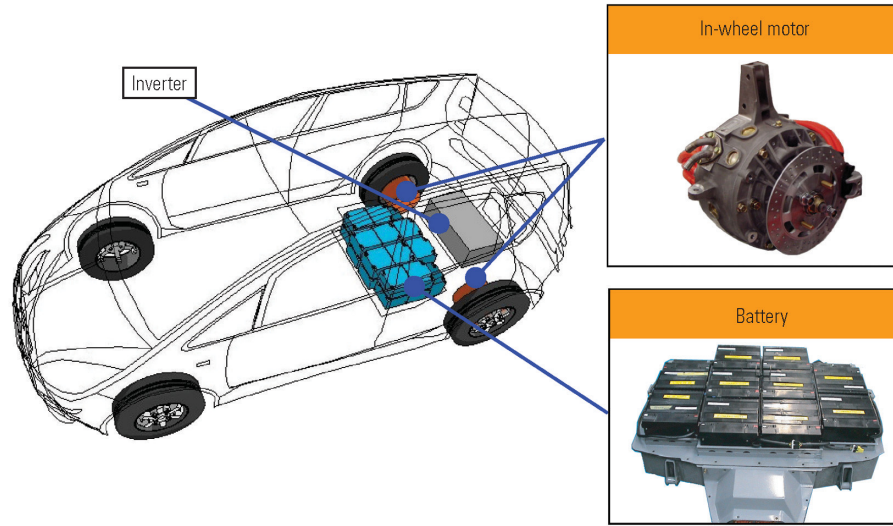


Fig. 2 Parts layout

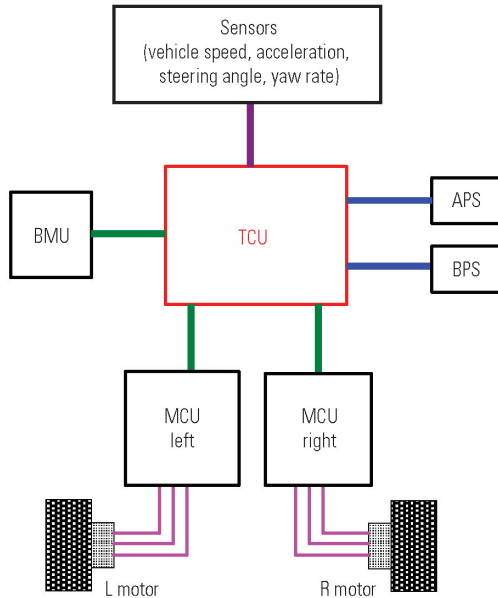


Fig. 3 System configuration

The torque commands are transmitted to the left and right motor control units (MCUs) via RS232C communication.

3. Vehicle model and DYC

3.1 Linear model of vehicle

When motor torques T_l and T_r are applied to the left and right wheels, respectively, of the IWM vehicle as shown in Fig. 4, the yaw moment M_z created about the vehicle's center of gravity by the motor-torque difference T_{dif} can be written using the following equation:

$$M_z = \frac{d}{2} \left(\frac{g_r T_r}{R} - \frac{g_r T_l}{R} \right) = \frac{g_r d}{2R} T_{dif} = K T_{dif} \quad (1)$$

Table 1 Vehicle specifications

Dimensions (L x W x H)		3,885 x 1,680 x 1,550 (mm)
Curb weight		1,150 kg (F: 467 kg + R: 683 kg)
Max. speed		150 km/h (93 mile/h)
Tires		185/55R15
Motors (per one unit)	Max. output	20 kW
	Max. torque	100 Nm
	Max. speed	9,000 min ⁻¹
	Internal reduction gear	Planetary gear (ratio: 6.0)
Battery	Type	Lithium-ion
	Capacity	40 Ah
	Voltage/Module	14.8 V x 22 modules

When a linear two-wheel model of the type shown in Fig. 5 is considered, the equation of motion can be written as shown below⁽²⁾.

$$\begin{bmatrix} \dot{\beta} \\ \dot{\gamma} \end{bmatrix} = \begin{bmatrix} -2 \frac{C_f + C_r}{MV} & -1 - 2 \frac{l_f C_f - l_r C_r}{MV^2} \\ -2 \frac{l_f C_f - l_r C_r}{I} & -2 \frac{l_f^2 C_f + l_r^2 C_r}{IV} \end{bmatrix} \begin{bmatrix} \beta \\ \gamma \end{bmatrix} + \begin{bmatrix} \frac{2C_f}{g_a MV} & 0 \\ \frac{2l_f C_f}{g_a I} & \frac{K}{I} \end{bmatrix} \begin{bmatrix} \theta \\ T_{dif} \end{bmatrix} \quad (2)$$

Here, θ is the steering angle, β is the sideslip angle of the center of gravity, and γ is the yaw rate. If a Laplace transform is performed on the equation, the transfer functions from θ and T_{dif} to γ can be written as follows:

$$\begin{aligned} \gamma &= \frac{A_G(1+T_{GS})}{1 + \frac{2\zeta}{\omega_n}s + \frac{1}{\omega_n^2}s^2} \theta + \frac{A_H(1+T_{HS})}{1 + \frac{2\zeta}{\omega_n}s + \frac{1}{\omega_n^2}s^2} T_{dif} \\ &= G(s)\theta + H(s)T_{dif} \end{aligned} \quad (3)$$

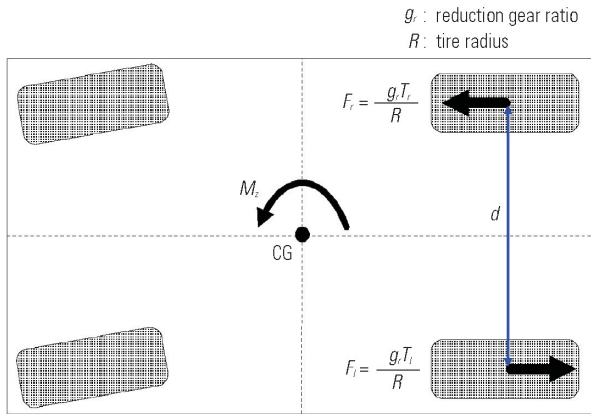


Fig. 4 Relationship between motor-torque difference and yaw moment

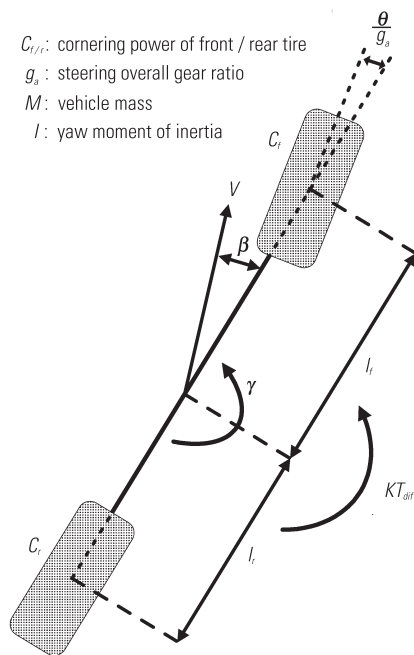


Fig. 5 Linear two-wheel model

Here, A_G and A_H are steady-state gains, T_G and T_H are lead-time constants, ζ is the damping coefficient, and ω_n is the natural frequency. Thus, the yaw rate is expressed as the linear sum of the steering response and motor-torque-difference response. As shown in **Fig. 6**, therefore, it is possible to effect control over the vehicle's motion (yaw rate) by applying an appropriate motor-torque difference. Such control is **DYC**.

3.2 Identification of vehicle model

The above-mentioned transfer functions $G(s)$ and $H(s)$ are experimentally identified.

3.2.1 Identification experiment for $G(s)$

The vehicle speed is kept constant (80 km/h in this paper), and the steering-angle input is applied in pulse form. The pulse width is set at approximately 0.5 s. To

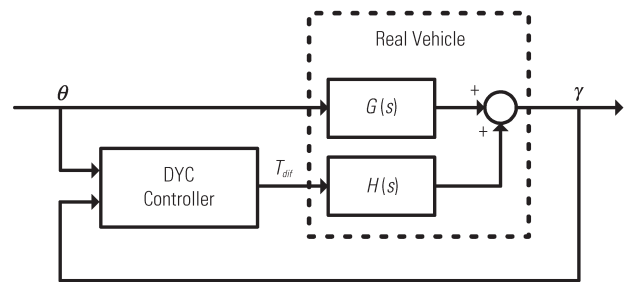


Fig. 6 Conceptual view of DYC

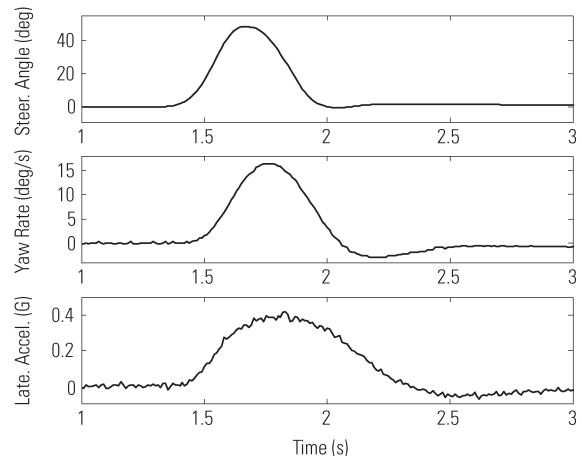


Fig. 7 Results of identification experiment (steering-angle input)

ensure the linearity of the tire characteristics, the steering-angle peak is applied such that the lateral-acceleration peak is approximately $0.4 G^{(3)}$. Time waveforms of experiment results are shown in **Fig. 7**. (The top part of **Fig. 7** corresponds to the steering angle, the middle part to the yaw rate, and the bottom part to the lateral acceleration.)

3.2.2 Identification experiment for $H(s)$

With the vehicle speed kept constant (80 km/h in this paper) and the steering wheel held in the 0° position, the motor-torque difference is applied in pulse form. The pulse width is set at 0.5 s, and the peak is set in the vicinity of the greatest torque difference obtainable at the set vehicle speed. Time waveforms of experiment results are shown in **Fig. 8**. (The top part of **Fig. 8** corresponds to the motor-torque difference, the middle part to the yaw rate, and the bottom part to the lateral acceleration.) The motor-torque difference is the difference between the torque-command values issued to the motors (before the reduction gears).

3.2.3 Identification calculation

A discrete Fourier transform is performed on each input (steering angle or motor-torque difference) and output (yaw rate), then the frequency response is calculated from the output/input ratio. The transfer function $G(s)$ or $H(s)$ is then approximated using a curve-fitting method. In accordance with equation (3), the denominators for both transfer functions are made common;

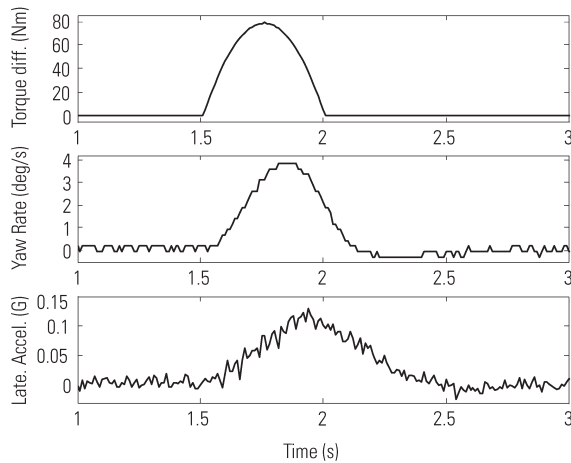


Fig. 8 Results of identification experiment (motor-torque-difference input)

the denominators are set to second order, and the numerators are set to first order. Bode diagrams of calculation results are shown in Fig. 9. In each part of Fig. 9, the solid line corresponds to transfer function $G(s)$ and the broken line corresponds to transfer function $H(s)$.

4. Evaluation of vehicle handling and stability; control objectives for DYC

With a focus on four key parameters of the identified transfer functions, the text hereafter describes the method used to evaluate vehicle handling and stability and discusses the setting of control objectives for DYC.

4.1 Evaluation parameters

Vehicle dynamic characteristics related to handling and stability include the yaw-rate response speed, yaw-rate damping characteristic, rotational ability, and lateral-acceleration response speed with respect to the steering-angle input. Here, the yaw-rate response speed corresponds to the speed of the rise in the yaw rate; the yaw-rate damping characteristic corresponds to the quality of the convergence of the yaw rate; the rotational ability corresponds to the magnitude of the steady-state value of the yaw rate; and the lateral-acceleration response speed corresponds to the speed of the rise in the lateral acceleration. It is known that the yaw-rate response speed corresponds to the yaw-rate natural frequency $f_n = \omega_n/2\pi$, that the yaw-rate damping characteristic corresponds to the yaw-rate damping coefficient ζ , that the rotational ability corresponds to the yaw-rate steady-state gain A , and that the lateral-acceleration response speed corresponds to the phase delay of the lateral acceleration (@1 Hz; hereafter designated ϕ)⁽⁴⁾. These four key parameters (f_n , ζ , A , and ϕ) are hereafter designated the “four parameters”.

4.2 Calculation of parameters

Among the four parameters, $f_n = \omega_n/2\pi$, $A = A_G$, and ζ can be deduced from identified transfer function $G(s)$.

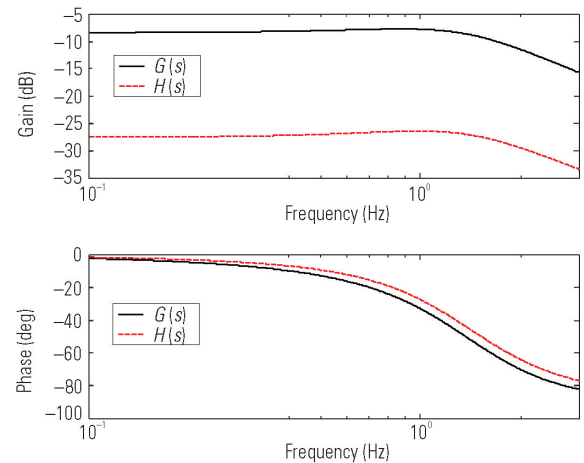


Fig. 9 Bode diagrams of identified transfer functions

Table 2 Four-parameter values (without DYC)

f_n	1.42 (Hz)
ζ	0.665
A	0.382 (l/s)
ϕ	-74.0 (deg)

The method for determining ϕ is the same as the method described in part 3.2.3 of this paper; the transfer function from the steering angle to the lateral acceleration is determined, and the phase delay is determined from the frequency response thereof. With regard to the orders of the transfer function, the numerator and denominator are set to the second order. The determined four parameters are shown in Table 2.

4.3 Establishment of DYC objectives

A vehicle's handling and stability are determined by the vehicle's weight, its front/rear weight distribution, its yaw moment of inertia, its wheelbase, its suspension characteristics, the cornering power of its front and rear tires, and other factors. When limits imposed by a vehicle's form and size preclude alteration of any of the aforementioned factors, it is desirable to be able to enhance the vehicle's handling and stability by means of DYC.

With a high-performance car, the four-parameter values are all typically high⁽⁴⁾. When the four-parameter values are plotted on a radar chart like the one shown in Fig. 10, therefore, the quadrangle is larger than that corresponding to a lower-performance car. In Fig. 10, the broken line corresponds to the COLT EV and the solid line corresponds to an MMC high-performance car. DYC can conceivably be used to improve handling and stability by enlarging all of the four-parameter values. In Fig. 10, ζ and A for the COLT EV are amply large relative to those of the high-performance car whereas f_n and ϕ are significantly smaller. (Conversion of the COLT to the IWM-equipped COLT EV increased the proportion of the vehicle weight distribution to the rear

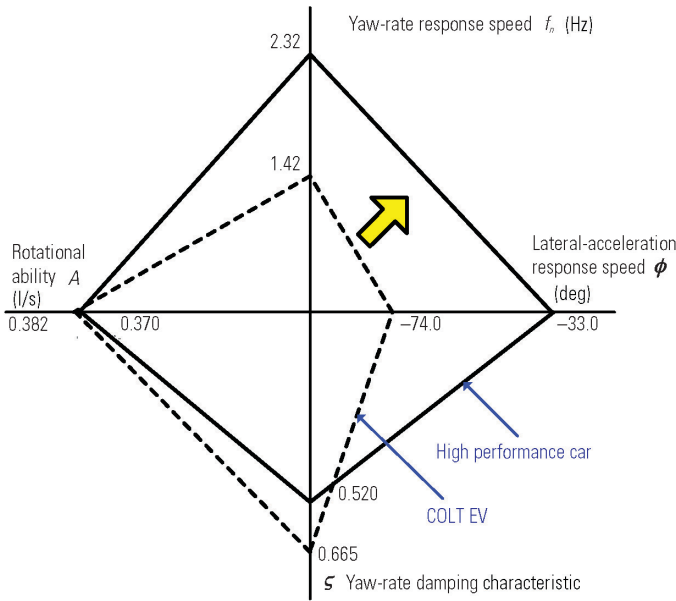


Fig. 10 Comparison of four-parameter values (without DYC)

wheels.) In this paper, therefore, the control objectives are focused on enlarging f_n and ϕ .

5. DYC and its effects

The text hereafter describes the implementation of DYC for improvement of handling and stability and the evaluation of its effects by means of experiments.

5.1 Establishment of target yaw rate

As stated in part 4.3 of this paper, the control objective is to increase f_n and ϕ . The ideal yaw-rate response with respect to the steering angle is thus imposed as the target yaw rate, and the actual yaw rate yielded by DYC is made to trace the target yaw rate. In this paper, a control method is constructed whereby a reference transfer function (a reference model) is provided and the actual transfer characteristics from the steering angle to the yaw rate are made to match the reference model as closely as possible.

For enlargement of f_n , the reference model $F(s)$ is established using the following equation, in which γ^* represents the target yaw rate.

$$\gamma^* = F(s)\theta = \frac{A_G(1+T_Gs)}{1 + \frac{2\zeta}{\omega_n}s + \frac{1}{\omega_n^2}s^2} \theta \quad (4)$$

As an example, Bode diagrams of $F(s)$ for $\omega'_n = 2\pi f_n \times 1.5$ are shown in Fig. 11. (In Fig. 11, the solid lines correspond to $F(s)$ and the broken lines correspond to $G(s)$.) It can be seen that the yaw-rate phase delay is improved by means of an increase in f_n . Thus it is expected that the lateral-acceleration phase delay ϕ is also improved. Verification of these phenomena by means of experiments is described in part 5.3 of this

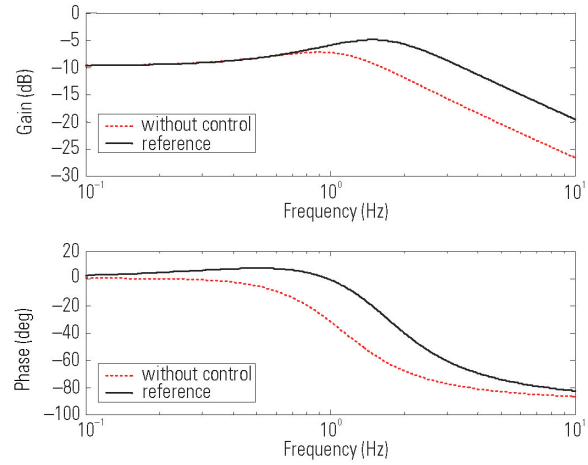


Fig. 11 Bode diagrams of reference model

paper.

5.2 DYC logic

For the target yaw rate and actual yaw rate to be equal, the following condition must be satisfied.

$$\gamma^* - \gamma = F(s)\theta - \{G(s)\theta + H(s)T_{dif}\} = 0 \quad (5)$$

In accordance with equation (5), the required motor-torque difference T_{dif} is shown by the following equation:

$$T_{dif} = \frac{F(s) - G(s)}{H(s)} \theta \quad (6)$$

Given the effects of modeling errors and disturbances with the real system, the target yaw rate and actual yaw rate will not match by application of equation (6) alone. Consequently, control logic is used whereby equation (6) is treated as a feedforward term and the deviation between the target yaw rate and actual yaw rate is added as a feedback term as shown in the following equation:

$$T_{dif} = \frac{F(s) - G(s)}{H(s)} \theta + K_{FB}(s)\{F(s)\theta - \gamma\} \quad (7)$$

Here, $K_{FB}(s)$ is an appropriate transfer function, for example, proportional-integral-derivative control. A block diagram of the control logic is shown in Fig. 12.

5.3 Experimental evaluation of DYC

The text hereafter describes the results of an experiment in which DYC was implemented using the aforementioned logic. The target yaw rate, equation (4) was set as $\omega'_n = 2\pi f_n \times 1.5$. For the feedback control term, proportional control was used. As in the identification experiment, the vehicle speed was 80 km/h.

5.3.1 Time-domain evaluation

The time-response results for application of steer-

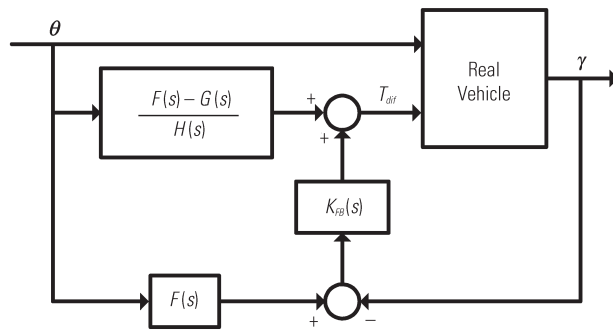


Fig. 12 Block diagram of DYC logic

Table 3 Four-parameter values (with DYC)

f_n	1.82 (Hz)
ζ	0.695
A	0.382 (l/s)
ϕ	-48.0 (deg)

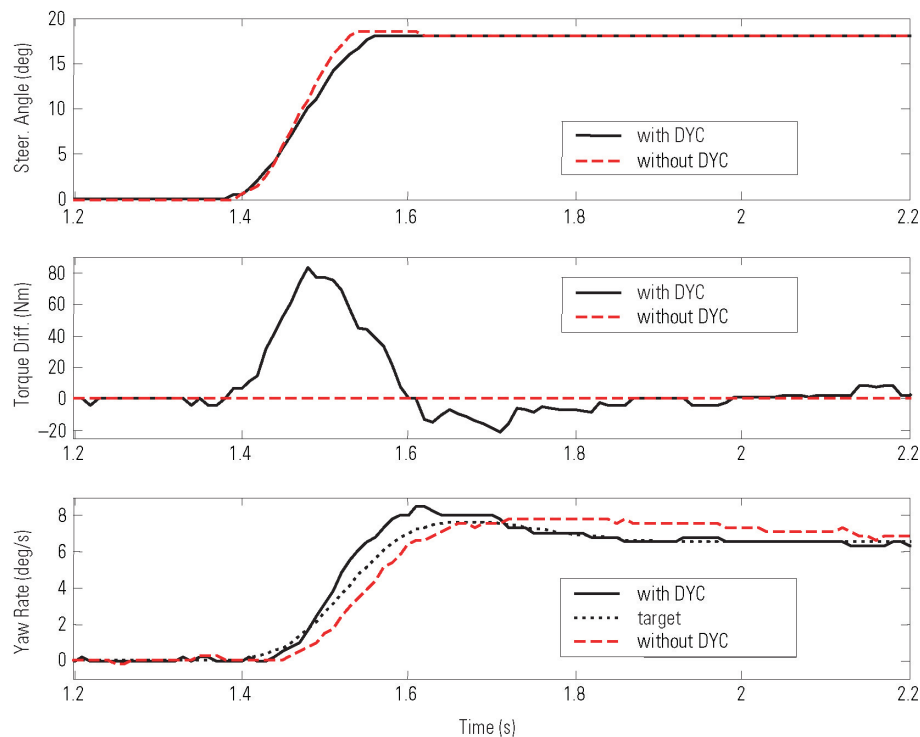


Fig. 13 Results of steering-angle step inputs

ing-angle step inputs are shown in Fig. 13. (The top part of Fig. 13 corresponds to the steering angle, the middle part to the control input, and the bottom part to the yaw rate.) The yaw rate with DYC (shown by the solid line) does not precisely track the target yaw rate (shown by the dotted line), indicating a need for improvement of the control parameters or logic. However, it can be seen that the speed of the rise and quality of the convergence with DYC is faster than those without DYC (shown by the broken line).

5.3.2 Four-parameter evaluation

The four parameters with DYC implemented are shown in Table 3. As shown, the control objective of enlarging f_n and ϕ is achieved. A four-parameter radar chart plotted for verification of the effects of control is shown in Fig. 14. (In Fig. 14, the broken line corresponds to the results without DYC and the solid line corresponds to the results with DYC.) Since the quadrangle corresponding to the results with DYC is larger than

the quadrangle corresponding to the results without DYC, it can be seen that the vehicle's handling and stability are improved by DYC.

6. Summary

In the work described in this paper, it was verified by means of experiments conducted with a COLT EV test vehicle that DYC (a feature of IWM-equipped electric vehicles) can be used to improve vehicle handling and stability.

MMC intends to study DYC for application in non-linear ranges such as those in which lateral acceleration is significantly large and those in which the vehicle is driven on low- μ surfaces. There is a particularly great need to suppress tire slip for higher stability on low- μ surfaces. Adhesion control that takes advantage of the quick, precise torque controllability of the motors (this control functionally corresponds to the control provid-

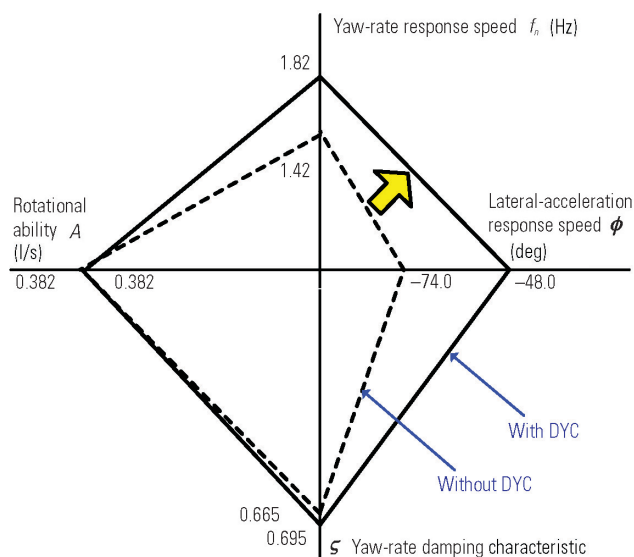


Fig. 14 Comparison of four-parameter values (with DYC)

ed by an antilock braking system or traction control system) is effective for this purpose.

With a vehicle equipped with an IWM in each of the four wheels, the left-right torque differences needed for DYC would be generated using all four wheels, permitting greater freedom in control of torque distribution. It is conceivable that this freedom could be exploited to

enable optimal control of the forces (longitudinal and lateral) produced by each tire and to enable active control of rolling and pitching motions. MMC intends to investigate these possibilities.

References

- (1) Hori: "Research on Future Vehicle Driven by Electricity and Control", FED Review, Research and Development Association for Future Electron Devices, Vol. 3, No. 4, 2004
- (2) Abe: "Automobile Dynamics and Control" (second edition), Sankaido Publishing Co., Ltd., 2003
- (3) "Lateral Transient Response Test Methods – Open Loop Test" (JASO Z110), Society of Automotive Engineers of Japan, 2003
- (4) Tani et al: "Relationship between Steering Response and Suspension Characteristics of Passenger Car", Mitsubishi Heavy Industries Technical Review, Vol. 25, No. 1, 1988



Makoto KAMACHI



Kevin WALTERS



Hiroaki YOSHIDA

Development of Technique for Predicting Roof Buckling Under Snow Load

Eiichi KOBAYASHI* Toshiyuki MIYACHI* Yoshinobu MATSUMURA**
Akinori YASUI*** Hiroyuki WATAKABE*** Hirotaka KANO***

Abstract

Implicit method structural analysis software was used in the past to analyze the buckling of vehicle roof under weight of snow, which is a major hurdle for a designer seeking to lighten the roof. However, calculation using this software resulted in mathematical divergence at a halfway point, and it was difficult to continue the analysis. In this study, we adopted explicit method structural analysis software, selecting appropriate analytical parameters, and succeeded in developing a technique for accurately predicting the behavior of roof buckling under weight of snow.

Key words: CAE, Strength Against Snow Load, Explicit Method, Implicit Method

1. Introduction

Lightening the top part of the vehicle, the roof, not only lighten the vehicle weight but also lowers the vehicle's center of gravity and shows the potential for the improvement of handling, but roof buckling under snow or other load is a major hurdle when trying to use a thinner roof panel.

The implicit method structural analysis software was preferred because of its higher analytical accuracy. However, the calculation led to mathematical divergence at a halfway point and the calculation took considerable time, so the software is unsuitable for our development project. Hence, we decided to apply the explicit method structural analysis software to the analysis of roof buckling.

2. Analytical method

The following equation can be obtained by discrete representation of the analytic area by the finite element method:

$$M\ddot{u} + C\dot{u} + Ku = f \quad (1)$$

where,

M : Mass matrix

C : Damping matrix

K : Stiffness matrix

u : Displacement vector

f : Force vector

To solve this dynamic equation, the time span t , $0 \leq t \leq T$, is divided into finite time increments, Δt , which form a set. An approximate solution is solved step by

step for each Δt by time integration. This is called direct time integration and is frequently used.

2.1 Implicit method

Suppose that the acceleration is constant between $t = t_i$ and $t = t_{i+1} = t_i + \Delta t$, and equal to the average of \ddot{u}_{i+1} and \ddot{u}_i . Then the speed and the displacement are represented by the following equations ($\alpha = 1/2$ and $\beta = 1/4$ in Newmark's integration formula):

$$\dot{u}_{i+1} = \dot{u}_i + (\ddot{u}_{i+1} + \ddot{u}_i) \frac{\Delta t}{2} \quad (2)$$

$$u_{i+1} = u_i + \dot{u}_i \Delta t + (\ddot{u}_{i+1} + \ddot{u}_i) \frac{(\Delta t)^2}{4} \quad (3)$$

Equation (4) below is derived from equation (3). Equation (5) below is obtained by substituting (4) for (2):

$$\ddot{u}_{i+1} = 4 \frac{u_{i+1} - u_i}{(\Delta t)^2} - \left(\ddot{u}_i + 4 \frac{\dot{u}_i}{\Delta t} + 4 \frac{u_i}{(\Delta t)^2} \right) \quad (4)$$

$$\dot{u}_{i+1} = 2 \frac{u_{i+1} - u_i}{\Delta t} - \left(\dot{u}_i + 2 \frac{u_i}{\Delta t} \right) \quad (5)$$

Equation (6) is obtained by substituting (4) and (5) for (1):

$$\left(\frac{4}{(\Delta t)^2} M + \frac{2}{\Delta t} C + K \right) u_{i+1} = f_{i+1} + M a_i + C b_i \quad (6)$$

* Digital Engineering Office, Development Planning Dept.

** Safety Testing Dept., Development Planning Dept.

***Thin Plate Processing Technology Research Dept., Steel Research Laboratory, JFE Steel Corporation

** Advanced Vehicle Engineering Dept., Development Planning Dept.

*** Development Planning Dept., Development Div., Mitsubishi Automotive Engineering Co., Ltd

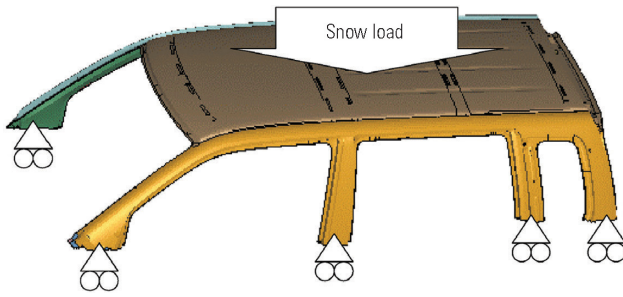


Fig. 1 Boundary conditions – analysis of roof buckling

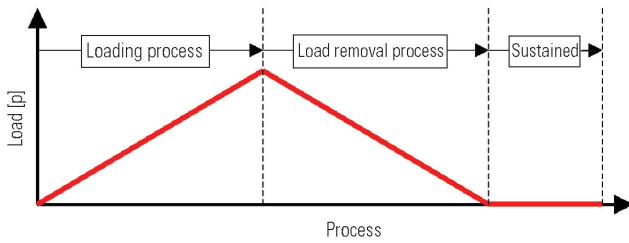


Fig. 2 Load – analysis of roof buckling

$$a_i = \ddot{u}_i + 4 \frac{\dot{u}_i}{\Delta t} + 4 \frac{u_i}{(\Delta t)^2} \quad (7)$$

$$b_i = \dot{u}_i + 2 \frac{\dot{u}_i}{\Delta t} \quad (8)$$

In other words, if values of u_i , \dot{u}_i and \ddot{u}_i are given, u_{i+1} can be calculated by using (6), and \ddot{u}_{i+1} and \dot{u}_{i+1} can be calculated by using (4) and (5).

Since the stiffness matrix, K , is included in the coefficient matrix on the left-hand side of (6), simultaneous linear equations must be solved; thus, this is an implicit method⁽¹⁾.

2.2 Explicit method

If the center difference approximation formula is applied in respect of time, equations (9) and (10) consist of regarding the speed and acceleration:

$$\dot{u}_i = (u_{i+1} - u_{i-1}) / (2\Delta t) \quad (9)$$

$$\ddot{u}_i = (u_{i+1} - 2u_i + u_{i-1}) / (\Delta t)^2 \quad (10)$$

Equation (11) below is obtained from (9) and (10) by substituting (1) for them:

$$\left\{ \frac{1}{(\Delta t)^2} M + \frac{1}{2\Delta t} C \right\} u_{i+1} = f_i - \left\{ K - \frac{2}{(\Delta t)^2} M \right\} u_i - \left\{ \frac{1}{(\Delta t)^2} M - \frac{1}{2\Delta t} C \right\} u_{i-1} \quad (11)$$

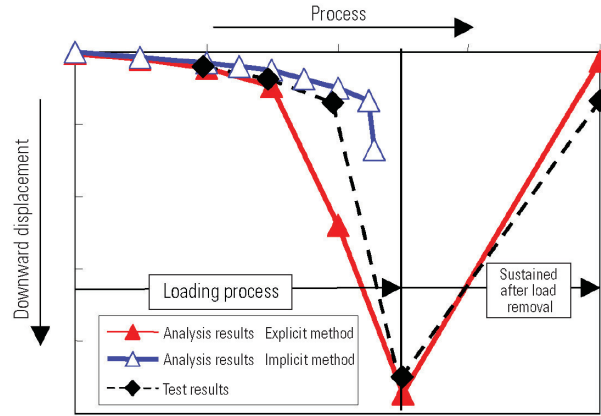


Fig. 3 Comparison of implicit method and explicit method calculations

If values of u_i and u_{i-1} are given, u_{i+1} can be calculated by using (11), and \dot{u}_{i+1} and \ddot{u}_{i+1} can be calculated by using (9) and (10).

Since the stiffness matrix, K , is not included in the coefficient matrix on the left-hand side of (11), there is no need to solve simultaneous linear equations if M and C are diagonal matrices; thus, this is an explicit method⁽¹⁾⁽²⁾.

3. Analysis of roof buckling under snow load

3.1 Study of analytical methods

Simultaneous equations must be solved under an implicit method. Mathematical divergence often occurs even if the arc-length method⁽³⁾ is used to analyze roof buckling under snow load.

We decided on a gross deformational analysis using MSC/NASTRAN, which is implicit method software. The area from the belt line up was selected as an analytical model, and the cut surface of the model was simply supported (Fig. 1). To reproduce the test condition, there are downward snow load (p) on the roof panel (Fig. 2).

LS-DYNA was used as explicit method software. The modeling area and boundary conditions were similar to those under the implicit method.

3.2 Comparison of analysis and test results

Fig. 3 shows a comparison between the analysis results and the test results. The displacement-to-load characteristic at the maximum displacement position on the roof panel is shown by the graph.

Under the implicit method, divergence occurred at a halfway point in the loading process. The situation when the calculation ended was studied by checking the test results. The divergence presumably occurred somewhere near the time the buckling started.

Under the explicit method, the calculation was completed from the loading process to the load removal process, and recovery from the buckling during the load removal process is apparent.

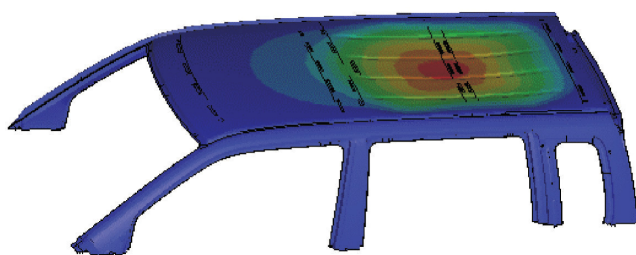


Fig. 4 Deformation mode under buckling

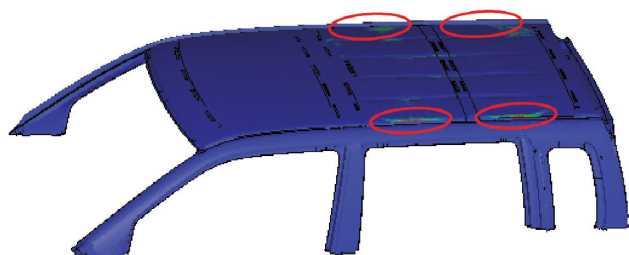
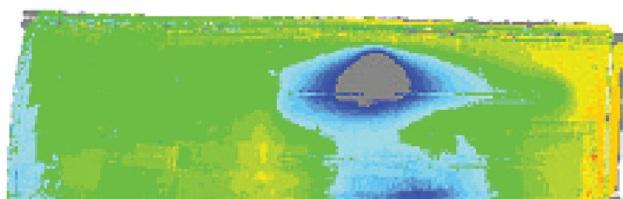
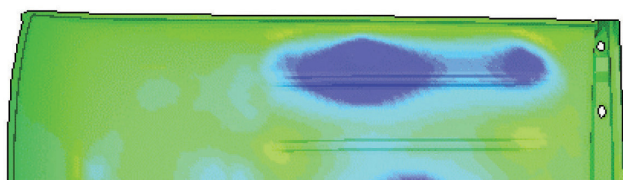


Fig. 5 Plastic strain distribution after load removal area with plastic strain



Residual displacement distribution Experiment results



Residual displacement distribution Calculated results

Fig. 6 Displacement distribution after load removal – comparison of test and analysis results

3.3 Explicit analysis results

Fig. 4 shows the deformation-mode distribution under the maximum load (buckling). It can be seen that the roof panel warps between the center pillar and the rear roof rail.

Fig. 5 shows the distribution in the deformation mode after the load removal process for the plastic strain. Recovery from the buckling after the load removal process is apparent, but plastic strain remains around the buckle.

The results of a test to determine vertical displacement after the load removal process and the results of

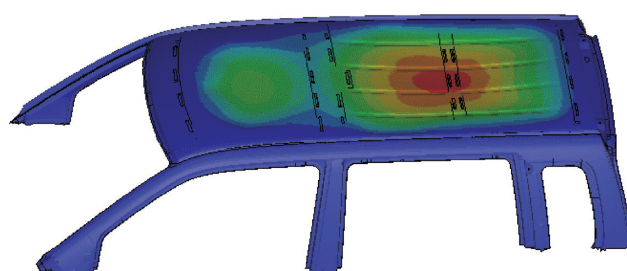


Fig. 7 Deformation mode under maximum load (reduction of roof panel thickness)

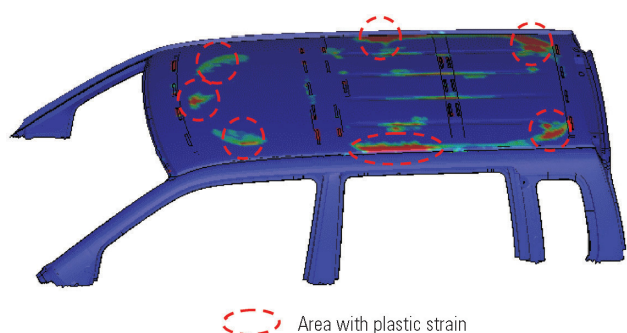


Fig. 8 Plastic strain distribution after load removal (reduction of roof panel thickness)

the analysis are compared in Fig. 6. As can be seen, they are in agreement.

We studied about reducing the roof panel thickness by two gauges.

Fig. 7 shows the deformation-mode distribution under the maximum load (buckling) about the panel thickness reduction conditions. This simulation result predicts the buckling in front of the center pillar.

Fig. 8 shows the plastic strain distribution after the load removal about the plate thickness reduction conditions. It shows that the plastic strain of thin roof panel is higher than thick roof panel.

4. Concluding remarks

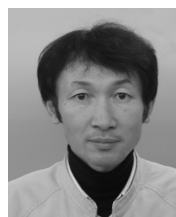
The explicit method analytical technique is free of mathematical divergence and capable of predicting roof buckling under a snow load with sufficiently high accuracy. The technique will be helpful for developing new models in future. We sincerely thank all those concerned inside and outside the company for their help in our research and development work.

References

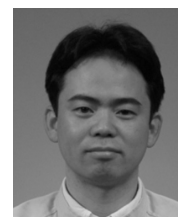
- (1) Japanese Society of Steel Construction: Theory and Application of the Finite Element Method in the Field of Structural Engineering, Chapter 3
- (2) The Japan Society of Mechanical Engineers: Calculational Dynamics Handbook (1. Finite Element Method, Structures), Chapter 4, Maruzen
- (3) Kyuichiro Washizu et al.: Finite Element Method Handbook 2, Applications, 5. Stabilization of Structure and Analysis of Gross Deformation, Baifukan



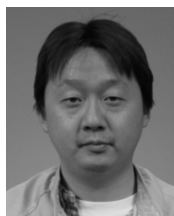
Eiichi KOBAYASHI



Toshiyuki MIYACHI



Yoshinobu MATSUMURA



Akinori YASUI



Hiroyuki WATAKABE



Hirotaka KANO

Development of Filter with New Function for Car Air-Conditioner

Makoto YAMAKAWA* Tadahiro NOMURA* Yuki ITO**
Osamu KANAMORI** Masanori KONO*** Tomoyasu OSAKI***
Daisuke TANAKA***

Abstract

In collaboration with Mitsubishi Heavy Industries, Ltd., we have developed the world's first*¹ car air-conditioning filter for decomposing and inactivating pollen, mites and other substances that cause allergies (allergens) accumulating on the filter through the action of an enzyme and urea (called "Bio-clear Filter") to improve the air quality in the cabin. This paper describes the technical features and performance evaluation of this filter.

*¹ World's first car air conditioner filter that decomposes and inactivates allergens such as pollen and mites using enzyme and urea. (As a result of our company's investigation, as of February 2005)

Key words: Filter, Air Conditioning, Amenity

1. Introduction

The rapid rise in sales of home air purifiers and home electric appliance manufacturers' introduction of a sanitizing function into their residential air-conditioners in recent years indicate that users are concerned about their own health and are becoming interested in improving the quality of air in their own rooms. Furthermore, a questionnaire about the air quality in a cabin completed by our company's employees (Fig. 1) indicated that they are strongly interested in the sanitizing and removal of pollen and other allergens as well as in dust removal and deodorization.

Noting this growing concern about health and cleanliness, we have jointly developed with Mitsubishi Heavy Industries, Ltd. a filter with a new function for a car air-conditioner (called "Bio-clear Filter"). This new filter is designed to purge the air in a cabin, based on new techniques⁽¹⁾⁽²⁾ developed by Mitsubishi Heavy Industries, Ltd. for decomposing and inactivating pollen, mites and other substances that cause allergies (called "allergens" hereafter) that accumulate on the filters for its residential air-conditioners.

This paper describes the technical features and performance evaluation of the air purging effect of the new filter.

2. Technical features of Bio-clear Filter

2.1 Problems of conventional filter

The conventional filter for a car air-conditioner is usually located upstream of the blower fan in the air-conditioner unit. The air inside the cabin and the air

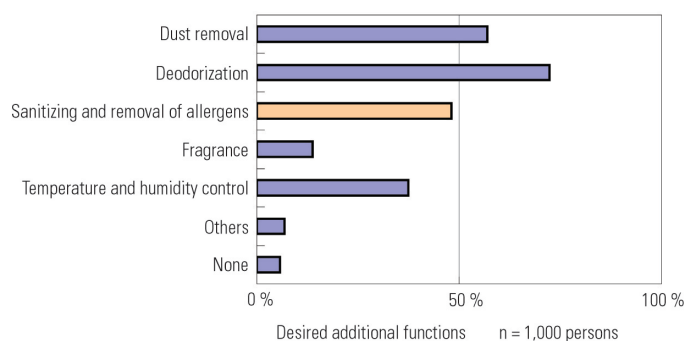


Fig. 1 Desired additional functions to improve the air quality in the cabin

outside it both flow through the filter while the air-conditioner is running. The dust, pollen, mites, etc. in the air are deposited inside the filter (Fig. 2).

However, some of the deposited dust, pollen, mites, etc. is dispersed again in the cabin due to the vibration of the moving car, the wind that gets into the filter (especially when the wind volume is at maximum), etc., which again deteriorate the air in the cabin.

2.2 Improvement of air quality by Bio-clear Filter

The Bio-clear Filter not only collects pollen and mites but also decomposes and inactivates the allergens collected on the filter. Even if part of the collected pollen and mites disperses again in the cabin, their allergens have decomposed and inactivated so that the air quality in the cabin has improved (Fig. 3).

* Interior Design Department., Development Engineering Office

** Advanced Vehicle Engineering Dept., Development Engineering Office

*** Nagoya Research & Development Center, Technical Headquarters, Mitsubishi Heavy Industries, Ltd.

** Material Engineering Dept., Development Engineering Office

** Auto Motive Thermal Systems Dept., Air-conditioning & Refrigeration Systems Headquarters, Mitsubishi Heavy Industries, Ltd.

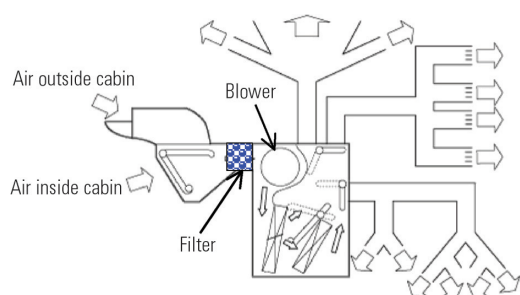


Fig. 2 Location of filter for car air-conditioner

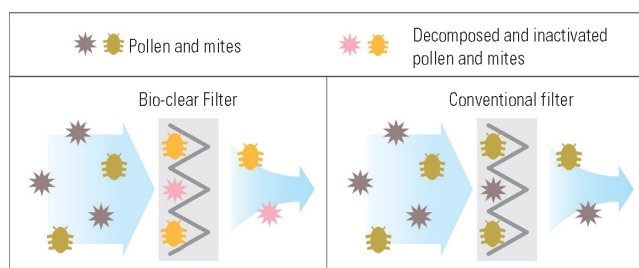


Fig. 3 Comparison of Bio-clear Filter and conventional filter

2.3 Outline of technique for decomposing and inactivating allergens

The primary component of pollen, mites and other allergens is protein. Protein is chemically stable because of its higher-order structure. Protein is generally considered difficult to decompose and inactivate except by high heat or a strong chemical agent, but we have developed a new process for decomposing and inactivating allergens in a cabin. This process is based on the sequential reactions of urea and an enzyme, which denature and decompose protein. The process is summarized below.

The above decomposition and inactivation of allergens are carried out through two stages (Fig. 4):

- ① The higher-order structure of the protein in the deposited pollen, mites and other allergens is turned into a composition that is readily decomposed, owing to the relaxation function of urea.
- ② Protein so altered is decomposed and inactivated by hydrolyze due to the catalyzing reaction of the enzyme.

The enzyme used in this process is natural organic matter (natural enzyme), while the urea is that contained in commercially available skin care cosmetics and the like, so they are harmless to the human body.

2.4 Composition of Bio-clear Filter

As the decomposition and inactivation of the allergens are performed on the filter, the Bio-clear Filter must be able to collect pollen and other fine particles of several tens of microns. If a finer filter media are used to collect a larger quantity of dust, however, the filter will soon become clogged. Hence, the filter has a three-

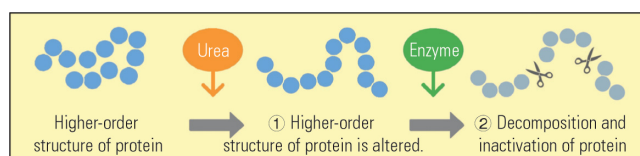


Fig. 4 Allergen decomposition and inactivation process



Fig. 5 Composition of filter media

layer laminated structure. The top and bottom layers mainly remove dust and the middle layer decomposes and inactivate allergens, thus ensuring excellent dust collection without clogging (Fig. 5).

3. Performance and effect of Bio-clear Filter

3.1 Decomposition and inactivation of allergens

The evaluation of the Bio-clear filter was performed using typical allergens – Japanese cedar pollen and mite allergens.

The extent of decomposition and inactivation of the Japanese cedar pollen allergen was determined. The decomposition and inactivation rate by the colorimetric ELISA method was approx. 85 % (the proportion of the specimen pollen which was decomposed and inactivated in one hour at 35 °C and 80 % RH; the pollen was put in the filter prior to the test). Fine decomposition and inactivation of the mite allergens. Allergen was also confirmed by the immunochromatographic method (Table 1).

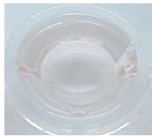
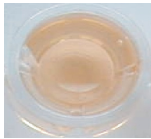
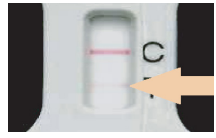
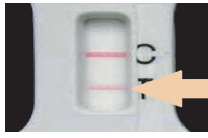
3.2 Environmental resistance

As described earlier, this Bio-clear Filter for car air-conditioner is an application of a technology for residential air-conditioner. The operation conditions of these air-conditioners are, however, extremely different (Table 2).

Whereas a residential air-conditioner takes in and purifies the air in a room which contains a relatively small quantity of dust, etc., a car air-conditioner takes in and purifies outside air which contains a large quantity of dust, etc. to refresh the air inside the cabin. Moreover, rain water or car-wash water may intrude into the car through the opening for outer air intake, while the temperature inside a cabin parked under the blazing sun rises alarmingly. Thus a car air-conditioner is subjected to severer conditions than a residential air-conditioner.

To ascertain the adaptability to and the durability under such harsh conditions, new check points were

Table 1 Decomposition and inactivation of pollen and mite allergens

	Bio-clear Filter	Conventional filter
<u>Decomposition and inactivation of pollen allergen</u> Deep color if the allergen is present in large quantities	 Decomposed and inactivated*	
<u>Decomposition and inactivation of mite allergen</u> Deep color if the allergen is present in large quantities	 Decomposed and inactivated*	

* Test method: Decomposition and inactivation of the pollen or mite allergen put on the filter medium specially prepared for the test
 Pollen: Colorimetric ELISA method
 Mites: Immunochromatographic method

Tested at Nagoya Research & Development Center, Mitsubishi Heavy Industries, Ltd.

Table 2 Comparison of car air-conditioner and residential air-conditioner

	Car air-conditioner	Residential air-conditioner
Air taken in	Air inside the cabin and air outside it	Air inside room alone
Deposition of water	Yes (rain water or car-wash water)	No
Highest ambient temperature	Approx. 60 °C	Approx. 40 °C

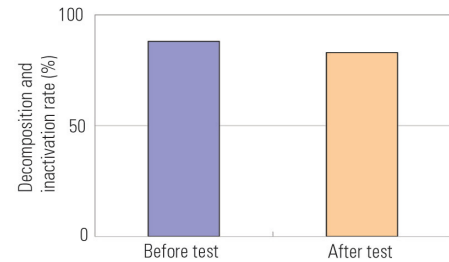
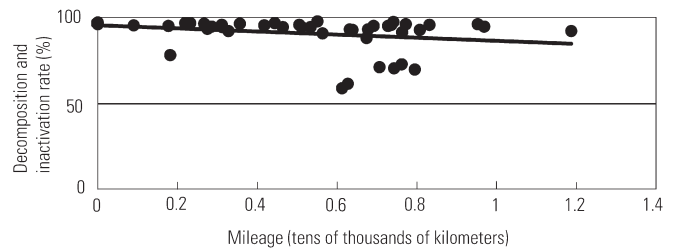
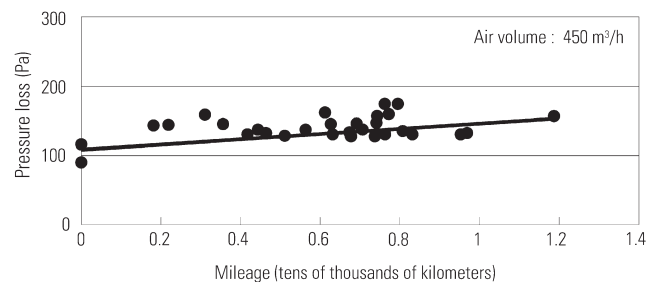
introduced for the filter for a car air-conditioner in addition to those for the filter for a residential air-conditioner. One of those new check points and a monitor test using a real car are described below.

3.2.1 Check points for filter for car air-conditioner and result of check

As noted, the temperature inside a car parked in the sun rises very high; the temperature around the filter may even exceed 60 °C. Hence, resistance to high temperature (resistance to heat) was added to the check points for the filter for a car air-conditioner, and was determined by checking for changes in the function and performance of the filter after endurance testing it in a thermostatic tank at 70 °C. The pollen decomposition and inactivation rate did not change greatly (Fig. 6).

3.2.2 Outline of monitor test with real car

The conditions under which a car air-conditioner is used vary with the time and place at which the car is used and the way it is used. A monitor test was therefore conducted. The Bio-clear Filter was attached to 60 cars owned by users, and the filter was checked for changes in function or performance after 6 months of use from March to September, which includes the season when Japanese cedar and other trees release pollen, as well as the rainy and sultry season.

**Fig. 6 Change in decomposition and inactivation rate after heat-resistance test****Fig. 7 Change in decomposition and inactivation rate after monitor test****Fig. 8 Change in the pressure loss after monitor test**

Figs. 7 and 8 show the change in the pollen decomposition and inactivation rate and the change in the resistance to the air flow due to clogging, etc. respectively. The decomposition and inactivation rate of the filter does not drop sharply, and the pressure loss does not increase sharply.

4. Conclusions

We have developed the world's first Bio-clear Filter for a car air-conditioner which can decompose and inactivate pollen, mites and other allergens, to improve the quality of air in the cabin and checked its adaptability and resistance to the conditions under which it is used. The Bio-clear Filter was incorporated first into the "Bloom Edition" Series – special editions for "COLT", "ek WAGON" and "PAJERO MINI" – released in May 2005 and was well received by users.

The Japan Automotive Industry Association is promoting voluntary efforts to reduce Volatile Organic

Compounds (VOC) inside cabin. In line with this, we are now developing an additional function to reduce VOC inside cabin to improve the cabin ambience even further.

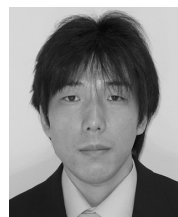
Finally, we wish to thank Mitsubishi Heavy Industries, Ltd. and all those concerned inside and outside our company for their cooperation in developing the Bio-clear Filter.

References

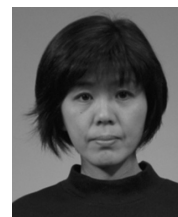
- (1) Miyazawa et al.: Residential Use Air-Conditioner with anti-Allergy Function, Mitsubishi Heavy Industries Technical Review, Vol. 41, No. 2, p. 58, 2004
- (2) Tanaka et al.: Technology for Improving Indoor Air Quality, Mitsubishi Heavy Industries Technical Review, Vol. 42, No. 1, p. 36, 2005



Makoto YAMAKAWA



Tadahiro NOMURA



Yuki ITO



Osamu KANAMORI



Masanori KONO



Tomoyasu OSAKI



Daisuke TANAKA

Parking-Guidance System Using Nose-View Cameras

Keiji UEMINAMI* Hitomi OHYABU* Takahiro MAEMURA*

Abstract

We have developed a system for providing voice and visual guidances during parallel and garage parking – two of the most disliked maneuvers among all common driving operations. Placing the priority on ease of use, we employed the nose-view cameras to realize an interface with no need for complicated initial settings, and which can be easily understood by all drivers, even those making use of the system for the first time. In addition, compensation for vehicle parameter unevenness allows the system to achieve highly-practical levels of position accuracy for parking.

Key words: *Intelligent Vehicle, Safety, Electric Equipment, Comfort, Human-Machine-Interface, Intelligent Transport Systems (ITS)*

1. Foreword

Many like to drive automobiles on account of the ability they afford to freely go wherever desired; however, a significant number of drivers have a negative impression of parallel and garage parking. In response, a wide range of different parking-support systems have been brought to market. In particular, drivers can become nervous when the space behind the vehicle cannot be seen, and they often have trouble determining how far to reverse; accordingly, the rear-view camera has been introduced in order to provide support for these specific aspects of parking. Similarly, corner sensors have been developed to help the driver determine how close the vehicle's hidden corners are to other objects. Nevertheless, even when equipped with these parking aids, certain drivers still need to repeat parking numerous times in order to get it right, and this state of affairs points to a failure thus far to eliminate other driver-specific factors, such as an inability to determine the initial stop position or the right time to turn the steering wheel.

In light of this situation, we employed the nose-view cameras (Fig. 1), which are installed on vehicles in order to watch the traffic conditions in intersections with poor visibility, in the development of an inexpensive and practical parking support system capable of satisfying the following requirements, and we launched this system as an integrated part of the new GRANDIS in May 2005.

<Requirements of this system>

- Simple determination of initial stop position by drivers of all ability levels
- Voice guidance of advance, reverse, stop, and steering wheel operations
- Support not only for parallel parking, but also highly-frequent garage parking



(a) Camera position



(b) Image on display

Fig. 1 Nose-view camera

2. System configuration

Fig. 2 presents a diagram of the system's configuration.

Images captured by a pair of nose-view cameras, one installed on each side of the front bumper, and by a rear-view camera installed at the rear of the vehicle, are input to a camera/parking guide control unit. This unit then superimposes menu items, a guide line and operation guidance onto the captured images, and displays the resultant images on a screen. Voice guidance is output via the vehicle's internal speakers, with vehicle-related information required for this guidance, such as steering-wheel turning angle and travel distances, being obtained from the corresponding devices via the Controller Area Network (CAN). Furthermore, a dedi-

* Electronics Engineering Dept., Development Engineering Office

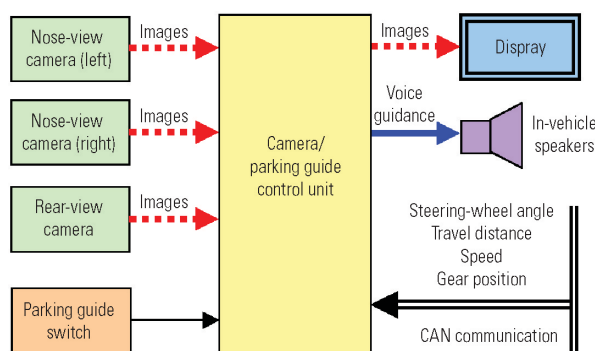


Fig. 2 System configuration

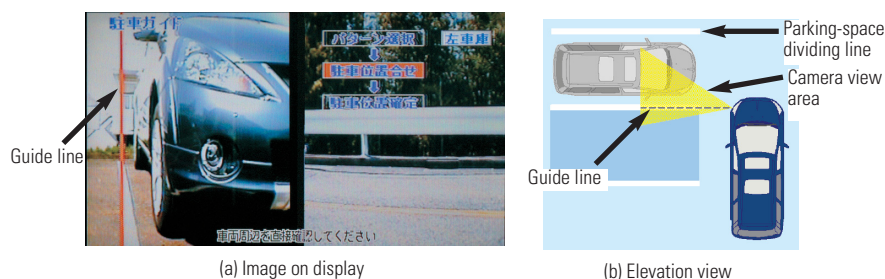


Fig. 3 Parking position alignment

cated parking-guide switch is provided inside the vehicle in order to allow the driver to startup the system and to make the required menu selections.

A guide line (Fig. 3 (a)) is superimposed on images from the nose-view cameras, and when the driver aligns this guide line with the parking-space dividing line displayed on the screen and stops the vehicle, the positional relationship between the vehicle and the parking space can be determined (Fig. 3 (b)). By assuming at this time that the vehicle is positioned either garage or parallel to the parking space, it is possible to calculate the parking trajectory. The calculated parking trajectory combines only forward and reverse in a straight line or at the maximum left and right steering angles, thus allowing garage parking to be completed in three steps, and longitudinal parking, in four (Fig. 4). The coordinates of the turning center (x_0, y_0) , (x_1, y_1) and the turning angles θ_0 , θ_1 are determined from vehicle data, nose-view camera mounting positions, and the turning radii R_0 , R_1 at the maximum left and right steering angles; furthermore, the travel distances $L_0 - L_3$ between the individual steps required for guidance are handled as parameters. The system then provides the necessary display-based and voice guidance to the driver in order that he or she can drive the vehicle along said route.

The following section will detail the conditions that determine whether or not a parking space is suitable for application of this system. In order to enable simple operations by the driver, the start position is determined using only one side of the parking space; however, route calculation is carried out at this time under the

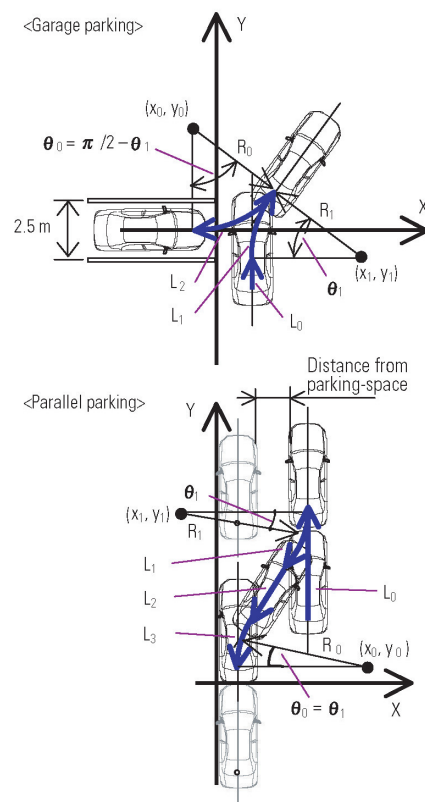


Fig. 4 Calculation of parking trajectory

assumption that the width of a garage parking space is 2.5 m. This assumption is based on the results of a survey showing the majority of parking spaces to be of this width. Furthermore, since it will affect the lateral (left/right) position of the vehicle at the end of guidance for parallel parking, the distance from the parking-space dividing line is assumed to be between 0.7 and 1.0 m at the time of position alignment.

As described above, this system has been designed to provide instructions regarding the parking procedure, and all such operations are performed fully by the driver. In addition, no functionality is provided for identification of obstacles in the vicinity of the vehicle or determination of whether or not the parking space is of a sufficient size; consequently, the driver must continue to follow normal driving practices and confirm safety while using the system.

3. Operation procedure and user interface

During the development of this system, particular attention was paid to the creation of an easy-to-understand user interface and operation procedure. Fig. 5 presents an overview of the operations performed during its usage.

This system's user interface was developed with priority given to the realization of operations that would be easily understood even by first time users, that would be easy to perform by persons not used to driving, and that could be performed in a comfortable, non-strenuous manner. The sequence of operations

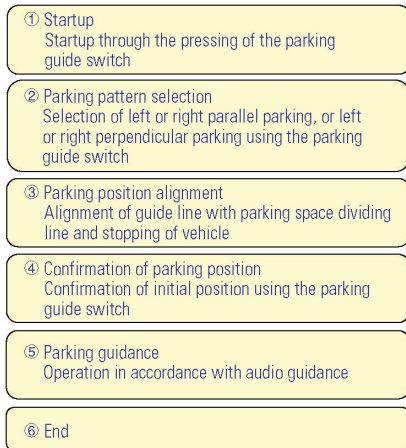


Fig. 5 System operation overview

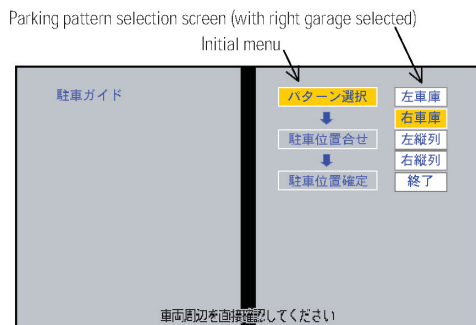


Fig. 6 Image of parking pattern selection

and the corresponding characteristics are described below.

- (1) **Startup:** Upon pressing of the parking guide switch, the initial menu is displayed to the right of the screen showing the nose-view camera images. This menu allows all subsequent operations to be quickly confirmed (Fig. 6).
- (2) **Parking pattern selection:** The message "Select parking pattern" is displayed upon startup, and since a list of valid parking patterns is displayed on the right of the screen, it is easy to understand even by a beginner. Each press of the parking guide switch changes the selected item, which is highlighted to improve ease of selection (Fig. 6).
- (3) **Parking position alignment:** As described above, the corresponding procedure is simple and straightforward, with the driver simply required to stop the vehicle at the position where the single guide line displayed on the screen coincides with the parking-space dividing line. As this simply involves stopping the vehicle in parallel with parking lot's driving lane, no difficult or troublesome operations are required on the part of the driver. At this time, furthermore, the guide line is displayed on the left of the screen in the case of left parallel or garage parking, or on the right of the screen in the case of right parallel or garage parking. This line is also flashed on and off in order to improve the ease of align-

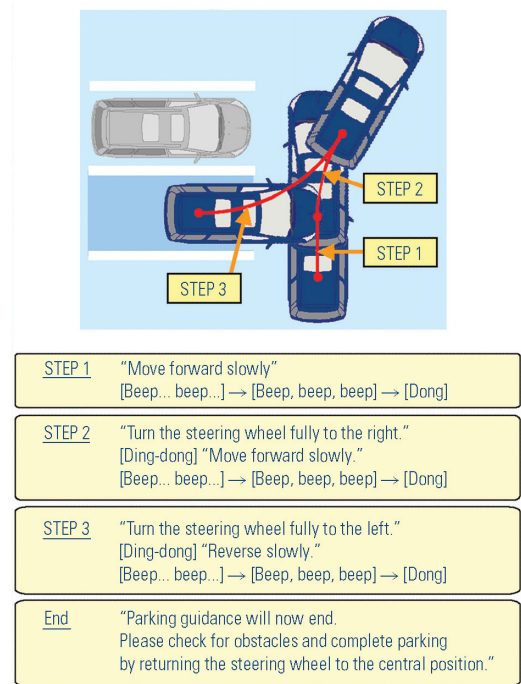


Fig. 7 Example of parking guidance (left garage parking)

ment.

- (4) **Confirmation of parking position:** As the driver presses the parking guide switch to confirm that the initial position has been determined, the system begins route guidance.
- (5) **Parking guidance:** Instructions for all subsequent operations are provided via voice guidance, and therefore, parking can be performed by anyone and with no need to rely on personal judgment. Fig. 7 presents an example of parking guidance provided for garage parking. Basic operations for garage parking and parallel parking are the same.

During parking guidance, the steering wheel is only operated while the vehicle is stationary, and the steering wheel is only maintained with in the fully-left, fully-right, or central position; accordingly, the driver can confirm safety around the vehicle much more easily than when performing normal driving. In addition, when providing motion guidance during forward or reverse driving, the interval between individual [Beep] sounds becomes shorter as the vehicle approaches the stop position, and a [Dong] sound informs the driver when the vehicle has reached this position.

In the rare event that the driver makes a mistake while trying to follow the guidance provided, this voice guidance is repeated. For example, if the vehicle were to be driven forward beyond the stop point, the driver would be requested to "Please reverse slowly", and this guidance would be repeated until the vehicle were successfully stopped at the correct point.

In order to cover for situations where the driver missed the voice instruction being given, operation details corresponding to these instructions are presented on the screen. Since this display uses a simple icon

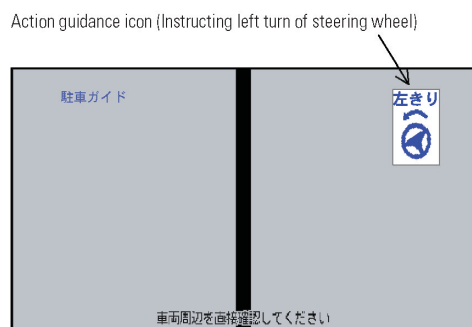


Fig. 8 Image of parking guidance

and text format that can be quickly understood at a glance, there is no need for the screen to be constantly monitored at the expense of confirmation of safety around the vehicle (Fig. 8).

In addition, even if the driver were to perform an action independently before voice guidance had come to an end, this guidance would be continued. Parking support via voice guidance is often considered to be time consuming when followed diligently, and drivers may feel that their own way of parking is much quicker. However, when a driver becomes familiar with this system and does not follow the instruction to its conclusion, he or she will be able to park in a trouble-free manner and with no significant difference in the time required when compared with unguided parking.

4. Parking position accuracy

In addition to assuring ease of operation during the development of this system, we also strove to improve the accuracy of vehicle positioning when parking in accordance with the guidance provided. Specifically, the target of development was to be able to park a vehicle within 100 mm to the left or right of the central position of a garage parking space, even in situations where there existed unevenness in each vehicle and driver-operation parameters that could affect accuracy.

In order to achieve the ease of operation that is this system's principle characteristic, steering is performed only at the fully-left and fully-right positions; however, the maximum steering angle depends on factors such as suspension assembly, varying each produced vehicle and also varying slightly between left and right turning. In situations where a vehicle's maximum steering angle differs from the design standard, the vehicle will deviate from the parking trajectory calculated based on those values, and therefore, the parking position at the end of guidance will not match the target position. Although it is necessary for any deviation in the maximum steering angle to be within a specific angular range in order that the targeted position accuracy be achieved, the vehicle's design standard range for maximum steering angles is larger than said specific range; accordingly, there is a possibility that certain vehicles may not be able to achieve the accuracy tar-

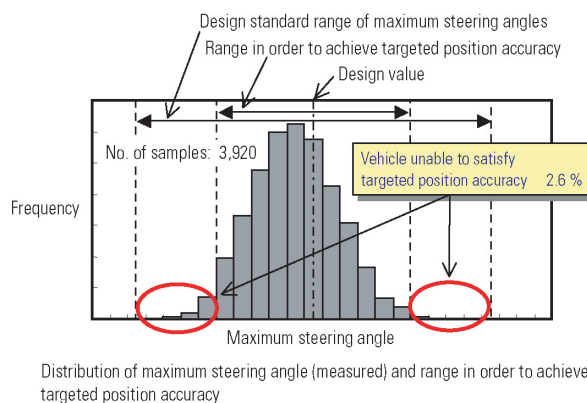


Fig. 9 Effect of deviation in maximum steering angle on parking accuracy

get. Numerous vehicles were measured in the production-line to make statistic analysis and checked the full-steer angles in each right and left. There were vehicles by 2.6 % which are not able to achieve the accuracy of targeted position in statistic (number of samples: 3,920) (Fig. 9). Accordingly, we decided to use maximum steering angles for each vehicle to calculate the parking trajectories, and to record the fully-left and fully-right steering angles of all vehicles at factory shipment.

On the other hand, some types of tires can be selectable even on a model depending on its grade. Although the distance traveled is calculated based on wheel revolutions, differences in the actual distance arise as a result of the size of tire fitted to the vehicle; accordingly, in situations where a number of different tire sizes can be selected based on vehicle model, it is necessary to convert the distance to reflect the fitted size. In this case also, we aim to improve parking accuracy by recording the varieties of tire fitted to vehicles at factory shipment.

In addition, it has also been considered that unevenness in the mounting position of the nose-view cameras could affect accuracy. If such unevenness does exist, the guide line superimposed onto the image obtained from the nose-view cameras may not correspond to the required direction, and consequently, the vehicle position will deviate from that of the parking space during alignment, thus adversely affecting position accuracy. Since the elimination of disparity in camera mounting positions cannot easily be achieved, the displayed positions of guide lines are adjusted prior to shipment from the factory, thus canceling the effect of any disparity.

5. Conclusion

- (1) Using nose-view cameras, it was possible to achieve a parking support system with extremely straightforward settings and simple operations from beginning to end.
- (2) The user interface, based on voice guidance, can be easily understood by first-time drivers and also

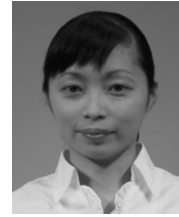
takes safety fully into consideration.

- (3) By compensating for unevenness in various vehicle parameters that can affect parking accuracy, it was possible to achieve a highly-practical level of accuracy.

Finally, we would like to express our sincere gratitude to Clarion Co., Ltd. and in-house departments such as Production Engineering and Vehicle Proving for their assistance in the development of this system.



Keiji UEMINAMI



Hitomi OHYABU



Takahiro MAEMURA

Latest Stamping Simulation Technique

Kuniomi MATSUYAMA* Takeo OHTSUKA*

Abstract

Considerable attention is now turning to simulation-based manufacturing methods as an effective means for making stamping parts highly accurate, reducing cost and achieving timely product delivery. The trend in the recent years has been toward adoption of complex design shapes and preference for aluminum or high strength steel sheets for lightening. Consequently, more sophisticated prediction is demanded in simulation methods.

The stamping simulation method actually applied by production engineering departments are described in this paper. Additionally, in consideration of the extensive use of the springback prediction method for ultra high strength steel sheets, we present a die shape compensation method based on computer-aided engineering (CAE).

Key words: CAE, Front-Loading, Springback, Die Compensation

1. Introduction

Stamping simulation involves finding the solution to a dynamically formulated boundary-value problem using the finite element method. Deformations such as cracks and wrinkles created during the process of forming stamping parts can be predicted through this simulation (Fig. 1).

The Production Engineering Department began applying the simulation technique to actual tasks in the latter half of the 1990s. It is now primarily used to predict cracks or wrinkles in a product and any compensated areas (addendum, blank hold surface, etc.). The technique is also applied to study such matters as process streamlining, parts integration, material yield, downgrading and suitability for the forming of aluminum, high strength steel sheets and tailored blank workpieces.

2. Features of our stamping simulation

2.1 Software used

We use two kinds of software intended for different purposes. Their features are described in Table 1, and the development schedule and times at which an simulation is conducted are given in Fig. 2.

Auto Form Incremental (AFI), which is used to conduct a product study, is applied at the designing and structure study stages to quickly detect any serious faults at the initial stage of development and to ensure that a remedy is reflected in the preparation-for-production chart.

PAM-STAMP (PAM), which is used to study a process, can perform a detailed simulation with the forming process taken into account, to determine the optimum method with respect to any addendum, blank hold surface, etc. and to ensure that a remedy is reflected in the production start chart.

The recently introduced AFI is indispensable for promoting front-loading by the Body Design Dept. and

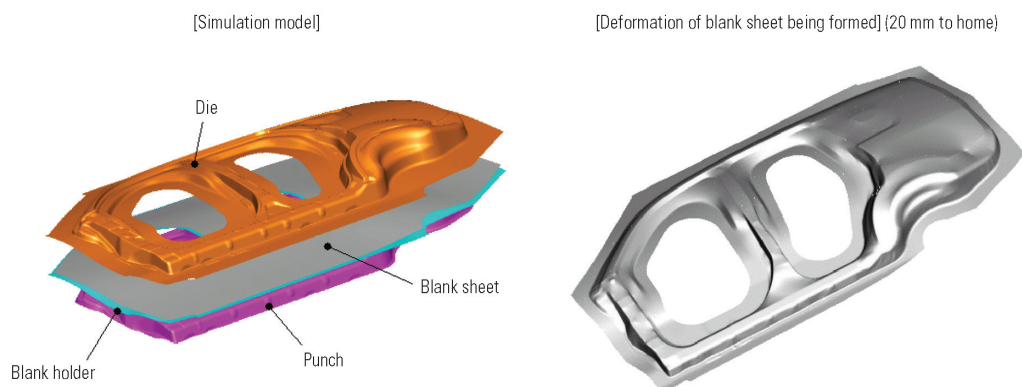
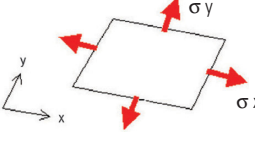
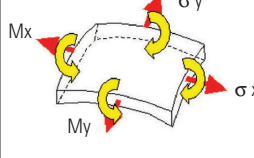
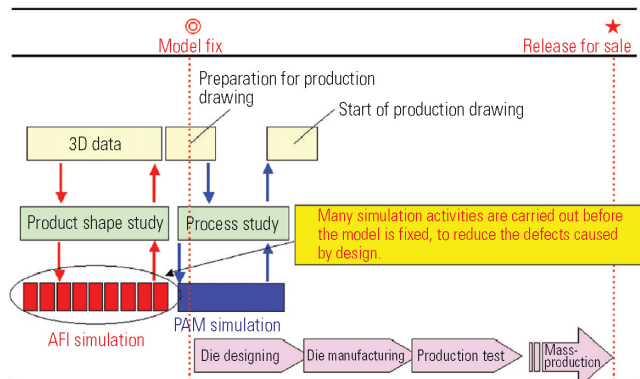
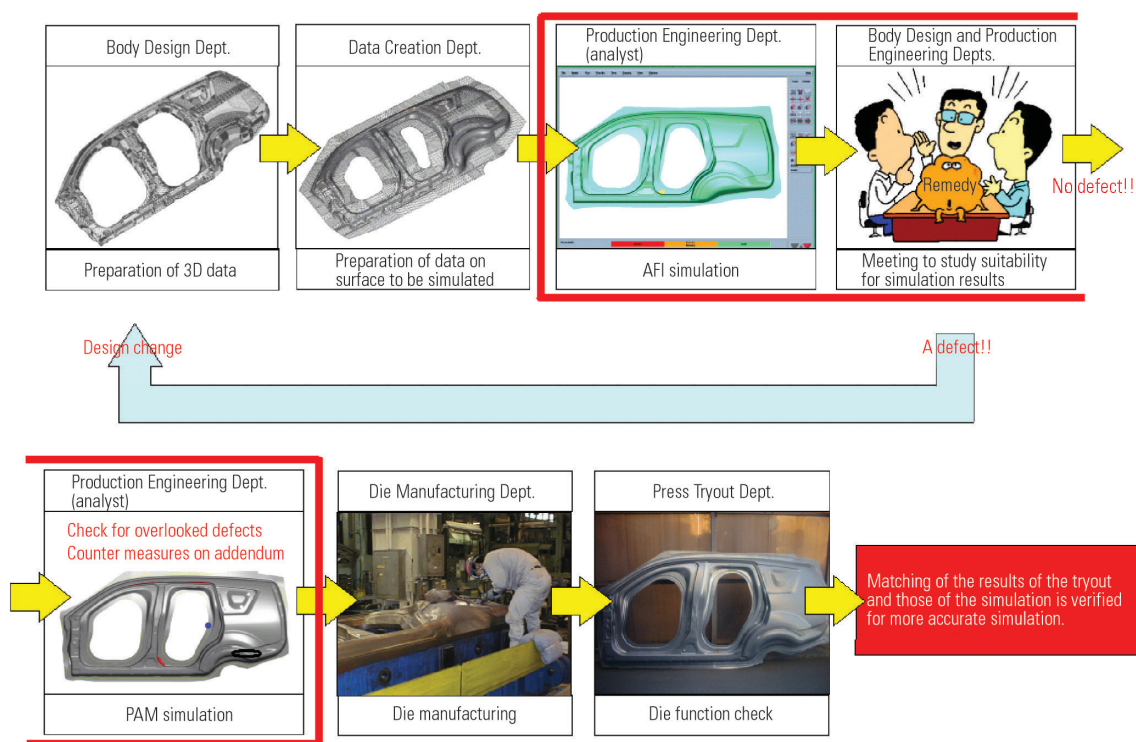


Fig. 1 Stamping simulation

* Production Engineering Body Dept., Production Engineering Office

Table 1 Features of stamping simulation software

Software	Auto Form Incremental (AFI)	PAM-STAMP (PAM)
Purpose	Searching cracks or wrinkles caused by design	Checking a stamping process to optimize a process planning
Features	Finite element – use of a film element (degrees of freedom 2)  σ : stress	Finite element – use of a shell element (degrees of freedom 4)  M: bending moment
Strong and weak points	<ul style="list-style-type: none"> • Faster simulation with lower-degree simultaneous equations • Medium simulation accuracy 	<ul style="list-style-type: none"> • High-precision simulation by accurately solving simultaneous equations. • Slow simulation
Usage	<ul style="list-style-type: none"> • All parts for die making in house • Some parts for die supplier (hard formability parts) 	<ul style="list-style-type: none"> • All parts for die making in house

**Fig. 2 Simulation activities under development schedule****Fig. 3 Stamping simulation workflow**

Production Engineering Dept., which is described later.

2.2 Simulation workflow

The flow of stamping simulation work is shown in Fig. 3.

First, after compensating for any addendum, blank hold surface, etc., the shape is determined based on 3D data from the Body Design Dept., and the AFI simulation is performed. With respect to detected cracks or

wrinkles, a remedy such as reshaping of the product or the addendum is adopted at a meeting for studying the suitability for simulation results. The necessary alterations are arranged with the Body Design Dept., and the AFI simulation is performed again, with the next batch of data taken in. The simulation is repeated until all serious defects are eliminated. PAM simulation, which provides a higher hit rate, is then performed to check for any overlooked defects. The analyst verifies the

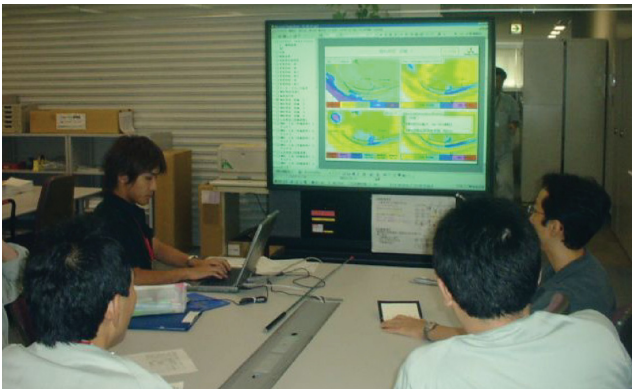


Fig. 4 Discussion with Designing Dept. on suitability for simulation results

Table 2 Theses to improve initial product quality of stamping parts

Item	Description
① Thorough feedback of product engineering requirements to Designing Dept.	<ul style="list-style-type: none">• Product design in compliance with the “Product Design Guideline for Promoting the Use of Base-grade Materials” (request)• Observing the rule to minimize the design change through Preparation for Production Drawing, Casting GO Drawing, and Start of Production Drawing (request)
② Further application of simulation	<ul style="list-style-type: none">• Improvement of prediction accuracy of simulation (on cracks and wrinkles)• Rule that precludes the possibility of a defect
③ Prediction of springback and surface distortion	<ul style="list-style-type: none">• Compensation of trim lines• Improvement of springback prediction accuracy• Quantification of surface distortion and improvement of its prediction accuracy

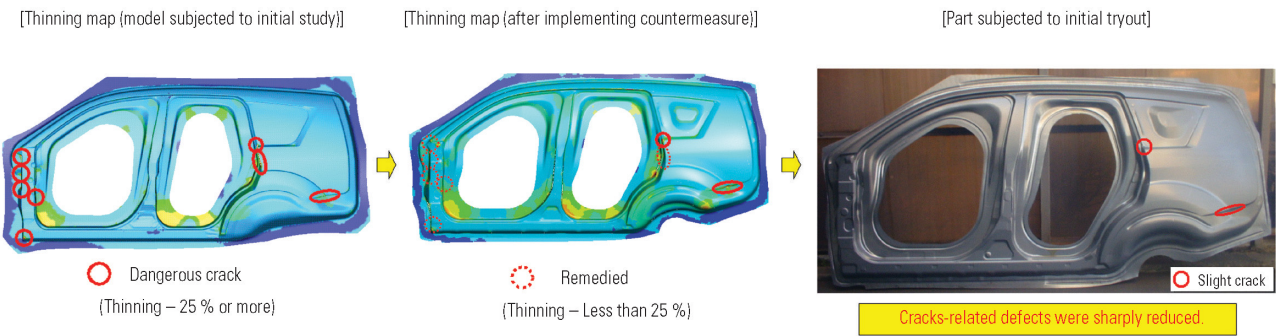


Fig. 5 Defect-reducing effect on side panel outer of OUTLANDER

matching of the results of the tryout and those of the simulation for more accurate simulation, and passes on the findings to the section that is to develop the next vehicle model.

3. Example of front-loading simulation

3.1 Collaboration with Body Design Dept.

In order to eliminate stamping defects at an early stage, simulation should begin at the designing stage where design changes are flexible and a remedy for defects should be reflected in the drawing by the feedback to the Body Design Dept.. In our company, a meeting is held between the Production Engineering Dept. and the Body Design Dept. to discuss the suitability for simulation results (Fig. 4). At this meeting, practical remedies are worked out for all identified shape-related defects of the product. The discussion is continued until the defects are eliminated, and an arrangement is subsequently made for scheduling the next simulation.

3.2 Defect-reducing effect by use of simulation

The effect of simulation using the outer side panel of the OUTLANDER is shown in Fig. 5. At an early stage of the study, 8 cracks were identified following the sim-

ulation. Remedies were repeatedly implemented until the number of cracks was reduced to 2 prior to manufacturing a die. A slight crack was detected on the piece subjected to the first tryout, but no disastrous defects were found. This evidences the defect-reducing effect of CAE.

3.3 Future steps

Aiming at zero defects at the end of the first tryout, we will appeal the Designing Dept. of the product design based on the “Product Design Guideline for Promoting the Use of Base-grade Materials” and tackle to further application of the simulation, improvement of dimensional accuracy and the countermeasures for surface distortion (Table 2).

4. Die shape compensating technique based on CAE as means to prevent springback

4.1 Problems associated with stamping ultra high strength steel sheet

Increasingly greater ultra high strength steel sheets (tensile strength: 590 MPa or more) are used to enhance safety against collision and reduce fuel costs by lightening body. However, these steel sheets are

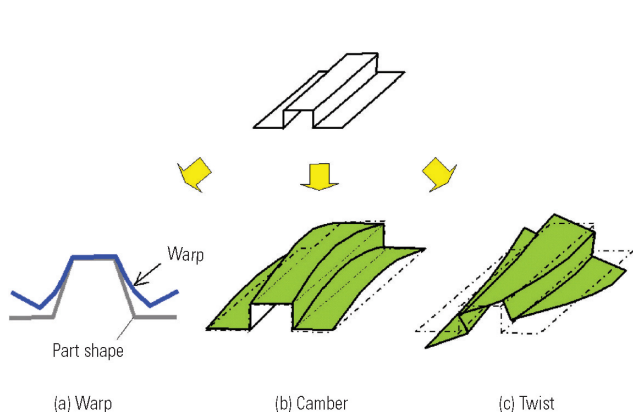


Fig. 6 Springback defects on formed ultra high strength steel sheets

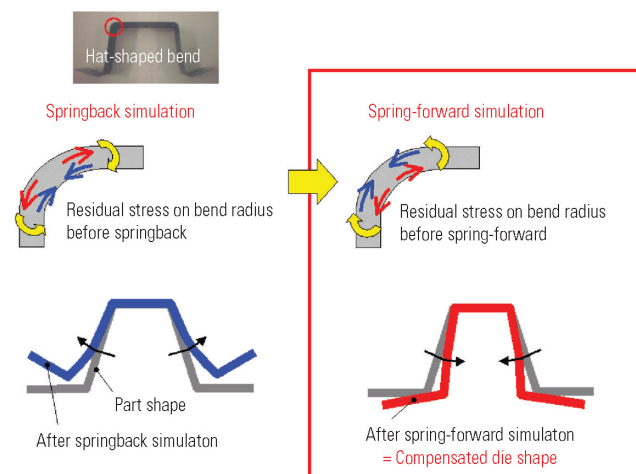


Fig. 7 Concept of spring-forward method

Process	Simulation	Die manufacturing	Press-tryout	Modification of die
Proposed method	Crack and wrinkle prediction only (no springback simulation)	Die milling matched with part shape	Springback detected ⇒ Measurement with instrument (jig) Unloading Tryout and error	Modification relying on feeling and experience Padding Re-milling
Conventional method	Compensation of die shape by spring-forward method	Processing of die into compensated shape	High-precision parts after first tryout ! Unloading	N/A

Fig. 8 Comparison of conventional die manufacturing process and proposed method

hard to form, and a serious dimensional change called “springback” occurs during the process. It is quite difficult to prevent springback in the present circumstances. Experience in using 980 MPa class steel sheets in particular is very scarce, and there is no way of predicting and dealing with three-dimensional springback such as warp, camber or twist (Fig. 6). Remedying the problem by tryout and error takes many man-hours on the production line.

4.2 Proposed method for compensated die design (Spring-forward Method)

Springback prediction by CAE is one of the most promising methods because it can be directly applied to vehicle body parts or other objects with a complex shape. Springback can be predicted by CAE and countermeasure, which will reduce tryout man-hours and raise the level of efficiency, ultimately leading to production without the need for preliminary tryouts.

What the designer needs to know is not the extent of springback deformation on a panel but the die shape for producing high-precision parts. Even with an accurate springback prediction by CAE, high-precision parts cannot be manufactured unless an optimum die shape can be designed based on the prediction data.

Recently, we proposed the Spring-forward Method, which is a new technique for compensating the die shape by CAE. Under this method, the plus and minus signs of the residual stress causing springback are reversed for simulation to orient the springback in the reverse direction of normal springback. The extent of deformation is reflected directly in the die shape (Fig. 7). The flowcharts for the conventional method and the proposed method are compared in Fig. 8. The die shape was automatically compensated by the proposed method following CAE, prior to manufacturing the die. Blank sheet were successfully formed with the die.

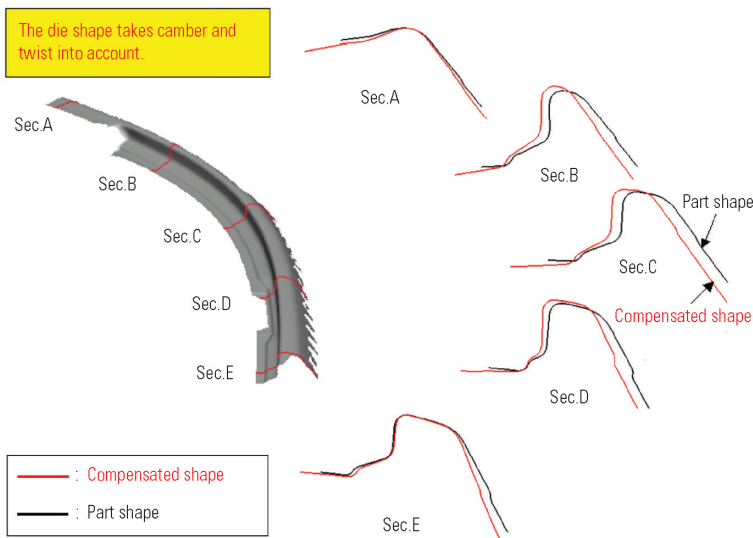


Fig. 9 Compensation of die shape by spring-forward method

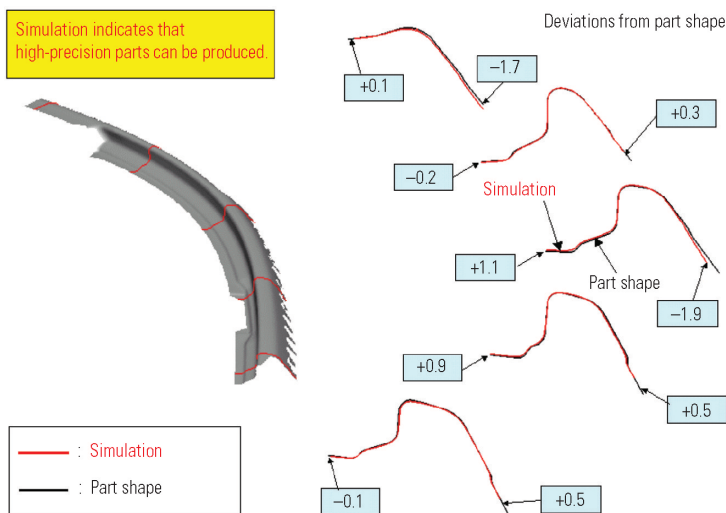


Fig. 10 Results of springback simulation

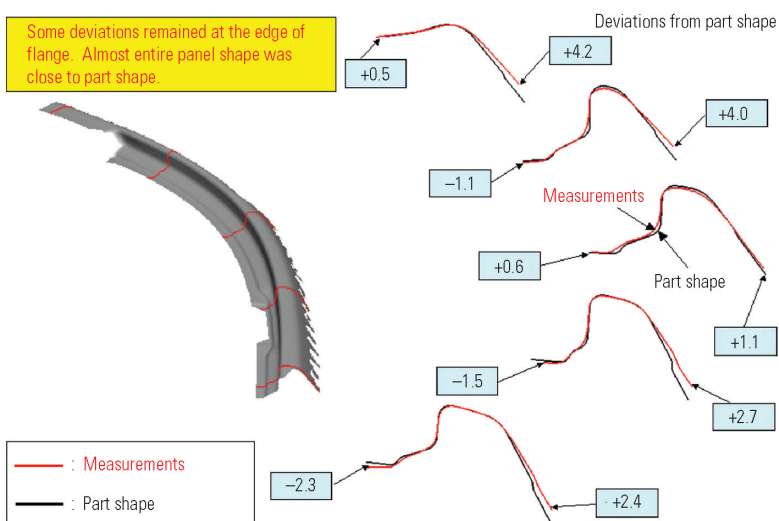


Fig. 11 Compensated die tryout results

Application of the spring-forward method is described next.

4.3 Example of die compensation by proposed method

(1) Compensation of die shape

The ultimate aim of the proposed method of compensation the die shape is to provide a die shape for producing high-precision parts. We decided to fabricate and use a test die to find out whether the proposed method is effective. Ultra high strength steel sheets were selected as trial parts, in consideration of safety against collision, and the upper part of a front pillar reinforcement, which is extremely hard to manufacture to a high precision, was also chosen. The shape of the trial part is based on the front pillar reinforcement for GRANDIS and is nearly the same as the part actually used on GRANDIS. A 980 MPa class ultra high strength sheet (adopted by OUTLANDER) was used as the trial material. A sectional view of the die shape compensated by the proposed method is shown in Fig. 9. This die shape allows for 3D deformation including twist and camber.

(2) Verification of simulation result

Fig. 10 shows the results of the spring-back simulation. The simulation indicates that high precision can be produced. An actual test die shaped like the simulated die was manufactured and then tested to determine the precision.

(3) Verification of tryout result

Fig. 11 shows the 3D measurements for the panel using the actually optimized test die. A slight deviation from the part shape was observed at the end of the flange, but twist, camber, etc. were sharply reduced.

4.4 Future tasks

Our future tasks include further improving the accuracy of springback simulation and developing a CAD function to translate the compensated shape into standard surface data for practical application.

5. Concluding remarks

Our stamping simulation process and the method we used to carry out the simulation are described in this paper. Further lightening will be demanded in the future, and ultra high strength steel sheets will be used in increasingly more sections of the product. We hope to upgrade method reliability and simulation

speed for early practical application. We would like to express our sincere gratitude for the cooperation of all those concerned inside and outside the company.



Kuniomi MATSUYAMA



Takeo OHTSUKA

The Road to "Concept-X"

Passionate Message from the Design Studio of Mitsubishi Motor R&D Europe GmbH (MRDE)

The "Concept-X" that enjoyed favorable reception at the exhibition in the 2005 Tokyo Motor Show was created at a design studio in Europe (belongs to MRDE located in the suburbs of Frankfurt, Germany).

Here is an article by 3 designers who were engaged in the "Concept-X" project to introduce the passionate heart of the designers and activities at design bases overseas.



A Glimpse into Creating a Design Icon – Understanding the Process and Method



Project Leader
Mikael CAZZATO

When one starts to analyze the content in mass produced products such as day to day things like a hair dryer, vacuum cleaner or cars, one is sometimes struck by the thought that there must have been people thinking about "how" or "why" things look like they do. Whereby the aesthetics and usability of products may be improved. Design aspects specified by the industrial designer may include the overall shape of the object, the location of details with respect to one another, colors, texture, sounds, and aspects concerning the use of the product ergonomics.

Additionally the industrial designer may specify aspects concerning the production process, choice of materials and the way the product is presented to the consumer at the point of sale. The flexible ideas of industrial designers in a product development process may lead to added values by improved usability, lowered production costs and more appealing products. Automotive design (especially with regard to exterior

designs) tends to differ from the other design disciplines in that it has an important kinetic dimension that involves emotion and dynamics. It is a defining feature of the car design that these qualities have a strong influence on the way designs are created.

The understanding of not only the product but also the "brand" image and identity is a must to enhance and conceive a successful new design for a product.

MRDE Design have had the luck and skill to contribute with the knowledge and professionalism required to create new products for Mitsubishi Motors Corporation (MMC). Although a small team we can say that we are a part in creating a new image and a new start for the brand.

As MRDE is situated in Europe, away from the mainstream production in Japan, we can sometimes take on a project with a different attitude or approach. With other words we can sometimes see a solution or a problem from a different angle. We also pick up dif-

ferent trends and movements in design from a European perspective, which sometimes is helpful also from a Japanese point of view as it gives the brand the diversity and different look that might distinguish MMC from other brands and thereby enhance the awareness of the brand for the customer world wide.

Late 2004 MRDE was asked to take on a project codenamed 05V later named Mitsubishi Concept-X. A small team of designers were assembled to take on this task, Omer Halilhodzic (Exterior Chief), Thomas Vaquerizo (Interior Designer) and Mikael Cazzato (Project Leader).

This project would be part of reinforcing the image of the brand at Tokyo Motor Show 2005. The general consensus was to create a successor to the famous LANCER EVOLUTION, or at least give the public a glimpse of what a "New EVO" could look like in the near future.

The LANCER "EVO" is and has been a product icon in the MMC product range for a long time, success in WRC and also famous for its performance and agility.

Although successful, the design or styling of the "EVO" have two camps, one that "loves it for its honesty and pure image", and one that think, "it's a great car but it's starting to look a bit old". Now how does one combine and enhance the image of such an "icon" as the LANCER EVOLUTION, not an easy task when starting to think about it, but one that is achievable if analyzed correctly and executed with love and care.

First the understanding of what the EVO is and stands for is essential. There is a lot of emotion in a product like a sports car, emotion that has to be interpreted and carefully studied. What makes a car radiate sportyness and at the same time clearly look like a MMC?

To answer these questions one have to look at the brand as a whole and try to understand what or which cars MMC have done in the past that in some way could be classified as "true" MMCs or "pure" products. Is it the PAJERO, which is another icon in the product range, or is it the DELICA?

I would say from a design point of view that one common point is that it is mature and a masculine feel to most of our products, of course there is other aspects that makes a product great or successful but to under-

stand what makes a MMC have that "feel" to it is crucial.

In creating the Concept-X we wanted to combine the WRC image with the pure sports car, in a sense what "EVO" stands for. At the same time we had to take care that the design did not become to stereotype and predictable.

We invited professional drivers and engineers from Ralliart to discuss and share ideas. We did not want the car to be a pure rally car, but we wanted to be "inspired" by the WRC world and let that come through in the design as a general theme, not be dominant but rather hint at it with certain features and treatments coming through as a reminder that this could be used as a pure racing machine.

When we talk about form language in MMC Design we sometimes have different ideas or directions but lately we use the word "Hagane" in design discussions as a key word, or "forged steel". This word is not used in the sense of the weapon or "Katana" but more in the sense of how one can shape metal to be soft but at the same time have solidity and a hardness that is beautiful and radiates quality and endurance. I believe that "Hagane" has been applied to both the exterior and interior of the Concept-X with success. The car radiates agility and softness but at the same time quality, endurance and power.

Another aspect of this project was to establish and forge MMC "Sport DNA". The Concept-X has certain "features" (front grill, headlamps, tail lamps, body section etc) that clearly expresses strength and quality; these elements are the result of careful study in proportion and balance as a whole. These features will also be used in future products carrying the "Sports DNA" and hopefully contribute to a global design language for new products.

I believe that in creating the Concept-X, MRDE has helped reinforcing and creating a "new look" of the MMC brand, a "look" that can be applied to other future products that will help and inspire MMC designers to reach new goals and create new and beautiful products to come.

A good balance of features proportion and stance and understanding what "EVO" stands for is what in the end made the Concept-X believable as a true successor to the LANCER EVOLUTION.

Mitsubishi Concept-X Exterior Design Story



Exterior Chief Designer

Omer HALIHODZIC

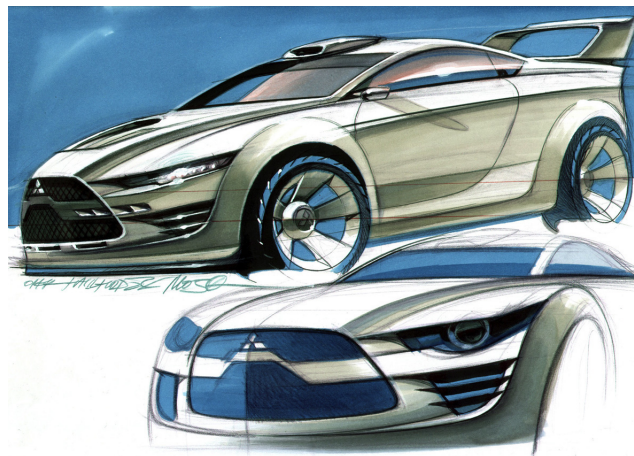
As I was involved in the creation of Concept-X from the early stage, it is clear to me that was a very straightforward project. First thing about creating "new EVO" was that we wanted to keep all the good things which car already has. It was clear to me that EVO has a special status in the product range of MMC and that car has cult status between followers and fans. So, we never thought about starting with a clean sheet of paper and reinventing EVO.

We got a completely new platform with new engine and new technology to start with. A new car should be a big step forward in all aspects of car design, functionality, aerodynamics, ergonomics, performance...etc. With that in mind I started working on the idea drawings and that was a short process.

And I was discussing my ideas with my colleague and management, especially Mr Nakanishi, Corporate General Manager of Design Office, MMC. It was very important to me, that new car should have a very strong character and pure Mitsubishi DNA. I did maybe three front sketches and some for the back. I imagined a car with sporty athletic body, sitting on big wheels with an aggressive and distinctive front and rear. A big air intake dominated the face of the car, together with narrow LED headlamps. The form of the front face and the rear of the car were constructed around three diamond Mitsubishi logo. For me it was very important that the three diamonds are proudly presented and that they fit to the car perfectly. The badge should not look like something added on or just an afterthought. I tried to put as much Mitsubishi DNA in Concept-X as was possible. I looked at the original PAJERO, last GALANT and LANCER and tried to understand which genes they share. I felt there was something from airplane design mixed into it.

To understand what EVO really is, I borrowed an EVO VII for a few weeks. That was big fun, I must admit! I had a chance to drive a BMW M3 and an AUDI S4 as competitor models. This driving test influenced me a lot and I got a very clear feeling what a new EVO should be and what it should not be. These feelings from the EVO driving I tried to replicate in my sketches.

After agreeing a general direction, I continued next to work on the full-scale model in Modarte Turin (Italy). As a base for the Concept-X we used the Evo X Commitment show car model. That car was built a few months before and my experience of working on that car influenced me a lot during work on the Concept-X. Major work was done to the cabin side profile and the pillars. The wheelbase was adjusted to accept the plat-



Original sketch which defined the exterior design

form of the donor car. The wheel size was increased to 20 inch so we had to rework the wheel-arches too. My goal was to keep the functionality and at the same time to achieve nice proportions and distinctive look which would appeal to a broader public.

The engine and turbo charger need as much air as possible, so design of the air intakes and outlets were done based on aerodynamic research in the wind tunnel. The same goes for the cabin silhouette, which developed a much nicer appearance, and has a better aerodynamic shape. The whole front of the car is designed so that the pedestrian protection norm is integrated in the design. Special care was taken that body sits well on the wheels and that the complete stance of the car should be dynamic, sporty and aggressive.

I was very pleased working with the team of very capable model makers from Modarte Turin. These guys are not only good modelers but also real artists; they took a job with a lot of passion. Working with them was a pleasure for me even though we did many hours of hard work. During work on the full-scale model I tried to encourage them to give personal contribution into the development of the surfaces and lines. We discussed many problems, which we encountered on the way and I was always mindful of their opinion.

Of course over all leadership was mine and I took decisions accordingly. The working atmosphere was very emotional, sometimes tense, but always positive. I hope that is visible in the final product.

Mr. Nakanishi, Corporate General Manager of



Mr. Halilhodzic working on the 1/1 exterior model



Final assembly process after the model painted

Design Office, MMC, and Mr. Tsujimoto, General Manager of Design Department, MRDE, visited Modarte a few times, to check progress of the work and give me their opinion and advice. I was happy to find that the general direction was OK and they were happy with the appearance of the model.

The next stage focused mainly on details like wheels, tires, mirrors, grille, head and tail lights...etc. Much of this job was done using computer modeling in MRDE Trebur Studio. Wah Tang and his team did a quick and brilliant job, based on the scan data from the model in Italy. Quality and detailing of the computer models was excellent and we transferred these into real models using stereo lithography. I was amazed myself how precise and exact everything fitted in the real car. TOORA Company milled alloy wheels from computer data with a very high quality. BREMBO supplied us with discs and calipers of our choice, size and design.

After finishing the full-scale model, we took casts and made negative tools for making fiberglass body panels. The front hood was hand crafted from aluminium sheet metal. The finished body panels were assembled over the donor car platform. After fitting and aligning all the parts on the car body, there was only one more step to go, paint-booth.

This was a very important stage, because here we could significantly improve the appearance of the car if it was well done, or destroy all the previous hard work if we made mistakes. I spent many hours and days with the painters during preparations for the final coat of the paint. Every line or radius should be checked and highlights should be examined and tuned if necessary. You must have a good eye for this job and a lot of experience – mathematics and books don't help!

After many layers of polyester and primer, and many hours of sanding and water sanding, it was time to apply the final coat. Maestro Pino did this job with a lot of care and attention. Many hours of fine polishing are done afterwards to give paint high gloss. Everybody was simply stunned when a car moved out of the booth.

Finally, we assembled all the parts and took care that everything functioned and that we didn't damage the paintwork or anything else. This was very precise work and it took some time. I was very happy that we didn't have any major problems with anything on the car and in all it went pretty smooth. I will never forget the moment when everything was finished – we started the engine and the car rolled forward on its own power. My work was done!

Creating an Interior Icon for Concept-X



Interior Designer

Thomas VAQUERIZO

The purpose of Concept-X, from an interior point of view is to provide a preview of the upcoming successor for the LANCER whilst creating an ambience that more closely links MMC's rally success to the road car. The interior also enhances MMC's sporty DNA philosophy, of which the EVO series are considered icons.

The overall ambience is one of minimalism, functionality, focus and clarity. Focus means that the layout is also as user friendly as possible, with all necessary switchgear laid out in front of the driver, clear and minimal meter cluster with integrated shift guide/traction setting monitor and the dual-clutch gearbox shifting located on the racing type steering wheel.

Inspired by the roll cage structure of the rally machine, the aluminium elements in the instrument panel (ip), doors, tunnel and roof replicate the tough secure feel of the rally car whilst providing the base for locating functional elements: in the ip it serves for locating the multimedia controller plus ventilation and switches; on the tunnel its serves for locating the HVAC regulator and extinguisher/water bottle; on the doors it provides for an armrest and window controls; finally on the roof it serves to provide additional ventilation whilst also serving as the location for the starter sequence, a position also inspired by the layout of combat helicopter cabins. The racing bucket seats – for all 4 occupants – together with their full race harnesses are inspired by jet fighter ejector seats, and as such have been designed as self-contained units with the harness being integrated into a central spine on the rear that also forms the base and mounting point to the cabin floor.

The multimedia system controls a slim-line monitor that rotates out of the main ip surface to provide access to all onboard functions, whether technical (e.g. engine performance, SAWC, tire pressure, navigation...) or media (e.g. on-board camera footage, music, telephone, internet...). This information is also available to the rear passengers, via the two monitors located in the headrests of the front bucket seats.

The colour and trim elements are minimalist inspired but tough – witness the ballistic nylon inspired ip and door trim, or the de-bossed leather inserts on the bucket seats – influenced by tactical body armour.

The dark colour choice provides a strong contrast to the aluminium detailing, and combined with the red accent lighting allows the cabin to be distraction free and focussed, like a submarine interior. The panels in the roof can also be illuminated to provide a diffused white ambient light, that with a computer-like technical



Front seat area of completed Concept-X

feel provides light where needed.

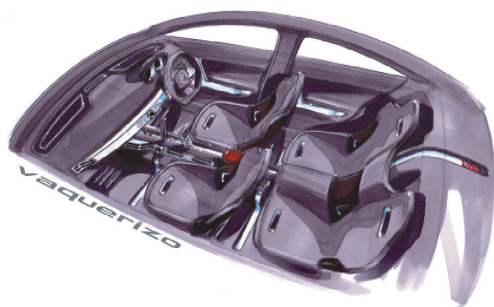
How the interior was born

Internal Design discussion at MRDE took place in early Spring 2005. After the basic direction was laid down by management, the designers began to realize this image first by sketch exploration. These sketches were further refined together with management input until a strong theme was established.

The next step for this theme would be to translate it into 3-D, using ALIAS (advanced CAD modelling), respective of the current exterior data and certain ergonomic requirements to further develop and define the volumes, surfaces and detail. This finished data was presented to Management shortly before Easter and was approved to continue to the next stage – full size modelling.

This modelling would take place in Turin, Italy using the preferred modelling/prototype company Modarte (Turin, as may or may not be known, is considered a center of excellence for the building of prototypes, where the designers work together with many highly skilled craftsmen and modellers to realize their dreams). The 3-D data was first milled in high density polyurethane, a stiff and lightweight material that can be easily tuned and modified as needed. Together with the Modarte staff the design model was developed over the summer months until the desired volume and detail had been achieved and approved.

The next stage would be to cast and reproduce all the parts, whether in glass fibre (doors, ip, tunnel, roof, pillars...) or in resin (for all the detail pieces). These pieces would then later be trimmed or painted respec-



Original sketch which defined the overall interior image



1/1 interior model under development

tively as specified. After completion these parts were then tentatively assembled inside the exterior over the internal architecture, to check for fit and finish, before being finally assembled. This stage is very critical to ensure the high quality of the finished product demanded by Design.

At this time, some final detailing was also added, including the addition of a fire extinguisher to sit on the tunnel, serving both as an intended useful safety feature and attracting attention visually at the same time. Prior to shipping however it was informed by MMC that due to internal regulations this feature could not be used in Japan, therefore Design was left to rack its brains and come up with a solution extremely quickly.

It was decided to turn the extinguisher into a water bottle, which could be exchanged for the extinguisher when the prototype was shown outside Japan. Proof indeed that Design provides rapid reaction and creative solutions when called upon.

The Concept-X prototype was duly finished on schedule at the end of August, before embarking on an intensive photo and video shoot near Turin ahead of a final clean up and shipping to MMC in Japan, where it now awaits successful presentation at the 2005 Tokyo Motor Show in October.



The OUTLANDER is the first all-new offering from the newly revived Mitsubishi Motors Corporation (MMC). With a new powertrain and a new platform, it was launched in October 2005.

1. Targets

In developing the OUTLANDER, MMC sought to bring together the driveability and on-road responsiveness of a sedan and the roominess and comfort of a class-eclipsing cabin. The all-round enjoyability of a Sports Utility Vehicle (SUV) is imbued with the company's performance DNA.

2. Features

2.1 Exterior design

The exterior design gives visual expression to the OUTLANDER's exhilarating performance in the form of sporty lines that wrap around a roomy and comfortable interior space. An intrepid and neat shape that conveys refinement and style is combined with a firm stance yielded by wide tracks and large-diameter wheels, with boldly shaped fender flares and front undercover expressing SUV-defining toughness.



2.2 Interior design

In the cabin, a design that expresses toughness and sophisticated sportiness combines a dynamically styled dashboard that sweeps across the width of the car with doors and floor console bearing a close resemblance to a motorcycle frame. The neat, elaborate design gives solid expression to the OUTLANDER's SUV-defining utility and functionality.

2.3 Enjoyable, responsive performance

In the OUTLANDER's powertrain, a newly developed 2.4-liter DOHC MIVEC engine with an aluminum cylinder block is mated to a newly developed INVECS-III Sport Mode six-speed continuously variable transmission (CVT) for class-leading dynamic performance, responsive, smooth acceleration, and low fuel consumption. In the highest grade, the driver's freedom to enjoy the OUTLANDER's performance is expanded by a standard-equipment paddle-shift system which can be controlled even in the D range shift position.

The OUTLANDER's newly developed platform incorporates technologies that reflect Mitsubishi's All Wheel Control (AWC) principles, and it forms the base for a high-rigidity body whose roof is made of aluminum to keep the center of gravity and roll-inertia moment low. (A high center of gravity and a high roll-inertia moment are weaknesses of conventional SUV design.) The rear suspension has monotube shock absorbers, which give superior damping response and contribute, together with the wide treads, to a pliant and flat ride comfort and to handling that's characterized by superior steering response with minimal roll. The 4WD system is a newly developed electronically controlled type with three driver-selectable modes: 4WD AUTO (this mode accommodates a wide range of road conditions); 4WD LOCK; and 2WD. To further promote stability in diverse conditions, Active Stability Control (ASC) functionality is standard in all OUTLANDER grades.



2.4 Roomy, comfortable cabin

Packaging that combines relatively large body dimensions (comparable to those of the largest conventional mid-size SUV) and a low luggage-area floor (600 mm from the ground) realizes class-eclipsing cabin spaciousness that's highlighted by luggage-area height (at tail gate opening) of 935 mm and second-row legroom of 875 mm. Even so, the OUTLANDER is highly maneuverable owing to a class-smallest minimum turning radius of 5.3 m.

Luggage-handling convenience is promoted by a tailgate that has two separately openable sections (upper and lower) and by a one-touch tumble mechanism whereby a switch located near the back of the luggage area causes the second-row seats to fold and tumble forward.

Two extra passengers can be accommodated using occasional-use third-row seats that are normally stowed under the flat luggage-area floor.

2.5 Premium sound system

The OUTLANDER is available with a 650 W, nine-speaker premium sound system developed jointly with Rockford Fosgate^(R), a leading car-audio maker in the United States. The front and rear doors are designed to serve as speaker boxes and are stiffened to deaden unwanted vibration, and the covers on the front tweeters are made of punched metal, which permits more openings than plastic. The overall result is powerful,



clear sound far surpassing that of conventional factory-fitted systems.

2.6 Safety and environmental compatibility

Although the new platform helps to minimize weight, it also contributes to crashworthiness corresponding to a 6☆ Japan New Car Assessment Program (JNCAP) rating as tested by MMC. Further, the OUTLANDER incorporates measures to reduce damage on small sized vehicles in case of collision, and also to enhance pedestrian protection.

With regard to environmental compatibility, the OUTLANDER realizes exhaust emissions level which is 75 % lower than the standard of Japan's 2005 emission regulations and also a 5 % higher level of fuel-efficiency than the recommended value of Japan's 2010 fuel-efficiency standards.

To give users even greater peace of mind, engine immobilizer, security-alarm system, and deodorizing ceiling are equipped as standard in all grades.

3. Major specifications

Major specifications of the OUTLANDER are shown in the following table.

Specifications	Model	Mitsubishi DBA-CW5W			
		4WD			
		M		G	
Seating capacity	(persons)	5	7	5	7
Overall length	(mm)	4,640			
Overall width	(mm)	1,800			
Overall height	(mm)	1,680			
Min. ground clearance	(mm)	210			
Vehicle weight	(kg)	1,550	1,590	1,580	1,620
Min. turning radius	(m)	5.3			
10-15-mode fuel consumption	(km/L)	11.6			
Engine model		4B12 2.4-L MIVEC			
Valve system and number of cylinders		DOHC, 16-valve, 4-cylinder			
Max. output	{ kW (PS) /min ⁻¹ (net) }	125 (170) /6,000			
Max. torque	{ Nm (kgf-m) /min ⁻¹ (net) }	226 (23.0) /4,100			
Transmission model		INVECS-III 6-speed sport mode CVT			
Suspension	Front	MacPherson strut type			
	Rear				
		Multi-link type			
Tires		215/70 R16		225/55 R18	

(C-seg Product Development Project, Product Development Group Headquarters: Murasaki, Kato)



The Mitsubishi “i” is an innovative premium small car in which a newly developed rear-midship layout realizes innovations in three key areas: styling; handling stability and ride comfort; and impact safety. Embodying totally new minicar values, the “i” was launched in Japan on January 24, 2006.

1. Targets

The “i” is aimed primarily at people who want to downsize from compact cars and at people who are dissatisfied with conventional minicars. Mitsubishi Motors Corporation (MMC) employed a rear-midship layout as a means of overcoming, within the dimensional constraints of the minicar category, the conventional tradeoffs between the following attributes:

- styling originality and comfort;
- comfort and impact safety; and
- handling and ride comfort.

2. Features

The rear-midship layout permits a wide range of features that can’t be achieved in conventional minicars.

2.1 Exterior design

The exterior design is distinguished by a “one-motion” silhouette that capitalizes on the rear-midship layout. Large-diameter wheels positioned in the extreme corners convey a sense of stability and strength. At the same time, a large windshield and “one-motion” rear

door-opening lines help to express a free-spirited individuality far surpassing minicar conventions.

Plus, sharply styled front and rear lamps combine with the body shape to project a “cool and cute” image that’s both intellectual and approachable.

The “i” is offered with a range of nine body colors including two chic, modern colors that were newly created (One of these colors was released on March 2006.).

2.2 Interior design

The large windshield and the spaciousness that stems from a long wheelbase help to realize a bright, open-feeling interior environment. Within this environment, a smoothly contoured instrument panel with simple, classy meters and a center panel offer user-friendliness and driving enjoyment.

And seats with simple, soft forms reminiscent of contemporary furniture gently wrap around the occupants.

A light-grey keynote color for the interior trim is, with all body colors, matched by a choice of red or dark grey for the seat upholstery. An upper tray in front of the front passenger seat is color-coordinated with the seats.

2.3 Packaging

The rear-midship layout realizes a wheelbase of 2,550 mm, which is comparable with the wheelbases of larger, compact cars. The cabin is concomitantly long. Positioning of the wheels at the extreme corners of the body complements the cabin length to realize impressive interior roominess (The positioning of the wheels also plays an important role with respect to handling stability



and ride comfort.). Nevertheless, a minimum turning radius comparable with that of conventional minicars ensures maneuverability.

For further convenience, the rear seat can be folded to create a long, flat, extended luggage surface.

2.4 Performance

(1) Powertrain

A newly developed three-cylinder MIVEC engine (model 3B20) is complemented by an intercooled turbocharger for high performance together with low fuel consumption and exhaust emissions throughout the rev range.

A high-rigidity aluminum cylinder block and a plastic intake manifold help make the engine light and compact. And mounting of the engine at a 45° inclination in a rear-midship position realizes a low center of gravity and superior space efficiency.

A silent timing chain with an automatic tensioner promotes reliability and durability.

Even though the engine is turbocharged, every "i" variant has exhaust emissions 50 % lower than those permitted by Japan's 2005 regulations and thus qualifies for a 3☆ rating as an ultra-low-emission vehicle. At the same time, fuel economy in Japan's 10-15-mode cycle satisfies Japan's 2010 fuel-economy regulations.

(2) Handling stability and ride comfort

Thanks to its rear-midship layout, the "i" is nimble enough for enjoyable driving on urban roads but offers a ride that feels comfortably stable.

The merits of the rear-midship layout are maximized by 45:55 front/rear weight distribution and by an optimally selected tire size.

With regard to hazard evasion, the "i" surpasses European compact cars in the double-lane-change test.

Impressively short braking distances and minimal nosediving during brake application further reflect the benefits of the rear-midship layout.

Also, maximal component stiffness and optimal positioning of soundproofing material realize quietness comparable with that of a larger, compact car.

2.5 Impact safety

Although the "i" has a short nose, the front of the body incorporates a sizeable crushable zone. The frame structure further promotes protection from impact forces in all directions; large-cross-section, straight side rails absorb and disperse collision energy in a frontal impact; optimally positioned crossmembers effectively absorb side-impact energy; and the floor and engine act in concert to absorb and disperse rear-impact energy.

The level of impact safety corresponds to a 5☆ Japan New Car Assessment Program (JNCAP) rating.

Further, pedestrian protection is promoted by ample energy-absorbing space under the hood and by shock-absorbing wiper pivots.

2.6 Utility and equipment

- (1) The windshield is made of glass that cuts the passage of ultraviolet and infrared radiation.
- (2) A keyless operation system allows the user to lock and unlock the doors and start and stop the engine without removing the key from his or her pocket or bag.
- (3) A CD player with AM/FM tuner has a unique panel design in which a large rotary dial promotes ease of use and a high-legibility liquid-crystal display provides information. A hard-disk-based navigation system with a seven-inch wide display is available as a factory-fitted option.
- (4) A fully automatic climate-control system incorporating an air filter works with a deodorizing roof liner to maintain a pleasant interior environment. The "i" achieves early compliance with the Japan Automobile Manufacturers Association's guidelines on minimization of volatile organic compounds in the cabin.
- (5) For environmental safety that gives cabin occupants even greater peace of mind, the "i" is the first Japanese car to have Oeko-Tex Standard 100-certified seat fabric.
- (6) An Electronic Time & Alarm Control System (ETACS) offers diverse functions including a security alarm and vehicle-speed-sensitive wiper operation.

3. Major specifications

The major specifications of the "i" are shown in the following table.

Specifications			Model	i	
				2WD	4WD
Dimensions	Overall length (mm)		4 A/T 3,395		
	Overall width (mm)		1,475		
	Overall height (mm)		1,600		
	Wheel base (mm)		2,550		
	Tread	Front (mm)	1,310		
		Rear (mm)	1,270		
	Interior length (mm)		1,775		
	Interior width (mm)		1,270		
	Interior height (mm)		1,250		
	Vehicle weight (kg)		900	960	
Min. turning radius (m)		4.5			
Engine	Model		3B20 with intercooler and turbocharger		
	Displacement (cc)		659		
	Valve system		DOHC MIVEC, 12-valve		
	No. of cylinders		3		
	Max. output {kW (PS)/min ⁻¹ (net)}		47 (64) / 6,000		
	Max. torque {Nm (kgf-m)/min ⁻¹ (net)}		94 (9.6) / 3,000		
Fuel supply system			ECI MULTI (electronically controlled fuel injection)		
Drivetrain	Steering		Rack & pinion (with power assistance)		
	Suspension	Front	MacPherson struts		
		Rear	3-link, de Dion axle		
	Brake	Front	Ventilated discs (13-inch)		
		Rear	Leading-trailing drums (8-inch)		
	Tires	Front	145/65R15		
Rear		175/55R15			

(Mini Car Product Development Project, Product Development Group Headquarters: Iwao, Kawamura, Masuda)

LANCER EVOLUTION WAGON



The LANCER EVOLUTION WAGON is a new, high-performance, four-wheel-drive (4WD) station wagon that combines the outstanding dynamic performance of the LANCER EVOLUTION IX with the superior utility of a wagon body, thereby extending the LANCER EVOLUTION's identity beyond the bounds of a sedan-only form. To accommodate easy driving on city streets and sporty driving on winding country roads, it is available not only manual but also automatic transmission. Production is limited to 2,500 units.

Sales began on September 7, 2005.

1. Targets

With the LANCER EVOLUTION WAGON, Mitsubishi Motors Corporation (MMC) sought to express its unique product-development direction in a new product combining the running, turning, and stopping performance realized by the company's proprietary All Wheel Control (AWC) technology in the LANCER EVOLUTION sedan with the superior practicality of the LANCER WAGON. With a view to developing the LANCER EVOLUTION WAGON quickly and economically, the company made the greatest possible use of parts from the base models.

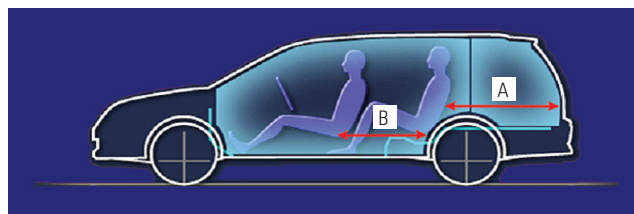
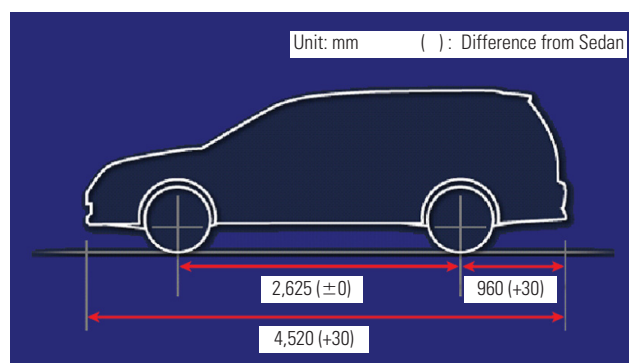
2. Target users

The LANCER EVOLUTION WAGON is aimed at active men aged 40+ who appreciate and desire high-performance cars, at people who are not potential buyers of the LANCER EVOLUTION sedan but are attracted to the newly realized utility of the wagon form, at people seeking an alternative to the MITSUBISHI GALANT LEGNUM VR-4 or MITSUBISHI LIBERO GT, and at people seeking an alternative to sporty cars made by other companies.

3. Features

3.1 Dimensions

Key dimensional attributes of the LANCER EVOLUTION WAGON are as follows:

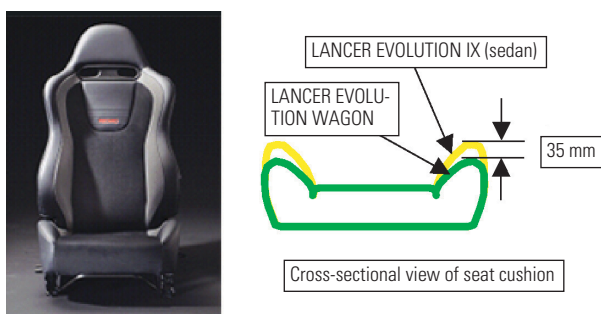


	LANCER EVOLUTION WAGON	LANCER WAGON	Competing wagon
Cargo length (A)	800 mm	800 mm	1,068 mm
Rear legroom (B)	785 mm	785 mm	768 mm

- The rear overhang is 30 mm longer than that of the LANCER EVOLUTION sedan.
- The luggage area is about the same length as that of the LANCER WAGON, but its capacity is about 10 % smaller because the LANCER EVOLUTION WAGON's 17-inch high-performance wheels necessitate larger wheel houses.
- The superior rear-seat roominess of earlier LANCER-series models is maintained.

3.2 Exterior

The body combines the front end of the LANCER EVOLUTION IX with a rear end in which wide, low proportions are emphasized by LANCER EVOLUTION IX design cues.



Interior environment with chrome-finished parts

3.3 Interior

The interior design is based on that of the LANCER EVOLUTION IX but is distinguished by chrome-finished parts, which add a classier touch. The thigh bolsters on the RECARO seats provide optimal hold but are 35 mm lower than those in the LANCER EVOLUTION IX to facilitate entry and exit.

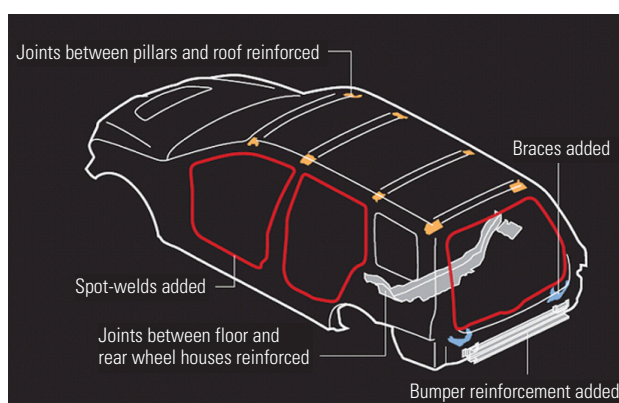
3.4 Body

To enable handling comparable with that of the LANCER EVOLUTION sedan, the rear of the body, the openings in the body, and the joints between the pillars and roof are reinforced for high rigidity.

To further enhance handling, a newly developed high-performance strut tower bar that links the left- and right-hand sides of the body behind the rear seat is available as a dealer-fitted option.

3.5 Performance technologies inherited from LANCER EVOLUTION sedan

The LANCER EVOLUTION WAGON has the same front and rear suspension as the LANCER EVOLUTION IX. The GT grade, which has a six-speed manual transmission, is fitted with the same engine as that for the LANCER EVOLUTION IX. The GT-A grade, which has a five-speed automatic transmission, is fitted with the LANCER EVOLUTION VII GT-A engine, which is well matched to the automatic transmission and gives good response. The 4WD system for each grade is based on that of the LANCER EVOLUTION IX and enables sporty performance.



	GT (6 M/T)	GT-A (5 A/T)
Center differential	Active Center Differential (ACD)	
Front differential	Helical limited-slip differential	Normal differential
Rear differential	Mechanical limited-slip differential	

For occupant comfort, interior noise levels are kept 1 – 3 dB lower than those in the LANCER EVOLUTION sedan.

3.6 Special equipment

User-friendly utility is realized by features including an underfloor box in the luggage area. In contrast to the LANCER EVOLUTION IX GT, the LANCER EVOLUTION WAGON also has the following standard features:

- High-intensity discharge headlamps (with fog lamps and an auto light system)
- Six speakers
- Privacy glass
- 12 V DC power socket (in luggage area)

4. Summary

MMC used its unique capabilities to create a station wagon that performance-oriented LANCER EVOLUTION fans can fully enjoy whether they choose to drive in towns and suburbs or head up to mountain passes for a more thrilling driving experience.

(C-seg Product Development Project, Product Development Group Headquarters: Iwata)

The TRITON is the fourth generation of the pickup, whose first three generations generated sales of 2.8 million units around the world, made by Mitsubishi Motors Corporation (MMC). Representing an evolution of the user benefits that MMC established and refined in the first three generations, it was developed in line with a concept of prioritizing basic functionality, establishing an MMC brand identity by means of high quality, and meeting the needs of a wide range of customers. MMC plans to market the TRITON in more than 140 countries. As a first step in implementing a global strategy, MMC launched the TRITON in Thailand on August 25, 2005.

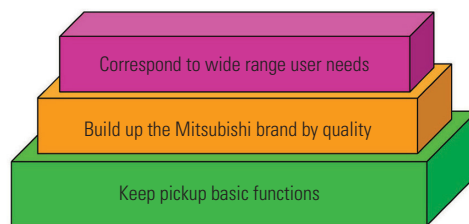


Fig. 1 Product concept

1. Targets

In developing the TRITON, MMC sought to meet a wide range of user needs by applying the pickup know-how that it has gained around the world. Three specific goals were as follows (**Fig. 1**):

- Deliver basic functionality by applying the reliability and durability know-how gained with the previous three generations of the MMC pickup.
- Establish an MMC brand identity by means of class-leading quality achieved through application of the Mitsubishi Motors Development System (MMDS).
- Realize attractive styling, comprehensive functionality, and comfort matched to contemporary lifestyles while also accommodating a wide range of business uses.

The development team focused on two key words: "ART" and "ACT" (**Fig. 2**). The former key word is an acronym of "Active Recreational Truck" and expresses the notion of expanding pickup possibilities in a new, recreational direction. The latter word is an acronym of "Active Commercial Truck" and expresses the notion of creating a pickup that embodies MMC's hallmark reliability and durability.

From the two key words, the development team established the broader goal of creating a distinctive pickup that would appeal not only to established pickup users but also to certain users of Sports Utility Vehicles (SUVs).

2. Features

2.1 Exterior

In pursuit of a distinctive pickup, the development team reflected the ideas behind the "ART" and "ACT" key words in various aspects of the TRITON's form.

2.1.1 Double Cab and Club Cab exterior-design features – ART

The front design of the Double Cab and Club Cab versions inherits the Mitsubishi SUV DNA seen in the PAJERO EVOLUTION, and it has a Mitsubishi three-diamond mark in its center. The body has a stable, road hugging stance that's emphasized by sculpted front fenders, and it has an impactful, dynamic form that's created by features including the A-pillars and roofline

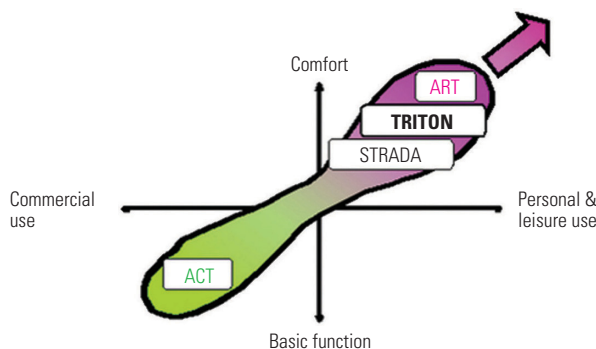


Fig. 2 Key word

(these are shaped to convey a sense of speed) and the belt line (this kicks up toward the rear). Doors and rear surfaces with taut contours like those of well-toned muscles combine with a matching, sloping rear gate to create a contemporary pickup look in which toughness is blended with the refinement of a passenger car. The cargo box has distinctive parting lines that make it appear to wrap onto the cabin, and on the Double Cab version of the TRITON it has curved side lines that match the roof line, creating a form that's fresh but pleasantly familiar (**Figs. 3 and 4**).

2.1.2 Single Cab exterior-design features – ACT

The front design of the Single Cab version inherits the Mitsubishi SUV DNA in common with that of the Double Cab and Club Cab versions, but a grille, headlamps, bumpers, and other items unique to the ACT theme create a stronger expression of reliability and durability (**Fig. 5**).

2.2 Interior-design features

The interior design reflects the pursuit of a fresh look that's matched to the exterior design. The instrument panel has a flowing wave shape and a geometrically striped surface treatment that together express a progressive identity. At the same time, a uniquely designed steering wheel, a large floor console, and bucket-type front seats realize the look and feel of a sporty passenger car (**Fig. 6**).

2.3 Packaging

The same as the previous model, MMC gives the



Fig. 3 Double Cab



Fig. 4 Club Cab



Fig. 5 Single Cab

TRITON dimensions suitable for markets around the world, thereby positioning the TRITON in the middle of the range of dimensions found in the light-pickup segment. The TRITON's wheelbase and treads are set to improve both the handling stability and ride comfort. Notably, the treads are widened by increasing the body width at front and rear wheel sections while keeping the door-to-door width unchanged. This wider treads realizes an increased maximum steering angle that permits a class-smallest minimum turning radius (5.9 m with four-wheel-drive (4WD) ; 5.7 m with two-wheel-drive (2WD)). Also, balance of the hood visible area from the driver's viewpoint has improved, and moreover, controllability in tight spaces has significantly improved. This improvement is noticeable sales point for new TRITON. With regard to cabin spaciousness, an increase

of approximately 150 mm in the interior length of the Double Cab version realizes SUV-level spaciousness for rear-seat occupants. Comfort-enhancing equipment such as leather seats and a retractable rear power window further distinguishes the TRITON's rear-passenger accommodation from that of a conventional pickup, giving passengers the impression that they are riding in an SUV.

2.4 Performance

2.4.1 Newly developed common-rail injection engine

In a first for an MMC pickup, the company developed two common-rail direct-injection diesel engines with two displacements: 2.5-liter and 3.2-liter. In the common-rail system, innovatively devised technology permits fuel under a pressure of 180 MPa to be injected



Fig. 6 Interior

with freely controllable timing. As a result, exhaust emissions clear the requirements of the European Union's (EU's) STEP 3 emission regulations, which have been implemented in Thailand. Nevertheless, power and fuel economy are approximately 20 % higher than those of diesel engines in the earlier MMC pickup, meaning that class-topping performance is combined with competitive fuel economy.

2.4.2 Platform

In the chassis, a rack-and-pinion steering gear accommodates increasingly high speeds of driving in Asia and elsewhere. Increased mounting rigidity for the front suspension is matched by updated rear suspension alignment for an optimal front/rear rigidity balance. A newly designed frame combines with these benefits to help realize SUV-level handling stability and ride comfort. With the Single Cab version, which is intended mainly for commercial use, stiff suspension is combined with a platform design that reflects the ART and ACT themes.

2.4.3 Crashworthiness

In light of plans to sell the TRITON in Europe, MMC targeted crashworthiness good enough for a 4★ rating in the European New Car Assessment Program (Euro NCAP). Consequently, the TRITON has highly rigid body framework and a newly designed chassis frame that's highly efficient in terms of absorbing impact energy. In the cabin, driver and passenger airbags are complemented by pretensioner- and force-limiter-equipped seatbelts for further occupant protection. In addition, a pedal structure that limits rearward pedal movement in a frontal impact helps protect the driver's lower legs.

2.4.4 Equipment

To make the TRITON acceptable to SUV users, MMC moved beyond the equipment specifications seen with conventional pickups. Highlight items of passenger-car-style equipment and pickup-style equipment newly adopted for the TRITON are as follows:

- Retractable rear power window

The window between the cabin and cargo bed can be raised and lowered electrically for easy access to the cargo bed.

It also has a ventilation position that permits fresh air to be introduced into the cabin. This is one of the specific features of the TRITON.

- Leather power seats
The highest grade of the Double Cab version is the first pickup to have leather-upholstered seats. The driver's seat has power adjustment (a feature that puts it in on a par with the driver's seat of an SUV).
- Liquid-crystal information panel
Instead of an information panel with three conventional mechanical meters, the TRITON has liquid-crystal meters that are superior in terms of legibility and styling. In addition to environmental information such as the altitude and outside temperature, the information panel shows driving-related information such as the average speed and average fuel consumption. If an MMC audio system is fitted, the information panel can also show audio information.
- Electronic devices
Electronic Time & Alarm Control System (ETACS) is fitted in all TRITON versions. The ETACS realizes diverse functions that can be customized using an MMC Multi-Use Tester (MUT). It also has comprehensive diagnosis functions.

2.4.5 Rough-road performance (4WD versions)

For stability at high speeds, the TRITON has a layout that makes its center of gravity lower than that of the previous model. As a result, the TRITON has less ground clearance than the previous model. However, the lowest parts of the TRITON are located as close as possible to the wheels, to prevent the adverse effect on the rough-road performance. Updated crossmember positioning permits a ramp-breakover angle (a key index of rough-road driveability) of 26.7 ° (an increase of 3.5 ° over the previous model), and the rebound

wheel strokes are longer (20 mm longer at the front; 13 mm longer at the rear) than those of the previous model. Notwithstanding its relatively low center of gravity, therefore, the TRITON surpasses the previous model in terms of rough-road performance.

2.4.6 Corrosion protection and environmental compatibility

For superior reliability and durability, the TRITON is sufficiently corrosion-resistant to be offered with a 12-

year corrosion warranty. Also, the TRITON achieves early compliance with EU directives on recycling and other aspects of environmental compatibility.

3. Major specifications

Major specifications of the TRITON are shown in the following table.

Item	Body shape		Single Cab	Club Cab				Double Cab								
	Model		KA4TNE NMFRU	KA4TNC NMFRU	KA4TNC NUZRU	KA4TNC RUZRU	KB4TGC NHZRU	KB8TGC NHZRU	KA4TNJ NMZRU	KA4TNJ NUZRU	KA4TNJ RUZRU	KB4TGJ NHZRU	KB8TGJ NHZRU	KB8TGJ NXZRU	KB8TGJ RXZRU	
Dimension & weight	Overall length (mm)		5,030	5,110				4,995								
	Overall width (mm)		1,750				1,800		1,750				1,800			
	Overall height (mm)		1,655	1,660	1,655		1,780		1,655	1,650		1,780				
	Wheel base (mm)		3,000													
	Track	Front (mm)	1,505				1,520		1,505		1,520					
		Rear (mm)	1,500				1,515		1,500		1,515					
	Bed interior length (mm)		2,220	1,805				1,325								
	Bed interior width (mm)		1,470													
	Bed interior height (mm)		405													
	Min. ground clearance (mm)		200		195		205		200	195		205				
	Cargo floor height (mm)		715	725	720		860		715	710		850				
	Vehicle weight (kg)		1,505	1,565	1,600		1,795	1,840	1,640		1,860	1,920	1,930	1,940		
Gross vehicle weight (kg)		2,495	2,285	2,330		2,535	2,605	2,330		2,535	2,605					
Seating capacity (person)		3	2				5									
Performance	Max. speed (km/h)		150	160	158	170	172	160		158	170	172				
	Min. turning radius (m)		5.7				5.9		5.7		5.9					
	Max. climbing ability (tan, q)		0.31		0.36		0.38	0.47	0.36		0.38	0.47				
	Towing capacity with brake (kg)		N/A													
	Towing capacity (full load) without brake (kg)		N/A													
Engine	Type		4D56IDI T/C		4D56CDI T/C		4D56CDI I/T	4M41CDI I/T	4D56CDI T/C		4D56CDI I/T	4M41CDI I/T				
	Displacement (cc)		2,477				3,200		2,477				3,200			
	Bore & stroke (mm)		91.1 x 95.0				98.5 x 105.0		91.1 x 95.0				98.5 x 105.0			
	Compression ratio		20.5		17.5		17.0		17.5				17.0			
	Max. output (din net) (kw/min ⁻¹)		66/4,000		85/4,000		103/4,000	121/3,800	85/4,000		103/4,000	121/3,800				
	Max. torque (din net) (Nm/min ⁻¹)		196/2,000		247/2,000		321/2,000	351/2,000	247/2,000		321/2,000	351/2,000				
Fuel system	Fuel supply system		Electrical fuel injection		Electrical fuel injection (commonrail)											
	Fuel tank capacity (L)		75													
Transmission	Type (manual floor change)		5 M/T (R5M21)		5 M/T (R5MB1)	4 A/T (R4AW4)	5 M/T (V5MB1)		5 M/T (R5MB1)		4 A/T (R4AW4)	5 M/T (V5MB1)		4 A/T (V4A5A)		
	1 st		3.967		4.313	2.452	4.313				2.452	4.313		2.842		
	2 nd		2.136		2.330	1.452	2.330				1.452	2.330		1.495		
	3 rd		1.360		1.436	1.000	1.436				1.000	1.436		1.000		
	4 th		1.000			0.688	1.000				0.688	1.000		0.731		
	5 th		0.856		0.789	—	0.789				—	0.789		—		
	Reverse		3.578		4.220	2.212	4.220				2.212	4.220		2.720		
	Transfer gear ratio	High	—				1.000		—		1.000					
		Low	—				1.900		—		1.900					
	Final gear ratio		4.222		3.909		4.100		3.909		4.100					
Steering			Rack & pinion with power steering													
Suspension		Front	Independent-wishbone, coil springs													
		Rear	Rigid, elliptic leaf springs													
Brake	Front	Ventilated discs (15-inch)				Ventilated discs (16-inch)		Ventilated discs (15-inch)			Ventilated discs (16-inch)					
	Rear	LT drums (10-inch)				LT drums (11.6-inch)		LT drums (10-inch)			LT drums (11.6-inch)					
Tires	Front	195R15C 8PR 106/104R		215/70R15C 6PR 106/104S		245/70R16 111S RF		195R15C 8P R 106/104R	215/70R15C 6PR 106/104S		245/70R16 111S RF					
	Rear	195R15C 8PR 106/104R		215/70R15C 6PR 106/104S		245/70R16 111S RF		195R15C 8P R 106/104R	215/70R15C 6PR 106/104S		245/70R16 111S RF					

(RV1 Product Development Project, Product Development Group Headquarters: Erami, Tomita, Konishi, Shibata)



In 2005, Mitsubishi Motors Corporation (MMC) performed the first full model change in eight years on the FREECA, a vehicle with versatile passenger-carrying and commercial capabilities that have made it popular in Taiwan, Indonesia, the Philippines, China, Vietnam, and other countries. For the full model change, MMC evolved the FREECA concept of meeting diverse passenger-carrying and commercial needs. The resulting new model, which is named the ZINGER, was launched in Taiwan by China Motor Corporation (CMC) in December 2005.

1. Targets

In Taiwan, China, and Southeast Asia, there is great demand for multipurpose vehicles that can meet commercial needs and passenger-carrying/leisure needs. Consequently, MMC developed the ZINGER in line with a concept that's summed up by the phrase "MICS-RV" (Fig. 1).

The letters of the concept phrase have the following meanings:

- M: Multi-purpose
- I : Interior roominess and riding comfort
- C: Compact body size
- S: Sophisticated styling

MICS-RV

Multi-purpose
Interior roominess & Riding comfort
Compact body size
Sophisticated Styling
 +
Rough-road running capability
Value for the money & Affordable price

Fig. 1 Concept key word

- R: Rough-road running capability
- V: Value for money and affordable price

In addition to reflecting each element of the concept phrase in the ZINGER, MMC provided the ZINGER with many storage spaces with a view to pursuing superior convenience (Fig. 2). MMC also sought to expand the versatility for commercial and passenger-carrying needs by specifying extensively rearrangeable seats including front and rear seats that can be folded fully flat and a rear seat that can be slide-adjusted.

2. Features

2.1 Exterior design

For international acceptability, the ZINGER has progressive styling that marries the utility of a commercial vehicle, the toughness of a Sports Utility Vehicle (SUV), and the luxury of a minivan by well-balanced proportions that appeal to users whose priorities are as diverse as family transportation and sporty driving. The strength of the Mitsubishi sports DNA that the ZINGER inherits can be seen in the front face that features large, stylish headlamps and in the side view in which sportiness and toughness of SUV are expressed by a wedge-style belt line and by flare garnishes that emphasize large-diameter wheels. At the rear of the body, the tail lamps have a passenger-car-style horizontal design that combines with a tailgate garnish to convey a sense of stability. At the same time, front and rear underguard garnishes emphasize a sense of SUV taste.

2.2 Interior design

The original exterior design is complemented by an interior design with futuristic relaxing wavy lines, fresh coloring and textures brought together in way to express quality and utility. The meters have bright blue illumination that gives them a futuristic look, and the steering wheel and floor console have silver-colored accents that

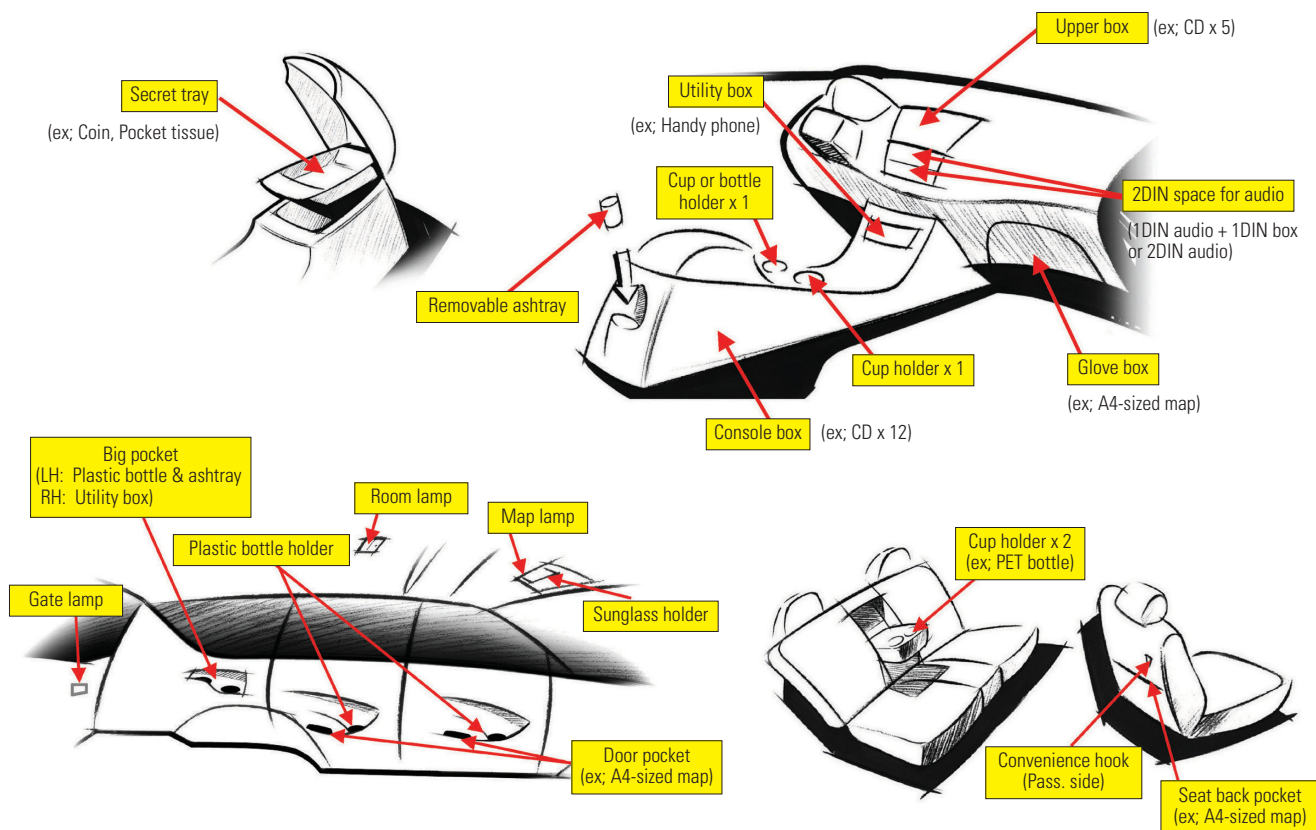


Fig. 2 Multi purpose: Utility

add a taste of sportiness. The instrument panel and door trim have two-tone coloring whose contrasting colors help to create a sense of openness and refinement. The air conditioner switch panel has large, colorful, easy-to-use knobs, and the audio panel is distinguished by a wood-grain finish that adds a taste of high quality. The trim coloring for high grades is maroon and beige (a combination that conveys a sense of high quality). The trim coloring for standard grades is blue and grey (a combination that conveys a sense of youthful sportiness).

2.3 Packaging

The ZINGER's overall length, overall width, overall height are similar to those of the previous model, so the ZINGER combines the high maneuverability of the previous model with a class-leading interior roominess. Notably, the ZINGER surpasses the previous model by 225 mm in terms of interior length and by 40 mm in terms of interior width. At the same time, a longer wheelbase and wider treads promise high level performance of handling stability and ride comfort.

The seats have large dimensions that promote relaxation. Together with ample head clearance, they help a comfortable environment for the driver and passengers.

2.4 Performance

2.4.1 Powertrain

Whereas the previous model had a 2.0-liter MPI gasoline engine, the ZINGER has a 2.4-liter engine whose larger displacement permits superior running performance. For transmission an electronically controlled four-speed automatic transmission is combined.

2.4.2 Handling stability and ride comfort

A newly designed high-rigidity chassis frame, front double-wishbone suspension, and rear three-link coil-spring suspension (an improvement over the previous model's rear leaf-spring suspension) achieve a superior SUV-level combination of handling stability and ride comfort. Whereas the previous model was lacking in terms of ride comfort, the ZINGER's ride comfort is improved not only by the newly specified rear three-link coil-spring suspension but also by passenger-car-type radial tires.

2.4.3 Quietness

The ZINGER is one of the quietest in the class.

To suppress noise and vibration, the ZINGER adopts high-rigidity chassis frame, a high-rigidity body, double door seals, spherical joints in the exhaust system, optimally positioned silencer and insulator and foam filler.

2.4.4 Body and steering-wheel vibration

Vibration in the body and steering wheel is suppressed not only by the high-rigidity chassis frame but also by superior rigidity in the joints of the deck cross-members and by optimal tuning of the rubber components used to mount the body on the frame.

2.4.5 Crashworthiness

In line with MMC's crashworthiness policy, the ZINGER's body is based on MMC's Reinforced Impact Safety Evolution (RISE) body structure. Even for markets where high crashworthiness is not legally required, the ZINGER satisfies European requirements including those for occupant protection in a 64 km/h impact with an offset deformable barrier. High hip points for the seats (more than 700 mm from the ground) make the ZINGER exempt from side-impact requirements. Nevertheless, in line with MMC's collision-safety policy, the ZINGER offers side-impact safety corresponding to the demands of relevant regulations. Pretensioner- and force-limiter-equipped seatbelts are used in airbag-equipped model of the ZINGER. Also, the steering column has a structure that prevents steering shaft from protruding into the cabin in the event of a collision.

2.4.6 Rough-road performance

Whereas passenger cars and minivans typically have minimum ground clearance of 150 – 160 mm, the ZINGER has minimum ground clearance of 180 mm for superior driveability on rough, flooded, and otherwise difficult road surfaces. Large approach and departure angles further promote the ZINGER's driveability in difficult conditions.

2.4.7 Corrosion resistance and environmental compatibility

In line with MMC's strategy on corrosion resistance and environmental compatibility, the ZINGER has superior corrosion resistance that promotes durability and reliability. In addition, none of the ZINGER's components contains environmentally harmful substances.

2.4.8 Equipment

To meet commercial, passenger-carrying, and recreational needs, the ZINGER has passenger-car-level equipment specifications. Highlight equipment items are as follows:

- Powered driver's seat (P and X lines)
- Leather seat upholstery (H, P, and X lines)
- Sunroof (P and X lines)
- Driver and front-passenger airbags (X line)
(Pretensioner- and force-limiter-equipped seatbelts are fitted together with the airbags.)
- High-intensity discharge headlamps (X line)
- Automatic air conditioner (P and X lines)
- Electronic Time & Alarm Control System (ETACS)*
(all lines)
(The ETACS realizes diverse driver-oriented functions that can be customized using a Multi-Use Tester. It also has comprehensive diagnosis functions.)

3. Major specifications

Major specifications of the ZINGER are shown in the following table.

NEW PRODUCTS

Specifications			Model				ZINGER			
			M		H		P		X	
			5 M/T		4 A/T					
Dimensions	Overall length	(mm)			4,585					
	Overall width	(mm)	1,760				1,775			
	Overall height	(mm)	1,800				1,805			
	Overhang	Front	(mm)		800					
		Rear	(mm)		1,065					
	Wheel base	(mm)			2,720					
	Tread	Front	(mm)		1,505					
		Rear	(mm)		1,500					
	Seating capacity	(persons)			5					
	Min. ground clearance	(mm)			180					
Engine	Min. turning radius	(m)			5.3					
	Vehicle weight	(kg)	1,640		1,660		1,720		1,725	
	Model				4G64					
	Valve system				SOHC 16 valve					
	Displacement				2,351					
	Bore and stroke				86.5 x 100					
	Compression ratio				9.0 : 1					
	Fuel supply system				MPI					
	Max. output	{kW (PS) /min ⁻¹ }			93.5 (127) /5,250					
	Max. torque	{Nm (kg-m) /min ⁻¹ }			193 (19.7) /4,000					
Transmission	Fuel tank capacity	(L)			65					
	Emission control				Unleaded (RON \geq 91)					
	Gear ratio	1st			3.967					
		2nd			2.136					
		3rd	1.360		2.826					
		4th	1.000		1.493					
		5th	0.856		1.000					
		Reverse	3.578		0.730					
		Final	4.222		4.636					
Drivetrain	Suspension	Front	(mm)		Double wishbone, coil spring, with stabilizer					
		Rear	(mm)		Rigid 3-link coil spring, with stabilizer					
	Brake	Front	(mm)		15-inch ventilated disc					
		Rear	(mm)		Leading trading drum					
	Steering				Rack & pinion					
	Tires				205/70R15		225/60R16			
	Wheels		15-inch steel/full cover		15-inch alloy		16-inch alloy			
	Spare tire				Ground tire/steel		Ground tire/alloy			

(RV2 Product Development Project, Product Development Group Headquarters: Watabe, Hazama, Kuzuoka, Akita, Yoshioka, Sakai, Kimura)

INTERNATIONAL NETWORK

Mitsubishi Motors North America, Inc.

6400 West Katella Avenue, Cypress,
CA 90630-0064, U.S.A.
Phone: 1-714-372-6000
Fax: 1-714-373-1020

MMNA (Manufacturing)

100 North Mitsubishi Motorway Normal,
Illinois 61761, U.S.A.
Phone: 1-309-888-8000
Telefax: 1-309-888-0130

Mitsubishi Motors R&D of America, Inc.

3735, Varsity Drive, Ann Arbor, Michigan
48108, U.S.A.
Phone: 734-971-0900
Fax: 734-971-0901

Mitsubishi Motors Sales of Canada, Inc.

2090 Matheson Blvd. E., Mississauga,
ON L4W 5P8
Phone: 1-888-576-4878

Mitsubishi Motors Sales of Caribbean, Inc.

Road 2 Km. 20.1 Candelaria Ward Toa Baja,
Puerto Rico 00949
(P.O. Box 192216 San Juan, PR 00919-2216)
Phone: 1-787-251-5591
Fax: 1-787-251-2953

Netherlands Car B.V. (NedCar)

Dr. Hub van Doorneweg 1,
6121 RD Born, The Netherlands
Phone: 31-46-489-4444
Fax: 31-46-489-5488

Mitsubishi Motors Europe B.V.

Beech Avenue 150 1119 PR Schiphol-Rijk,
The Netherlands
(P.O. Box 22922, 1100 DK Amsterdam Zuidoost)
Phone: 31-20-4468111
Fax: 31-20-4468143

Mitsubishi Motor Sales Nederland B.V.

Beech Avenue 150, 1119 PR Schiphol-Rijk,
The Netherlands
(P.O. Box 22934, 1100 DK, Amsterdam Zuidoost)
Phone: 31-20-8512277
Fax: 31-20-6541485
email: klanteninfo@mmsn.nl

Mitsubishi Motor Sales Sweden AB

Fagerstagatan 29 Box 8144, S-163 08 Spanga,
Sweden
Phone: 46-8-474-5400
Fax: 46-8-621-1794

MMC Automoviles Espana S.A.

Calle Francisco Gervás 4 28108
Alcobendas Madrid, Spain
Phone: 34-91-387-7400
Fax: 34-91-387-7458

Mitsubishi Motors Deutschland (GmbH)

Hessenauer Strasse 2, 65468
Trebur, Germany
Phone: 49-6147-20701
Fax: 49-6147-207220

Mitsubishi Motor R&D Europe GmbH

Diamant-Strasse 1 65468
Trebur, Germany
Phone: 49-6147-9141-0
Fax: 49-6147-3312

Mitsubishi Motors Corporation France SAS

9 Chausse Jules Csar, BP 10051 OSNY, 95521
CERGY PONTOISE Cedex, France
Phone: 33-1 34 35 84 00

Mitsubishi Motors Belgium N.V.

Uitbreidingsstraat 2-8,
2600 Berchem, Belgium
Phone: 32-3-280-8484
Fax: 32-3-280-8485

Mitsubishi Motors de Portugal, S.A.

Rua. Dr. Jos-Espirito Santo, 38, 1950-097 Lisboa,
Portugal
Phone: 351-218-312-100
Fax: 351-218-312-232

Mitsubishi Motors Australia, Ltd.

1284 South Road, Clovelly Park,
SA 5042, Australia
(P.O. Box 8, Melrose Park SA 5039)
Phone: 61-8-82757111
Fax: 61-8-82756841

Mitsubishi Motors New Zealand, Ltd.

Private Bag 50914, Porirua, New Zealand
Phone: 64-4-237-2439
Fax: 64-4-237-4495

Mitsubishi Motors (Thailand) Co., Ltd.

88 Phaholyothin Road, Klongluang,
Phatumthai 12120, Thailand
Phone: 66-2-908-8000
Fax: 66-2-908-8285

Mitsubishi Motors Philippines Corporation

Ortigas Avenue Extension, Cainta Rizal,
P.O. Box 4592, Manila, Philippines
Phone: 63-2-658-0109
Fax: 63-2-658-0671

MITSUBISHI MOTORS CORPORATION

- **Head Office**

16-4, Kohnan 2-chome, Minato-ku, Tokyo 108-8410, Japan
Phone: +81-3-6719-2111
Telefax: +81-3-6719-0034

- **Design Center**

Tama Design Center

1-16-1, Karakida, Tama-shi, Tokyo 206-0035, Japan
Phone: +81-423-89-7307

- **Engineering Offices**

Research & Development Office

1, Nakashinkiri, Hashime-cho, Okazaki-shi, Aichi Pref. 444-8501, Japan
Phone: +81-564-31-3100
[Tokachi Proving Ground]
22-1, Osarushi, Otofuke-cho, Kato-gun, Hokkaido 080-0271, Japan
Phone: +81-155-32-7111

- **Plants**

Nagoya Plant

1, Nakashinkiri, Hashime-cho, Okazaki-shi, Aichi Pref. 444-8501, Japan
Phone: +81-564-31-3100

Powertrain Plant

[Powertrain Plant – Kyoto]
1, Uzumasa Tatsumi-cho, Ukyo-ku, Kyoto-shi 616-8501, Japan
Phone: +81-75-864-8000
[Powertrain Plant – Shiga]
2-1, Kosuna-cho, Konan-shi, Shiga Pref. 520-3212, Japan
Phone: +81-748-75-3131

Mizushima Plant

1-1, Mizushima Kaigandori, Kurashiki-shi, Okayama Pref. 712-8501, Japan
Phone: +81-86-444-4114

- **Pajero Manufacturing Co., Ltd.**

2079, Sakagura, Sakahogi-cho, Kamo-gun, Gifu Pref. 505-8505, Japan
Phone: +81-574-28-5100

